The Dissertation Committee for Daniela D'Amico Certifies that this is the approved version of the following dissertation:

HIV-Associated Neurocognitive Disorders: Role of Viral Reservoirs and Lipid Dysregulation

Committee:

Eliseo A. Eugenin

Brendan Prideaux

Giulio Taglialatela

Joan W. Berman

Shelly Buffington

Shao-Jun Tang

HIV-Associated Neurocognitive Disorders: Role of Viral Reservoirs and Lipid Dysregulation

by

Daniela D'Amico, Ph.D.

Dissertation

Presented to the Faculty of the Graduate School of

The University of Texas Medical Branch

in Partial Fulfillment

of the Requirements

for the Degree of

Doctor of Philosophy

The University of Texas Medical Branch

June 2022

Dedication

To my beloved daughter, Marta Joy, who has been nicely my source of inspiration and gave me strength when I thought of giving up.

Acknowledgments

It is my pleasure to acknowledge several people who were essential for completing my Ph.D. research. First, I wish to thank all my committee members.
I particularly thank Dr. Eliseo A. Eugenin and Dr. Brendan Prideaux, as my tutors and responsible for my research activity at the Department of Neuroscience, Cell Biology, and Anatomy. They provided me the scientific rigor and precious methodical and personal advice.

These acknowledgments would not be complete without mentioning all the Post Docs (Dr. Anna Maria Gorska, Dr. Silvana Valdebenito, Dr. Maribel Donoso, Dr. David Ajasin, and Dr. Matthias Holzlechner) in Dr. Eugenin's laboratory for being friends and supporting me during my research activity and in the realization of this work.

Finally, I wish to express deep gratitude to the most important people in my life, allowing me to reach this important achievement, which is full of troubles but very satisfying.

To my daughter Marta Joy for her unaware support that gave me strength when I thought of giving up.

To my husband Gabriele for his inestimable presence, his daily love, his tireless patience and for his crazy attitude to come with me to Texas and to assist me in this amazing experience.

To my dad, my powerful angel, who always believed in me and worked hard to allow me to become a doctor.

To my mum, my sister, my nieces, and my best friend, indispensable presence in my life, who were a thousand kilometers far, but they have never made me feel alone.

HIV-Associated Neurocognitive Disorders: Role of Viral Reservoirs and Lipid Dysregulation

Publication No._____

Daniela D'Amico, Ph.D.

The University of Texas Medical Branch, 2022

Supervisor: Eliseo A. Eugenin

Abstract: HIV infection has become a chronic and manageable disease due to the effective use of combined anti-retroviral therapies (cART). However, several chronic aging-related comorbidities, including HIV-associated neurocognitive disorders (HAND), persist in the HIV-infected population; but the mechanisms are unknown. We hypothesized that neurocognitive decline in the HIV-infected population is dependent on CNS viral reservoirs by mechanisms of damage amplification mediated by host lipids. HIV CNS damage, in the current cART era, is mediated by a low number of HIV DNA positive macrophages/microglia and astrocytes that support a residual viral mRNA and protein synthesis. Some HIV proteins are secreted and taken into the neighboring uninfected cells, generating bystander damage in the CNS. Viral reservoirs are associated with local myelin structure compromise resulting in the release of several myelin components, including the lipid sulfatide. Soluble sulfatide compromises gap junctional communication and calcium waves, which contribute to the amplification of CNS damage and cognitive impairment that distress the HIV-infected population.

Our pending experiments aim to categorize Cx43 interacting proteins after sulfatide treatment by proteomics, to identify specific astrocyte populations that become susceptible to HIV infection or bystander damage by single-cell RNA sequencing, and detect lipid dysregulation in primary human cultures of HIV-infected astrocytes using MALDI-MSI or MALDI-2 MSI.

To further examine lipid dysregulation, we also developed a MALDI-2 MSI method to detect lipid classes and species that are not detected with regular MALDI-MSI, using the brain tissue sections of the AD 3xTg mouse model. We proved that this assessment is compatible with subsequent immunofluorescence and histological analyses in the same tissue section. This approach is innovative and helpful in performing a multi-omics characterization for several pathologies, including HAND.

TABLE OF CONTENTS

List of Tables

List of Figures

List of Abbreviations

AA - arachidonic acid

9-AA - 9-aminoacridine

Aβ - amyloid-β

aCDase - acid ceramidase

ACTN1/4 - Actin

AD - Alzheimer's diseases

AGA - 18-α-glycerritenic acid

AIDS - Acquired Immune Deficiency Syndrome

αKG - alpha-ketoglutarate

AML - acute myeloid leukemia

ANI - asymptomatic neurocognitive impairment

ANXA1/5 - annexin 1/5

AP - alkaline phosphatase

ASA - arylsulfatase A

ASL - arterial spin labeling

aSMase - acid sphingomyelinase

ATP - adenosine triphosphate

aWM - abnormal white matter

Bax - Bcl-2-associated X protein

BBB - Blood Brain Barrier

Bcl-2 - B cell lymphoma 2 gene

Bim - Bcl-2-like protein 11

BOLD - blood oxygen level dependent imaging

BRD4 - bromodomain-containing protein 4

^{11}C - $^{11}Carbon$

CA - cytosine-adenine

cART - combined Antiretroviral Therapy

CCL2 - Monocyte chemoattractant protein-1

CCR5 - C-C chemokine receptor 5

cDNA - complementary DNA

CDK9 - cyclin-dependent kinase 9

CDK11/CycL - cellular CDK/cyclin complex

Cer - Ceramide

Cer1-P - ceramide-1 phosphate

CERT - ceramide transfer protein

CEs - cholesteryl esters

cFLIP - cellular FLICE (FADD-like IL-1β-converting enzyme)-inhibitory protein

CGT - ceramide galactosyltransferase

CHARTER - CNS HIV Anti-Retroviral Therapy Effects Research

CHCA - α-Cyano-4-hydroxycinnamic acid

CHO - choline

CIP75 - Connexin Interacting Protein of 75 k.Da.

CKAP4 - Cytoskeleton Associated Protein 4

CNS - Central Nervous System

Cr - Creatine

CSF - Cerebrospinal fluid

CST - cerebroside sulfotransferase

Cx43 - Connexin43

CXCR4 - co-receptor C-X-C chemokine receptor type 4

CycT1 - Cyclin T1

DA - Dopamine

DAG - Diacylglycerol

DAN - 1,5-Diaminonaphthalene

DAPI - 4',6-diamidyno-2-fenyloindol

DAT - dopamine transporters

DBN - Debrin

dCA - didehydro-cortistatin A

DES - dihydroceramide desaturase

DESI - desorption electrospray ionization

DHB - 2,5-dihydroxybenzoic acid

dhCer - dihydroceramide

dhSph - dihydrosphingosine

dihydroCS - (Dihydro)ceramide synthase

DKK1 - dickkopf-1 protein

DNA - deoxyribonucleic acid

dsDNA - double helix DNA molecule

DSIF - DRB-sensitivity inducing factor

DTI - diffusion tensor imaging

Env - envelope

EP - E-prostanoid

EP MALDI - Elevated Pressure Matrix-Assisted Laser/Desorption Ionization

ER - endoplasmic reticulum

EXR - Ezrin

^{18}F - $^{18}Fluorine$

FA - fatty acid

Fadd - Fas-associated protein with death domain

FAPP2 - phosphate adaptor protein 2

FFAs - free fatty acid

FFPE - Formalin-fixed paraffin embedded

fMRI - functional Magnetic Resonance Imaging

GFAP - Glial fibrillary acidic protein

GJs - gap junctions

Gln - Glutamine

GLT1/EAAT1 - Excitatory amino acid transporter 1

GLAST/EAAT2 - Excitatory amino acid transporter 2

Glu - Glutamate

GluCer - Glucosylceramide

Glx - glutamate-glutamine

GM - gray matter

GMs - Gangliosides

Gp120 - envelope protein gp120

GSL - Glycosphingolipids

HAND - HIV-associated neurocognitive disorders

HAD - HIV-associated dementia

HDAC - histone deacetylases

HDL - high-density lipoprotein

H&E - Hematoxylin and Eosin

HexCers - hexosylceramides

HIV - Human Immunodeficiency Virus

HIVE - HIV encephalitic brains

H-MRS/MRS - proton-magnetic resonance spectroscopy

HMTs - histone methyltransferases

HSP90 - Heat shock protein 90

Iba-1 - Ionized calcium-binding adaptor protein-1

ICAM5 - intercellular adhesion molecule-5

IF - immunofluorescence

IFN-α - interferon Alpha

IHC - immunohistochemical

ILK - integrin-linked kinase

IL-6 - Interleukin-6

IN - Integrase

INSTI - integrase strand transfer inhibitors

IP_3 - inositol triphosphate

IP-10 - interferon-γ-Inducible Protein

IPA - Ingenuity Pathway Analysis

3KdhSph - 3-keto-dihydrosphingosine

3KSR - 3-keto-dihydrosphingosine reductase

LCM - Laser Capture Microdissection

LC-MS/MS- Liquid Chromatography with tandem mass spectrometry

LDs - lipid droplets

LDL - low-density lipoprotein

LPA - latency promoting agent

LPS - Lipopolysaccharide

LRAs - latency reversing agents

LRPPRC - Leucine Rich Pentatricopeptide Repeat Containing

L-ser - L-serine

LTRs - long terminal repeats

LY - Lucifer yellow

M - neutral analyte molecules

MAG - myelin-associated glycoprotein

MALDI-MSI - Matrix-assisted laser desorption ionization-mass spectrometry imaging

MAP-2 - Microtubule-associated protein 2

MAPK - mitogen-activated protein kinase

MBP - myelin basic protein

Mcl-1 - Myeloid leukemia 1

MCMD - HIV-associated minor cognitive/motor disorder

MCP-1- monocyte chemoattractant protein-1

MI - Myoinositol

MMP2 - matrix metalloprotease

MND - mild neurocognitive disorder

MOG - myelin oligodendrocyte glycoprotein

MRI - magnetic resonance imaging

mRNA - messenger RNA

MS - Multiple Sclerosis

MSI - mass spectrometry imaging

mTOR - mammalian target of rapamycin

NAA - N-acetylaspartate

NAPA - silicon nanopost array

Nef - negative factor

NELF - negative elongation factor

NFAT - nuclear factor of activated T cells

NFkB - nuclear factor kappa B

NK - Natural Killer

NNRTI - non-nucleoside reverse transcriptase inhibitor

NPCs - nuclear pore complexes

NPM - non-pacemaker

NRM - Norharmane

NRTI - nucleoside reverse transcriptase inhibitor

NSF - N-Ethylmaleimide Sensitive Factor

OCT - Octanol

ORF - open reding frames

OXPHOS - oxidative phosphorylation

PA - Phosphatidic acid

PalmitylCoA - palmityl coenzyme A

Panx-1- Pannexin 1

PBMCs - peripheral blood mononuclear cells

PCR - polymerase chain reaction

PD - Parkinson's diseases

PE - Phosphatidylethanolamine

PET - positron emission tomography

PGE_2 - Prostaglandin E_2

PHA - Phytohaemagglutinin

PI - protease inhibitor or phosphatidyl inositol

PIC - pre-integration complex

PIP - polyphosphoinositol

PKA - protein kinase A

PKC - protein kinase C

PLP - proteolipid protein

PM - plasma membrane

PMA - phorbol myristate acetate

PPIA - Peptidylprolyl Isomerase A

PPP1CA - Protein Phosphatase 1 Catalytic Subunit Alpha

PRC - polycomb repressive complex

P-TEFb - positive transcription elongation factor b

PUFAs - polyunsaturated fatty acids

qRT-PCR - Quantitative real-time PCR

QVOA - Quantitative Viral Outgrowth Assay

REMPI - resonance-enhanced two-photon ionization

Rev - regulator of expression of viral protein

RNA - ribonucleic acid

RNase - Ribonuclease

RNAPII - RNA polymerase II

ROS - Reactive oxygen species

rsfMRI - resting-state fMRI

S - Serine

sap B - saposin B

S100B- calcium-binding protein B

shRNA - short hairpin RNA

SIMS - MSI including secondary ion

SIV - Simian Immunodeficiency Virus

SK - sphingosine kinase

SM - Sphingomyelin

S1P - sphingosine-1-phosphate

SPECT - single photon emission computer tomography

Sph - Sphingosine

SPT - serine palmitoyltransferase

SPT5 - subunit of DSIF

SPTAN1 - Spectrin

SVZ - subventricular zone

TAGs - triacylglycerides

TAR - Transactivation Response Element

Tat - trans-activator of transcription protein

TBI - traumatic brain injury

TC - total cholesterol

TCA - tricarboxylic acid

THAP - 2,4,6-Trihydroxyacetophenone

TILDA - Tat/rev Induced Limiting Dilution Assay

TLR - toll-like receptor

TNF-α - Tumor Necrosis Factor Alpha

TNTs - tunneling nanotubes

tRNA - transfer RNA

TXN - Thioredoxin

uHCs - unopposed hemichannels

UV - ultraviolet

VDAC1/2 - Voltage Dependent Anion Channel 1/2

Vif - virion infectivity factor

Vpr - viral protein r

Vpu - viral protein u

WM - white matter

XPO1 - Exportin 1

ZO-1 - Zonula occludens-1

CHAPTER 1: GENERAL INTRODUCTION

PART 1 – HUMAN IMMUNODEFICIENCY VIRUS

Epidemiology

Human Immunodeficiency Virus (HIV) is a major public health concern, with 37.7 million infected individuals worldwide in 2020. Since the start of the epidemic, 79.3 million people have become infected with HIV, and 36.3 million have died from Acquired Immune Deficiency Syndrome (AIDS)-related illnesses. Last year, 1.5 million people were newly infected, and 680,000 died from AIDS-related illnesses (http://www.unaids.org/en/, 2021). 73% of individuals that know their status have access to combined anti-retroviral therapy (cART), resulting in an extended lifespan. Although clinically successful, cART is not a cure. Most anti-retroviral drugs are potent small molecules targeting entry, reverse transcriptase, protease maturation, and integration steps of the HIV life cycle (Arts and Hazuda 2012), but these drugs do not target viral genome transcription and translation. Even though cART suppresses systemic virus replication, decreases the risk of transmission, and restores the immune competence, it cannot deplete circulating or tissue-associated HIV reservoirs, which remains one of the main obstacles to curing HIV infection (Vanhamel, Bruggemans et al. 2019).

HIV classification

HIV was identified in 1983 (Barre-Sinoussi, Chermann et al. 1983), and it was considered the causative agent of AIDS, which was first diagnosed in 1981 in the USA (Gottlieb, Schroff et al. 1981). It is accepted that the origin of HIV occurred by a cross-species adaptation, which started from Simian Immunodeficiency Virus (SIV) infected

monkeys and progressed to great apes and ultimately humans (Sharp and Hahn 2011). Two types of HIV have been identified, HIV-1 and HIV-2, with comparable structure, tropism, and transmission pathophysiology. HIV-1 is more virulent and responsible for 95% of infections worldwide. HIV-1 strains are subdivided into four groups: M, N, O, and P. The M group, or "Major" group, is responsible for the global HIV epidemy. Within group M, there are nine genetically distinct and phylogenetically equidistant clades (A, B, C, D, F, G, H, J, and K) (Hemelaar 2012). From them, clade C is globally dominant and responsible for approximately 50% of infections, especially in South Africa and India (McCutchan 2006). HIV-1 N group consists of a recombinant virus between two ancestral strains, one ancestor related to HIV-1 group M and one related to SIV chimpanzee strains found in Cameroon (Simon, Mauclere et al. 1998). This group is not so common in the global population, and all the cases identified are from Cameroon (Mourez, Simon et al. 2013). The O group is present in 1-2% of the population, especially in Cameroon and some European countries (Belgium, France, and Spain) (Bush and Tebit 2015). The last group is the P group, which accounts for just 0.06% of infections in the global population (Vallari, Holzmayer et al. 2011). In contrast to HIV-1, HIV-2 is mostly asymptomatic and predominately found in West Africa. HIV-2 can be classified into nine groups (A to I), which derive from 9 different cross-species transmissions involving SIV (Marlink 1996). Groups A and B are the most common in the population, and the other seven groups account for just one patient each (Visseaux, Damond et al. 2016).

Time course of HIV infection

HIV transmission is principally due to sharing biological fluids, including mucosal and blood (Shaw and Hunter 2012). The progression of HIV infection can be divided into 4 phases: primary infection, acute infection, chronic or latent infection, and AIDS (Fig. 1.1) (Coffin and Swanstrom 2013). As indicated in Fig. 1.1, the cluster of

differentiation four positive T ($CD4^+$ T) cell count is between 500 and 1500 cells/µl of blood prior to infection. In the early stages of infection, plasma viremia increases and $CD4^+$ T cell count in the blood decreases. The subsequent acute phase (weeks 2-9) is therefore characterized by high levels of viral RNA in the blood (>10^7 copies of viral RNA/ml) and the spreading of infection to susceptible tissues. In immune tissues, the adaptive immune response induces the production of antibodies against HIV proteins (Tomaras and Haynes 2009, Cohen, Shaw et al. 2011), and the $CD8^+$ cytotoxic T lymphocytes attack the productively infected $CD4^+$ T lymphocytes contributing to the CD4 count decrease (Jones and Walker 2016). Typically, people show flu-like symptoms, such as fever, headache, and rash. The following phase corresponds to the clinical latency that can last 2-12 years (Moss and Bacchetti 1989, Lemp, Payne et al. 1990), but in cART virally suppressed individuals, this period can be extended for years or decades (Nakagawa, May et al. 2013). Plasma viremia is low or undetectable during this phase due to cART (~50 copies of HIV RNA/ml plasma). However, $CD4^+$ T lymphocytes progressively decline due to the chronic immune exhaustion and inflammation (Coffin and Swanstrom 2013). The last phase of the disease or AIDS, which is not observed in HIV-infected individuals under effective cART, is defined by $CD4^+$ T lymphocytes decline (<350 $CD4^+$ T cells/µl of blood) and high viremia levels (>10^6 copies of viral RNA/ml plasma), causing the loss of immune control and leading to opportunistic infections and cancers (Cribbs, Crothers et al. 2019, McNally 2019, Shi, Zhou et al. 2019). Therefore, the demise of the HIV-infected population is mainly due to immunological disorders, opportunistic infections, and aging-related issues in the current cART era (Escota, O'Halloran et al. 2018, Chauvin and Sauce 2022).

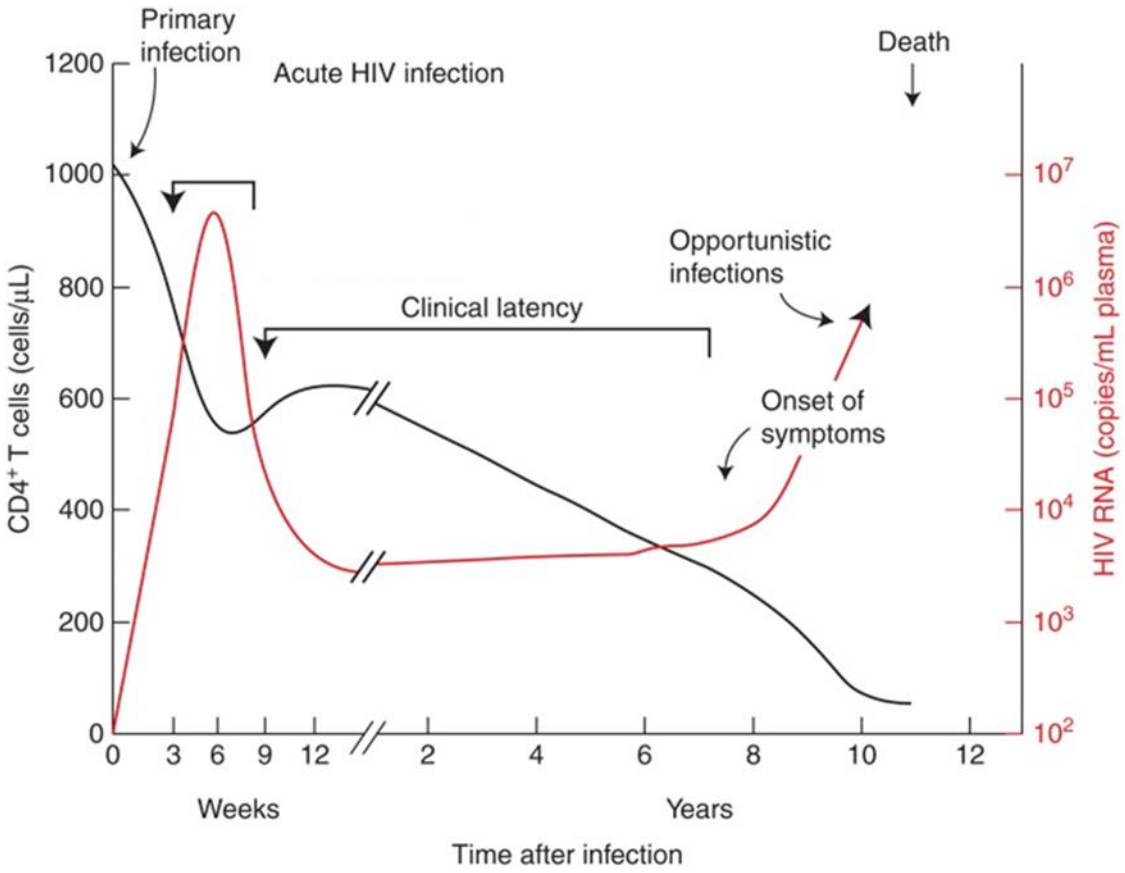

Figure 1.1. Clinic time-line of HIV infection, replication, and CD4 counts in humans, reproduced with permission of (Fauci and Desrosiers 1997).

The black line represents the amount of $CD4^+$ cells in the blood, and the red line shows the amount of HIV RNA copies in the plasma of HIV-infected individuals. Early after primary infection, viral replication increases and CD4 count decreases. These parameters also characterize the acute phase of infection with high levels of viral RNA in the plasma ($>10^7$ copies of viral RNA/ml) and decreased $CD4^+$ T lymphocytes, but with the spreading of infection in several tissues. The long clinical latency phase is characterized by low or undetectable plasma viremia and a progressive reduction of $CD4^+$ T lymphocytes. In the last phase, $CD4^+$ T lymphocytes continue to decline, and plasma viremia rapidly increases, causing opportunistic infections and HIV-related cancers, leading to death.

HIV life cycle

HIV is a positive-sense single-stranded enveloped RNA virus. HIV is classified as a retrovirus, and its RNA genome is structured in nine-open reding frames (ORF) (German Advisory Committee Blood 2016). Three major ORFs are retrovirus common: gag, pol, and env, which encode the polyprotein precursors of structural proteins. Specifically, gag encodes for a polyprotein cleaved to form 6 structural proteins: matrix protein p17, capsid proteins p24, p7 and p6, and two spacer peptides. The matrix protein p17 ensures capsid integrity, while p24, p7, p6 and the spacer peptides are essential for capsid assembly (Freed 1998). The pol ORF encodes for reverse transcriptase, integrase, and protease, providing critical enzymatic functions for infection, integration, and virion maturation. Reverse transcriptase transcribes viral RNA into double-stranded cDNA; integrase modulates the insertion of viral cDNA into the host cell genome; HIV protease is involved in the final maturation of the released virions after budding (Tekeste, Wilkinson et al. 2015). The env gene encodes for the envelope protein Gp160, which trimerizes to $(Gp160)_3$ and then undergoes cleavage by a host furin protease into the receptor-binding fragment Gp120 and the fusion fragment Gp41 (Harrison 2008, Checkley, Luttge et al. 2011). Three copies of each fragment constitute the mature viral spike (Gp120/Gp41). The other six ORFs of the HIV genome encode for regulatory and accessory proteins such as trans-activator of transcription protein (Tat), regulator of expression of viral protein (Rev), negative factor (Nef), virion infectivity factor (Vif), viral protein r (Vpr), and viral protein u (Vpu) (Karn and Stoltzfus 2012). Tat facilitates activation of viral transcription after integration, stabilizing the interaction between the RNA polymerase II and the integrated viral DNA and phosphorylating the RNA polymerase II C-terminal domain inducing the elongation process. Rev and Vpr regulate the transport. Nef, Vif, and Vpu manipulate the host cell signaling and the immunity to attenuate immune surveillance (Turner and Summers 1999, Freed and Mouland 2006).

HIV infection is initiated by Env-mediated adhesion viral particles binding to host attachment factors present on the surface of targeted cells (heparan sulfate proteoglycans for macrophages, α4β7 integrin for T cells, and dendritic cell-specific intercellular adhesion molecule-3-grabbing non-integrin for dendritic cells), as well as by HIV envelope protein Gp120 interacting with the CD4 receptor. Binding to CD4 induces a conformational change in Gp120 that facilitates binding to the co-receptor C-X-C chemokine receptor type 4 (CXCR4) and/or C-C chemokine receptor 5 (CCR5) (Kwong, Wyatt et al. 1998). After Gp120 binding to CD4 and its co-receptor, the N terminal fusion peptide of Gp41 translocates and inserts into the target cell membrane. Subsequent refolding of Gp41 makes a postfusion hairpin conformation. Formation of the fusion pore ensues membrane fusion and entry of the viral capsid into the target cell (Freed, Delwart et al. 1992, Shugars, Wild et al. 1996).

Once viral fusion with the plasma membrane of the host cell is completed, the HIV capsid containing two strands of viral RNA is deposited into the host cytoplasm to begin the process of reverse transcription (Campbell and Hope 2015). Reverse transcription is performed by reverse transcriptase, which has two enzymatic activities. Reverse transcriptase DNA polymerase activity allows copying of either RNA or DNA template, and reverse transcriptase ribonuclease (RNase) H activity permits RNA degradation of the RNA–DNA duplex (Hu and Hughes 2012). Through its RNase H active site, the reverse transcriptase begins the reverse transcription of viral RNA starting at the primer binding site to obtain an RNA/DNA hybrid double helix. Then, the RNase H site breaks down the RNA strand, and the polymerase active site of the reverse transcriptase completes a complementary DNA strand to form a double helix DNA molecule (dsDNA) with long terminal repeats (LTRs) sequences at the 5’ and 3’ ends. These repeats contain all the useful elements for gene expression (enhancer, promoter, transcription terminator, and polyadenylation signal). They are also used as a substrate for HIV protein Integrase, allowing HIV DNA insertion into the host cell genome (Klaver

and Berkhout 1994). Specifically, the viral DNA made by reverse transcription within the cytoplasm is part of a large nucleoprotein complex, the pre-integration complex (PIC) (Bowerman, Brown et al. 1989), which allows the crossing of the nuclear membrane through the nuclear pore complexes (NPCs). The nuclear import process is crucial in establishing infection, and several viral proteins such as Integrase, Vpr, Matrix, Capsid, HIV-1 central DNA flap, and host importin proteins with host tRNAs are involved (Jayappa, Ao et al. 2012). In the nucleus, Integrase catalyzes the reaction generating a hydroxyl nucleophile for DNA strand insertion in a LTR region adjacent to a cytosine-adenine (CA) dinucleotide sequence of the host genome (Roth, Schwartzberg et al. 1989). Later, the hydroxyl group cleaves the host cell DNA and becomes integrated following strand transfer and DNA repair (Engelman, Mizuuchi et al. 1991). The integration of HIV DNA into the host cell genome does not guarantee viral production. HIV integration is not random and preferentially occurs in host DNA areas with actively transcribed genes, gene-rich regions, and intronic regions and largely avoids promoter regions (Anderson and Maldarelli 2018). Therefore, the nuclear topography of HIV integration may impact HIV replication (Lusic, Marini et al. 2013). For instance, the HIV PIC preferentially targets those areas of open chromatin that are proximal to the nuclear pore, excluding the internal regions in the nucleus and the peripheral regions associated with the nuclear lamina. When the HIV genome is transcribed by the host RNA polymerase II, the full-length (unspliced), singly spliced, and multiply spliced RNAs are recognized by Rev and transported to the cytoplasm by host exportin 1 (XPO1)-RanGTP nuclear export pathway (Dayton 2004, Mahboobi, Javanpour et al. 2015), where they can be translated in polyprotein precursors, regulatory, and accessory proteins. HIV transcription and translation occur with the early synthesis of regulatory HIV-1 proteins Tat and Rev. Specifically, Tat binds to the TAR (Transactivation Response Element) site and stimulates the transcription and the formation of longer RNA transcripts. Rev facilitates the transcription of longer RNA transcripts and the expression of structural and

enzymatic genes and inhibits the production of regulatory proteins, therefore promoting the formation of mature viral particles. In addition, Gag and Gag-Pol polyproteins are localized to the cell membrane and the immature virion begins to bud from the cell surface to infect other cells (Sundquist and Krausslich 2012). This classical process of infection mediated by the virions is called "cell-free spread" (Fig. 1.2). Recent studies recognized a more efficient and predominant spreading process called "cell-to-cell spread" (Martin, Welsch et al. 2010). Its higher effectiveness is due to the protection from neutralizing antibodies and the ability to overcome the inhibitory effects of some anti-viral restriction factors (Zhong, Agosto et al. 2013). The cell-to-cell spread mechanism influences viral pathogenesis using intercellular structures such as immunological synapses, gap junctions (GJs) and tunneling nanotubes (TNTs) that transfer ions, small molecules, organelles, and pathogens, between the connected cells (Eugenin, Gaskill et al. 2009, Ariazi, Benowitz et al. 2017, Okafo, Prevedel et al. 2017, Bracq, Xie et al. 2018). Part of this thesis also involved a detailed description of the Connexin43 (Cx43) GJ communication system in the context of HIV spread (see Part 2 of General introduction).

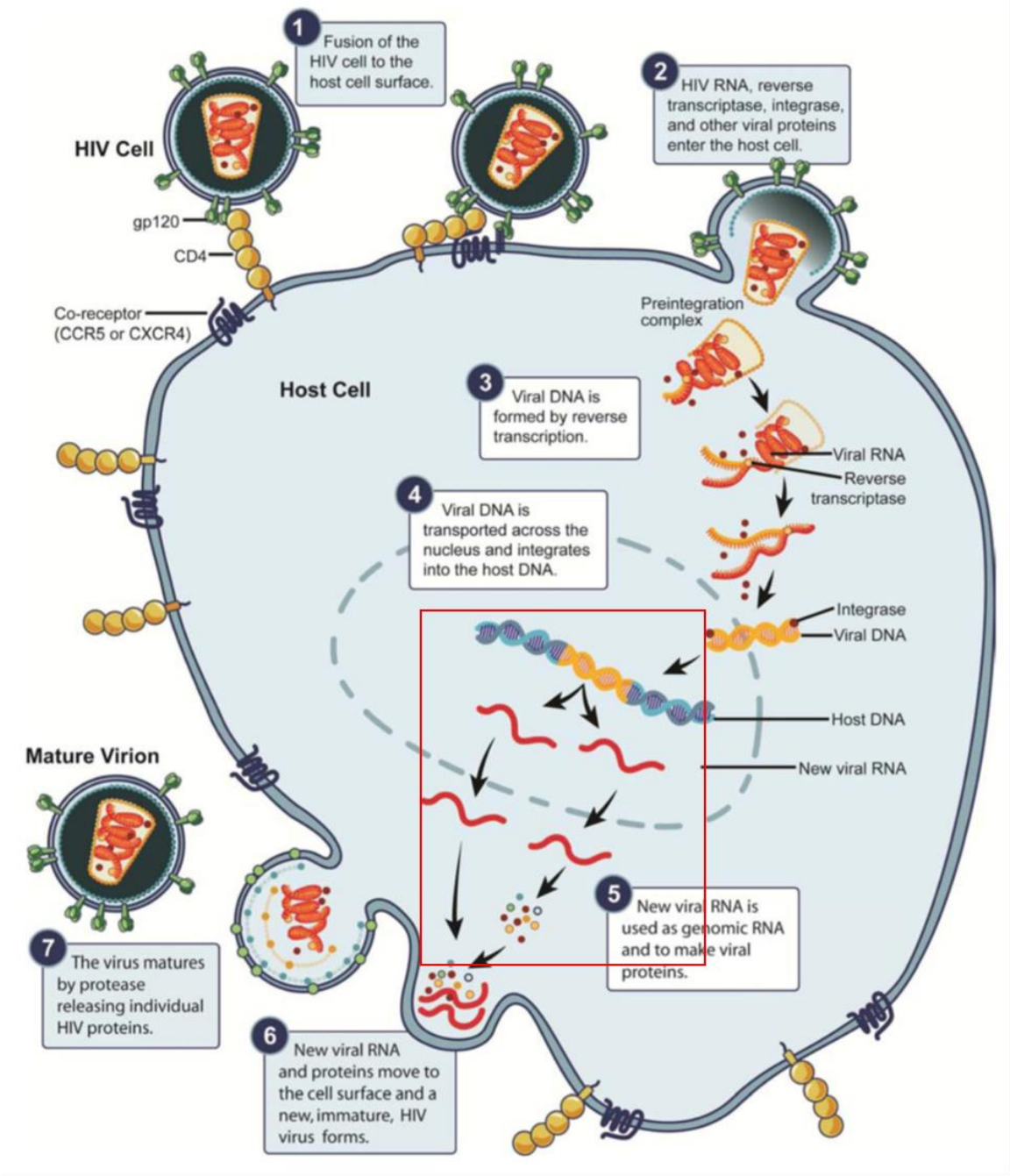

Figure 1.2. HIV life cycle, reproduced with permission of (Pau and George 2014).

(1) Attachment. HIV infection starts with the Env-mediated adhesion viral particles binding to host attachment factors present on the surface of targeted cells, as well as by HIV envelop protein Gp120 interacting with the CD4 receptor and co-receptor (CXCR4 or CCR5); later, Gp41 inserts into the outer leaflet to facilitate the fusion between the HIV envelope and the host plasma membranes. (2) Fusion. The viral genome, the PIC, and proteins from capsid such as p24 are released in the cytoplasm of the host cells. (3) Reverse transcription. It is performed by reverse transcriptase to convert HIV RNA into

HIV dsDNA. (4) Integration. It is conducted by an intermediate PIC which includes reverse transcriptase and integrase to transport the HIV dsDNA into the nucleus to be integrated into the host genome. HIV begins to use the cell machinery to transcribe HIV mRNAs transported to the cytoplasm. (5) HIV protein production. This occurs in the cytoplasm, where HIV proteins are synthetized from viral mRNA. (6) Assembly. The new synthetized HIV proteins and HIV RNA accumulate and move to the host plasma membrane to generate immature virions. (7) Budding. Newly immature-formed virions are released into the extracellular space. Protease induces the maturation of the virions to become infectious. The red box in the figure indicates the topic of this thesis: HIV-integrated DNA, HIV mRNA production, and HIV protein synthesis.

Antiretroviral therapies

The first anti-retroviral agent was introduced in 1987. However, over 50% of patients treated with a singular drug for longer than six months developed drug resistance (Larder, Darby et al. 1989). Currently, HIV-infected individuals are administered a well-defined combined anti-retroviral therapy (cART), transforming HIV infection from a deadly to a manageable chronic disease (Taylor, Tieu et al. 2019). The first combined treatment, which blocks viral replication at multiple stages of the HIV life cycle, was introduced in 1996 (https://www.niaid.nih.gov/diseases-conditions/antiretroviral-drug-development). A combined ART regimen consists of several anti-retroviral drugs to reduce the viral load resulting in delayed disease progression and prolongation of patient survival. The first therapy combinations commonly prescribed include a "backbone" of 2 inhibitors of the HIV reverse transcriptase (nucleoside reverse transcriptase inhibitor NRTI) plus a non-nucleoside reverse transcriptase inhibitor (NNRTI), an integrase strand transfer inhibitor (INSTI), or a protease inhibitor (PI) boosted with cobicistat or ritonavir (https://aidsinfo.nih.gov/understanding-hiv-aids/fact-sheets/21/53/what-to-start-choosing-an-hiv-regimen). Cobicistat and ritonavir are pharmacokinetic enhancers of PIs by acting as potent inhibitors of the cytochrome P450 3A4 isoenzyme (Xu and Desai 2009, Tseng, Hughes et al. 2017).

Other new drugs include CCR5 antagonists, fusion inhibitors, and post-attachment inhibitors (Sinxadi, Khoo et al. 2021). The NRTIs are prodrugs that must be

activated into diphosphate or triphosphate metabolites. They inhibit the reverse transcriptase enzyme for the insertion of nucleotide analog. NNRTIs inactivate the reverse transcriptase enzyme-inducing conformational change and do not require intracellular phosphorylation to be active. The PIs block proteolytic activities necessary for the formation of mature infectious virions. The INSTIs work by preventing the integration of viral DNA into the host genome. In addition, the CCR5 antagonists and the fusion inhibitors obstruct the fusion process blocking the interaction of the HIV-Gp120 and the CCR5 receptor and avoiding conformational changes of Gp41, respectively. The last class of drugs include the post-attachment inhibitors or entry inhibitors, which are competitive inhibitors for the CD4 receptor. The current clinical HIV practice aims to modify cART regimens to reduce risks of long-term toxicity and avoid interactions with other drugs (Wood 2019). Together, these drugs comprise the cART targeting different viral replication steps to improve $CD4^+$ T cell count, prolong patient survival, and reduce the risk of transmission. However, long-term cART can provoke side effects, virologic failures and resistance, and it still does not eradicate HIV (Wood 2019).

Moreover, cART must be administrated regularly and constantly because viral rebound occurs rapidly after treatment discontinuation due to long-lasting tissue-associated viral reservoirs (https://aidsinfo.nih.gov/guidelin, https://aidsinfo.nih.gov/understanding-hiv-aids/fact-sheets/21/58/fda-approved-hiv-medicines). Even though cART blocks peripheral viral replication, cART does not prevent viral mRNA and protein expression. Thus, damage in the absence of viral production is still ongoing.

HIV latency

Stable and productive HIV DNA integration is the most important aspect of HIV latency (Lafeuillade and Stevenson 2011). Productively infected cells can become

latently infected through viral silencing mechanisms, which are still under investigation (Mok and Lever 2007, Kim, Hosmane et al. 2014). Several transcriptional and post-transcriptional molecular mechanisms have been proposed and demonstrated (Bruner, Murray et al. 2016, Hiener, Horsburgh et al. 2017). It is well known that multiple cellular signaling pathways can control HIV transcription positively: positive transcription elongation factor b (P-TEFb) pathway, the nuclear factor kappa B (NF-kB) pathway (Chan and Greene 2011), the nuclear factor of activated T cells (NFAT) pathway (Siliciano and Greene 2011), the mitogen-activated protein kinase (MAPK) pathway (Yang, Chen et al. 1999), the toll-like receptor (TLR) pathway (Macedo, Novis et al. 2019), and the mammalian target of rapamycin (mTOR) pathway (Besnard, Hakre et al. 2016). Conversely, other cellular signaling pathways can control HIV transcription negatively: the polycomb repressive complex (PRC) pathway (Kim, Kim et al. 2011), the Cullin 3 E3 ligase pathway (Langer, Yin et al. 2020), and the zinc-finger protein 304 pathway (Krasnopolsky, Kuzmina et al. 2020). During acute and chronic infection, in the initial phase (Tat protein is absent), the host RNA polymerase II (RNAPII) is delayed by negative elongation factor (NELF) and DRB-sensitivity inducing factor (DSIF), generating short premature RNAs that form stem-loop structures called transactivation response (TAR) element (Asamitsu, Fujinaga et al. 2018). When the amount of HIV Tat is sufficient, it binds to TAR and the cyclin T1 (CycT1) subunit of P-TEFb. The cyclin-dependent kinase 9 (CDK9) subunit of P-TEFb then hyperphosphorylates the C-terminal domain of RNAPII, NELF, and the SPT5 subunit of DSIF. Thus, NELF is downregulated to overcome the elongation pausing, and the positive transcription factor DSIF supports the RNAPII activity (Jadlowsky, Wong et al. 2014). In the late stage of HIV transcription, the cellular CDK/cyclin complex (CDK11/CycL) is engaged in RNAII elongation complex transcribing HIV (Pak, Eifler et al. 2015). CDK11 phosphorylates RNAPII and recruits the transcription export (TREX/THO) complex, promoting the cleavage and polyadenylation of HIV transcripts, stabilizing HIV mRNAs, and enhancing

their nuclear export and translation of viral proteins (Pak, Eifler et al. 2015). When HIV is integrated into a transcriptionally active gene, HIV transcription is silenced by transcription interference. RNAPII reads through the boundary between the host gene and HIV provirus, preventing viral transcription initiated at the 5′-LTR (Shan, Yang et al. 2011). When the HIV provirus is integrated into the opposite direction to the cellular gene, the HIV RNAs are not transcribed and do not synthetize HIV proteins (Lenasi, Contreras et al. 2008). Other mechanisms, characterized by occlusion of transcription initiation or elongation complexes, involve the regulation of the essential Tat-cofactor P-TEFb, NF-κB, and NFAT (Kim, Mbonye et al. 2011).

Post-integration latency can be dependent on epigenetic modifications of histones that promote chromatin condensation and HIV silencing (Kumar, Darcis et al. 2015, Turner and Margolis 2017). Repressive histone marks such as methylation at histone 3 lysine 9 (H3K9me), methylation at histone 3 lysine 27 (H3K27me), methylation at histone 4 lysine 20 (Boros, Arnoult et al. 2014, Turner and Margolis 2017), deacetylation at histone 3 lysine 4 and 27 (Smith, Yeung et al. 2010), and crotonylation at histone H1, H2A, H2B, H3 and H4 in 28 different lysine sites (Tan, Luo et al. 2011, Jiang, Nguyen et al. 2018, Wan, Liu et al. 2019) can be found at the integrated HIV LTR in latently infected cells. Specifically, H3K9 methylation on the HIV LTR occurs *via* various histone methyltransferases (HMTs): SUV39H (Bernhard, Barreto et al. 2011), G9a, and/or SETDB1 (Imai, Togami et al. 2010). H3K27 methylation is mediated by EZH HMT (Tripathy, McManamy et al. 2015).

Post-integration latency also includes post-transcriptional mechanisms. One of the most interesting post-transcriptional mechanisms involves microRNAs that downregulate the levels of cyclin T1 protein, which is essential for viral replication (Chiang, Sung et al. 2012).

Recent studies have proposed a new therapeutic approach based on the reactivation of latently infected reservoirs by small molecules called latency-reversing

agents (LRAs) that reactivate the virus, stimulating the immune system to kill the viral reservoirs. This is called the “shock and kill” strategy (Petravic, Rasmussen et al. 2017, Schwartz, Bouchat et al. 2017). There are several categories of LRAs in trials: HDAC inhibitors (Archin, Liberty et al. 2012), P-TEFb releaser/activators (Rice 2016), protein kinase c (PKC) agonist/canonical NF-κB inducers (Jiang and Dandekar 2015, Wong and Jiang 2021, Okoye, Fromentin et al. 2022), non-canonical NF-κB inducers (Wong and Jiang 2021), Toll-like receptor agonists (Jiang and Dandekar 2015, Rasmussen and Sogaard 2018), epigenetic modifiers (Mbonye and Karn 2011), mammalian mechanistic target of rapamycin (mTOR) inhibitors (Besnard, Hakre et al. 2016), and MAPK agonists (Schlaepfer and Speck 2011). HDAC inhibitors such as vorinostat were among the first compounds used in clinical trials for HIV latency reversal and functional cure (Archin, Kirchherr et al. 2017).

Another proposed approach is to promote a state of “deep latency” that permanently prevents transcriptional activation of the viral genome as a “block-and-lock” mechanism (Mousseau, Kessing et al. 2015). This block-and-lock approach uses latency promoting agents (LPAs) such as didehydro-cortistatin A (dCA), which is a Tat inhibitor that silences HIV transcription (Kessing, Nixon et al. 2017, Li, Mousseau et al. 2019). Other LPAs include small molecule inhibitors of the interaction between HIV Integrase (IN) and the cellular chromatin-tethering factor LEDGF/p75 named ‘LEDGINs’, anticancer compounds, RNA-based strategies like short interfering (si) or short hairpin (sh) RNAs, Heat shock protein 90 (HSP90) inhibitors, Jak-STAT pathway inhibitors, bromodomain-containing protein 4 (BRD4) modulators, mTOR inhibitors, kinase inhibitors, CRISPR/Cas9 system editing of the CCR5 gene, and triptolide, which is a diterpenoid epoxide derived from a Chinese herb that possesses anti-inflammatory, immunosuppressive, and anti-tumor activities (Moranguinho and Valente 2020, Vansant, Bruggemans et al. 2020).

Although the proposed approaches aim to kill latently infected cells by host immune activity (Shan, Deng et al. 2012), virus-induced cytotoxicity (Doitsh, Galloway et al. 2014), or using LRAs and LPAs (Mousseau, Kessing et al. 2015, Li, Kaiser et al. 2016, Kim, Anderson et al. 2018), none of them are safe, effective, scalable, and durable interventions to achieve HIV-1 remission or cure. This suggests a gap between the signals required for reactivation of some viruses, depending on where they are integrated, the degree of epigenetic modulation and specific response to different stimuli to induce reactivation.

Viral reservoirs

As discussed above, HIV remains incurable due to the early viral seeding and generation of latently-infected cells in several tissues. Viral reservoirs are a cell type in which a replication-competent form of HIV persists, and they function as long-lived viral sanctuaries scattered throughout the body. HIV reservoirs have a slow decay rate ($t_{1/2}$=3.7 years) (Siliciano, Kajdas et al. 2003). Thus, the virus remains integrated into the host genome and can be reactivated. The transient increase of HIV RNA in plasma, called blips, is common in HIV patients under cART and is typically related to viral rebound (Grennan, Loutfy et al. 2012). This stochastic reactivation of viral reservoirs may be due to gaps in circulating concentration, toxicity, or discontinuation of the cART regimen.

Currently, the best described viral reservoirs are resting $CD4^+$ T lymphocytes, including central memory T cells, transitional T cells, effector T cells, and naïve T cells (Stein, Storcksdieck Genannt Bonsmann et al. 2016). However, other viral reservoirs are also described in circulation and tissues, such as peripheral blood monocytes, dendritic cells, macrophages (such as microglial), astrocytes, and other myeloid cells (Eugenin, Clements et al. 2011, Castellano, Prevedel et al. 2017, Ganor, Real et al. 2019, Mitchell, Laws et al. 2019). The Siliciano group has investigated how T cells survive and become latent by creating a CD4 cell line transduced with the B cell Lymphoma 2 gene (Bcl-2)

(Yang, Xing et al. 2009). Bcl-2 is a family of pro-apoptotic members that regulate the mitochondrial outer membrane pore formation inducing apoptosis. The Siliciano group showed that the Bcl-2 cell line survives infection and later can revert to the latent state suggesting that the Bcl-2 pathway can explain the survival mechanism of lymphoid viral reservoirs (Kim, Hosmane et al. 2014).

Other cell survival mechanisms are associated with upregulated anti-apoptotic proteins such as cFLIP and Mcl-1 or downregulated pro-apoptotic proteins such as Bax and Fadd (Timilsina and Gaur 2016), suggesting that blocking apoptosis contributes to viral reservoir survival.

Data in our laboratory demonstrated that macrophage survival, in response to HIV infection, has a metabolic and an anti-apoptotic component. Latent macrophages show mitochondrial fusion, lipid accumulation, and reduced mitochondrial ATP production, in addition to using glutamine/glutamate as a primary energy source (Castellano, Prevedel et al. 2019). Therefore, it is necessary to define the importance of myeloid cells as viral reservoirs. Three landmark clinical cases that demonstrate the effective role of myeloid cells in HIV infection are the "Berlin Patient," the "Mississippi baby," and the "London Patient." The first case achieved viral remission after a bone marrow transplant with stem cells from a homozygous donor for CCR5 delta32 used to cure acute myeloid leukemia (AML) (Hutter, Nowak et al. 2009). In the case of the "Mississippi baby" after an early administration of cART (30 hours after birth), plasma viremia was undetectable after interrupting cART for 27 months before the rebound, suggesting a crucial role of the myeloid reservoirs in viral persistence during the earliest stage of infection (Persaud, Gay et al. 2013). Another case was the "London Patient", who remained in HIV-1 remission for more than 18 months. Unlike the Berlin patient, the London patient was homozygous for wild-type CCR5 before transplant; he received chemotherapy for relapsed Hodgkin's lymphoma and did not undergo whole-body irradiation (Gupta, Abdul-Jawad et al. 2019). In addition, rare individuals called "elite" controllers can maintain the viral load below

the limit of detection even in the absence of cART, suggesting that their proviruses are in a deeper state of latency (Jiang, Lian et al. 2020).

Therefore, the major barrier to HIV cure is this population of infected, long-lived cells containing persistent and latent viral genomes that host defenses cannot detect or eliminate. Three mechanisms that contribute to the clonal expansion of viral reservoirs are the integration of the viral genome in or near genes involved in cell division, the capacity to maintain their homeostatic proliferation despite immune system activation, and the antigen-driven proliferation in case of co-infection and chronic exposure to antigens (Cohn, Chomont et al. 2020).

Several strategies have been proposed to study and target the viral reservoirs, using the shock and kill/block and lock mechanisms or using cell transplant and gene therapy to modify CCR5 in myeloid compartments (Mitchell, Laws et al. 2019). None of these strategies turned out to be safe due to the stochastic interval of viral rebound that is not easy to predict and their widespread off-target effects that can affect host gene expression (Centlivre, Legrand et al. 2013, Elliott, Wightman et al. 2014, Pitman, Lau et al. 2018, Vansant, Bruggemans et al. 2020).

Current methods to detect viral reservoirs

Available methods to detect viral reservoirs cannot precisely measure either their amount or the cell type involved. Currently, most viral reservoirs are detected in blood, but these are a poor representation of viral reservoirs in tissues. Quantitative Viral Outgrowth Assay (QVOA), Tat/Rev Induced Limiting Dilution Assay (TILDA), other Quantitative PCR assays for total HIV RNA or HIV DNA, and flow cytometry-based fluorescence in situ hybridization (Flow-FISH) are frequently used to detect viral reservoirs. QVOA is a cultured-based assay that identifies reservoirs in circulating cells (Finzi, Hermankova et al. 1997). TILDA is a PCR-based assay that measures the frequency of cells harboring HIV-integrated genomes. Other PCR-based methods can

also measure the frequency of cells harboring HIV-integrated and unintegrated DNA. QVOA is performed in the blood $CD4^+$ T lymphocytes, which are stimulated with phytohemagglutinin (PHA) in irradiated allogeneic peripheral blood mononuclear cells (PBMCs) that induce global T cell activation of HIV-integrated genomes. HIV-p24 ELISA detects the replication of the virus on the media of 2–3-week cultures combined with $CD4^+$ lymphoblasts from HIV-negative donors (Finzi, Hermankova et al. 1997). TILDA measures the frequency of cells harboring viral genomes that produce tat/rev multiply spliced HIV RNA upon maximal stimulation. It also requires isolation of the total $CD4^+$ T lymphocytes stimulated with PMA and ionomycin for 12 hours to induce the maximal production of tat/rev RNA. Later, the qRT-PCR is used to quantify tat/rev transcripts. TILDA requires 10 ml of blood and can be completed in 2-3 days (Procopio, Fromentin et al. 2015). Other PCR assays such as digital droplet PCR for total HIV DNA/RNA or integrated HIV sequences (Alu or 2 LTR) can quantify HIV DNA or RNA in peripheral blood mononuclear cells (PBMCs), in purified $CD4^+$ T cells or plasma (Gaebler, Falcinelli et al. 2021). However, they are expensive, use a large number of starting materials, are time-consuming, and overestimate the amount of the latent reservoirs (Eriksson, Graf et al. 2013). Flow-FISH uses markers to detect cell-type specificity, viral tropism, cell functionality, and cellular state (latent or active), but it requires cellular activation, and it is limited to isolated cell populations (Freen-van Heeren 2021).

Overall, QVOA, TILDA, other PCR-based techniques, and Flow-FISH have major limitations such as timing, cost, accuracy, precision, sensitivity, and use of a large blood volume. Additionally, they detect just one component of the viral cell cycle and are limited to only detecting circulating viral reservoirs. Generally, they can produce data which are readily misinterpreted and incorrectly estimate the replication-competent viruses within the viral reservoir pools (Shen and Siliciano 2008).

Recently Dr. Eugenin's laboratory generated a highly sensitive and innovative protocol specific for viral DNA, viral RNA, and several viral proteins and characterizes circulating and tissue-associated viral reservoirs in HIV-infected individuals (Prevedel, Ruel et al. 2019). This technique is based on improved staining and confocal microscopy analysis. It determines the viral life cycle stage by detecting, quantifying, and localizing concurrently HIV DNA, HIV mRNA, HIV proteins, and host cell markers *in vitro* and *in vivo* (Prevedel, Ruel et al. 2019). HIV reservoir identification and localization are necessary to study the mechanism of viral reservoir-induced damage and find new molecular targets for HIV efficacious treatments. Our laboratory has developed techniques to identify viral reservoirs in urethral tissue (Ganor, Real et al. 2019) and other human tissues such as bone marrow (Real, Capron et al. 2020). This thesis presents data about the localization, identification, and quantification of viral reservoirs in the brain in Chapter 2.

PART 2 – HIV IN CNS

HIV CNS infection

HIV infection of the Central Nervous System (CNS) arises very early after primary infection (15 days). It is accepted that HIV transmigration into the brain occurs by the "Trojan Horse" mechanism (Hazleton, Berman et al. 2010). Briefly, circulating HIV-infected monocytes, specifically $CD14^{+}CD16^{+}$ intermediate monocytes, cross the Blood-Brain Barrier (BBB) in response to chemotactic signals such as CCL2 and CXCL12 (Eugenin, Osiecki et al. 2006, Williams, Eugenin et al. 2012). The high sensitivity of HIV-infected cells to sense these chemokines is due to the enhanced capacity of HIV-infected cells to recognize physiological chemokine gradients such as CCL2 (Eugenin, Osiecki et al. 2006). During the process of transmigration of HIV-infected cells in response to CCL2, the BBB becomes compromised, further contributing to local inflammation. In the CNS, migrated HIV-infected monocytes infect resident cells such as microglia, perivascular macrophages and a small population of astrocytes (Williams, Veenstra et al. 2014). Overall, microglial cells and perivascular macrophages are the major productively infected cells by HIV in the early stages of brain invasion (Cosenza, Zhao et al. 2002).

On the contrary, astrocytes support a low viral replication. Astrocytes are CD4 negative cells, and they are infected by HIV using a mannose receptor that mediates vesicle endocytosis from the membrane avoiding endolysosomal destruction or via viral synapses using cell-to-cell contact with infected lymphocytes (Liu, Liu et al. 2004, Do, Murphy et al. 2014, Galloway, Doitsh et al. 2015). Their mediated apoptosis of surrounding uninfected cells is regulated by inter-organelle interactions among the mitochondria/Golgi/endoplasmic reticulum system and the associated signaling of inositol triphosphate (IP_3) and calcium *via* gap junctions (Malik, Valdebenito et al. 2021).

During active CNS infection, the formation of multinucleated giant cells and neuronal and glial cell death were common in infected individuals in the pre-ART era. However, upon cART introduction, damage still occurs but is more controlled.

Viral reservoirs within the CNS

During the acute phase of HIV infection, human microglia/macrophages and astrocytes are in an inflammatory phenotype due to the release of cytokines and chemokines, causing massive apoptosis (Castellano, Prevedel et al. 2017). However, a small population of HIV-infected cells survive and become latently infected (Eugenin and Berman 2007, Eugenin, Clements et al. 2011, Eugenin and Berman 2013, Orellana, Saez et al. 2014, Castellano, Prevedel et al. 2017). Macrophages/microglia are the primary CNS target of HIV (Wong and Yukl 2016). It was shown that uninfected macrophages derived from recently transmigrated monocytes die in a few days (Bellingan, Caldwell et al. 1996). In contrast, microglia, perivascular, and alveolar macrophages have a long half-life (months-years) (Lassmann and Hickey 1993). Latently HIV-infected macrophages are terminally differentiated, and non-dividing cells derived from circulating monocytes residing in all tissues. They can survive HIV infection principally due to metabolic alterations and apoptosis inhibition (Castellano, Prevedel et al. 2017, Castellano, Prevedel et al. 2019). In latently HIV-infected microglia/macrophages, the pro- and anti-apoptotic pathways are blocked, and Bim, a highly pro-apoptotic negative regulator of Bcl-2, is upregulated and recruited into the mitochondria preventing apoptosis (Castellano, Prevedel et al. 2017). Thus, their survival mechanism is different from $CD4^+$ T cells mediated by Bcl-2 (Kim, Hosmane et al. 2014). In microglia/macrophage reservoirs, the mitochondria become larger, accumulate lipids, and produce less ATP for the compromised metabolic steps in the tricarboxylic acid (TCA) cycle preceding oxidative phosphorylation (OXPHOS). While HIV-infected macrophages use fatty acids and glucose as primary sources of energy the same way as

the uninfected cells, they also use glutamine/glutamate and alpha-ketoglutarate (αKG) as an alternative energy supply (Castellano, Prevedel et al. 2019).

Latently HIV-infected astrocyte survival is principally due to cytochrome C mislocalization from the mitochondria to the cytoplasm and the subsequent alterations in IP_3, IP_3 receptors, and calcium that block the formation of the apoptosome, as well as to the compromised mitochondria/Golgi/ER interactions (Fig. 1.3) (Eugenin and Berman 2013, Malik, Valdebenito et al. 2021). Even though only a small fraction of astrocytes become infected, they induce bystander apoptosis of neighboring cells through a cell-to-cell mechanism (Eugenin and Berman 2007, Eugenin, Clements et al. 2011). Thus, macrophages and astrocytes have different survival mechanisms than $CD4^+$ T cells. Moreover, HIV envelope sequencing studies from blood, brain, and other non-brain tissues such as bone marrow, colon, lung, and liver showed an HIV macrophage tropism with a different HIV compartmentalization and evolution within the blood and the tissues (Holman, Mefford et al. 2010), suggesting that viral reservoirs are different in each compartment.

Data shown in this thesis demonstrate the adaptation of myeloid and glial networks to limited HIV replication in the current cART era. Briefly, we have quantified the viral reservoirs in the brain of HIV-infected individuals with undetectable, low, and high viral replication (see details in Chapter 2).

Novel mechanism of bystander CNS damage in the current cART era

HIV-associated neurocognitive disorders (HAND) are present in around 50% of HIV-infected individuals in the post-cART era (Rumbaugh and Tyor 2015). In 90% of autopsied brains, CNS damage was identified in HIV-infected patients displaying chronic neuroinflammation in association with neurocognitive impairment even after receiving cART for many years (Lamers, Rose et al. 2016). Moreover, HAND can be exacerbated by HIV-related infections, cART-related toxicities, cART discontinuation, and

comorbidities (alcohol and substance abuse) (Justice, Sullivan et al. 2010, Byrd, Fellows et al. 2011, Tedaldi, Minniti et al. 2015). According to the severity of the clinical manifestations, HAND is divided into asymptomatic neurocognitive impairment (ANI), minor neurocognitive disorder (MND), and HIV-associated dementia (HAD) (Antinori, Arendt et al. 2007). In the post-cART era, the proportion of HIV-infected individuals with neurocognitive symptoms is the same as the pre-cART era, but the percentage of infected patients with HAD has decreased in favor of ANI and MND (Heaton, Clifford et al. 2010, Saylor, Dickens et al. 2016). The symptoms displayed in the milder forms of HAND include memory loss, problems in concentration, difficulty learning new tasks, diminished reflexes, personality changes, and mood swings. However, people diagnosed with HAD have severe memory and concentration problems, wild mood swings, symptoms of psychosis and loss of physical coordination (Eggers, Arendt et al. 2017).

Nowadays, HAND diagnosis and monitoring are based on neuropsychiatric performance tests, blood tests, CSF analysis, and neuroimaging (Clifford and Ances 2013). These techniques may identify metabolic and structural alteration in the blood and the brain. However, techniques to identify viral reservoirs are lacking. Chapter 2 describes a novel method to identify, localize, and quantify viral reservoirs in circulation and tissues. In addition, in Chapter 3, we show that myelin damage and sulfatide dysregulation can have a crucial role in HAND. Later, we will discuss enhancing the bystander effect by sulfatide through GJ.

Our laboratory identified that viral reservoirs could promote bystander damage to neighboring cells via GJ-mediated mechanisms. Gap junctions are expressed in most cell types of the nervous system, including astrocytes, neurons, oligodendrocytes, neuronal stem cells, endothelial cells, and under inflammatory conditions in microglia/macrophages (Kielian 2008, Eugenin, Basilio et al. 2012, Palacios-Prado, Hoge et al. 2013, Vejar, Oyarzun et al. 2019). Gap junctions are low-resistance bridges that perform electrical and metabolic functions. They connect the cytoplasm of adjacent cells

and allow the exchange of electrical signals and intracellular messengers, such as IP_3, calcium, cyclic nucleotides, metabolites, neurotransmitters, and viral peptides (Yeager and Nicholson 1996). Gap junctions consist of connexin (Cx) dodecamer channels formed of two hexameric unopposed hemichannels (uHCs), one from each of the coupled adjacent cells (Harris 2001). Connexin-containing uHCs are defined as homomeric when six monomers of Cx that comprise it are the same, or heteromeric when the Cxs are different. Gap junctions can be docked by two identical (homotypic) or different (heterotypic) subunits of HCs. Homo- and hetero-combinations generate channels with different biophysical properties and permeability (Harris 2007). Hemichannels and GJ channels have an internal pore of approximately 12 A° enabling the diffusion of molecules up to 1.2 k.Da. (Villanelo, Escalona et al. 2017). The role of HCs and GJs in HIV infection has acquired an increased interest. Although uHCs exist physiologically in a closed state, HIV infection is one of the few cases where uHCs become open, enabling the release of pro-apoptotic and pro-inflammatory factors such as prostaglandin E_2 (PGE_2) and adenosine triphosphate (ATP) in the extracellular space (Eugenin 2014). For instance, in HIV-infected astrocytes the opening of Cx43 containing uHCs allows the secretion of dickkopf-1 protein (DKK1) that is a soluble Wnt pathway inhibitor. It has been shown that neuron and astrocyte mixed cultures treated with DKK1 resulted in a significant collapse of neuronal processes (Orellana, Saez et al. 2014). Thus, it can explain the synaptic compromise and the cognitive decline observed in HIV-infected individuals. GJs regulated to control synaptic function, are permanently open following HIV infection, and are used by the virus to spread and maintain infection in the CNS. Specifically, HIV reservoirs mediate bystander damage into the neighboring cells *via* Connexin-43 (Cx43), containing GJs and uHCs (Malik, Theis et al. 2017). To prove GJs crucial role in CNS damage, the Cx43-GJ blockers 18-α-glycerritenic acid (AGA) and octanol were used to treat HIV-infected astrocyte cultures resulting in a decreased level of apoptosis in the neighboring HIV-uninfected cells (Eugenin and Berman 2007). In

addition, bystander apoptosis was related to IP_3 and intracellular calcium (Fig. 1.3), dysregulation of lipoxygenase/cyclooxygenase, BK calcium channels, and ATP receptor activation within astrocytes (Eugenin and Berman 2013). It was demonstrated that HIV-Tat protein enhances Cx43 expression in human primary astrocytes to maintain communication between the few HIV-infected cells and surrounding uninfected cells, suggesting a critical link between HIV proteins, commonly present in the brain of virally-suppressed infected individuals, and cell-to-cell communication (Malik, Theis et al. 2017). To conclude, we can remark that viral reservoir pools use unique cell-type mechanisms to survive infection and generate toxicity in neighboring uninfected cells. Cx43 containing the GJ system will be considered in Chapter 3.

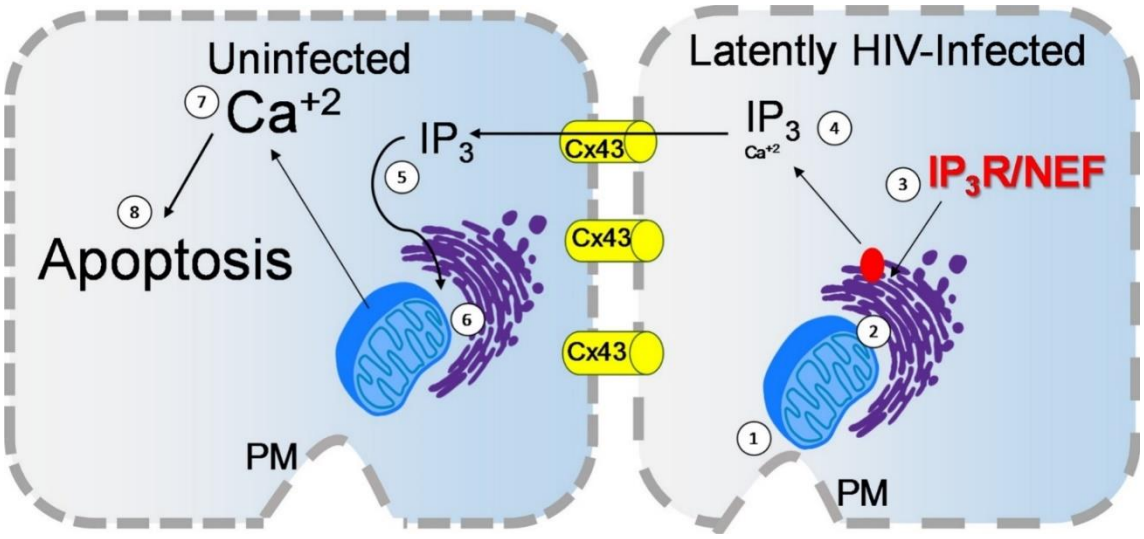

Figure 1.3. The proposed model of HIV-infected astrocytes for survival and bystander damage is mediated by Cx43 containing GJs, reproduced with permission of (Malik et al., 2021).

HIV-infected astrocyte survives apoptosis by altering the interactions between the plasma membrane (PM), mitochondria, and the ER (1, 2), binding of HIV-Nef protein to the IP_3R_1 (3) and increasing intracellular IP_3 levels (4) that protect from calcium improvement and apoptosis. The maintenance of Cx43 containing GJ enables the diffusion of IP_3 into neighboring uninfected cells (5), resulting in ER signaling (6), increasing calcium (7), and activating the apoptotic process (8).

Neuroimaging used to diagnose and monitor HAND in the current cART-era

Neuroimaging includes multiple techniques that directly or indirectly image the brain to assess metabolic, structural, and functional changes. They can be partially useful to generate a diagnosis and monitor the clinical course of HAND (Clifford and Ances 2013). The more common non-invasive techniques for metabolic imaging are proton-magnetic resonance spectroscopy (H-MRS or MRS), positron emission tomography (PET), and single-photon emission computer tomography (SPECT). H-MRS gives information on brain pathophysiology by measuring signals from hydrogen atoms of specific brain metabolites, such as N-acetyl aspartate (NAA), myoinositol (MI), choline (CHO), and glutamate-glutamine (Glx) (Van Zijl and Barker 1997). N-acetyl aspartate is a functional neuronal marker, and it is synthetized due to the reaction between aspartate and acetyl coenzyme A (Baslow 2003). Myoinositol is an astrocyte marker associated with inflammation, astrocytosis, and gliosis (Harris, Choi et al. 2015). Choline is a cell membrane marker that tracks the membrane lipid turnover and reflects macrophage infiltration and inflammation (Lin, Ross et al. 2005). Glutamate (Glu) is the major excitatory neurotransmitter in the brain, stored as glutamine (Gln) in glial cells.

Glutamate-glutamine balance cycling is essential for the normal functioning of brain cells. Astrocytes are responsible for the uptake of most extracellular glutamate *via* glutamate transporters GLT1 (or EAAT1) and GLAST (or EAAT2) to maintain Glu extracellular concentration and avoid excitotoxicity (Schousboe and Waagepetersen 2005). During MRS, the magnet strength is not always enough to resolve Glu from Gln, and it is for this reason, in some cases, they are combined as Glx (Ramadan, Lin et al. 2013). Moreover, some MRS data are expressed as a ratio of the specific metabolites compared to creatine (Cr), which is a reference marker (Vigneswaran, Rojas et al. 2015). The most common MRS features in HIV seropositive population are increased levels of CHO and MI, suggesting inflammation and microglial proliferation, and decreased levels of NAA and Glx that are related to neuronal-axonal injury or dysfunction (Mohamed,

Barker et al. 2010). During HIV infection, MRS is also used to monitor changes in brain inflammation and neuronal integrity associated with cART effects (Chaganti and Brew 2021). The biggest limit of MRS is that the analysis results are restricted to certain brain regions. During acute HIV infection, brain metabolites have been measured in frontal grey and white matter, occipital grey matter, and basal ganglia. Elevated levels of CHO/Cr in the basal ganglia and in the occipital grey matter of acute HIV cases (14 days after HIV infection) were detected compared to uninfected controls and chronic HIV subjects. These values became normal after six months of cART administration (Sailasuta, Ross et al. 2012). Moreover, the levels of Cho/Cr, NAA/Cr, Glu/Cr and MI/Cr have been shown to be increased in frontal white matter, parietal grey matter, and basal ganglia, but after cART initiation their excitotoxicity and neuronal injury effects were attenuated (Young, Yiannoutsos et al. 2014). In addition, the relationship between HIV-cognitive impairment and brain metabolism was investigated in older HIV-infected individuals under cART and it was shown that NAA and Glu were lower and correlated with worse performance on neuropsychological tests in MND or HAD individuals (Mohamed, Barker et al. 2018). Although MRS can detect several brain metabolites, only one study mentions the possibility to detect lipid molecules (Bairwa, Kumar et al. 2016), without identifying either the class or their specific alteration.

Other techniques that can be applied for metabolic investigation in HIV pathology are PET and SPECT. They have been applied to study HIV patients with or without HAND. PET and SPECT are used to evaluate glucose metabolism or cerebral perfusion by applying nuclear medicine tracers (^{18}F-deoxyglucose - ^{99}Tc-HMPAO) that specifically bind to a positron-emitting radioisotope, such as ^{18}fluorine (^{18}F) or ^{11}carbon (^{11}C) (Sathekge, McFarren et al. 2014). Decreased glucose metabolism in the frontal cortex detected by PET in HIV seropositive patients may reflect neuronal injury or dysfunction (Andersen, Law et al. 2010). PET imaging is also used to assess dopamine (DA) function in HIV-infected patients because HIV-infected patients with HAND often present

psychomotor slowing and parkinsonian symptoms. For this technique, (11C)-cocaine and (11C)-raclopride is used to measure the presynaptic dopaminergic transporter and postsynaptic D2 dopaminergic receptor, respectively. These tracers demonstrated lower levels of dopamine transporters (DAT) that are associated with a dopaminergic neuronal injury, especially in HIV-positive patients with HAD (Wang, Chang et al. 2004) and worst neurocognitive performance (Chang, Wang et al. 2008). Likewise, SPECT is utilized to evidence the central dysfunction of the dopaminergic pathways in HIV infection, and ^{123}I-FP-CIT and ^{123}I-IBZM are the trackers used for these analyses (Scheller, Arendt et al. 2010). Current studies are focusing on the development of radiotracers ((^{11}C)PK11195, (^{11}C)PBR18, (^{11}C)DPA-713, and (^{11}C)PBR28) specific for microglia to quantify and localize brain inflammation in HIV-infected patients (Hammoud, Endres et al. 2005, Chang and Shukla 2018).

Two structural neuroimaging techniques have been applied to investigate HAND: volumetric analysis and diffusion tensor imaging (DTI). Structural neuroimaging involves brain tissue contrast based on differences in proton density and relaxation times among brain structures (Ashburner and Friston 2000, Good, Ashburner et al. 2001, Sanford, Fernandez Cruz et al. 2017). The measurement of cortical and subcortical grey matter and total and abnormal white matter (aWM) volumes showed that HAD and MND patients had smaller grey and white matter volumes and more aWM than neurocognitively unimpaired patients (Alakkas, Ellis et al. 2019). DTI is an MRI-based neuroimaging technique used for the detection of microarchitectural changes. Microstructural disruptions were localized in the frontal and motor white-matter regions of the HIV-infected individuals and ventral tegmental area, pallidum, and nucleus accumbens in correlation with depression (Wright, Heaps et al. 2012).

Current functional neuroimaging techniques include magnetic resonance imaging (MRI) for blood oxygen level-dependent imaging (BOLD) and perfusion. BOLD fMRI signal investigates the ratio of oxygenated to deoxygenated hemoglobin in the

microvasculature. Although HIV regional injury can be associated with a partial dysfunction of the brain networks, BOLD task-activated fMRI and resting-state fMRI (rs-fMRI) are used to evaluate functional networks (Fox and Raichle 2007). For instance, HIV seropositive patients showed a selective activation for networks involving attention, working memory, hippocampal function, and risky choices (Connolly, Bischoff-Grethe et al. 2014). On the other hand, rsfMRI showed lesser connectivity within the front striatal, motor, and executive networks and within the precuneus seed and the prefrontal cortex in the HAND population, suggesting a compromised brain activity even in the current cART era (Ann, Jun et al. 2016, Chaganti, Heinecke et al. 2017). Perfusion MRI is another functional method using the arterial spin labeling (ASL) technique to measure the proton spins associated with endogenous oxyhemoglobin and deoxyhemoglobin to calculate the arterial function. Using ASL, low levels of cerebral blood flow were demonstrated in HIV seropositive population that can be partially restored after cART (Blokhuis, Mutsaerts et al. 2017).

Together, these *in vivo* neuroimaging techniques are useful to assess HAND onset and progression, but better markers in terms of prediction and selectivity are required. Several of these neuroimaging techniques can measure different species of lipids, but this remains largely unexplored. In this thesis, we study sulfatide metabolic alteration in the brain of HIV-infected patients and correlate them with neurocognitive impairments using an *ex vivo* mass spectrometry imaging (MSI) approach.

Brain volume changes and white matter structure in HAND

Neuroimaging data have shown that volumetric and structural changes involve the brain of HIV-infected patients virally suppressed with cART (Alakkas, Ellis et al. 2019). By DTI, it was demonstrated that white matter deficits comprise dramatic thinning of the corpus callosum, reduction in blood flow, loss of structural integrity and volume of the superior longitudinal fasciculus, superior corona radiata, and the internal capsule (Leite,

Correa et al. 2013, Correa, Zimmermann et al. 2015). A CNS HIV Anti-Retroviral Therapy Effects Research (CHARTER) study used structural MRI to assess reduced white matter volume in HIV-infected individuals with HAD and MND compared with neurocognitively normal patients virally suppressed with cART (Alakkas, Ellis et al. 2019). MRI also detected white matter hyperintensities and microstructural changes in the brain of HIV-positive patients (van Zoest, Underwood et al. 2017, Trentalange, Prochet et al. 2020). These persistent white matter abnormalities raise the possibility that HIV infection can perturb oligodendrocyte maturation, function and/or survival to affect myelin sheath structure and electrical impulse conduction (Liu, Xu et al. 2016, van Zoest, Underwood et al. 2017). In addition, a global and local reorganization of the white matter network was investigated in the right postcentral gyrus, right precuneus, right inferior parietal lobule, right transverse temporal gyrus, right inferior temporal gyrus, right putamen, and right pallidum of patients with HAND despite viral control through cART (Di Cio, Minosse et al. 2021).

HIV-infected individuals of the post-cART era displayed synaptic-dendritic damage (Ellis, Langford et al. 2007) with prominent atrophy in subcortical structures, such as caudate, putamen, amygdala, hippocampus, and thalamus, instead of neuronal loss often observed in pre-cART era (Harezlak, Buchthal et al. 2011, Ances, Ortega et al. 2012). In addition, cortical thinning or regional volume loss affects parietal white matter, orbitofrontal cortex, cingulate cortex, primary motor and sensory cortices frontal and temporal lobes suggesting worst cognitive performance (Sanford, Fernandez Cruz et al. 2017). One cross-sectional study performed using a volumetric analysis compared HIV-infected patients virally unsuppressed and suppressed to uninfected individuals showed that reduced brain volumes in the corpus callosum, amygdala, caudate, thalamus, and putamen volumes are independent of cART because both HIV positive groups displayed similar changes. As discussed previously, volumetric reductions of subcortical regions occur despite cART, suggesting a faster morphometry change after persistent

seroconversion in the virologically suppressed cohorts (Ances, Ortega et al. 2012). It is still unclear whether changes in white matter underlie the clinical manifestation seen in patients or whether they result from persistent viral reservoirs in the CNS. In chapter 2, we quantified, identified, quantified, and characterized the amount of HIV DNA, HIV DNA/RNA, and HIV DNA/RNA/proteins positive cells in the brain of HIV-infected individuals under long-term cART.

Long-term cART has no significant effects on HIV-mediated CNS structural changes (Brier, Wu et al. 2015). Thus, we propose it cannot fully prevent HIV-induced myelin damage and subsequent lipid dysregulation. Our combined efforts for this thesis have been directed to study sulfatide dysregulation due to its known importance in myelin structure (see Chapter 3). Our future direction aims to fully elucidate the pathways involved as potential targets for therapeutic intervention.

PART 3 – LIPIDS IN HAND

General introduction to lipids in the brain

Lipids are amphipathic biomolecules (Fahy, Cotter et al. 2011). Lipids assist several important cellular functions; they are structural elements of the lipid bilayers, chemical energy sources, and precursors for several second messengers (Glatz 2015). Lipids can also work as chaperones, signal transduction molecules, electron carriers, hormones, vitamins, and antioxidants (Sunshine and Iruela-Arispe 2017, Budin, de Rond et al. 2018, Dowhan, Vitrac et al. 2019, Montesinos, Guardia-Laguarta et al. 2020). They are classified into eight categories based on the ketoacyl groups and the isoprene groups: glycerophospholipids, fatty acyls, glycerolipids, sphingolipids, sterol lipids, prenol lipids, saccharolipids, and polyketides (Fahy, Subramaniam et al. 2005). Here, we categorized them into phospholipids, neutral lipids, and glycolipids to simplify their metabolic characterization.

Phospholipids are the major class of lipids present in all cells, and they can be divided into glycerophospholipids and sphingomyelins. Glycerophospholipids include phosphatidylcholine, phosphatidylethanolamine, phosphatidylserine, phosphatidylinositol, phosphatidic acid, phosphatidylglycerol, and cardiolipin. They all have a structural function in the cellular membranes and are asymmetrically distributed in the bilayer (Fadeel and Xue 2009). The major phospholipid component in cell membranes is phosphatidylcholine, representing 40-50% of the total phospholipid pool. Moreover, phosphatidylcholine is a precursor of several signaling molecules such as phosphatidic acid, diacylglycerol, lysophosphatidylcholine, platelet-activating factor, and arachidonic acid (Billah and Anthes 1990). Phosphatidylethanolamine is the second most abundant phospholipid in the membrane representing 20-30% of the total cell phospholipid. Its function is to stabilize the membrane proteins in the bilayer. Phosphatidylserine is a minor membrane phospholipid, and it is involved in the early

phases of apoptosis and the production of anti-inflammatory mediators (Vance and Steenbergen 2005, Bratton and Henson 2008). Phosphatidylinositol is also a minor lipid in most mammalian cells and involved in several signaling processes. However, it is particularly enriched in the brain where it may account for up to 10% of membrane phospholipid content (Raghu, Joseph et al. 2019). It is the precursor of polyphosphoinositol lipids (PIP, PIP_2, and PIP_3), which regulate intracellular calcium signaling, gene transcription, RNA editing, nuclear export, and protein phosphorylation (Di Paolo and De Camilli 2006). Other glycerophospholipids such as phosphatidic acid, phosphatidylglycerol, and cardiolipin present at lower abundance. Specifically, phosphatidic acid is less than 1% abundant in the membrane but is a very important intermediate for synthesizing membrane phospholipids and an important regulator of signal transduction, membrane trafficking, secretion, and cytoskeletal rearrangement (Jenkins and Frohman 2005). Phosphatidylglycerol is more expressed in the mitochondrial membranes, and it is the precursor of cardiolipin, which is necessary for normal electron transport and oxidative phosphorylation (Claypool 2009).

Sphingomyelins are also important components of cell membranes and amount to 10% of the total phospholipids. Specific sphingomyelin metabolites such as ceramide (Cer), sphingosine (Sph), sphingosine-1-phosphate (S1P), diacylglycerol (DAG) and gangliosides (GMs) are also involved in cell signaling (Merrill, Schmelz et al. 1997). Ceramide is a crucial metabolite for sphingolipid metabolism. It is involved in cellular apoptosis (Hannun and Obeid 1995), cell differentiation (Okazaki, Bielawska et al. 1990), and inflammatory responses (Masini, Giannini et al. 2008). Sphingosine and S1P are cofactors of inflammatory signaling; Sph inhibits proliferation and promotes apoptosis, and S1P mediates cell growth arrest and apoptosis inhibition (Hannun and Obeid 2008). DAG is a second messenger that supports the biosynthesis (and degradation) of glycerolipids regulating protein kinase C (PKC) activity (Bishop and Bell 1988). Gangliosides are predominantly localized in the outer leaflets of neuronal plasma

membranes, contributing to cell-cell recognition, adhesion, and signal transduction (Yu, Tsai et al. 2011, Kolter 2012).

Neutral lipids are comprised of sterols and glycerolipids. Sterols play a key role in the membrane integrity, maintaining its microfluid state. The most abundant sterol in the cellular membranes is cholesterol (Dufourc 2008). Glycerolipids include triacylglycerols and steryl esters and are typically used as energy stores (Athenstaedt and Daum 2006).

Glycolipids are glycans with a lipidic portion that binds to monosaccharide or polysaccharide chains extended into the extracellular space. Glycolipids include glyceroglycolipids, lipopolysaccharides, glycosphingolipids, and glycosylphosphatidyl-inositols. They have a structural role in the cellular membrane and participate in immune responses to bacterial infections and cell-to-cell communication (Paulick and Bertozzi 2008, Zajonc and Kronenberg 2009).

Lipids are pivotal elements of the brain's structure and function (Montesinos, Guardia-Laguarta et al. 2020). They are involved in brain structural development, impulse conduction, insulation, neurogenesis, synaptogenesis, and myelin sheath formation. The brain is a lipid-rich organ, second only to the adipose tissue, and 50% of the brain’s dry weight consists of lipids. Cholesterol, fatty acids, sphingolipids, and glycerophospholipids are important structural components of neuronal cells. In the neuron, lipid dynamics control essential cellular processes such as signal transduction and trans-membrane gradients (Sonnino, Aureli et al. 2015).

Within CNS, cholesterol has a common structural role, but it also facilitates the extension of axons and promotes the neurons survival, synaptogenesis, axonal plasticity, glial cell proliferation, and myelin formation (Huntemer-Silveira, Patil et al. 2020). Cholesterol and sphingolipid dynamics support neurotransmitter release, modulation of ion channels, and downstream signaling (Borroni, Valles et al. 2016). Fatty acids determine membrane fluidity and plasticity of neuronal membranes, also serving as signaling molecules. They are classified according to saturated fatty acids made by single

bonds between neighbor carbons and unsaturated fatty acids that present one or more carbon-carbon double-bonds. The neuronal membranes are mostly composed of polyunsaturated fatty acids (PUFAs), which are abundant in the myelin sheath (Hooijmans and Kiliaan 2008). Glycerophospholipids and sphingolipids maintain structural integrity in the neuronal membrane (Olsen and Faergeman 2017). Sphingolipids are also involved in synaptic transmission, neuronal differentiation, and myelin sheath stability (Schnaar, Gerardy-Schahn et al. 2014). In the brain, sphingomyelins among the membranes regulate cell-to-cell and cell-to-matrix interactions and contact other signaling molecules to ensure cell proliferation and differentiation (Schnaar, Gerardy-Schahn et al. 2014, Itokazu, Wang et al. 2018).

Lipids are active compounds involved in important physiological and pathological processes. Altered disruption or imbalance in lipid composition or metabolism is observed in various diseases, including infectious and neurocognitive diseases (Lee, Olson et al. 2003) Altered lipid metabolism and changes in lipids concentration were presented in neurodegenerative disorders, such as Alzheimer's (AD) and Parkinson's diseases (PD) (Hussain, Anwar et al. 2020). The main changes in the brain of Parkinson's and Alzheimer's individuals were described as altered levels of cholesterol and sphingolipids (Hussain, Anwar et al. 2020), but also fatty acids and glycerophospholipid alterations were shown to contribute to the CNS structural compromise. For example, the high cholesterol content causes the incorporation of amyloid-β (Aβ) into the membrane in AD and the accumulation of α-synuclein in PD, leading to neuronal death (Abramov, Ionov et al. 2011, Galvagnion, Buell et al. 2015).

Moreover, specific fatty acids speed up AD progression by enhancing the production of Aβ (Amtul, Uhrig et al. 2011). It has also been demonstrated that in patients with AD, the expression of Cer, the precursor of sphingolipids, in the membrane was increased, whereas the level of sphingomyelin was reduced because of sphingomyelinase activation (He, Huang et al. 2010). Thus, it induces synaptic loss and

neuronal cell death in response to amyloid accumulation (Couttas, Kain et al. 2014). Altered levels of sphingolipids were also observed in the brains of Parkinson's patients. Interestingly, oxidative stress activates the neutral sphingomyelinase enzyme, resulting in increased levels of Cer following apoptosis in the substantia nigra (Posse de Chaves and Sipione 2010). Moreover, glycerophospholipids, especially phosphatidylethanolamines, phosphatidylinositols, and phosphatidylcholines, are significantly reduced in the neural membrane during the progression of AD (Kosicek and Hecimovic 2013, Gonzalez-Dominguez, Garcia-Barrera et al. 2014) This excessive degradation of glycerophospholipids may be due to stimulation of phospholipase A2 producing arachidonic acid (and eicosanoid metabolites) that induces the release of inflammatory cytokines (Frisardi, Panza et al. 2011).

Lipid balance is crucial to sustaining optimal brain health. Like other neurocognitive diseases (Adibhatla and Hatcher 2007, Xicota, Ichou et al. 2019), HAND has been linked to lipid dysregulation, including structural, signaling, and circulating lipids (Bandaru, Mielke et al. 2013, Kelesidis and Currier 2014, Kearns, Gordon et al. 2017). However, brain lipid dysregulation during HAND pathogenesis remains to be fully explored. Matrix-assisted laser desorption ionization-mass spectrometry imaging (MALDI-MSI) is a powerful technique that provides molecular and spatial information within a tissue section. Thus, we propose investigating lipid alteration by MALDI-MSI in human brain tissues from HIV-infected individuals undergoing cART with normal CD4 count and without detectable viral replication who develop mild or severe neurocognitive disorders (see Chapter 3). We suggest that HAND is associated with the presence of viral reservoirs and host amplification systems mediated by lipids and specific channels as described in the current Ph.D. thesis.

Myelin structural lipids

Myelin is a lipid-rich electrical insulating layer that wraps around axons. This membrane organelle has specific lipid-associated proteins contributing to its function (Chrast, Saher et al. 2011). The transcripts encoding structural myelin proteins and enzymes involved in myelin lipid biosynthesis are highly synchronized to manage the myelin sheath assembly (Chrast, Saher et al. 2011). The myelin structure significantly increases nerve conduction velocity due to the saltatory impulse propagation and a decrease in axonal energy consumption (Hartline and Colman 2007). In the CNS, myelinating glia cells are represented by the oligodendrocytes. Oligodendrocytes can synthesize lipids and uptake them from external sources, including the circulating cells (Marangon, Boccazzi et al. 2020). However, the mechanism of myelin lipid turnover is poorly understood (Ando, Tanaka et al. 2003).

Compared to the other cell membranes, myelin has a high lipid-to-protein ratio. It has been estimated that lipids account for the 71% of the dry weight myelin content (Chrast, Saher et al. 2011). Myelin lipid classes include cholesterol, glycosphingolipids (galactosylceramide and sulfatide), and saturated long-chain fatty acids. Cholesterol accounts for 26% of weight (Chrast, Saher et al. 2011), galactosylceramide and sulfatide for 14%–26% and 2%–7% (Stoffel and Bosio 1997, Chrast, Saher et al. 2011)), and less than 5% for the saturated long-chain fatty acids (O'Brien and Sampson 1965, Chrast, Saher et al. 2011). This specific myelin lipid composition is necessary for appropriate packing of the myelin sheath and for generation of lipid rafts, which mediate myelin protein interactions (Simons, Kramer et al. 2000, Lingwood and Simons 2010). Changes in lipid structure, ratios, and interactions with myelin-specific proteins have been associated with mild and severe disease forms including spinal cord/brain injury, multiple sclerosis, and other neurodegenerative diseases (Simons, Kramer et al. 2000, Hu, Doudevski et al. 2004).

Cholesterol is the major regulator of myelin biogenesis, differentiation of oligodendrocytes, and organization of the mature myelin (Saher, Brugger et al. 2005, Saher and Simons 2010, Saher and Stumpf 2015). Neurons synthesize cholesterol as a myelin resource during embryogenesis, oligodendrocytes at a postnatal stage, and astrocytes in adults (Berghoff, Spieth et al. 2021). The main function of cholesterol is to regulate membrane fluidity and permeability to polar molecules (Subczynski, Pasenkiewicz-Gierula et al. 2017). This provides the insulating property of the myelin sheath around the axons (Posse de Chaves and Sipione 2010). Glycosphingolipids are predominantly present in the outer leaflet of the myelin. Together with cholesterol, glycosphingolipids control fluidity and curvature of myelin membranes (Chrast, Saher et al. 2011). The high content of saturated FA in the myelin contributes to thick permeability for ions and electric insulation of the axon (Poitelon, Kopec et al. 2020).

Defects that involve all the myelin-enriched lipids can be distinguished as hypomyelination (decreased myelin production), dysmyelination (abnormally formed myelin), and demyelination (degenerative loss of myelin) (Chrast, Saher et al. 2011). These defects are caused by reduced expression levels of myelin-enriched lipid or lipotoxicity, a consequence of the accumulation of lipids that prove toxic for oligodendrocyte maturation and myelin structure development (Chrast, Saher et al. 2011, Duncan and Radcliff 2016).

Therapeutic approaches to target myelin lipid metabolism in HIV-positive individuals suffering from HAND are required to restore or maintain myelin structure (Haughey, Cutler et al. 2004, Jensen, Monnerie et al. 2015). However, a detailed analysis of myelin structure for HAND has not been performed. In work presented in chapter 3, we analyzed myelin structural changes and visualized sulfatide relative expression in human brain tissues from HIV-infected patients with mild and severe HAND.

MBP and PLP as Inflammatory Stimuli

The myelin sheath contains myelin-specific proteins such as myelin basic protein (MBP) and proteolipid protein (PLP). Myelin basic protein is a peripheral membrane protein that amounts to 30% of the total CNS myelin protein content (Boggs 2006). It is necessary for myelin formation and maintenance (Hallpike and Adams 1969). It is considered the glue of the myelin bilayers, taking advantage of electrostatic and hydrophobic forces (Aggarwal, Yurlova et al. 2011). Twelve MBP isoforms are present in human adults and they differ in size and charge. MBP size isoforms are derived from alternative splicing of a single mRNA transcript, and they are 21.5, 20.2, 18.5, and 17.2 k.Da. (Boggs 2006). MBP charge isoforms result from post-translational modifications of the 18.5 k.Da. isoform. MBP interacts with several cytoskeletal proteins to trigger numerous signaling pathways and negatively charged lipids to stabilize myelin structure (Boggs 2006, Boggs, Rangaraj et al. 2011, Vassall, Bamm et al. 2015, Raasakka, Ruskamo et al. 2017). MBP protein has been suggested as a possible biomarker for several neurodegenerative diseases, both in serum and in the CSF (Frid, Einstein et al. 2015, Zhan, Jickling et al. 2015, Wang, Yang et al. 2018, Santaella, Kuiperij et al. 2020). Even in HIV-infected individuals, high CSF MBP levels showed a proportional correlation with the size of white matter lesions detected by MRI (de Almeida, Rotta et al. 2017). In addition, HIV-positive individuals affected by neurocognitive disorders show white matter abnormalities associated with altered gene expression profiles. Despite effective cART, decreased myelin protein mRNAs, including MBP, were detected (Borjabad, Morgello et al. 2011). MBP has also been proposed to play a role in the pathogenesis of Multiple Sclerosis (MS) (Adiele and Adiele 2019). MS is a neurodegenerative disease distinguished by multifocal inflammatory lesions, demyelination, and oligodendrocyte loss (Lassmann 2018). MBP functions as an inflammatory stimulus in mediating the pathogenesis of MS. Endothelial cells treated with MBP secrete CCL2 and IL-6 by p38 MAPK phosphorylation, decrease tight

junction proteins (occludin and claudin-1), and increase the secretion of matrix metalloprotease (MMP2) resulting in the disruption of the BBB and accelerating the demyelination process (D'Aversa, Eugenin et al. 2013). The infiltration supports demyelination in MS patients in the white matter of $CD4^+$ and $CD8^+$ T cells and macrophages. The inflammatory response mediated by MBP stimulates $CD8^+$ T cells. Specifically, MBP induces reactive oxygen species (ROS) production in MBP-specific $CD8^+$ T cells expressing Fas ligand (FasL) (Wagner, Roque et al. 2020). Thus, soluble MBP is not only a structural protein but also, in soluble conditions, could become an immune and/or inflammatory signal.

PLP is the major transmembrane protein; it accounts for about 50% of adult CNS myelin protein content (Aggarwal, Yurlova et al. 2011). PLP plays a role in adhesion membrane phospholipids (Nadon and West 1998, Palaniyar, Semotok et al. 1998). Regulation of PLP expression is necessary for oligodendrocyte differentiation and maturation (Lourenco, Paes de Faria et al. 2016). PLP has a splicing isoform, DM20, expressed earlier during embryogenesis in neural and oligodendrocyte progenitors. Otherwise, PLP is expressed in mature myelin (Michalski, Anderson et al. 2011). Although PLP is the most abundant protein in myelin, it was not directly identified as a specific marker for the detection of demyelination. Nevertheless, it is considered a key mediator of inflammation and myelin structure damage (Greer, Trifilieff et al. 2020). In particular, PLP generates autoreactivity in MS patients exacerbating myelin damage. It was demonstrated that PLP peptide-specific $CD8^+$ T cells are the sources of pro-inflammatory soluble mediators that mediated myelin structure alterations (Biddison, Taub et al. 1997).

In chapter 3, we examined the levels and distribution of MBP and PLP, and through their expression, we evaluated myelin thickness and length changes in the HIV-infected population with neurocognitive disorders.

Sulfatide as a possible indicator of HAND

Although current investigated biomarkers represent HAND onset and progression, few studies have investigated lipids as a possible indicator of neurocognitive impairment in HAND. Dysregulation in lipid metabolism is known to occur in the CNS and the CSF/blood of HIV-infected populations (Haughey, Cutler et al. 2004, Farooqui, Horrocks et al. 2007, Jensen, Monnerie et al. 2015); however, a direct or indirect link to HAND has never been associated.

One of the most dysregulated lipidic pathways observed in the CNS of HIV-infected patients is the ceramide pathway. Ceramide is a fundamental mediator of cell differentiation, proliferation, survival, and apoptosis (Andrieu-Abadie, Gouaze et al. 2001). It is a metabolic and structural precursor for many sphingolipids, such as sphingomyelin (SM), ceramide-1 phosphate (Cer1-P) and glucosylceramide. The de novo synthesis of ceramide originates in the endoplasmic reticulum (ER) through a series of condensation and reduction reactions. Specifically, serine palmitoyltransferase (SPT) catalyzes the conversion of L-serine (L-ser) and palmityl coenzyme A (PalmitylCoA) in 3-keto-dihydrosphingosine (3KdhSph) that is translated in dihydrosphingosine (dhSph) by 3-keto-dihydrosphingosine reductase (3KSR). (Dihydro)ceramide synthase (dihydroCS) removes sphingoid bases and produces dihydroceramide (dhCer), which is converted into Cer by dihydroceramide desaturase (DES). Next, Cer is transported via non-vesicular transport by ceramide transfer protein (CERT) and *via* vesicular transport by the four-phosphate adaptor protein 2 (FAPP2) to the Golgi apparatus. There, Cer is modified to make SM, Cer1-P, and glucosylceramide (GluCer). Glucosylceramide is the precursor for complex glycosphingolipids (GSL). After Cer synthesis in the Golgi apparatus, SM and complex GSL are delivered to the plasma membrane by vesicular transport. Several sphingolipid metabolic enzymes are present at the plasma membrane to regulate SM, Cer, Sph, and sphingosine-1-phosphate (S1P) levels. The latter is produced from Sph by sphingosine kinase (SK) and may also take part in the salvage pathway for

the generation of Cer. Coordination between S1P and Cer1-P is crucial for eicosanoid inflammatory mediator production, such as prostaglandins (Hannun and Obeid 2008). During endocytosis, membrane sphingolipids are internalized and transported to the lysosome *via* endocytic vesicles, where acid sphingomyelinase (aSMase), acid ceramidase (aCDase), and glycosidase catalyze the hydrolysis (Bartke and Hannun 2009).

Sulfatide is an important Cer-related metabolite because it is the major lipidic component of the myelin sheath with galactosylceramide (2%–7%). The myelin sheath has a specific compartmentalization of sulfatide and myelin structural proteins, MBP and PLP. The myelin proteins MBP and PLP mostly colocalize with galactosylceramide in the juxtaparanode and internode areas of the compacted myelin, whereas sulfatide is mainly located in the paranodal areas of non-compacted myelin (Fig. 1.4) (Maier, Hoekstra et al. 2008, Blomqvist, Zetterberg et al. 2021). Sulfatide is synthesized in the Golgi apparatus of oligodendrocytes and Schwann cells. Sulfatide is a class of anionic sulfoglycolipids mainly found in the outer leaflet of the plasma membranes of cells (Honke 2013). Its presence is not exclusive to oligodendrocytes and Schwann cells in the plasma membrane; it is also produced in neurons and astrocytes located in intracellular compartments (Ishizuka 1997). The precursor of sulfatide, galactosylceramide, undergoes 3-O-sulfation of the galactose residue by the enzyme 3′-phosphoadenosine-5′-phosphosulfate: cerebroside sulfotransferase (CST). Galactosylceramide is synthesized in the ER from ceramide and UDP-galactose by the enzyme UDP-galactose: ceramide galactosyltransferase (CGT), is then transported to the Golgi apparatus before sulfation to sulfatide. Sulfatide is specifically degraded by a sulfatase (arylsulfatase A) in the lysosome (Fig. 1.4) (Eckhardt 2008).

As discussed, HIV infection and subsequent treatment with cART are often associated with perturbations in lipid profiles (Griffin, Wesselingh et al. 1994, Archibald, McCutchan et al. 2014, Padmapriyadarsini, Ramesh et al. 2017) but no studies have investigated their altered metabolism in the myelin sheath. For instance, HIV-infected

populations show decreased levels of high-density lipoprotein (HDL) cholesterol and increased levels of low-density lipoprotein (LDL) cholesterol, total cholesterol (TC) and triglycerides in the blood (Archibald, McCutchan et al. 2014, Padmapriyadarsini, Ramesh et al. 2017). Interestingly, the Cer pathway has foreshadowed its direct or indirect function in HAND, but limited data are present in the literature. Some investigations have been performed for Cer metabolites in the brain of HIV-infected patients. Levels of Cer and SM are significantly increased in brain tissues and CSF of HIV-infected patients with dementia compared to individuals mildly demented and HIV-infected without cognitive disorders (Haughey, Cutler et al. 2004). The same group demonstrated elevated levels of Cer and SM in hippocampal neuronal cultures after stimulation with HIV-Tat or HIV-Gp120 proteins, which induce apoptosis (Haughey, Cutler et al. 2004). This suggests a possible correlation between lipid secretion and the presence of HIV proteins.

In conclusion, our studies aim to demonstrate that dysregulated sulfatide metabolism associated with myelin structural damage can fill an important gap in the field of NeuroHIV. The screening of these structural lipids may potentially be used to diagnose and follow up on the HIV aviremic population affected by HAND. A recent study by MRS showed increased lipids in HIV patients with CNS lesions versus asymptomatic HIV individuals and healthy controls (Bairwa, Kumar et al. 2016). While they demonstrated increased lipid levels in HIV patients with CNS lesions, suggesting a critical role for inflammatory lipids in HAND pathophysiology, the lipid species involved were not elucidated. To fully understand lipidomic and metabolic changes occurring due to advancing disease state, lipid classes and fatty acid composition must be fully identified at the molecular level. Mass spectrometry has emerged as the leading technique for accurate, sensitive, and detailed lipid analysis (Han and Gross 2003). Advanced mass spectrometry technologies such as matrix-assisted laser desorption/ionization (MALDI) are useful for elucidating lipidic signatures in multiple disease conditions, including HAND.

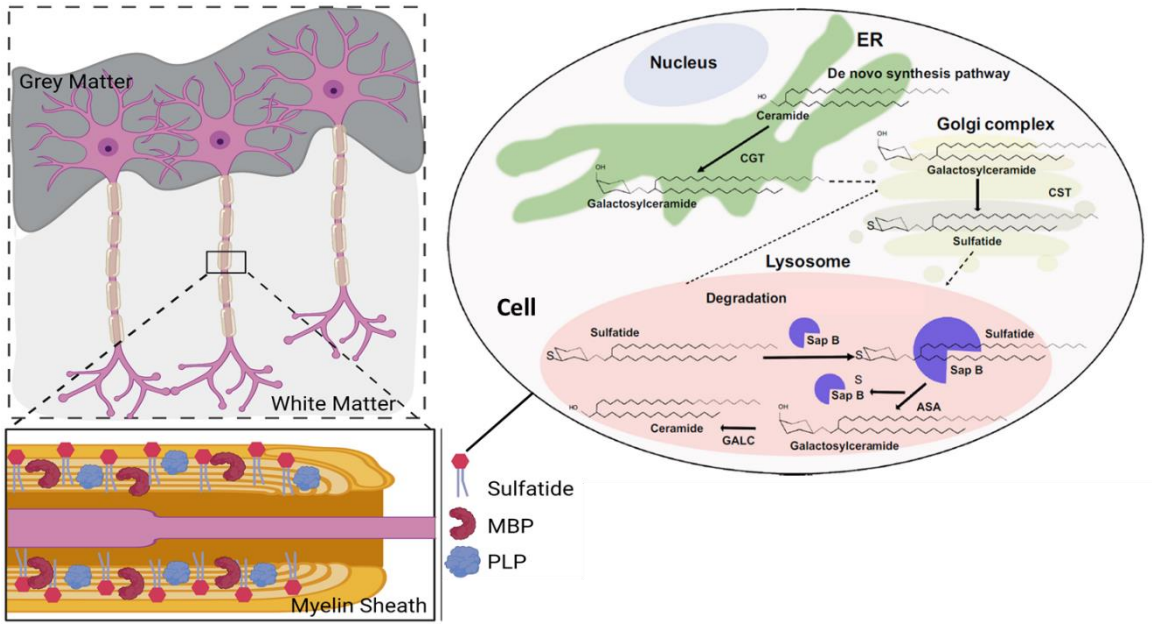

Figure 1.4. Localization and metabolism of Sulfatide, adapted and reproduced with permission of (Blomqvist et al., 2021).

Sulfatide is the major lipid in the myelin sheath that properly compartmentalizes structural lipids and proteins. The myelin proteins MBP and PLP mostly localize in the compacted myelin, whereas sulfatide is mainly located in the non-compacted myelin. At the cellular level sulfatide precursor, ceramide, is generated by the de novo synthesis in the Golgi apparatus, where Galactosylceramide is sulfated by cerebroside sulfotransferase (CST). Sulfatide degradation occurs through hydrolysis in the lysosomal compartment by the action of arylsulfatase A (ASA) in the presence of the activator protein, saposin B (sap B).

Mass Spectrometry Imaging

Mass spectrometry imaging (MSI) is a powerful tool allowing molecule investigations without extraction, purification, separation, or labeling of biological samples (Chughtai and Heeren 2010). MSI was introduced in 1994 by Spengler B., Hubert M. and Kaufmann R. at the 42nd Annual Conference on Mass Spectrometry and it has been applied to examine various analytes such as lipids (Jackson, Baldwin et al. 2014), proteins (Seeley and Caprioli 2008), peptides (Schober, Guenther et al. 2012), metabolites (Bhandari, Schott et al. 2015), and drugs (Prideaux and Stoeckli 2012) in biological tissues, cells, and microbial cultures (Hoffmann and Dorrestein 2015, Li,

Zhang et al. 2018). Mass spectrometry imaging is applied to evaluate the distribution of molecules present in biological samples by direct ionization from the tissue surface. Many different ionization sources have been used for molecular MSI including secondary ion (SIMS), desorption electrospray ionization (DESI), and Matrix-assisted laser desorption/ionization (MALDI). MALDI is the most sensitive ionization technique used for MSI and has the widest dynamic range of ions enabling direct analysis of molecules ranging from small metabolites to large intact proteins (Leopold, Popkova et al. 2018). Formalin-fixed paraffin-embedded (FFPE) tissues have only been used for limited MALDI-MSI studies (most typically for analysis of proteins due to delocalization of small molecules during the fixation and antigen retrieval sample processing stages). Hence, for most MALDI-MSI, fresh frozen samples are used, which are later sectioned (~10 μm thickness), thaw-mounted onto the microscope slides (e.g., indium tin oxide coated glass slides for MALDI-MSI lipidomics) and placed into a desiccator for preservation and not to compromise molecules distribution and structures. MALDI requires matrix or nanoparticles application to the tissue surface prior to laser irradiation. The matrix facilitates the production of charged ions and the choice of matrix is optimized dependent upon the chemical properties of the desired analytes. Commonly used matrices for lipids and small molecules include: 2,5-dihydroxybenzoic acid (DHB), 9-aminoacridine (9-AA), 1,5-Diaminonaphthalene (DAN), and norharmane (NRM) (Goto-Inoue, Hayasaka et al. 2011). The matrix is most-commonly applied to the tissue in solution by airspray deposition (Agar, Yang et al. 2007). This approach enables substantial extraction of the desired analytes from the tissue by the applied solvent system. However, care must be taken that the solvent deposition is not too wet as this may result in delocalization of the analyte and loss of vital spatial information. Dry matrix application (usually *via* sublimation of pure matrix powder) is optimal for maintaining spatial integrity of the analytes yet suffers significantly due to the lack of a solvent to extract analytes from within the tissue cells. The matrix absorbs the energy of

the UV laser resulting in thermal desorption and ionization of the co-crystal analytes in the gas phase, where they are measured using a mass analyzer (Karas and Kruger 2003). The exact mechanisms for ionization during MALDI remain to be confirmed, but the main hypotheses are based on thermal desorption (Knochenmuss and Zhigilei 2010) and phase explosion (Soltwisch, Jaskolla et al. 2013). During ionization the tissue remains intact, and the same section can be washed free of matrix with solvents and used for downstream histological examinations (Schwamborn and Caprioli 2010). MALDI is compatible with all types of mass spectrometer and mass analyzers. However, the direct ionization and the lack of chromatographic separation leads to the production of highly-complex spectra and isomers that make identification of specific analytes challenging.

During the imaging acquisition, a mass spectrum is acquired for every position the laser is fired (ultimately becoming a voxel in the resultant mass spectrometry dataset). After completion of data acquisition, a 2D ion map can be reconstructed for any generated ion in which relative ion intensity can be represented either as the contrast of a single color or as a “heat map”. This 2D ion map shows the distribution and relative intensity of any detected analyte of interest within the tissue section (Buchberger, DeLaney et al. 2018). The use of high-mass resolution and high mass accuracy analyzers (such as the Orbitrap) aids in resolving desired analytes (such as drugs, metabolites, and low abundance lipids) from endogenous background species or matrix-derived spectral peaks. In addition, with sufficient mass resolution they can provide specific and unequivocal information about the elemental composition of the desorbed ion from the tissue (Landgraf, Prieto Conaway et al. 2009). Due to recent increases in MS and laser technology the voxels (in the full dataset) or pixels (in an extracted 2D ion image) may be as small as 1 μm (Niehaus, Soltwisch et al. 2019) making intracellular MALDI-MSI feasible.

Lipids are abundant molecules in the cells, especially in the membranes, and they can be easily ionized to generate abundant positive or negative ions during the MALDI

process. Moreover, many (but not all) lipids have molecular weights below 1,000 Daltons, which is an optimal mass range for their diffusion into the matrix crystals and for the sensitive operation of MALDI (Berry, Hankin et al. 2011). Whether lipids can be detected in positive or negative mode depends upon the charge of the head group. Several types of lipids, such as phospholipids (Zaima, Hayasaka et al. 2009), neutral lipids (Hayasaka, Goto-Inoue et al. 2009), glycolipids (Goto-Inoue, Hayasaka et al. 2011), and fatty acids (Hayasaka, Goto-Inoue et al. 2010) have been investigated by MSI. Multiple lipid species have been identified as potential markers for diseases including cancer (Paine, Liu et al. 2019), cardiovascular infarction (Menger, Stutts et al. 2012), Alzheimer's (Hong, Kang et al. 2016), and hepatitis B (Park, Lee et al. 2014).

In a published example of MSI applied to infectious disease research, MALDI-MSI was used to investigate specific host lipidic dysregulation occurring in pulmonary TB. In addition to identifying lipids accumulating within necrotic pulmonary granulomas, the group also identified the precise localization of mycobacterium tuberculosis within the granulomas by visualizing specific bacterial membrane lipids. In serial sections, the distributions of anti-TB drugs were determined by MALDI-MSI. Thus, the authors obtained a perfect map of drugs colocalizing with specific metabolites and bacterial target populations, which could be used to answer whether administered drugs were reaching their intended target (Prideaux, ElNaggar et al. 2015, Prideaux, Via et al. 2015, Blanc, Lenaerts et al. 2018, Zimmerman, Blanc et al. 2018). Using a similar approach, we have applied MALDI-MSI lipidomic analysis to investigate lipidic dysregulations that are very common in pathological conditions such as HAND (see Chapter 3). In post-mortem HIV brain tissues from patients undergoing successful cART and symptomatic HAND, we identified significant relative intensity changes for select species of sulfatides, even in tissues without notable alterations in morphology. Thus, we found that MALDI-MSI is an important technique for the characterization of neurological molecular dysfunction, and we propose that sulfatide can be a potential indicator of myelin damage in neuroHIV.

PART 4 – AIMS OF THE STUDY

This Ph.D. thesis aims to test the hypothesis that "chronic brain damage in HIV-infected population is dependent on CNS viral reservoirs by mechanisms of damage amplification mediated by lipids". This assumption is because HIV reservoirs in the brain are associated with compromised myelin structures resulting in the release of sulfatide, the major structural lipid of the myelin sheath. Soluble sulfatide improves Cx43 gap junctional communication and impairs calcium waves, contributing to the amplification of CNS damage and cognitive impairment that distress the HIV-infected population.

To address this hypothesis, we generated a protocol to identify, localize, and quantify viral reservoirs in HIV-infected brain tissues. We identified that the cells with HIV-integrated DNA are macrophages/microglia and a small population of astrocytes. These cells are not silent and still produce residual viral mRNA and proteins even in patients under efficient cART. In addition, some viral proteins synthesized in HIV-infected cells can be released and taken up by neighboring uninfected cells to spread toxicity into the brain areas without viral reservoirs. Therefore, viral reservoirs generate CNS damage using a bystander mechanism.

Using histology coupled with high-resolution confocal microscopy and image analysis, we determined that viral reservoirs correlate with myelin structure alteration in the brain of HIV-infected individuals with mild and severe cognitive impairment. To further examine the mechanism of myelin compromise induced by HIV-infected cells, we used MALDI-MSI to identify a key lipid involved in maintaining myelin structure and a potential indicator for HAND pathogenesis, sulfatide.

Subsequently, *in vitro*, we investigated changes induced by soluble sulfatide exposure on key molecules involved in cell-to-cell communication, such as Connexin43 (Cx43) and Zonula Occludens-1 (ZO-1). Additionally, we examined the extracellular

effects of sulfatide on calcium waves, which are essential for neuronal synchronization and firing pattern.

We intend to provide evidence for a new mechanism to justify CNS viral reservoirs and lipid alternation connection in HAND through the following aims. In the future, we will complete and expand our study to larger clinical cohorts and animal models to confirm whether sulfatide plays a causative role in neuroHIV and whether its biosynthetic pathways can be potential pharmaceutical targets to alleviate the debilitating neurocognitive effects present in HIV-infected patients under cART.

We also described our plan to complete pending experiments involving proteomics of Cx43 interacting proteins, single-cell RNA sequencing to identify specific astrocyte populations that become susceptible to HIV infection or bystander damage, and MALDI-MSI or MALDI-2 MSI to detect lipid dysregulation in primary human cultures of HIV-infected astrocytes.

For future application to elucidate lipid dysregulation in neurocognitive disorders, we also established a MALDI-2 MSI method to detect lipid classes and species that are not detected with regular MALDI-MSI, using the brain tissue sections of the 3xTg AD mouse model. We demonstrate that this assessment is compatible with subsequent immunofluorescence and histological analyses in the same tissue section. This approach is innovative and will be critical for performing a multi-omics characterization for several pathologies, including HAND.

CHAPTER 2 – IDENTIFICATION AND QUANTIFICATION OF HIV VIRAL RESERVOIRS USING IMPROVED STAINING AND MICROSCOPY TECHNIQUE IN HUMAN BRAIN TISSUES

Donoso Maribel[1]; D'Amico Daniela[1,2]; Valdebenito Silvana[1]; Hernandez Christian[1]; Prideaux Brendan[1]; Eugenin Eliseo A.[1]

[1]University of Texas Medical Branch (UTMB), Department of Neuroscience, Cell Biology and Anatomy, Galveston, TX, USA

[2]University of Palermo (UniPa), Department of Biomedicine, Neuroscience and Advanced Diagnostics, Palermo, Italy

The National NeuroAIDS Tissue Consortium (NNTC) and the NeuroBioBank provided all human samples. The NNTC is made possible through funding from the NIMH and NINDS by the following grants: Manhattan HIV Brain Bank (MHBB): U24MH100931; Texas NeuroAIDS Research Center (TNRC): U24MH100930; National Neurological AIDS Bank (NNAB); U24MH100292; California NeuroAIDS tissue Network (CNTN): U24MH100928; and Data Coordinating Center (DCC): U24MH100925. This work was funded by The National Institute of Mental Health grant, MH096625, MH128028, the National Institute of Neurological Disorders and Stroke, NS105584, and UTMB internal funding (to E.A.E).

Adapted paper: Donoso M., D'Amico D., Valdebenito S., Hernandez C., Prideaux B. and Eugenin E.A. "Identification, quantification, and characterization of HIV-1 reservoirs in the human brain". Submitted to Cell Molecular Medicine Journal, under the second review.

INTRODUCTION

HIV persists in the body of infected individuals despite effective cART due to the presence of viral reservoirs in different tissues (Blankson, Persaud et al. 2002, Balcom, Roda et al. 2019). Viral reservoirs are characterized as a small population of cells with integrated HIV DNA into the host DNA that either does not produce or only produces low levels of virus or viral proteins. This process is called latency (Dahabieh, Battivelli et al. 2015). Upon cART interruption, the virus rebounds and repopulates the body in a few weeks (Sengupta and Siliciano 2018). Most viral reservoir studies are currently performed in the blood due to the ease of access and the large amount of available biological material. Using current techniques, the clinical limit of viral detection is 20-50 HIV RNA copies (Tan, Carrington et al. 2018). Crucially, recent advances in the field indicate that most viral reservoirs are present in different tissue compartments in addition to those circulating with the blood (Lamers, Rose et al. 2016). Several tissues have been proposed as anatomical compartments for viral reservoirs including gastrointestinal mucosa, liver, brain, associated lymphatic tissues (spleen, thymus, lymph nodes, gut-associated lymphoid tissue), platelets/megakaryocytes/bone marrow, lungs, kidneys, adipose tissue, and genitourinary systems (Svicher, Ceccherini-Silberstein et al. 2014, Wong and Yukl 2016, Abreu, Shirk et al. 2019, Denton, Sogaard et al. 2019, Ganor, Real et al. 2019, Chaillon, Gianella et al. 2020, Real, Capron et al. 2020, Martin, Bender et al. 2021). Currently, there are two schools of thought concerning viral reservoir compartmentalization; one describes that there is no difference between viral strains and evolution in tissues versus the blood (Bozzi, Simonetti et al. 2019), and the second indicates that virus and viral reservoirs in different tissues can evolve differently than blood strains (De Scheerder, Vrancken et al. 2019). Most of these viewpoints are based only on data derived from sequencing of HIV strains as there are no available techniques to detect viral reservoirs present within tissues in a reliable manner. Also, all the

techniques that detect and quantify viral reservoirs are based on the detection of only one virus component, such as viral DNA, mRNA, or proteins (De-Scheerder, Depelseneer et al. 2020). In general, the techniques amplify the viral reservoirs populations or component by inducing proliferation and selection by viral reactivation with phytohaemagglutinin (PHA) and phorbol myristate acetate (PMA). However, these amplification systems over-represent or only detect a partial amount of the total viral reservoirs pool (Finzi, Hermankova et al. 1997, Massanella, Yek et al. 2018). Thus, resulting in significant limitations including accuracy, precision, sensitivity, cost, testing times, and requirement for a large volume of blood from patients (Eriksson, Graf et al. 2013, Graf and O'Doherty 2013, Strain and Richman 2013, Deere, Kauffman et al. 2014, Salantes, Zheng et al. 2018, Siliciano and Siliciano 2018)

Viral reservoirs are characterized by containing potentially productive HIV DNA integrated into the host DNA (Pinzone and O'Doherty 2018). Moreover, HIV DNA integration cannot assure viral replication because several mechanisms could compromise HIV replication, including mutations, incorrect site or direction of integration, and epigenetic regulation (Abbas and Herbein 2012, Cary, Fujinaga et al. 2016). If the HIV DNA enables viral production, viral mRNA will be produced upon infection or reactivation. Viral mRNA expression results in viral protein synthesis and subsequent viral particle assembly and release of mature virions. However, HIV integration, viral RNA, and protein production ratio are unknown in viral reservoirs in the current cART era. Viral proteins are secreted as soluble proteins inducing inflammation and bystander damage in the neighboring uninfected cells. However, there is a lack of *in vivo* data showing this mechanism due to the inability to correctly identify, localize, and quantify latent HIV reservoirs in the circulation and tissues of HIV-infected individuals under cART.

One of the major objectives of my thesis was to design, test, and validate a method to detect, localize, and quantify viral reservoirs in human brain tissues from the

HIV-infected population using a multi-probe and antibody-based system visualized by microscopy. Our method identifies HIV-integrated DNA, HIV mRNA, and several viral proteins in a single test. This approach demonstrated that HIV-infected macrophages/microglia and a smaller population of astrocytes are the main cell types infected with HIV in the current cART era. Overall, our findings show that viral brain reservoirs still produce viral mRNA and proteins. HIV-p24, Gp120, Nef, Vpr, and Tat proteins, but not Integrase, are synthesized in HIV-infected cells, released, and taken up by neighboring uninfected cells to spread toxicity even in the current cART era.

MATERIALS AND METHODS

Staining

Sample Preparation: Human brain blocks were obtained from the National NeuroAIDS Tissue Consortium (NNTC). Fixed and unfixed tissue blocks were cut in ten μm thick serial sections using a Leica RM2235 cryostat and thaw-mounted onto frosted glass microscope slides.

Rehydration of samples: Paraffin-embedded slides containing the tissue samples were immersed in the following solutions consecutively: xylene for 5 min (2 times), 100% EtOH for 3 min (2 times), 95% EtOH for 3 min, 90% EtOH for 3 min, 70% EtOH for 3 min, 60% EtOH for 3 min, 50% EtOH for 3 min, miliQ H_2O for 3 min. Then, tissue was encircled with ImmEdge Pen to reduce the reagent volume needed to cover the specimens. Finally, slides were immersed in miliQ H_2O for 3 min.

Pre-treatment with proteinase K: Tissues were incubated with proteinase K (0.01 mol/ml, K5201, Dako products-Agilent Technologies, Santa Clara, CA) diluted 1:10 in 1X TBS (*PNA ISH kit*, K520111-2, Dako products-Agilent Technologies, Santa Clara, CA) for 10 min at RT in a humidity chamber. Slides were immersed in miliQ H_2O for 3 min, then immersed in 95% EtOH for 20 sec and finally, the slides were let air-dry for 5 min.

HIV DNA Probe Hybridization: Tissues were incubated with a PNA DNA probe 10 μM for Nef-PNA Alexa Fluor 488 (Alexa488-GCAGCTTCCTCATTGATGG) and Alu-PNA Cy5 (Cy5- GCCTCCCAAAGTCGTGGGATTACAG) (PNA Bio, Thousand Oaks, CA). Slides were placed in a pre-warmed humidity chamber and incubated at 42°C for 30 min, then the temperature was raised to 55ºC for an additional 1 h of incubation. Following, tissues were incubated using Preheat Stringent Wash working solution (PNA ISH kit, K520111-2, Dako products-Agilent Technologies, Santa Clara, CA) diluted 1:60 in 1X TBS for 25 min in an orbital shaker at 55ºC. Slides were equilibrated to RT by brief immersion in TBS for 20 sec.

HIV mRNA detection: The manufacturer's protocol was followed for RNAscope 2.5 HD Detection Reagent-RED (322360, ACD). A probe for HIV-gagpol was added to the tissue samples and incubated for 30 min at 42°C and then 50 min at 55°C. Samples were incubated in Preheat Stringent Wash working solution diluted 1:60 in 1X TBS (PNA ISH kit, K520111-2, Dako products-Agilent Technologies, Santa Clara, CA) for 15 min in an orbital shaker at 55ºC. Slides were immersed in 1X TBS for 20 sec. The colorimetric method was performed as described by the manufacturer. The development of the viral mRNA signal needs to be low, so we did not overdevelop. The reaction was stopped as soon as a red color was observed. Samples were washed three times with miliQ H_2O. Slides should be kept at 4°C in the dark to minimize fluorescence decay. Note: The detection of RNA-scope by color was unreliable, especially for archival or tissues in formalin or other fixatives for long periods. Thus, the detection of viral mRNA was done by fluorescence instead of colorimetric analysis.

HIV or cellular protein detection: Antigen retrieval was performed by incubating slide sections in commercial Antigen retrieval solution (S1700, Dako products-Agilent Technologies, Santa Clara, CA) for 30 min at close to 80ºC water bath. Slides were removed from the bath and then allowed to cool down in 1X TBS. Samples were permeabilized with 0.1% Triton X-100 (X-100, Sigma-Aldrich, St. Luis, MO) for 2 min

and then washed in 1X TBS for 5 min three times. Unspecific antibody binding sites were blocked by incubating samples with a freshly prepared blocking solution. Sections were incubated overnight at 4ºC using a humidity chamber (10 ml of Blocking solution: 1 mL 0.5 M EDTA, 100 ul Fish Gelatin from cold water 45%, 0.1 g Albumin from Bovine serum Fraction V, 100 ul horse serum, 5% human serum, 9 mL miliQ H_2O). A primary antibody (viral proteins: p24 GXT40774, Irvine, CA; Integrase NIH 7374; Gp120 NIH 1476; Tat NIH 705; Nef NIH 2949; Vpr NIH 3951; and cellular markers Iba-1, anti-goat, dilution 1:200, ab5076, Cambridge, UK; and GFAP, anti-mouse, dilution 1:100, G3893, Sigma-Aldrich, St. Luis, MO) was added to the samples diluted in blocking solution and incubated at 4ºC overnight. Slides were washed in 1X TBS 5 min three times to eliminate unbound antibodies. Secondary antibodies were added at the appropriate dilutions and incubated for 2 h at RT. Slides were washed in 1X TBS 5 min three times to eliminate unbound antibodies. Slides were mounted using Prolong Diamond Antifade Mount medium containing DAPI (P36930, Thermo Fisher Scientific, Waltham, MA). Slides were kept in the dark at 4ºC.

Analysis: Nikon A1 confocal microscopy with spectral detection was used to identify the probes and the antibodies. The absorption and emission of each fluorophore were examined using spectral detection to narrow the wavelengths to 20-40 nm. These analyses were also performed using RNAscope due to the significant red color in uninfected samples. The fluorescent detection of RNAscope precipitate was only found in HIV-infected samples. NIS Elements (Japan) and other proprietary software were used for further analysis.

Neurocognitive examination

NNTC and CHARTER perform a comprehensive neurocognitive test battery every 6 months, including motor function (perceptual-motor speed), verbal fluency, executive function, attention/working memory, speed of information processing, learning,

and memory (Woods, Rippeth et al. 2004, Heaton, Clifford et al. 2010, Jernigan, Archibald et al. 2011), for details, see http://www.mountsinai.org/patient-care/service-areas/neurology/areas-of-care/neuroaids-program or https://nntc.org/.

Statistical analysis

Statistical analyses were performed using Prism 5.0 software (GraphPad Software, Inc., San Diego, CA). Analysis of variance was used to compare the different groups; *$p \leq 0.005$ for all statistical analyses performed in this study.

RESULTS

Detection of viral reservoirs in human brain tissue samples

In collaboration with the National NeuroAIDS Tissue Consortium (NNTC) and the NeuroBioBank, we collected 34 brain tissue samples from individuals who were uninfected, HIV-infected, and uninfected with Alzheimer's disease (cortex and/or hippocampus). Samples from HIV-infected individuals have different degrees of cognitive impairment and viral replication (see Table 1 for details). There were no significant differences in age between HIV-negative and HIV-positive groups (HIV-positive, mean = 49.9 ± 2.6 years; HIV-negative, mean = 50.4 ± 5.2 years; Table 1) and sex (HIV-positive = 38% female and 62% male; HIV-negative = 20% female and 80% male; Table 1). The HIV-positive cohort had an average of 14.9 ± 1.9 years living with HIV, which we could subdivide into three groups according to systemic viral replication upon demise: HIV-positive with undetectable replication (Patients N° 6-13, HIV_{un} with a range of plasma HIV RNA of 0 to <50 copies/mL and an average $CD4^+$ T cell count of 727 ± 177 cells/mm^3); low replication (Patients N° 14-19, HIV_{low}) with a range of plasma HIV RNA of 275 to 12,352 copies/mL and an average $CD4^+$ T cell count of 444 ± 147 cells/mm^3; and high replication (Patients N° 20-26, HIV_{high}) with a range of plasma HIV RNA of 165,862 to >750,000 copies/mL and an average $CD4^+$ T cell count of 22.4 ± 12.4

cells/mm^3 (see Table 1 for details). Among the HIV-positive participants, 72% had some degree of cognitive impairment as determined by neuropsychological tests (Table 1). Also, we included archival cases of AIDS and encephalitis (HIVE, patients Nº 27-31) as a positive control and acute cases of Alzheimer's disease as a negative control (AD, patients Nº 32-34). To assure an unbiased assessment, all samples were received and analyzed blindly. After the data was acquired, the clinical and HIV status was requested to assure proper scientific rigor.

Brain cells containing HIV-integrated DNA accumulate in cell clusters containing macrophages/microglia and astrocytes in the current cART era

To identify viral reservoirs containing HIV DNA in the nucleus within the human brain, we used a combination of tissue staining, confocal microscopy, 3D reconstruction, deconvolution, and imaging analysis. A graphical example of the approach is denoted in Fig. 2.1A, and the protocol is described in detail in the materials and methods section. Large brain tissue pieces were serially sectioned to characterize the brain structures and cell types to identify viral reservoirs (cortex and hippocampal sections, sizes were 6.7±3.03 cm^2, 11 to 12 serial sections of 10 μm each). The reason for using large tissue pieces was the low abundance of viral reservoirs in some tissues. In our approach, the first and the last sections were used for hematoxylin and eosin (H&E); the second section for trichrome staining; and the subsequent sections were stained for DAPI to identify nuclei, HIV DNA probe for the nef DNA sequence (DNA^{nef} or HIV DNA), HIV mRNA probe for HIV-gag-pol mRNA sequence (HIV-mRNA or $mRNA^{gagpol}$), Alu-repeats probe as control of host DNA (Alu), and HIV-p24 protein (HIV-p24 prot or $protein^{p24}$) to quantify the overall number of cells with integrated DNA that are producing or not viral mRNA and HIV-p24 proteins versus the total number of cells (Alu-repeats and DAPI positive). The following section was stained using DAPI for nuclei, HIV DNA probe for nef, Iba-1 protein to quantify macrophage/microglia, and GFAP to quantify astrocytes.

The subsequent tissue section was used to identify viral protein expression in particular cell types by identifying cell types with HIV-integrated DNA. After nine sections, we repeated the staining for the HIV DNA probe for nef, Alu-repeats probe, and DAPI to reposition the brain structures, clusters of HIV-infected cells, and cell types identified (Fig. 2.1A).

Using the staining and imaging approaches described above, we identified, quantified, and characterized low abundance HIV components (viral DNA, mRNA, and proteins as described in Fig. 2.1A) and the cell types present in the human brain obtained from individuals under cART. We identified that most cells with HIV-integrated DNA (triple positive nucleus staining for DAPI, Alu-repeats, and the HIV-nef probe) were organized in cell clusters of 2-9 cells (Fig. 2.1B-G). The brain tissue sections obtained from uninfected or Alzheimer's individuals shows DAPI, Alu-repeats, and cellular markers (Iba-1 and GFAP) and no nonspecific staining for HIV DNA, mRNA, or HIV-p24 protein. In brain tissues obtained from HIV-infected individuals, cell clusters containing HIV DNA staining were positive for the macrophage/microglia marker, Iba-1 protein, and surrounded by enlarged hyper-reactive GFAP positive astrocytes (Fig. 2.1B to G, a representative example). The number of HIV DNA positive clusters per tissue section corresponded to a total of 2.67±1.2, 5.38±1.1, and 22.40±10.09 in brain tissues obtained from HIV-infected individuals with undetectable replication (HIV_{un}), low replication (HIV_{low}), and high replication (HIV_{high}), respectively (Fig. 2.1H, *$p \leq 0.005$ compared to uninfected conditions, #$p \leq 0.005$ compared to HIV_{un} conditions, and &$p \leq 0.005$ compared to HIV_{un} or HIV_{low} conditions, n=34 tissues analyzed and 21 tissues compared to uninfected tissues, Un and AD, each point represent 3-5 different areas per tissue analyzed). In HIVE brains, 46.83±14.74 cell clusters were detected (Fig. 2.1H, *$p \leq 0.005$ compared to uninfected conditions, #$p \leq 0.005$ compared to HIV_{un} conditions, and &$p \leq 0.005$ compared to HIV_{un} or HIV_{low} conditions, n=5 HIVE tissues compared to uninfected tissues, n=8, each point represent 3-5 different areas per tissue analyzed).

HIVE conditions correspond to archival tissues from the early stages of the AIDS epidemics without cART or monotherapy. We determined that the extent of HIV systemic replication (see Table 1) could predict the numbers of clusters with HIV-infected cells (Fig. 2.1H, compare HIV_{un}, HIV_{low}, and HIV_{high}, or HIVE). We have to note that large tissue areas were negative for HIV DNA, and the examples in the figures focus on the positive areas. Also, in HIV_{un}, HIV_{low}, and HIV_{high} conditions, there was a correlative number of HIV-positive clusters and cART status, suggesting that long-term cART reduces the number of clusters of HIV-infected cells (Fig. 2.1H, F_{value}=222.9721, ANOVA). No HIV DNA staining was detected in uninfected tissues (brains obtained from uninfected, Un, and Alzheimer's patients, AD, Fig. 2.1H). In addition, we did not detect HIV reservoirs using Alu-PCR or ultra-sensitive PCR as described (Siliciano and Siliciano 2018, Abdel-Mohsen, Richman et al. 2020) using the brain tissues obtained from individuals with undetectable replication and low replication. However, Alu-PCR and ultra-sensitive PCR reliably detected viral reservoirs in brain tissues obtained from high replication and HIVE tissues (data not shown).

Most cell clusters positive for HIV DNA signal were also positive for HIV-mRNA, 0.86±0.51 for HIV_{un}, 1.88±0.52 for HIV_{low}, and 14.22±8.3 for $HIV_{high,}$ indicating that approximately 1/3 of the cells containing HIV DNA could express viral mRNA (Fig. 2.1I, *p≤0.005 compared to uninfected conditions, #p≤0.005 compared to HIV_{un} conditions, and &p≤0.005 compared to HIV_{un} or HIV_{low} conditions, n=34 tissues analyzed and 21 tissues compared to uninfected tissues, Un and AD, each point represent 3-5 different areas per tissue analyzed). In contrast, in HIVE conditions, the cell numbers containing HIV DNA match the cells expressing HIV-mRNA supporting highly productive infection (Fig. 2.1I, HIVE). Further analysis of the cell clusters for HIV-p24 protein expression indicates that 0.37±0.32 for HIV_{un}, 1.16±0.37 for HIV_{low}, and 9.88±6.9 for $HIV_{high,}$ indicating that approximately 1/3 of the cells containing HIV DNA and HIV-mRNA still express HIV-p24 in these cell clusters (Fig. 2.1J, *p≤0.005

compared to uninfected conditions, #p≤0.005 compared to HIV_{un} conditions, and &p≤0.005 compared to HIV_{un} or HIV_{low} conditions, n=34 tissues analyzed and 21 tissues compared to uninfected tissues, Un and AD, each point represent 3-5 different areas per tissue analyzed). In HIVE conditions, HIV-p24 expression correlates with HIV DNA and HIV-mRNA expression (Fig. 2.1J, HIVE).

Overall, in the cART era, the number of clusters in HIV-infected tissues decreased by about 2/3 compared to HIV_{high} and HIVE conditions (Fig. 2.1H to J) and confirmed some of the ratios described for T cells reservoirs (Bruner, Hosmane et al. 2015, Churchill, Deeks et al. 2016, Abdel-Mohsen, Richman et al. 2020). Further, there was a decrease in the overall intensity of HIV-mRNA and HIV-p24 signals between low replication (HIV_{un} and HIV_{low}) and high replication groups (HIV_{high} and HIVE) of 78.34±20.41 % for HIV-mRNA and 83.04±16.54 % for HIV-p24 (Fig. 2.2.1I-J), indicating that in the cART era, viral mRNA and protein were expressed at lower levels (data not represented, p≤0.001 compared to HIVE conditions, respectively). Analysis of brain tissue sections obtained from uninfected individuals (uninfected, Un, and Alzheimer's disease, AD) showed DAPI, Alu-repeats, and cellular markers (Iba-1 and GFAP), but no nonspecific staining for HIV DNA, HIV-mRNA, or HIV-p24 as expected. Moreover, there was no correlation between the numbers of cell clusters, numbers of clusters per tissue, and the ratio among HIV DNA/HIV-mRNA/HIV-p24 with the degree of cognitive decline in the population analyzed (HIV-associated minor cognitive/motor disorder, MCMD or HIV-associated dementia, HAD data not represented). In conclusion, long-term cART and reduction in systemic replication reduce the numbers of HIV-infected clusters in the brain, but a significant number of HIV-infected cell clusters remain in the human brain producing residual viral mRNA and HIV-p24.

Brain cells, microglia/macrophages, and astrocytes containing HIV-integrated DNA still produce low levels of HIV-mRNA and HIV-p24 in the current cART era

Subsequently, we expanded our analysis to larger cortical and subcortical areas to quantify the frequency of viral components present within different cell types (see details in Table 1, cortex and hippocampus). Representative images of unstained and H&E-stained conditions are shown in Fig. 2.2A and B, respectively. The blue boxes in both figures denote the presence of clusters with HIV-infected cells (HIV DNA positive cells, Fig. 2.2A and B). Upon identification of the coordinates with HIV DNA staining and colocalization with Alu-repeats and DAPI, we enlarged the selected areas to examine the expression and distribution of DAPI (nuclear marker, Fig. 2.2C), HIV DNA (Fig. 2.2D, HIV-nef-DNA), HIV gag-pol mRNA (HIV-mRNA, Fig. 2.2E), HIV-p24 (Fig. 2.2F), Alu-repeats (Fig. 2.2G) and the merge/colocalization of all colors (Fig. 2.2H, Merge) as described in the materials and methods section. To quantify and identify which cell types contained HIV-integrated DNA and the degree of viral mRNA and protein expression, we quantified the HIV DNA signal in a cell-specific manner (Iba-1 or GFAP positive cells to identify macrophage/microglia or astrocytes, respectively) in the different tissues analyzed (see Table 1).

In brain tissues obtained from HIV-infected individuals with undetectable replication (HIV_{un}, Fig. 2.2I), macrophage/microglia corresponded to 21.48±13.50 and astrocytes corresponded to 74.85±15.85 cells containing HIV DNA per tissue analyzed (Fig. 2.2I, HIV_{un}). In brain tissues obtained from HIV-infected individuals with low systemic replication, 131.1±28.17 cells corresponded to macrophage/microglia and 76.73±16.11 cells corresponded to astrocytes (Fig. 2.2I, HIV_{low}). In brains obtained from HIV-infected individuals with high systemic replication, most HIV DNA positive cells corresponded to macrophage/microglia, 307.23±87.73 cells, and 44.43±19.11 cells corresponded to astrocytes (Fig. 2.2I, $HIV_{high,}$ *$p \leq 0.005$ compared to uninfected conditions, #$p \leq 0.005$ compared to HIV_{un} conditions, and &$p \leq 0.005$ compared to HIV_{un} or HIV_{low} conditions, n=34 tissues analyzed and 21 tissues compared to uninfected tissues, Un, each point represent 3-5 different areas per tissue analyzed).

Our data indicate that macrophage/microglia are the predominant cells infected with HIV in patients with low to high systemic replication (Fig. 2.2I, HIV_{low} and HIV_{high}). However, in HIV conditions with undetectable replication, the number of HIV-positive macrophage/microglia decreased significantly (Fig. 2.2I, HIV_{un}, F=287.5331 for ANOVA to compare all the groups). In contrast, in GFAP-positive cells (astrocytes), the numbers of astrocytes containing HIV DNA in the nucleus were not altered by systemic replication (Fig. 2.2I, HIV_{un}, HIV_{low}, and HIV_{high}, no significant differences). Overall, our data indicate that the HIV-infected astrocyte population is more stable upon long-term cART than the myeloid-infected population (Fig. 2.2I, compare macrophage/microglia and astrocytes).

To determine the expression of viral mRNA within the cells containing HIV DNA, we quantified the numbers of HIV-mRNA and HIV DNA positive cells. Analyses of brains obtained from HIV-infected individuals with undetectable replication and stained for Iba-1 indicate that only 5.85±2.9 cells per tissue expressed viral mRNA (Fig. 2.2J, HIV_{un}), yet 21.48±13.49 cells per tissue show viral DNA in the nucleus (compared to Fig. 2.2J to 2I, for the quantification of HIV DNA containing cells). In brain tissues obtained from individuals with low systemic HIV replication, only 47.65±20.02 cells per tissue analyzed were positive for HIV DNA and viral mRNA (Fig. 2.2J, HIV_{low}). In contrast, in brain tissues obtained from individuals with high viral replication, the population of macrophages/microglia cells positive for HIV DNA and viral mRNA was similar (HIV DNA, 307.22±87.7 versus 224.32±106.42, viral mRNA), suggesting that effective cART reduces the replication of the virus in myeloid cells (Fig. 2.2J, *$p \leq 0.005$ compared to uninfected conditions, #$p \leq 0.005$ compared to HIV_{un} conditions, and &$p \leq 0.005$ compared to HIV_{un} or HIV_{low} conditions, n=34 tissues analyzed and 21 tissues compared to uninfected tissues, Un, each point represent 3-5 different areas per tissue analyzed).

In contrast, quantifying viral mRNA expression in HIV DNA positive astrocytes indicates that despite different levels of HIV replication, viral mRNA expression was maintained, 55.45±15.16 HIV_{un}, 62.63±16.69 HIV_{low}, and 40.65±18.31 HIV_{high} (Fig. 2.2J, *p≤0.005 compared to uninfected conditions and significant differences between the HIV-infected groups. ANOVA analysis among the HIV-infected groups was insignificant, suggesting that astrocytes are less sensitive to cART than myeloid cells).

To determine whether cells containing HIV DNA and viral mRNA could produce viral proteins, we first quantified the expression of HIV-p24. Quantification of triple-positive cells, HIV DNA, mRNA and HIV-p24 signals in macrophage/microglia indicates that in the brain obtained from individuals with undetectable replication, the numbers of cells per tissue analyzed were 1.68±0.94 cells (Fig. 2.2K, HIV_{un}). Analysis of brains from individuals with low systemic replication indicates that 32.7±22.6 of macrophage/microglia (Fig. 2.2K, HIV_{low}) were triple positive. Lastly, analysis of brains obtained from HIV-infected individuals with high systemic viral replication indicates that 202.22±101.52 of macrophage/microglia were triple positive (Fig. 2.2K, HIV_{high}, *p≤0.005 compared to uninfected conditions, #p≤0.005 compared to HIV_{un} conditions, and &p≤0.005 compared to HIV_{un} or HIV_{low} conditions, n=34 tissues analyzed and 21 tissues compared to uninfected tissues, Un, each point represent 3-5 different areas per tissue analyzed).

These data indicate that despite long-term cART and effective systemic viral suppression, a population of macrophages/microglia in the brain still expresses HIV-p24 (Fig. 2.2K). In contrast, in astrocytes containing HIV DNA and viral mRNA, a conserved HIV-p24 expression despite differences in systemic replication was observed, HIV_{un}, 42.58±11.79 cells; HIV_{low}, 37.1±17.68, and HIV_{high}, 37.92±17.47 cells, indicating that viral replication and HIV-p24 production in astrocytes are stable and no affected by cART (Fig. 2.2K). Analysis of astrocytes for triple-positive cells (HIV DNA/viral RNA/ HIV-p24) indicates that HIV-infected astrocytes are not susceptible to systemic

replication as the expression of HIV-p24 remains equal under all the conditions analyzed (Fig. 2.2K, Astrocytes). Overall, we demonstrate that first, even in the current cART era, viral reservoirs are present in the brain in macrophage/microglia and astrocytes; second, HIV-infected macrophage/microglia, but not astrocytes, are susceptible to long-term cART reducing viral or protein production within the brain (HIV DNA/mRNA and HIV-p24); third, cART reduced residual viral replication or viral protein production in HIV-infected macrophage/microglia but not in HIV-infected astrocytes and lastly, HIV-infected astrocytes are a more stable viral reservoir than macrophage/microglia after long term infection and cART administration.

To compare the amount of the current viral reservoir under long-term cART to the early stages of the AIDS epidemic, we used HIV encephalic tissues (see Table 1 for patient information) to quantify infection and cell numbers per tissue. First, HIV infection (HIV DNA, mRNA, and protein) in HIVE tissues was more widespread than the localized infection in clusters observed in the HIV_{un}, HIV_{low}, and HIV_{high} tissues analyzed (see Table 1). Second, the total HIV DNA cells corresponded to 1,606±368 cells in a comparable tissue volume analyzed (compared to Fig. 2.2L). The HIV-infected population was mostly HIV-infected microglia/macrophages (945±305 cells) and a small astrocyte population (430±208 cells). Thus, a significant difference in the numbers and ratios between microglia/macrophages and astrocytes can be observed between current cART and HIVE conditions.

A critical piece of data from our analysis of tissues obtained from HIV-infected individuals with undetectable, low, and high systemic replication is the lack of colocalization of HIV-p24 protein with cells containing HIV-integrated DNA or viral mRNA surrounding the clusters of HIV-infected cells suggesting a local secretion and bystander uptake. Our findings indicate that most cells with HIV DNA and HIV gag-pol mRNA express HIV-p24 (Fig. 2.2L, HIV DNA (+), combined numbers for HIV_{un}, HIV_{low} and HIV_{high}); however, HIV-p24 protein was found in neighboring uninfected cells,

suggesting its release and uptake by neighboring uninfected cells (452.12±113.64 cells, Fig. 2.2L, HIV DNA (-), *p≤0.005 compared to uninfected conditions and #p≤0.005 compared to HIV DNA (+) conditions). In contrast, analysis of brain tissues obtained from the early and pre-cART era with encephalitis (HIVE) demonstrates that most HIV-p24 proteins were localized in HIV DNA positive cells (HIVE DNA (+)). Low secretion into uninfected cells was detected (Fig. 2.2L, HIVE DNA (+),1,497±459 total cells, or HIVE DNA (-), 890±278 total cells, *p≤0.005 compared to uninfected conditions). We did not detect any nonspecific staining for HIV DNA, viral mRNA or HIV-p24 in uninfected tissues, Un, or tissues obtained from Alzheimer's individuals (AD). Overall, our data indicate that HIV-p24 is still produced by latently infected cells and released into neighboring cells even in the current cART era.

HIV-Gp120 is locally synthesized and released from HIV-infected cells and accumulates in neighboring uninfected cells even in the cART era

Several manuscripts have described the toxic effects of soluble viral proteins within the CNS, including HIV-Gp120, Integrase, Nef, Vpr, and Tat (Kehn-Hall, Guendel et al. 2011, Chompre, Cruz et al. 2013, Datta, Deshmane et al. 2016, Sami Saribas, Cicalese et al. 2017, Yarandi, Robinson et al. 2020), but conclusive data about production, release, and associated bystander toxicity are lacking in the current long-term cART era. HIV-Gp120 is the envelope protein, and it is required for HIV entry into cells, and it is neurotoxic if applied as a soluble protein (Bachis, Aden et al. 2006, Wenzel, Bachis et al. 2017). Further, several animal models have been developed to examine the toxic effects of these viral proteins (Evans and Silvestri 2013, Bar, Coronado et al. 2019, Su, Cheng et al. 2019), but it is unclear whether HIV-Gp120 protein is produced and secreted in the cART era compared to the early stages of the AIDS epidemic and its significant role in HIV-associated cognitive impairment.

HIV-Gp120 distribution was similar to HIV-p24; most brain tissue was negative for HIV-Gp120; however, HIV-Gp120 expression was associated with specific cell clusters positive for HIV DNA signal. A representative cell cluster is shown (Fig. 2.3A-E, arrows indicate cells with HIV DNA and HIV-Gp120 expression). However, as indicated in Fig. 2.3E, cells lacking HIV DNA were also positive for Gp120 protein (Fig. 2.3E, white staining). Also, it is important to note that several cells with HIV-integrated DNA do not express HIV-Gp120 (Fig. 2.3). Quantifying the total numbers of macrophage/microglia with HIV-integrated DNA and expressing HIV-mRNA that were also positive for HIV-Gp120 protein indicates that a total of 1.98±1.61 cells were triple positive within brain tissues obtained from HIV-infected individuals with undetectable replication (HIV_{un}, Fig. 2.3F). In brain tissues obtained from HIV-infected individuals with low and high systemic replication, triple positive macrophage/microglia increased to 14.68±7.1 and 189.4±88.89 cells, respectively (Fig. 2.3F, HIV_{low} and HIV_{high} conditions, *$p \leq 0.005$ compared to uninfected conditions, #$p \leq 0.005$ compared to HIV_{un} conditions, and &$p \leq 0.005$ compared to HIV_{un} or HIV_{low} conditions, n=34 tissues analyzed and 21 tissues compared to uninfected tissues, Un, each point represent 3-5 different areas per tissue analyzed). Thus, our data indicate that HIV-Gp120 is still expressed in the cART era despite a significant reduction in macrophage/microglia expressing this viral protein upon viral suppression (Fig. 2.3F, F=165,4816, by ANOVA to compare the different HIV groups).

In contrast, in astrocytes, the triple expression of HIV DNA, viral mRNA, and HIV-Gp120 was stable and independent of the cART status (Fig. 2.3F, astrocytes, HIV_{un}, HIV_{low} or HIV_{high}), suggesting significant differences compared to myeloid cells. The numbers of positive astrocytes in HIV undetectable replication conditions corresponded to 41.25±12.49 astrocytes per tissue analyzed (Fig. 2.3F, $HIV_{un,}$ *$p \leq 0.005$ compared to uninfected conditions, each point represents 3-5 different areas per tissue analyzed), HIV low replication conditions corresponded to 37.42±17.21 astrocytes per tissue analyzed

(Fig. 2.3F, $HIV_{low,}$ *p≤0.005 compared to uninfected conditions, each point represent 3-5 different areas per tissue analyzed), and HIV high replication conditions corresponded to 37.25±15.01 astrocytes per tissue analyzed (Fig. 2.3F, $HIV_{high,}$ *p≤0.005 compared to uninfected conditions, each point represents 3-5 different areas per tissue analyzed. ANOVA analysis among the HIV-infected groups did not show any significant difference). Our data indicate that HIV reservoirs in macrophage/microglia are responsive to changes in systemic replication but not for HIV-infected astrocytes. In contrast, in HIVE conditions, HIV-Gp120 protein correlated with the total numbers of HIV-infected cells containing HIV DNA and HIV-mRNA and was mostly concentrated in macrophages rather than astrocytes (data not represented, 876±458 cells for macrophages, and 624±287 for astrocytes, triple-positive cells), however, cART or better disease management reduce the expression of Gp120 in macrophage/microglia and astrocytes.

Similar to our HIV-p24 data, most HIV-Gp120 staining was localized in cells lacking HIV DNA signal but in close contact with HIV-infected cells (750.61±164.85 cells, HIV DNA (-), Fig.3G, *p≤0.005 compared to uninfected conditions and #p≤0.005 compared to cells with HIV DNA (+)). In brains obtained from individuals with undetectable, low, and high systemic HIV replication, the combined numbers of triple-positive cells corresponded to 10.45±3.65 cells, suggesting that HIV-Gp120 production, release, and bystander uptake is an important mechanism of HIV-Gp120 spread within the brain even in the cART era (Fig. 2.3G). In contrast, in HIVE brains, there was a perfect correlation between HIV-Gp120 production in HIV DNA positive and negative cells in the greatest numbers compared to the cART era (Fig. 2.3G, HIVE DNA (+), 1,345±349, and HIVE DNA (-), 901±302 cells).

Further, in brain tissues obtained from individuals with undetected, low, and high HIV replication, we calculated the diffusion of the HIV-Gp120 protein from the HIV-positive clusters reaching distances up to 345.8±89.71 μm (data not represented). All

tissues showed a similar HIV-Gp120 expression and distribution. In addition, the pixel intensity between long-term cART and HIVE conditions indicates that cells with high HIV-Gp120 protein expression were reduced by 29.56±8.71 %. We did not find any correlation between HIV DNA, HIV-mRNA, HIV-Gp120 protein expression and cognitive impairment. No nonspecific staining for HIV-Gp120 and other viral components was detected in brain sections obtained from uninfected individuals. Our data indicate that HIV-Gp120 protein is still synthesized, released, and taken up by neighboring uninfected cells despite long-term cART supporting multiple claims that residual Gp120 mediated toxicity and production.

HIV-Integrase is poorly expressed in the brain of HIV-infected individuals under effective cART

Integrase is a key HIV enzyme required for HIV DNA integration into the host DNA (Zhang, Zhang et al. 2016, Wadhwa, Jain et al. 2018, Koneru, Francis et al. 2019). Its association with neurotoxicity is unclear and controversial (Gill, Hassan et al. 2019). Our staining results indicate that Integrase had a highly localized expression (Fig. 2.4A-E) that did not correlate with the presence of clusters containing HIV-infected cells. However, as observed in the merge (Fig. 2.4E), some cells had a nuclear accumulation of Integrase (Fig. 2.4, asterisk). Still, this viral protein's overall expression was low compared to other HIV proteins, likely due to the nature and limited expression of Integrase with the viral DNA (Craigie and Bushman 2012). Quantification of the Integrase staining corroborates our observations that minimal to non-expression of Integrase is present in the brains of individuals with undetectable, low, and high replication due to cART (Fig. 2.4A to E, white arrows indicate cells with HIV-integrated DNA; the asterisk indicates cells with nuclear Integrase. Fig. 2.4E). Quantification of the numbers of macrophage/microglia containing HIV DNA, HIV-mRNA, and Integrase protein shows that in brain tissues obtained from HIV-infected individuals with

undetectable replication, the pool of cells expressing Integrase corresponded to 0.75±0.8 macrophage/microglia per tissue analyzed (HIV_{un}, Fig. 2.4F). Brain tissues obtained from HIV-infected individuals with low systemic replication corresponded to 6.53±1.98 macrophage/microglia, suggesting that cART and systemic replication significantly impact the numbers of cells expressing Integrase (Fig. 2.4F, HIV_{un} and HIV_{low}). The differences in Integrase expression within the brain and related to cART become evident when brains of individuals with high systemic replication were analyzed with 325.05±85.69 cells positive for Integrase in macrophage/microglia (Fig. 2.4F, HIV_{high}, *$p \leq 0.005$ compared to uninfected conditions, #$p \leq 0.005$ compared to HIV_{un} conditions, and &$p \leq 0.005$ compared to HIV_{un} or HIV_{low} conditions, n=34 tissues analyzed and 21 tissues compared to uninfected tissues, Un, each point represent 3-5 different areas per tissue analyzed; comparisons of the HIV-infected groups for ANOVA indicate that HIV_{high} was significantly different from HIV_{un} and HIV_{low} groups, F=552.3771). Further, the pixel intensity for Integrase corresponded only to 8.54±3.75 % of the pixel intensity observed for HIV-Gp120 and HIV-p24 in HIV_{un} and HIV_{low} conditions in macrophage/microglia (data not represented).

In contrast, in HIV-infected astrocytes producing viral mRNA, Integrase was expressed higher than HIV_{un} and HIV_{low} in macrophage/microglia (Fig. 2.4F). However, there were no differences in the numbers of triple-positive cells despite differences in systemic replication; 26.38±6.5 cells (HIV_{un}), 20.85±4.27 cells (HIV_{low}), and 25.35±9.7 cells (HIV_{high}), suggesting an even low expression or stability of Integrase in HIV-infected astrocytes (Fig. 2.4F, Astrocytes). If we compare these data to HIVE conditions, Integrase was expressed in 905±357 microglia/macrophages and 569±299 astrocytes (HIVE, data not show) supporting that cART or better disease management reduce the expression of Integrase in macrophage/microglia and astrocytes.

To quantify whether Integrase is accumulated in uninfected cells as described for HIV-p24 and HIV-Gp120, we quantified colocalization with HIV DNA. Our data

indicate that Integrase is expressed at low levels in HIV DNA (+) cells, 11.22±8.52 cells (Fig. 2.4G and compared to Fig. 2.4F, *p≤0.005 compared to uninfected conditions). Quantification of Integrase in HIV DNA negative cells indicates that 4.21±2.46 cells contain Integrase indicating that it is poorly secreted and accumulated in neighboring cells (Fig. 2.4G, HIV DNA (-), *p≤0.05 compared to uninfected conditions). In contrast, the examination of HIVE tissues indicates that most HIV DNA (+) cells, 1,406±425 cells (Fig. 2.4G, HIVE-DNA (+)), are positive for Integrase and HIV DNA negative cells corresponded to 905±357 cells (Fig. 2.4G, HIVE-DNA (-), *p≤0.005 compared to uninfected conditions). Nonspecific staining was not observed in tissues obtained from uninfected individuals. Thus, the expression of Integrase protein was low but significant compared to uninfected tissues but was not comparable to the expression or distribution observed for other HIV proteins such as HIV-p24 and Gp120.

HIV-Nef protein is expressed in HIV-infected and surrounding uninfected cells, even in individuals without detectable systemic replication

HIV-Nef has been involved in many neuronal/glial/immune toxicity mechanisms even in the current cART era (Fields, Dumaop et al. 2015, Cheney, Guzik et al. 2020, Yarandi, Duggan et al. 2020). Thus, we evaluated HIV-Nef expression and distribution as described for the other HIV proteins.

Experiments using brains from HIV-infected individuals with undetectable and low systemic viral replication indicate that HIV-Nef is expressed in association with HIV-positive clusters. Here, we show a selected region containing HIV-positive DNA cells containing HIV-Nef; however, we must note that most brain areas were negative for HIV DNA and HIV-Nef protein (Fig. 2.5A-E). The confocal analysis identified cells containing HIV DNA (Fig. 2.5A-E, arrows), but also cells with high Nef protein accumulation but negative for HIV DNA (Fig. 2.5A-E, see asterisks for cells with high expression or accumulation, Fig. 2.5E)

Quantification of HIV-Nef protein expression in macrophage/microglia indicates that triple-positive cells (HIV DNA, viral mRNA, and HIV-Nef protein) are present in all HIV conditions, including undetected, low, and high systemic replication (Fig. 2.5F, macrophage/microglia) with an abundance of 10.65±4 cells (HIV_{un}), 40.4±20.50 (HIV_{low}) and 371.48±70.82 cells (HIV_{high}) per tissue analyzed (Fig. 2.5F). Interestingly, a similar trend was observed for the other viral proteins analyzed, HIV-p24, HIV-Gp120, and HIV-Integrase, in correlation with systemic viral replication (Fig. 2.5F, *$p \leq 0.005$ compared to uninfected conditions, #$p \leq 0.005$ compared to HIV_{un} conditions, and &$p \leq 0.005$ compared to HIV_{un} or HIV_{low} conditions, n=34 tissues analyzed and 21 tissues compared to uninfected tissues, Un, each point represent 3-5 different areas per tissue analyzed; comparisons of the HIV-infected groups for ANOVA indicate that HIV_{high} was significantly different from HIV_{un} and HIV_{low} groups, F=883.0321).

In astrocytes, HIV-Nef protein expression in HIV DNA and HIV-mRNA positive astrocytes was significant in all HIV conditions, including undetectable, low, and high systemic replication (Fig. 2.5F, Astrocytes). The numbers of positive astrocytes were 25.28±15.62 cells and 43.73±27.21 in undetectable (HIV_{un}) and low replication (HIV_{low}) (Fig. 2.5F, *$p \leq 0.005$ compared to uninfected conditions, #$p \leq 0.005$ compared to HIV_{un} conditions, and &$p \leq 0.005$ compared to HIV_{un} or HIV_{low} conditions, n=34 tissues analyzed, and 21 tissues compared to uninfected tissues, Un, each point represent 3-5 different areas per tissue analyzed). In brain tissues obtained from individuals with high systemic viral replication, astrocytes corresponded to 247.88±118.13 cells per tissue analyzed. However, and in contrast to the analysis of HIV-p24, HIV-Gp120, and Integrase, HIV-Nef expression in astrocytes was dependent on systemic viral replication (Fig. 2.5F, Astrocytes, ANOVA indicates that HIV_{high} was significantly different than HIV_{un} and HIV_{low} groups, F=122.5936) in a similar manner to other viral proteins in macrophage/microglia. Also, quantifying HIV-Nef expression in HIVE tissues indicates that the total number of cells with HIV DNA, HIV-mRNA, and HIV-Nef protein

corresponded to 1,233±277 (HIVE, data not represented). In HIVE tissues, most of these triple-positive cells were microglia/macrophages, 975±345, and astrocytes were 605±278. Overall, the data indicate that HIV-Nef protein expression in macrophage/microglia and astrocytes is dependent on systemic viral replication. These data indicate that long-term cART can affect different viral proteins in a cell type-specific manner.

To quantify whether HIV-Nef could be released into neighboring uninfected cells, we analyzed HIV DNA positive and negative cells as described above. Quantification of HIV-Nef protein in HIV DNA and HIV-mRNA indicates that 17.15±2.81 cells per tissue were positive (Fig. 2.5G, HIV DNA (+)). However, most HIV-Nef was localized in HIV-nef DNA negative cells, 341.63±107.68 cells, but always in close contact with clusters of HIV-nef DNA positive cells suggesting that most HIV-Nef protein accumulates in surrounding uninfected cells (Fig. 2.5G, HIV-nef DNA (-), *$p \leq 0.005$ compared to uninfected conditions, n=34 tissues analyzed, n=21 infected tissues compared to uninfected tissues, each point represent 3-5 different areas per tissue analyzed). In contrast, in HIVE conditions, most HIV-Nef proteins were associated with HIV DNA positive cells, 1,468±236 cells, and only 958±387 cells without HIV-integrated DNA showed Nef protein (HIVE-DNA (-), Fig. 2.5G, *$p \leq 0.005$ compared to uninfected conditions). Quantification of the pixel intensity indicates that cells with high HIV-Nef protein intracellular content only had a reduction in HIV-Nef staining of 33.78±7.09% as compared to HIV_{high} and HIVE conditions, suggesting that specific areas of the brain can accumulate large amounts of HIV-Nef protein even in the cART era. Also, we calculated that HIV-Nef diffused from HIV DNA positive cells into neighboring uninfected cells reaching distances of 493.02±104.5 μm from the clusters of HIV-infected cells suggesting an active mechanism of synthesis, release, and bystander uptake. Overall, our data indicate that HIV-Nef protein is still synthesized, released, and taken up by neighboring uninfected cells despite suppression of replication.

HIV-Vpr protein is expressed within the brain of HIV-infected individuals under cART

HIV-Vpr is the multifunctional HIV accessory protein essential for transporting the pre-integration complex into the nucleus (Kogan and Rappaport 2011). HIV-Vpr has also been associated with the pathogenesis of NeuroHIV, but whether this viral protein is expressed within the human brain in the cART era is unknown.

To evaluate the expression and distribution of HIV-Vpr, staining of brain tissues obtained from uninfected and HIV-infected individuals with undetectable (HIV_{un}), low (HIV_{low}), and high replication (HIV_{high}) for HIV-Vpr protein, DAPI, HIV DNA, and HIV mRNA was performed (Fig. 2.6 A-E). Analysis of the staining indicates a low expression and scattered distribution (Fig. 2.6A-E, arrows denote cells with integrated HIV DNA and asterisk denote cells with high HIV-Vpr accumulation). In the case of HIV-Vpr, the protein could not establish a diffusion pattern from HIV-infected clusters as established for HIV-Gp120 and HIV-Nef; however, HIV-Vpr, like HIV-Nef, also highly accumulated in particular cells (Fig. 2.6E, asterisks).

Quantification of the numbers of macrophage/microglia per tissue analyzed indicates that HIV-Vpr expression depended on systemic viral replication with 1.88±1.67 cells in tissues obtained from individuals with undetectable replication (HIV_{un}), 34.08±21.5 cells in low replication, and 222.5±134.59 cells in high replication conditions (Fig. 2.6F, macrophage/microglia). Interestingly, there was a correlation between systemic replication and the numbers of HIV-infected macrophage/microglia cells (Fig. 2.6F, *$p \leq 0.005$ compared to uninfected conditions, #$p \leq 0.005$ compared to HIV_{un} conditions, and &$p \leq 0.005$ compared to HIV_{un} or HIV_{low} conditions, n=33 tissues compared to uninfected tissues, each point represents 3-5 different areas per tissue analyzed).

Quantification of astrocytes containing HIV-nef DNA, HIV-mRNA, and HIV-Vpr protein indicates that HIV-Vpr expression depends on systemic viral replication (Fig. 2.6F, Astrocytes). The astrocyte numbers corresponded to 35.55±13.07 in brain tissues

obtained from individuals with undetectable systemic replication (HIV_{un}), 59.5±18.83 in brain tissues obtained from individuals with low systemic replication (HIV_{low}), and 74.63±21 cells in brain tissues obtained from individuals with high systemic replication (HIV_{high}) (Fig. 2.6F, astrocytes, *p≤0.005 compared to uninfected conditions, #p≤0.005 compared to HIV_{un} conditions, and &p≤0.005 compared to HIV_{un} or HIV_{low} conditions, n=34 tissues analyzed and 21 tissues compared to uninfected tissues, Un, each point represent 3-5 different areas per tissue analyzed). In HIVE conditions, 1,198±315 cells were positive for HIV DNA, HIV-mRNA, and HIV-Vpr protein. Most of the cells were microglia/macrophages, 846±208 cells, and astrocytes, 623±277 cells (HIVE, data not represented). In addition, the pixel intensity was 74.08±18.39% lower in $HIV_{un/low}$ than in HIV_{high} and HIVE conditions (data not represented).

To quantify bystander uptake of HIV-Vpr, we measured HIV-Vpr in HIV DNA positive and negative cells spatially. In a similar manner to HIV-Gp120 and HIV-Nef data, most infected cells expressed residual Vpr (Fig. 2.6G, 9.68±2.70 cells); however, most HIV-Vpr signals were located in uninfected cells (Fig. 2.6F, HIV DNA negative cells, HIV DNA (-), 855.83±257.45), but we could not establish an association or diffusion pattern similar to HIV-Gp120 and HIV-Nef proteins (Fig. 2.6G, *p≤0.005 compared to uninfected conditions and #p≤0.005 compared to HIV DNA (+) cells). In HIVE conditions, most HIV-Vpr was located in HIV-positive DNA cells, 1289±245 cells, and 920±105 cells with HIV-negative signals (Fig. 2.6G, HIVE DNA (+) or (-)). Unspecific staining for HIV DNA or HIV-Vpr was not observed in tissues obtained from uninfected individuals. Overall, HIV-Vpr synthesis and bystander secretion are still significant in the current cART era.

HIV-Tat protein is expressed and secreted within the CNS

HIV-Tat corresponds to the transactivator of the virus, and its main function is to drive HIV transcription (Hategan, Masliah et al. 2019, Spector, Mele et al. 2019).

Multiple laboratories, including us, identified that soluble HIV-Tat has neurotoxic effects (Eugenin, D'Aversa et al. 2003, Clark, Nava et al. 2017, Al-Harti, Joseph et al. 2018, Ajasin and Eugenin 2020) and it has been reported in the CSF of HIV-infected individuals under cART (Henderson, Johnson et al. 2019). However, it is debatable whether HIV-Tat is produced significantly during long-term HIV infection and cART administration.

Staining of brain tissues obtained from uninfected and HIV-infected individuals with undetectable, low, and high systemic replication for HIV-Tat protein, DAPI, HIV DNA, and HIV-mRNA shows that HIV-Tat was expressed and widely distributed around clusters of cells containing HIV DNA (Fig. 2.7 A-E, arrows represent cells with integrated HIV DNA signal and asterisk represent cells with high HIV-Tat accumulation). Also, as described for HIV-Gp120 and HIV-Nef, and now for HIV-Tat, the viral protein distribution was highly localized into brain areas with clusters of HIV-infected cells; however, most of the tissue was negative for viral components (Fig. 2.7A-E, represent a cluster of HIV-infected cells). We calculated that HIV-Tat could diffuse from HIV DNA positive clusters into neighboring uninfected cells, reaching distances up to 492.1±145.68 μm.

Quantification of the total numbers of macrophage/microglia with integrated HIV DNA, producing HIV-mRNA, and positive for HIV-Tat protein shows that in the brain obtained from individuals with undetectable replication, the numbers of triple-positive cells corresponded to 8.38±4.4 cells (HIV_{un}, Fig. 2.7F), in samples with low replication the cell number was 48.8±15.9 (HIV_{low}, Fig. 2.7F), and in samples with high replication the numbers corresponded to 365.68±68.05 cells (HIV_{high}, Fig. 2.7F, macrophage/microglia, *$p \leq 0.005$ compared to uninfected conditions, #$p \leq 0.005$ compared to HIV_{un} conditions, and &$p \leq 0.005$ compared to HIV_{un} or HIV_{low} conditions, n=34 tissues analyzed and 21 tissues compared to uninfected tissues, Un, each point represent 3-5 different areas per tissue analyzed). Interestingly, the numbers of triple-positive cells

were correlated with the degree of systemic replication, suggesting that systemic replication significantly impacted the production of HIV-Tat within the brain (Fig. 2.7F). However, HIV-Tat production is still highly significant even in HIV-infected individuals with undetectable replication. ANOVA analysis of the macrophage/microglia HIV-infected groups indicates that brain tissues from low and high viral systemic replication were significantly different than brain obtained from individuals with undetectable replication (Fig. 2.7F, comparisons of the HIV infected groups for ANOVA indicates that HIV_{high} was significantly different than HIV_{un} and HIV_{low} groups, F=936.9699).

The HIV-Tat accumulation in astrocytes indicates that HIV-Tat expression was systemic viral replication-dependent (Fig. 2.7F, Astrocytes). The numbers of triple-positive astrocytes in tissues from individuals with undetectable replication were 50.53±18.03 cells (HIV_{un}, Fig. 2.7F, astrocytes), in low replication were 143.93±102.1 cells, and in high replication conditions were 385.25±66.34 cells (Fig. 2.7, F, astrocytes, *$p \leq 0.005$ compared to uninfected conditions, #$p \leq 0.005$ compared to HIV_{un} conditions, and &$p \leq 0.005$ compared to HIV_{un} or HIV_{low} conditions, n=34 tissues analyzed and 21 tissues compared to uninfected tissues, Un, each point represent 3-5 different areas per tissue analyzed). In astrocytes, HIV-Tat expression depended on systemic viral replication like HIV-Nef and HIV-Vpr, but not HIV-p24 and Integrase, suggesting a different mechanism of expression and cART-mediated regulation. The accumulation of HIV-Tat protein in astrocytes follows a similar distribution to Nef and Vpr, but not for HIV-p24 or Integrase, suggesting differential stability or expression for some viral proteins. In contrast, in HIVE conditions, a total of 1,193±244 cells were identified in a similar volume analyzed in samples under long-term cART. Most HIV-infected cells containing HIV-Tat proteins were macrophage/microglia, 801±197, and astrocytes, 685±297 (data not represented).

To evaluate bystander release and uptake, we quantified the amount of HIV-Tat in cells with HIV DNA and neighboring uninfected cells (Fig. 2.7G). HIV-Tat was present

in most HIV-infected cells (HIV DNA (+), Fig. 2.7G, 13.96±3.65 positive cells for HIV DNA and HIV-Tat), but most HIV-Tat proteins were accumulated in neighboring uninfected cells lacking HIV DNA or HIV gag-pol mRNA, 1,383.71±164.85 (HIV DNA (-), Fig. 2.7G). The quantification of HIV-Tat positive cells' pixel intensity indicates two populations of cells: first, a low but consistent HIV-Tat intracellular expression (cytoplasm and nucleus) localization and a second profile with high cytoplasmic/nuclear accumulation. Interestingly, the expression of HIV-Tat in neighboring cells could reach numbers similar to the one on HIVE (Fig. 2.7G, HIVE in HIV positive and negative cells), indicating that even in the cART era, some areas of the brain still produce and accumulate significant amounts of HIV-Tat within the brain. In HIVE conditions, most HIV-Tat was localized in microglia/macrophages, 1,306±306 cells, and 934±277 cells corresponded to astrocytes (Fig. 2.7G, *$p \leq 0.005$ compared to uninfected conditions and #$p \leq 0.005$ compared to HIV DNA (+) cells). Overall, we demonstrated that HIV-Gp120, HIV-Nef, HIV-Vpr, and HIV-Tat proteins, but not HIV-Integrase protein, are still produced significantly within the brains of HIV-infected individuals, but expression and distribution were dependent on systemic viral replication.

Table 1: Patient information for the samples analyzed

Nº	Patient Group	HIV	Age	Sex	Cognitive Status	CD4 cells/ mm^3	CD8, cells/ mm^3	Viral Load, copies/mL	Years with HIV	cART	Brain Area
1	Un	-	44	M	None	-	-	-	-	-	B
2	Un	-	50	M	None	-	-	-	-	-	B
3	Un	-	69	M	None	-	-	-	-	-	B
4	Un	-	38	M	None	-	-	-	-	-	C
5	Un	-	51	F	None	-	-	-	-	-	B
6	HIV_{un}	+	70	M	MCMD	741	N.R.	<50	26	ziagen, epivir, fosamprenavir , ritonavir	B
7	HIV_{un}	+	69	F	MCMD	616	1190	<50	22	ziagen, epivir, fosamprenavir	C
8	HIV_{un}	+	61	F	MCMD	488	465	<50	24	efavirenz, ziagen, epivir	B
9	HIV_{un}	+	68	F	None	1306	380	0	15	emtricitabine, tenofovir alafenamide, elvitegravir, cobicistat	B
10	HIV_{un}	+	48	M	MCMD	1658	50	<50	13	etravirine, ritonavir, maraviroc, darunavir	C
11	HIV_{un}	+	36	M	None	293	881	<50	11	zidovudine, lamivudine, nelfinavir	C
12	HIV_{un}	+	59	M	None	428	768	<50	26	lamivudine, darunavir, raltegravir, ritonavir, etravirine	B
13	HIV_{un}	+	43	F	None	282	376	<50	24	emtricitabine, tenofovir alafenamide, darunavir, cobicistat	C
14	HIV_{low}	+	38	M	None	973	864	<400	14	etravirine, abacavir, zidovudine, lamivudine	B
15	HIV_{low}	+	53	M	Prob. HAD	101	396	<400	18	lamivudine, nevirapine, zidovudine	C
16	HIV_{low}	+	62	F	None	750	647	275	25	darunavir, ritonavir, emtricitabine, tenofovir	C
17	HIV_{low}	+	51	M	Prob. MCMD	126	N.R.	349	1	lamivudine, abacavir, nelfinavir	B
18	HIV_{low}	+	46	M	Prob. MCMD	214	1330	12352	25	darunavir, raltegravir, etravirine, emtricitabine, tenofovir	B

19	HIV_{low}	+	61	M	Prob. HAD	500	1077	<400	18	atazanavir, emtricitabine, nevirapine, ritonavir	C
20	HIV_{high}	+	49	M	Prob. MCMD	3	71	>750000	21	amprenavir, stavudine, lopinavir	C
21	HIV_{high}	+	44	F	Prob. HAD	1	139	>750000	9	stavudine, didanosine, nevirapine, nelfinavir	C
22	HIV_{high}	+	42	M	Prob. HAD	37	1683	691338	6	didanosine, efavirenz, nelfinavir	B
23	HIV_{high}	+	37	F	Prob. HAD	1	1101	>750000	3	zidovudine, didanosine, lopinavir, ritonavir	C
24	HIV_{high}	+	40	F	Prob. HAD	14	N.R.	>750000	4	indinavir, zidovudine	C
25	HIV_{high}	+	34	M	Prob. HAD	10	545	165862	6	zidovudine, nelfinavir, indinavir, didanosine, lamivudine, abacavir, saquinavir-sgc	B
26	HIV_{high}	+	37	M	Prob. MCMD	91	N.R.	>750000	2	efavirenz, lopinavir, ritonavir, nevirapine, tenofovir, abacavir, zidovudine, lamivudine	C
27	HIVE	+	43	M	HAD	7	N.R.	119000	6	None	B
28	HIVE	+	40	F	HAD	5	N.R.	750000	8	atazanavir	H
29	HIVE	+	43	M	HAD	21	N.R.	172000	5	None	B
30	HIVE	+	38	M	HAD	185	N.R.	46284	3	None	C
31	HIVE	+	44	F	HAD	64	N.R.	750000	5	emtricitabine, tenofovir	B
32	AD	-	62	F	-	-	-	-	-	-	C
33	AD	-	68	M	-	-	-	-	-	-	C
34	AD	-	62	M	-	-	-	-	-	-	C

Information for all 34 individual donors of brain tissue samples regarding HIV status, age, sex, cognitive status, $CD4^+$ T cell counts (cells/mm^3), CD8+ T cells (cells/mm^3), viral load (copies/mL), years living with HIV, and cART treatment description. Patient Group - Un: Uninfected/HIV negative group, HIV_{un}: HIV positive, viral load under the limit of detection, HIV_{low}: HIV positive, low viral load group, HIV_{high}: HIV positive, high viral load group, HIVE: HIV positive, archival encephalitic group, AD: Alzheimer's group. Cognitive status - MCMD: minor neurocognitive and motor disorder, HAD: HIV-associated dementia. ART: antiretroviral. CD4, CD8 T cell counts - N.R.: not reported. Brain Section – C: cortex, H: hippocampus, B: both cortex and hippocampus.

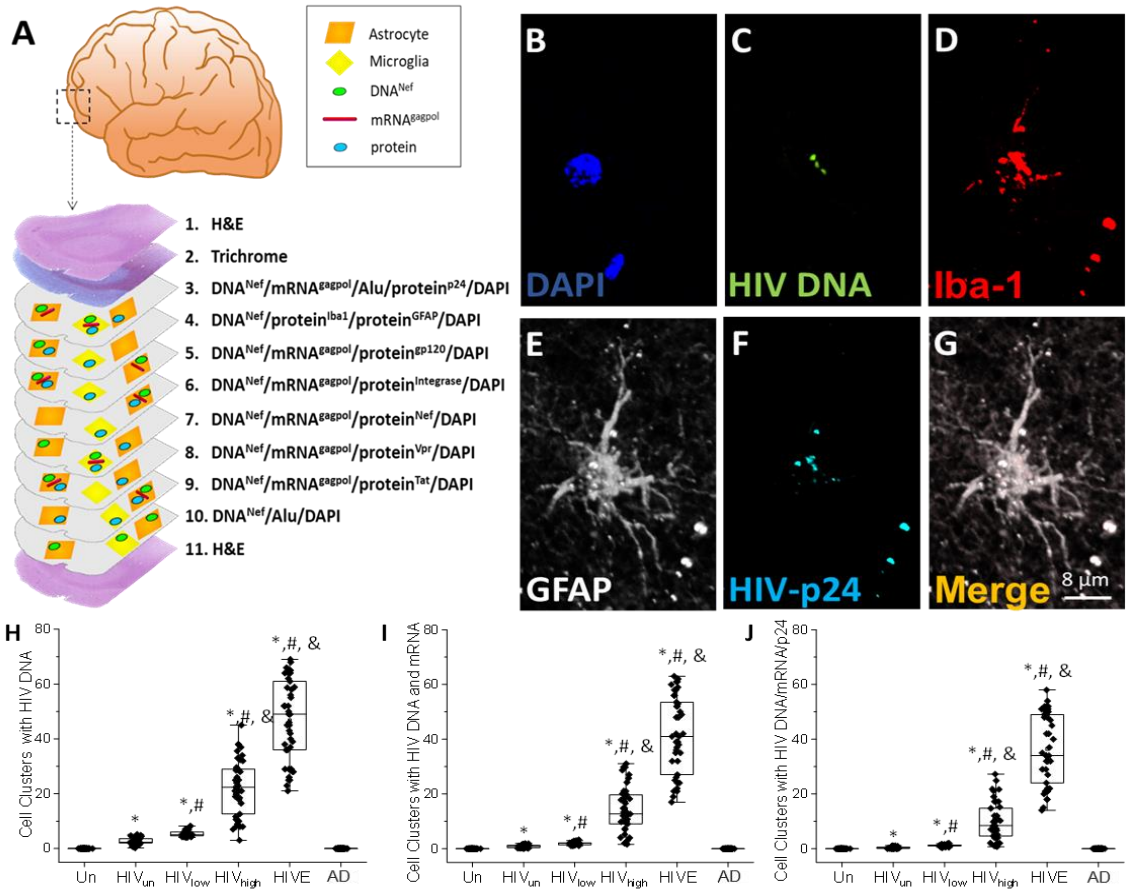

Figure 2.1. HIV reservoirs are organized in small clusters within the brain of HIV-infected individuals

(A) The cartoon shows the detection strategy of HIV DNA, viral mRNA, viral proteins, and cellular markers using 11 slide sections per tissue. The first and last sections were stained for H&E; the second section was used for a Trichrome stain; the following sections were sequentially stained for DAPI, HIV DNA, HIV-mRNA, HIV proteins (p24, Gp120, Integrase, Nef, Vpr or Tat), Alu repeats, or markers for astrocytes (GFAP) and macrophage/microglia (Iba-1) as indicated. (B-G) Confocal images show a cell cluster labeled with DAPI, containing HIV DNA, positive for macrophage/microglia marker and enlarged astrocytes, indicated by Iba-1 protein and GFAP, respectively, and expressing HIV-p24 protein cells. (H-J) Quantification of cell clusters positive for HIV DNA in tissues obtained from uninfected brains (Un), HIV infected brains with undetectable replication (HIV_{un}), HIV infected brains with low replication (HIV_{low}), and HIV infected brains with high replication (HIV_{high}). As a control, we used HIV encephalitic (HIVE) brains and uninfected cases from healthy and Alzheimer's individuals, AD (n=34 brains analyzed and each point corresponding to the mean of at least 3-5 different quantifications per tissue). (H) Correspond to the quantification of cell clusters containing HIV DNA in the nucleus (colocalizing with DAPI and Alu repeats). (I) Quantification of double-positive cell clusters for HIV DNA and viral mRNA. (J) Quantification of cell clusters positive for HIV DNA, viral mRNA and HIV-p24. *p≤0.005 compared to

uninfected conditions, #p≤0.005 compared to HIV_{un} conditions, and &p≤0.005 compared to HIV_{un} or HIV_{low} conditions, n=34 tissues analyzed, and 21 tissues compared to uninfected tissues, Un and AD, each point represent 3-5 different areas per tissue analyzed. Comparisons of the HIV-infected groups were perfumed by ANOVA and described in the text. Bar: 8 μm.

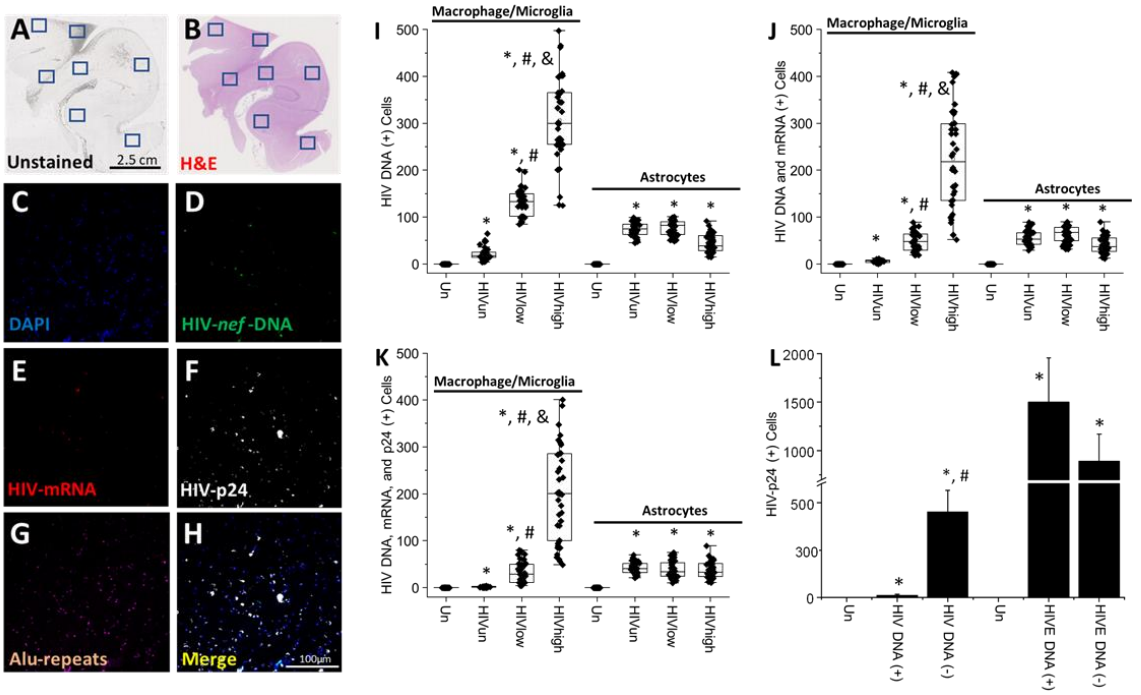

Figure 2.2. Quantification of myeloid and glial viral reservoirs in cortical and subcortical human brain areas

Representative confocal images of the areas analyzed for (A) Unstained and (B) H&E-stained tissue. Areas detected with HIV DNA are represented in blue boxes. (C-H) Representative confocal images of the brain areas containing HIV-integrated DNA and positive labeling for (C) DAPI, (D) HIV DNA, (E) HIV-mRNA, (F) HIV-p24, (G) Alu-repeats, and (H) the merge of all colors. (I-K) Quantification of cells positive for (I) HIV-integrated DNA in macrophages/microglia (Iba-1 positive cells) and astrocytes (GFAP positive cells) in human tissues obtained from individuals with undetectable, low, and high systemic replication, *p≤0.005 compared to uninfected conditions, #p≤0.005 compared to HIV_{un} conditions, and &p≤0.005 compared to HIV_{un} or HIV_{low} conditions, n=34 tissues analyzed and 21 tissues compared to uninfected tissues, Un (including also AD tissues), each point represent 3-5 different areas per tissue analyzed. Comparisons of the HIV-infected groups by ANOVA are described in the text and Star Method Section), (J) HIV-integrated DNA and HIV-mRNA in macrophage/microglia and astrocytes in human tissues obtained from individuals with undetectable, low and high systemic replication (*p≤0.005 compared to uninfected conditions and #p≤0.005 compared to HIV conditions), (K) HIV-integrated DNA, HIV-mRNA and HIV-p24 in macrophage/microglia and astrocytes in human tissues obtained from individuals with undetectable, low, and high systemic replication (*p≤0.005 compared to uninfected conditions, #p≤0.005 compared to HIV_{un} conditions, and &p≤0.005 compared to HIV_{un} or HIV_{low} conditions, n=34 tissues analyzed and 21 tissues compared to uninfected tissues, Un (including also AD tissues), each point represent 3-5 different areas per tissue analyzed). (L) Quantification of cells expressing HIV-p24 in HIV and HIVE cells positive for HIV DNA (HIV DNA (+) and HIVE-DNA (+)) and negative for HIV DNA

(HIV DNA (-) and HIVE-DNA (-)) (*$p \leq 0.005$ compared to uninfected conditions and #$p \leq 0.005$ compared to HIV DNA (+) conditions). Bar: 100 μm.

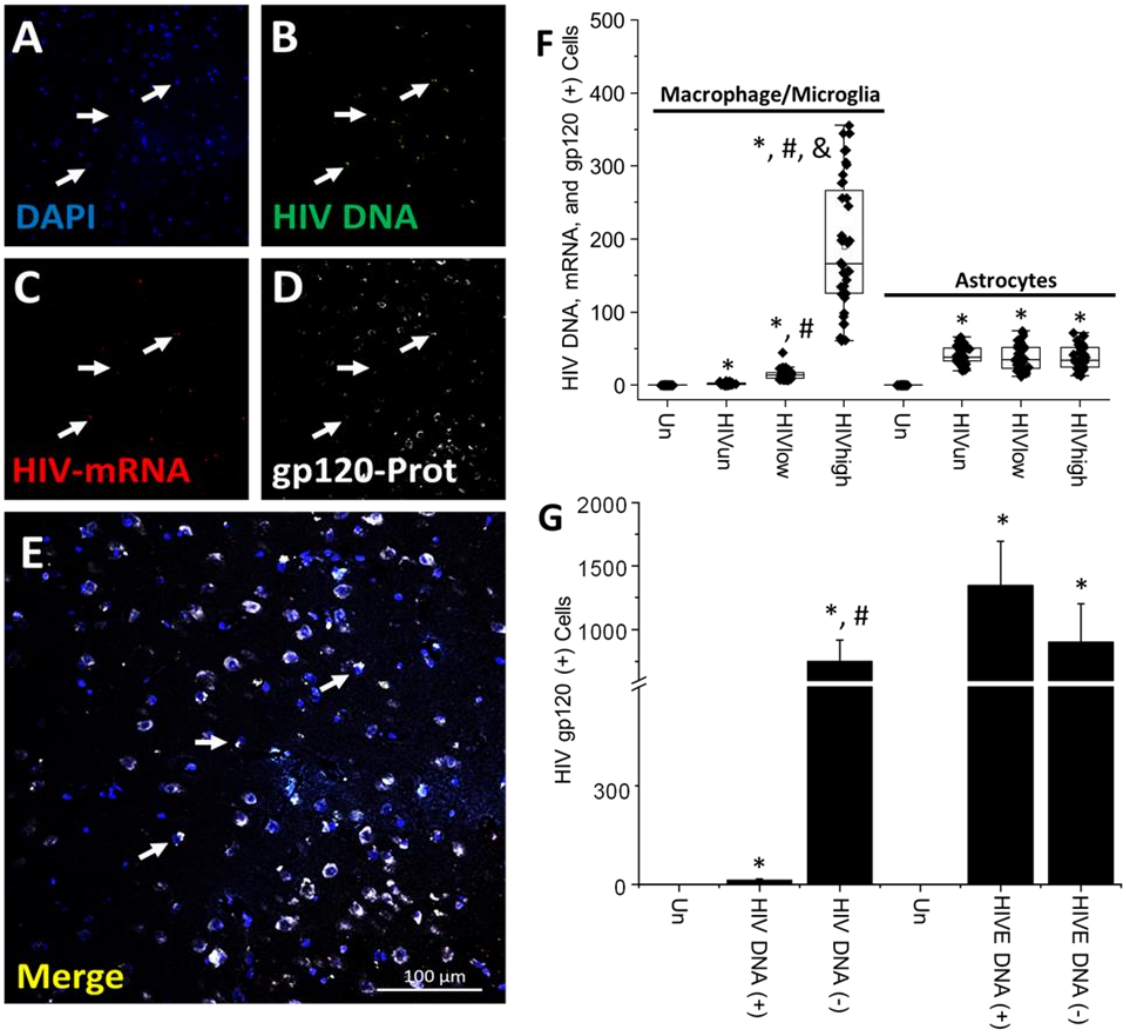

Figure 2.3. HIV-Gp120 protein is expressed in myeloid and glial viral reservoirs and surrounding uninfected cells: potential bystander toxicity under the current cART era

(A-E) Representative confocal images showing (A) DAPI staining, (B) HIV DNA, (C) microglia/macrophage marker Iba-1 protein, (D) HIV-Gp120 protein (arrows denote triple-positive cells), and (E) corresponds to the merge of all colors. (F) Quantified macrophage/microglia and astrocyte cells with HIV-integrated DNA, producing HIV-mRNA, and HIV-Gp120 according to the viral replication status, including undetectable, low and high replication *p≤0.005 compared to uninfected conditions, #p≤0.005 compared to HIV_{un} conditions, and &p≤0.005 compared to HIV_{un} or HIV_{low} conditions, n=34 tissues analyzed, and 21 tissues compared to uninfected tissues, Un (including also AD tissues), each point represent 3-5 different areas per tissue analyzed). HIVE total numbers were 1,364±279 cells, 876±458 for macrophages, and 624±287 for astrocytes under HIVE conditions (data not plotted). (G) Quantification of cells positive for HIV-Gp120 detected in uninfected cells (HIV DNA (-)) surrounding the clusters containing HIV-integrated DNA (HIV DNA (+)) corresponded to 750.61±164.85 cells, suggesting bystander damage within the CNS (*p≤0.005 compared to uninfected conditions and

#p≤0.005 compared to HIV DNA (+) cells). In contrast, only 10.45±3.65 cells with HIV-integrated DNA accumulated HIV-Gp120 protein. In HIVE conditions, cells with HIV-integrated DNA (HIVE-DNA (+)) were 1,364±349 cells, and uninfected cells (HIVE-DNA (-)) were 901±302 cells; thus, local numbers of cells containing HIV-Gp120 could be comparable to HIVE conditions but with a significantly lower expression or accumulation as well as extremely localized. Bar: 100 μm.

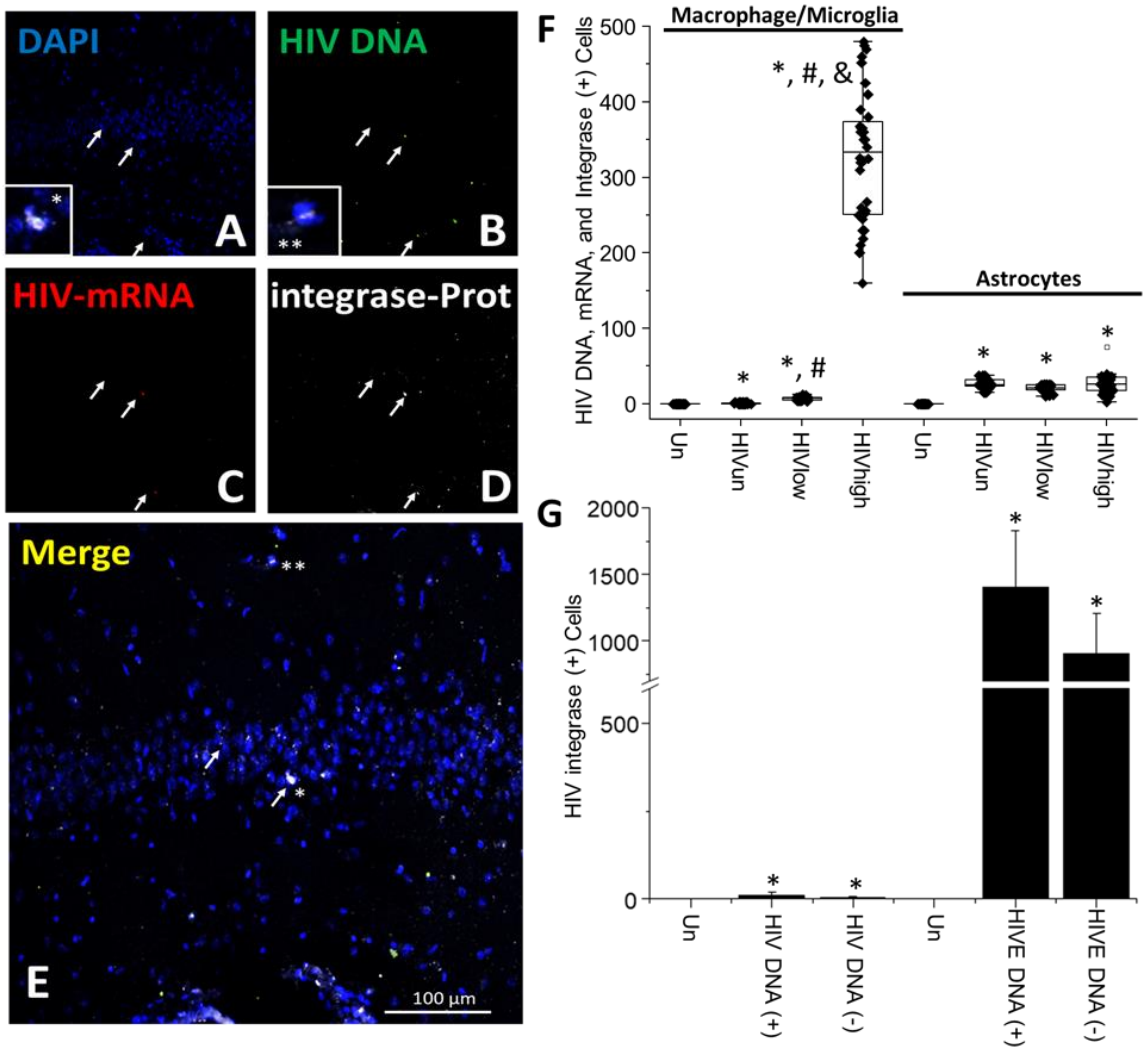

Figure 2.4. HIV-Integrase protein is poorly expressed in HIV-infected cells under cART

(A-E) Representative confocal images showing the expression and distribution of integrase in the HIV-infected cells, showing minimal to no expression of Integrase, where labeling corresponds to (A) DAPI, (B) HIV DNA, (C) HIV-mRNA, (D) HIV-Integrase protein, and (E) merge of all colors. White arrows indicate cells with HIV-integrated DNA. Asterisks indicate cells with high levels of cytoplasmic and nuclear Integrase protein. The insets indicate the colocalization of DAPI, HIV DNA, and Integrase. (F) Quantification of the cells with HIV-integrated DNA, viral mRNA, and HIV-Integrase protein according to its localization in macrophage/microglia or astrocytes in human brain tissues obtained from individuals with undetectable, low, and high viral replication *$p \leq 0.005$ compared to uninfected conditions, #$p \leq 0.005$ compared to HIV_{un} conditions, and &$p \leq 0.005$ compared to HIV_{un} or HIV_{low} conditions, n=34 tissues analyzed and 21 tissues compared to uninfected tissues, Un (including also AD tissues), each point represent 3-5 different areas per tissue analyzed). The quantification of the total numbers of cells in HIVE conditions was 1,406±425 cells, 905±357 cells were macrophages, and

569±299 cells were astrocytes (data not plotted). (G) Quantification of cells expressing HIV-Integrase protein detected in HIV positive and negative cells, 11.22±8.52 and 4.21±2.46 cells, respectively. In contrast, in HIVE conditions, most integrase was accumulated in HIV DNA positive cells, 1,406±425 cells (HIV DNA (+)), and HIV DNA negative cells (HIV DNA (-)) 904±305 cells, surrounding HIV-infected clusters. *$p \leq 0.005$ compared to uninfected conditions. Bar: 100 μm.

.

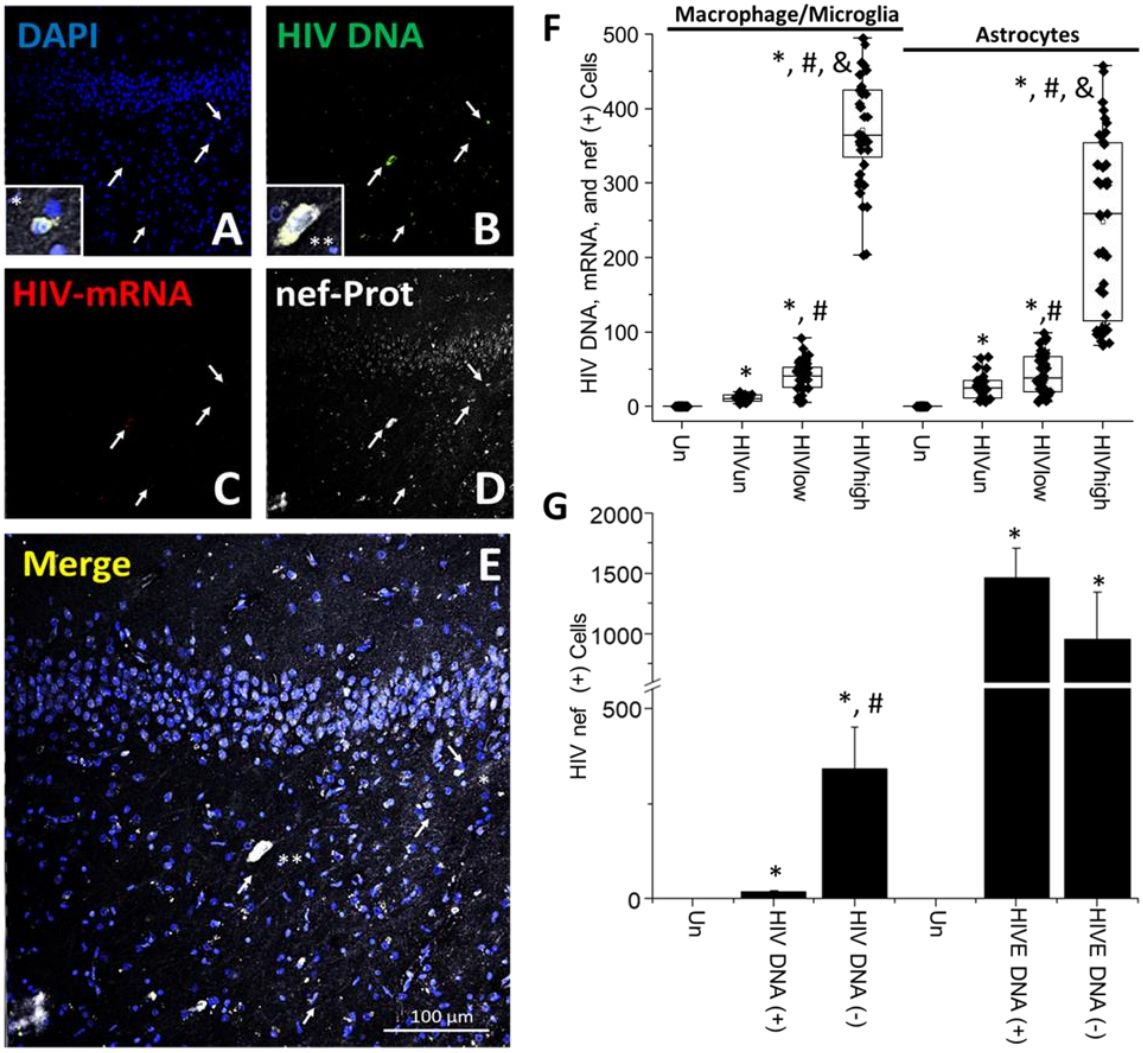

Figure 2.5. HIV-Nef is expressed in HIV-infected and surrounding uninfected cells, even in cART conditions

(A-E) Representative confocal images show the expression and distribution of Nef protein in the HIV-infected cells. Labeling corresponds to (A) DAPI, (B) HIV DNA, (C) HIV-mRNA, (D) HIV-Nef protein showing wide distribution in cells containing HIV-integrated DNA (white arrows) and cells without integrated DNA, and (E) merge of all colors. The asterisks represent cells with a high HIV-Nef protein expression. The insets show cells with DAPI, HIV DNA, and HIV-Nef protein. (F) Quantification of the cells with HIV-integrated DNA, viral mRNA, and HIV-Nef protein in macrophage/microglia and astrocyte cells according to the tissue analyzed based on systemic replication, including undetectable, low, and high replication (*$p \leq 0.005$ compared to uninfected conditions, #$p \leq 0.005$ compared to HIV_{un} conditions, and &$p \leq 0.005$ compared to HIV_{un} or HIV_{low} conditions, n=34 tissues analyzed and 21 tissues compared to uninfected tissues, Un (including also AD tissues), each point represent 3-5 different areas per tissue analyzed). (G) Quantification of cells positive for HIV-Nef protein in HIV-infected cells

(HIV DNA (+)) was 17.15±2.81 cells compared to neighboring uninfected cells (HIV DNA (-)) containing HIV-Nef protein 341.63±107.68 cells. This indicates a strong Nef expression within the CNS in the current cART era, especially in neighboring uninfected cells. *$p \leq 0.005$ compared to uninfected conditions, #$p \leq 0.005$ compared to HIV_{un} conditions. Bar: 100 μm.

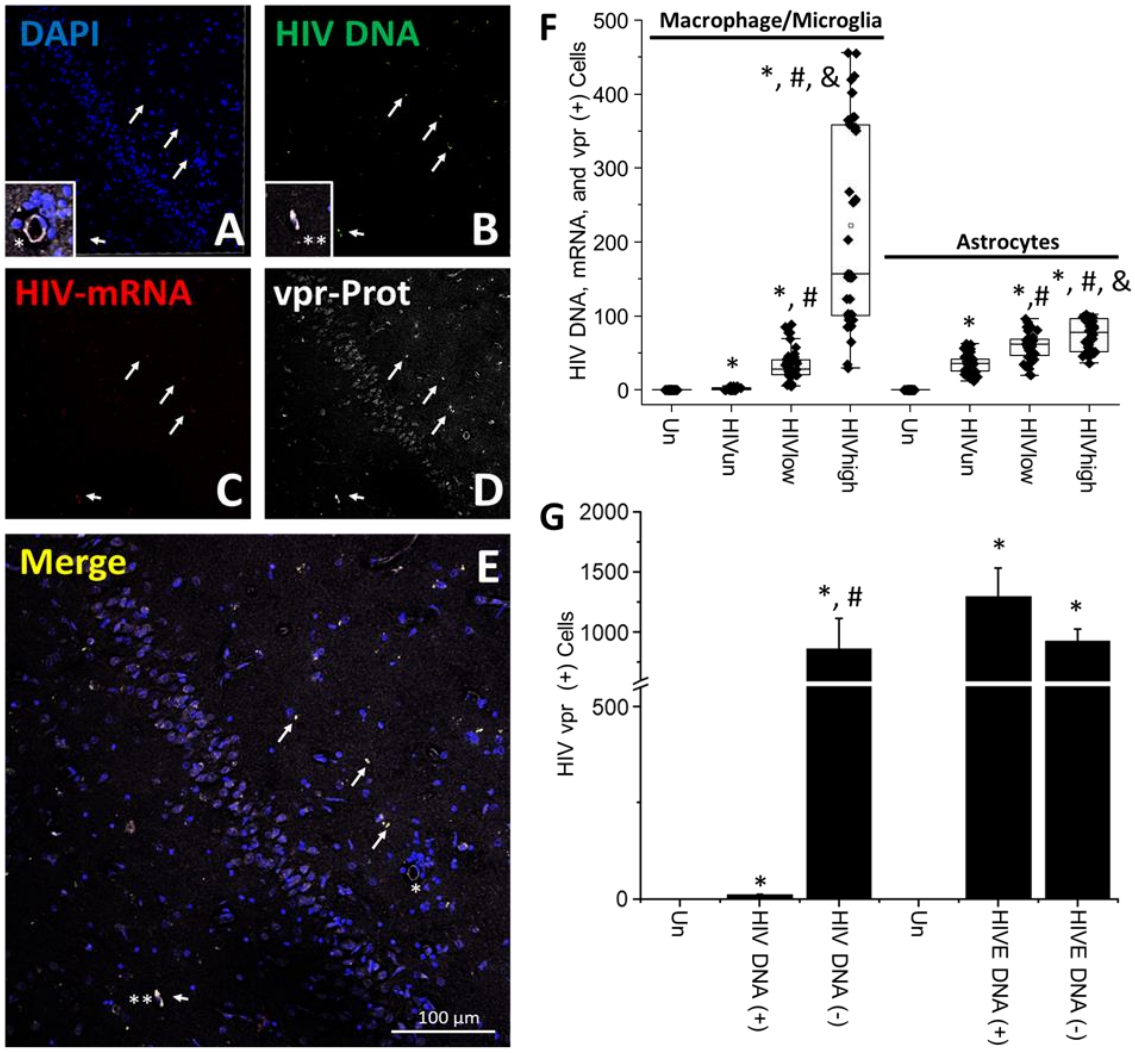

Figure 2.6. HIV-Vpr is expressed in HIV-infected cells under effective cART

(A-E) Representative confocal images show the expression and distribution of Vpr protein in the HIV-infected cells. We identified that HIV-Vpr was expressed in HIV-infected cells and cells without DNA. Labeling corresponds to (A) DAPI, (B) HIV DNA, (C) HIV-mRNA, (D) HIV-Vpr protein was not possible to establish a diffusion pattern like Gp120 and Nef proteins. HIV-Vpr positive cells were scattered within the brain (arrows represent HIV-infected cells producing HIV-Vpr, * or ** represent cells with high HIV-Vpr expression without association to HIV-infected cells), (E) merge of all colors. The insets indicate cells positive for DAPI, HIV DNA, and Vpr protein. (F) Quantification of cells with HIV-integrated DNA, producing HIV-mRNA and HIV-Vpr protein in macrophage/microglia and astrocyte cells according to the brain tissue analyzed based on systemic replication, including undetectable, low and high replication (*$p \leq 0.005$ compared to uninfected conditions, #$p \leq 0.005$ compared to HIV_{un} conditions, and &$p \leq 0.005$ compared to HIV_{un} or HIV_{low} conditions, n=34 tissues analyzed and 21 tissues compared to uninfected tissues, Un (including also AD tissues), each point

represent 3-5 different areas per tissue analyzed). In HIVE conditions, HIV-Vpr colocalized mostly with HIV-infected cells with total numbers (HIVE) of 1,289±245, macrophages 920±105 cells, and astrocytes 623±277 positive cells. (G) Quantification of cells expressing HIV-Vpr protein in uninfected cells (HIV DNA (-)) positive for Vpr was 855.83±257.45 cells around the clusters containing cells with HIV-integrated DNA, as compared to HIV DNA positive cells (HIV DNA (+)) with 9.68±2.70 cells, suggesting a bystander secretion and uptake (*$p \leq 0.005$ compared to uninfected conditions and #$p \leq 0.005$ compared to HIV DNA (+) cells). In HIVE conditions, quantification shows most Vpr was in cells with HIV-integrated DNA (HIVE-DNA (+)), with 1,289±245 cells, and minimal amounts present in uninfected cells (HIVE-DNA (-)), with 920±105 cells. Bar: 100 μm.

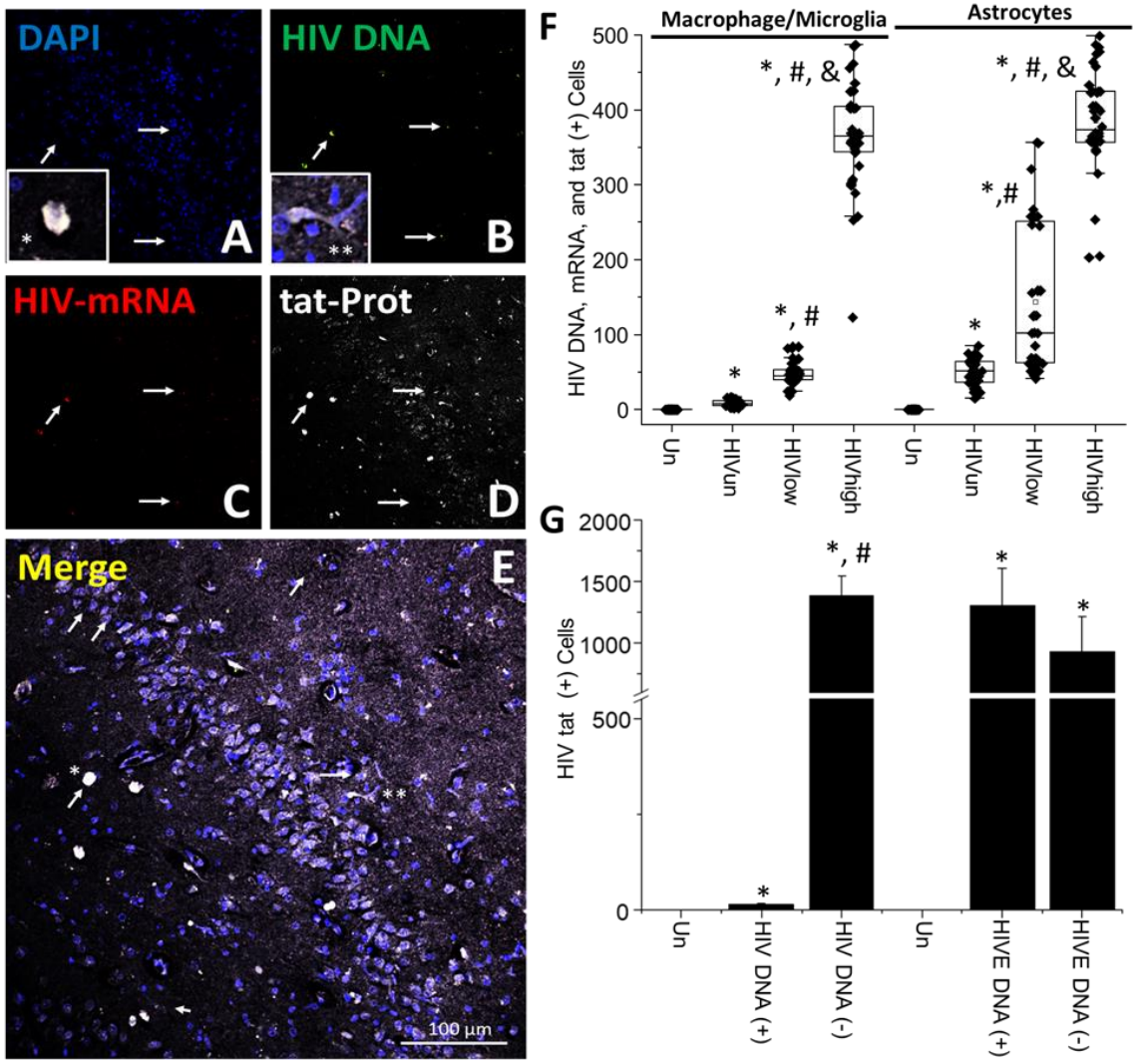

Figure 2.7. HIV-Tat protein is expressed within the CNS, even in the cART era

(A-E) Representative confocal images show the expression and distribution of Tat protein in the HIV-infected cells and surrounding uninfected cells. Labeling corresponds to (A) DAPI, (B) HIV DNA, (C) HIV-mRNA, (D) HIV-Tat protein showing diffusion from HIV DNA positive cells into neighboring uninfected cells (white arrows indicate cells with HIV-integrated DNA and * indicated cells without HIV-integrated DNA but highly positive for HIV-Tat), (E) merge of all colors. The insets indicate cells positive for DAPI, HIV DNA, and Tat protein. (F) Quantification of cells with HIV-integrated DNA, producing HIV-mRNA, and HIV-Tat in microglia/macrophages and astrocyte cells in brain tissues obtained from HIV-infected individuals with undetectable, low, and high replication (*p≤0.005 compared to uninfected conditions, #p≤0.005 compared to HIV_{un} conditions, and &p≤0.005 compared to HIV_{un} or HIV_{low} conditions, n=34 tissues analyzed and 21 tissues compared to uninfected tissues, Un (including also AD tissues), each point represent 3-5 different areas per tissue analyzed). In encephalitic conditions (HIVE), HIV-Tat colocalized mostly with HIV-infected cells, total numbers (HIVE,

1,193±244), macrophages/microglia (801±197 cells), and astrocytes (685±297 cells) (data not show). (G) Quantification of cells positive for Tat protein-containing HIV-integrated DNA (HIV DNA (+)) indicates only 13.96±3.65 cells, whereas 1,383.71±164.85 uninfected surrounding cells (HIV DNA (-)) contained Tat protein. A similar number of cells were found in HIV encephalitic brains (HIVE), 1,306±306 cells expressed Tat in HIV-infected cells (HIVE DNA (+)), and only 934±277 cells without HIV DNA showed HIV-Tat staining (HIV DNA (-), *$p \leq 0.005$ compared to uninfected conditions, #$p \leq 0.005$ compared to HIV DNA (+) cells. Bar: 100 μm.

DISCUSSION

HIV, as well as other viruses, has evolved to persist within the host. The major barrier to cure HIV infection is the early generation and extended survival of HIV reservoirs that remain undetectable in several cellular and anatomical sites (Denton, Sogaard et al. 2019). As discussed in the general introduction, most current techniques to detect viral reservoirs only identify one component of the viral cell cycle and require amplification or cell proliferation for efficient detection. Our method is extremely sensitive, reliable, and specific for all the components analyzed. It is useful to detect HIV DNA, viral mRNA, and proteins in a cell type-dependent manner and with high spatial resolution in brain tissues, even in tissues obtained from individuals under long-term infection and cART. Our findings provide a unique technique to detect and quantify viral reservoirs (silent, active, or with residual mRNA and protein production) within the CNS of HIV-infected individuals; to highlight the distribution of viral reservoirs within the brain; to quantify the cell types with HIV-integrated DNA and the ones with HIV-integrated DNA that still are producing viral mRNA and synthesizing proteins within the CNS of individuals under cART; to recognize several viral proteins, but not all that are produced, secreted, and taken up by neighboring uninfected cells; to prove that efficient systemic cART reduces the brain reservoir pool and prevents the synthesis of some viral proteins, and to quantify viral reservoirs within the CNS.

Overall, the numbers of detected viral reservoirs were lower than the described data in isolated microglia/macrophage and astrocytes (Churchill, Wesselingh et al. 2009, Thompson, Cherry et al. 2011, Castellano, Prevedel et al. 2017, Russell, Chojnacki et al. 2017). Thus, our data *ex vivo* may represent the more realistic number of viral reservoirs in HIV-infected individuals under effective cART, with low numbers of HIV-infected cells and minimal viral mRNA and protein synthesis. Also, in the current cART era, not

all the microglia/macrophages and astrocytes contain HIV. Thus, there is a selection mechanism that is not fully known.

An important point to discuss is that for the first time, we can detect basal synthesis and release of several HIV proteins in tissue samples from HIV-infected individuals under effective cART, with normal CD4 counts and undetectable systemic replication. This result is unique and validates the multiple papers describing the toxic and inflammatory effects of viral proteins in tissue cultures and animal models without active HIV replication (Kanmogne, Kennedy et al. 2002, Nath 2002, Jaeger and Nath 2012, Kovalevich and Langford 2012).

Contrary to the belief that viral reservoirs are only present in different kinds of $CD4^+$ T cells with low drug penetrance or biological barrier that enables survival and residual replication (Siliciano, Kajdas et al. 2003, Hosmane, Kwon et al. 2017, Bruner, Wang et al. 2019), the identification of infected microglia/macrophages and astrocytes indicate that several cells may be infected with HIV (Chauhan 2015, Kasparov 2016, Li, Henderson et al. 2016, Marban, Forouzanfar et al. 2016, Russell, Chojnacki et al. 2017, Barat, Proust et al. 2018, Ko, Kang et al. 2019, Wallet, De Rovere et al. 2019). In fact, numerous groups propose that circulating reservoirs may be a poor reflection of the actual/real viral reservoirs present in tissues (Churchill, Deeks et al. 2016, Lorenzo-Redondo, Fryer et al. 2016, Wang, Simonetti et al. 2018, Abdel-Mohsen, Richman et al. 2020, Chaillon, Gianella et al. 2020, Henderson, Reoma et al. 2020). Our laboratory indicated that macrophages of the urethral tissue and megakaryocytes could be infected as positive HIV-integrated cells (Ganor, Real et al. 2019). Furthermore, data from human macrophages identified several mechanisms of survival that are not present in $CD4^+$ T cells and require urgent examination. Recent data has demonstrated that a few HIV-infected astrocytes can amplify infection into the periphery, proving that although these reservoirs are low in numbers and highly compartmentalized, they can still repopulate the entire body with the virus (Lutgen, Narasipura et al. 2020, Valdebenito, Castellano et al.

2021). Thus, eliminating all viral reservoirs is required to achieve an HIV cure, including those present in the brain.

The brain has been proposed to be a major viral reservoir tissue due to its immune privilege and the presence of the blood-brain barrier that limits immune trafficking/surveillance and some cART drug penetration. In addition, a new understanding of the brain's role is emerging because at least 50% of the HIV-infected population has HAND signs, even in the current cART era. HIV-related neurocognitive disorders, deeply discussed in Part 2 of Chapter 1, have been associated with cART's neurotoxicity, chronic inflammation, comorbidities, presence of quiescent/latent infected cells, and residual production and secretion of viral proteins. However, most of these mechanisms have been examined using *in vitro* and several animal models, but whether these mechanisms are present *in vivo*, the extent of the associated damage or the amount of the viral reservoirs, and the viral protein synthesis is poorly explored in human tissues. Our findings show that cART can reduce the amount of the reservoirs in the brain, but residual viral protein synthesis and secretion are differentially affected by cART in a cell type-dependent manner.

In the human brain of HIV-infected individuals under cART, we identified that microglia/macrophages and a small population of astrocytes are the main cells with HIV-integrated DNA. We quantified the frequency of these HIV-infected cells in large tissue areas to provide a more accurate description of viral reservoirs within the brain in the current cART era. The imaging system's specificity enabled cell type identification, 3D reconstructions, and the evolution of several viral markers (HIV DNA, HIV-mRNA, and viral proteins) in a single analysis. Only one-third of the cells with HIV-integrated DNA expressed viral mRNA, and one-third of these double-positive cells synthetized viral proteins. Surprisingly, we identified viral proteins such as p24, Gp120, Nef, Vpr, and Tat accumulated in uninfected cells around HIV-infected cells suggesting an active local production, secretion, and bystander uptake. Our data also provided critical information

on residual viral protein expression and secretion into neighboring uninfected cells that support multiple *in vitro* data about the toxic role of viral protein even in the current cART era. Although HIV-infected microglia/macrophages (Castellano, Prevedel et al. 2017) and astrocytes (Eugenin, Clements et al. 2011, Eugenin, Basilio et al. 2012, Eugenin and Berman 2013, Eugenin 2014, Orellana, Saez et al. 2014) are protected from apoptosis by several mechanisms, including preventing the formation of the apoptosome, changing their metabolism, modifying the inter-organelle interactions and using cell-to-cell communication mechanisms to spread toxicity and local inflammation, neighboring cells undergo viral protein-mediated toxicity.

One of the consequences of HIV infection in the brain is neuronal cell death and CNS inflammation due to immune activation, oxidative stress, and neurotoxicity. It has been described that in the CNS, HIV infects astrocytes and macrophages/microglia, but not neurons. Several neurotoxic substances, especially HIV proteins (HIV-Tat, HIV-Gp120, and HIV-Nef) released by infected astrocytes and macrophages/microglia, induce cell death in neurons (Huang, Zhao et al. 2011, Wang, Zhang et al. 2017). These findings support multiple claims of bystander damage and cognitive impairment associated with HIV infection. It seems that eradicating viral reservoirs in the CNS is the major barrier to improving the treatment and complete recovery of HIV-infected patients' neurological function.

Further, we identified that long-term cART reduced the pool of myeloid viral reservoirs but minimally reduced the pool of HIV-infected astrocytes, supporting specific eradication mechanisms due to the significant differences in the anatomical sites.

In conclusion, our accurate identification, localization, and quantification process is essential for developing therapeutic strategies targeting specific areas of viral reservoirs and treating HIV comorbidities such as the neurocognitive manifestations seen in HAND.

CHAPTER 3 – CHRONIC BRAIN DAMAGE IN HIV-INFECTED INDIVIDUALS UNDER COMBINED ANTI-RETROVIRAL THERAPY IS ASSOCIATED WITH VIRAL RESERVOIRS, SULFATIDE RELEASE, AND COMPROMISED CELL-TO-CELL COMMUNICATION

D'Amico Daniela[1,2], Barone Rosario[2], Di Felice Valentina[2], Ances Beau M.[3], Prideaux Brendan [1], Eugenin Eliseo A.[1]

[1]University of Texas Medical Branch (UTMB), Department of Neuroscience, Cell Biology and Anatomy, Galveston, TX, USA

[2]University of Palermo (UniPa), Department of Biomedicine, Neuroscience and Advanced Diagnostics, Palermo, Italy

[3]Washington University School of Medicine, Department of Neurology, St. Louis, Missouri, USA.

The National NeuroAIDS Tissue Consortium (NNTC) and the NeuroBioBank provided all human samples. The NNTC is made possible through funding from the NIMH and NINDS by the following grants: Manhattan HIV Brain Bank (MHBB): U24MH100931; Texas NeuroAIDS Research Center (TNRC): U24MH100930; National Neurological AIDS Bank (NNAB); U24MH100292; California NeuroAIDS tissue Network (CNTN): U24MH100928; and Data Coordinating Center (DCC): U24MH100925. This work was funded by The National Institute of Mental Health grant, MH096625, MH128028, the National Institute of Neurological Disorders and Stroke, NS105584, and UTMB internal funding (to E.A.E).

Adapted paper: D'Amico D., Barone R., Di Felice V., Ances B. M., Prideaux B., Eugenin E. A. "Chronic Brain Damage in HIV-Infected Individuals under Combined Anti-Retroviral Therapy is Associated with Viral Reservoirs, Sulfatide Release, and Compromised Cell-to-Cell Communication". Cells Journal. Under the second review.

INTRODUCTION

The failure to eradicate HIV is due to latent viral reservoirs in different anatomical compartments, including the brain. Viral reservoirs can repopulate the body with the virus upon cART interruption (Wang and Xu 2021). We demonstrate in Chapter 2 that, even in the absence of viral replication, chronic HIV CNS injury is supported by long-lasting latent cells (microglia/macrophages and astrocytes) that continue to produce HIV mRNAs and viral proteins. The brain damage induced by HIV infection has been investigated using multiple techniques, including diffusion basis spectral imaging (DBSI), MRI/MRS, postmortem analyses, and cognitive assessment screening tools (Strain, Burdo et al. 2017). As we discuss in Chapter 1, in the chronic HIV-infected population under cART, most noninvasive imaging approaches proved a decrease in gray matter volumes and the presence of white matter microstructural abnormalities, called hyper-densities, compared to uninfected individuals (Underwood, Cole et al. 2017, van Zoest, Underwood et al. 2017). These hyper-densities areas have been associated with inflammation, compromised blood vessels, or mini "stroke" areas based on cellularity (Su, Wit et al. 2016, Eggers, Arendt et al. 2017, Strain, Burdo et al. 2017, Sanford, Strain et al. 2019). Furthermore, diffuse myelin pallor, diminished white matter tracts, and decreased myelin protein mRNAs can prove myelin sheath injury legitimizing HAND (Jensen, Monnerie et al. 2015). However, the nature and mechanism of CNS damage in the current cART were unknown.

To detect early signs of brain damage in HIV-infected individuals, several sera and CSF potential biomarkers have been proposed, including adenosine triphosphate (Velasquez, Prevedel et al. 2020), neurofilament light chain (Freeman, Castro et al. 1986, Abdulle, Mellgren et al. 2007, Jessen Krut, Mellberg et al. 2014, Gisslen, Price et al. 2016, Yilmaz, Blennow et al. 2017, Guha, Mukerji et al. 2019), β-Amyloid$_{1-42}$ (de Almeida, Ribeiro et al. 2018, Howdle, Quide et al. 2020), calcium-binding protein B (Du

Pasquier, Jilek et al. 2013, Guha, Mukerji et al. 2019), extracellular vesicles (Guha, Mukerji et al. 2019, Urbanelli, Buratta et al. 2019), and the wnt-related proteins (Al-Harthi 2012). Other groups identified immune markers such as soluble CD14 (Lyons, Uno et al. 2011, Jumare, Akolo et al. 2020), soluble CD163 (Burdo, Lentz et al. 2011, Burdo, Weiffenbach et al. 2013, Perez-Santiago, Schrier et al. 2016, Jumare, Akolo et al. 2020), neopterin (Valcour, Ananworanich et al. 2013, Farhadian, Patel et al. 2017), Cathepsin B (Cantres-Rosario, Plaud-Valentin et al. 2013), kynurenine to tryptophan ratio (Adu-Gyamfi, Snyman et al. 2017, Gelpi, Hartling et al. 2017, Scheri, Fard et al. 2017, Adu-Gyamfi, Snyman et al. 2020, Adu-Gyamfi, Savulescu et al. 2021), monocyte chemoattractant protein-1 (Eugenin, Osiecki et al. 2006, Williams, Eugenin et al. 2012, Burlacu, Umlauf et al. 2020), Tumor Necrosis Factor Alpha (Oliveira, Chaillon et al. 2017, Jumare, Akolo et al. 2020), interleukin-6 (Oliveira, Chaillon et al. 2017, Burlacu, Umlauf et al. 2020), interferon-γ-Inducible Protein (Yuan, Liu et al. 2015, Burlacu, Umlauf et al. 2020), interleukin-8 (Yuan, Liu et al. 2015, Ozturk, Kollhoff et al. 2019), interleukin-1 (Mamik, Banerjee et al. 2011, de Almeida, Rotta et al. 2016), interferon Alpha (Cassol, Misra et al. 2013, Anderson, Lennox et al. 2017), intercellular adhesion molecule-5 (Yuan, Wei et al. 2017), lipopolysaccharide (Lyons, Uno et al. 2011, Vassallo, Dunais et al. 2013) and several growth factors (Kallianpur, Gittleman et al. 2019). Despite the long list of potential biomarkers of HIV CNS disease, most are associated with late events of tissue destruction or significant immune activation. However, no clear biomarkers can predict early or chronic stages of CNS compromise or explain chronic CNS damage in the current cART era when systemic viral replication is low to undetectable.

Only recently, our group demonstrated that one of these mechanisms of chronic brain damage is also mediated by gap junction (GJ) and hemichannel (HC) from a few HIV-infected astrocytes into neighboring uninfected cells even in the absence of viral replication (Eugenin, Clements et al. 2011, Eugenin and Berman 2013, Berman, Carvallo

et al. 2016, Malik, Theis et al. 2017, Gorska, Donoso et al. 2021, Malik, Valdebenito et al. 2021, Valdebenito, Castellano et al. 2021). We identified that residual expression of HIV-tat upregulates connexin43 (Cx43) expression (Berman, Carvallo et al. 2016), resulting in enhanced GJ and HC communication enabling the diffusion of toxic host factors into vast areas of the brain (Eugenin and Berman 2007, Eugenin, Clements et al. 2011, Eugenin and Berman 2013, Castellano and Eugenin 2014, Eugenin 2014, Berman, Carvallo et al. 2016, Malik, Theis et al. 2017, Malik, Valdebenito et al. 2021). We demonstrated that HIV-infected astrocytes and microglia are the reservoirs within the brain. These cells are protected from apoptosis by regulating the formation of the transition pore on the mitochondria, the secretion of cytochrome C to form the apoptosome, the inter-organelle interactions to prevent overactivation, and their metabolism and viral replication (Malik, Theis et al. 2017, Eugenin 2019, Malik, Valdebenito et al. 2021).

However, the role of sulfatide in the control of Cx43 GJ in NeuroHIV is unknown.

In a similar manner to other neurocognitive diseases (Adibhatla and Hatcher 2007, Xicota, Ichou et al. 2019), HIV-associated neurocognitive disease has been linked to lipid dysregulation, including structural, signaling, and circulating lipids (Bandaru, Mielke et al. 2013, Kelesidis and Currier 2014, Kearns, Gordon et al. 2017). Thus, we propose that HAND is dependent on the viral reservoirs present within the brain, and one of the mechanisms of damage amplification is mediated by host lipids. Data from our laboratory also supported our interest in structural/signaling lipids and showed peripheral lipid dysregulation in HIV-infected patients. The levels of PGE_2 (a bioactive eicosanoid lipid mediator) in the sera of HIV-infected individuals virally suppressed with cART were elevated compared to the uninfected individuals (Velasquez, Prevedel et al. 2020). In addition, PGE_2 secretion in the media of the peripheral blood mononuclear cells isolated from HIV-infected individuals or isolated from uninfected individuals and stimulated

with HIV-Gp120 protein was higher than the secretion obtained in PBMCs isolated from uninfected individuals (Velasquez, Prevedel et al. 2020). PGE_2 is an eicosanoid synthetized from arachidonic acid (AA) *via* cyclooxygenase 2 and prostaglandin E synthase. It is a potent inflammatory lipid mediator (Park, Pillinger et al. 2006) that, according to our laboratory data, can be secreted *via* pannexin 1 (Panx-1) channels into the extracellular space (Velasquez, Prevedel et al. 2020), where it binds to E-prostanoid (EP) receptors to trigger toxic signaling pathways into the neighboring cells (Andreasson 2010). Thus, we used MALDI-MSI with a high spatial resolution and high mass accuracy to investigate altered structural/signaling lipid distribution in HIV-infected brain tissues compared to uninfected controls. We used an untargeted lipidomics approach to identify the major lipid spectral peaks corresponding to sulfatide highly abundant in the brain.

In this chapter, we demonstrate that HIV reservoirs, myeloid and glial, locally compromise the myelin sheath resulting in the release of sulfatide species, but not myelin basic protein (MBP) and proteolipid proteins (PLP), into the extracellular space. MBP and PLP are involved in myelin compaction to generate the closely apposed multilayered structure of mature myelin (Fulton, Paez et al. 2010). Previously, in multiple sclerosis, we demonstrated that soluble MBP is an inflammatory stimulus that results in microglial activation and associated inflammation (D'Aversa, Eugenin et al. 2013). However, the role of Sulfatide in NeuroHIV is unknown.

Sulfatide is a glycosphingolipid class that exhibits a galactosyl-3-O-sulfate polar head group and a ceramide moiety composed of a fatty acid and a long-chain base (Ishizuka 1997). Sulfatide is highly expressed in brain tissue (Isaac, Pernber et al. 2006) and is mainly localized in the myelin sheath (Moyano, Li et al. 2014), composed of 70% to 85% of phospholipids, cholesterols, and complex sphingolipids in a particular proportion (Folch-Pi 1972, Dupree and Pomicter 2010, Darios, Mochel et al. 2020). Sulfatide and the enzymes involved in its synthesis and degradation have been associated with several diseases, including brain cancer, subcortical dementia (Svensson, Blomqvist

et al. 2021), multiple sclerosis (Novakova, Singh et al. 2018), endothelial damage (Li, Hu et al. 2015), Alzheimer's disease (Flirski and Sobow 2005, Jonsson, Zetterberg et al. 2010), and Parkinson's disease (Fabelo, Martin et al. 2011). Also, like MBP and PLP, there are a description of autoreactive NK (Stax, Tuengel et al. 2017) and γδ-T cells (Luoma, Castro et al. 2013) cells to sulfatide, suggesting that our immune system is not sufficiently exposed to this lipid antigen.

In this chapter, we hypothesize that HIV reservoirs compromise myelin structures resulting in the release of sulfatide. Soluble sulfatide compromised gap junctional communication and calcium waves, promoting the amplification of chronic CNS damage observed in the HIV-infected population under cART.

MATERIALS AND METHODS

Human tissue sections and myelin structure analysis

Human brain tissues were obtained from the NeuroBioBank (https://neurobiobank.nih.gov/) and the National NeuroAIDS Tissue Consortium (NNTC; https://www.nimh.nih.gov/about/organization/dar/hiv-neuropathogenesis-genetics-and-therapeutics-branch/national-neuroaids-tissue-consortium). The patient information is summarized in Table 2 and for all tissues analyzed the postmortem interval was similar, <24 h. Frozen fresh tissues were cut in 25 μm thick serial sections using a Leica CM1850 cryostat (Buffalo Grove, IL) and thaw-mounted onto frosted glass microscope slides. Serial sections were fixed with PFA 4% (Cat# 15710-S, Electron Microscopy Science, Hatfield, PA) for 20 min and stored at 4°C. The first two serial sections of human frontal cortex fixed tissues were stained for Luxol fast blue, and Hematoxylin and Eosin by the UTMB anatomical pathology core facility and scanned with the NanoZoomer.2ORS (Hamamatsu Photonics, Japan). Subsequent serial sections were incubated with proteinase K (Cat# AM2546, Thermo Fisher Scientific, Waltham, MA) for 10 min at RT,

then the HIV DNA probe hybridization (Nef-PNA Alexa 488, Alexa488-GCAGCTTCCTCATTGATGG, PNA Bio, Thousand Oaks, CA) was perfomed. The probe was washed in preheated stringent wash working solution (PNA ISH kit, Cat# K520111-2, Dako products-Agilent Technologies, Santa Clara, CA) diluted at 1:60 at 55°C. To perform antigen retrieval, the sections were incubated in antigen retrieval solution (Cat# S1700, Dako products-Agilent Technologies) at 80°C for 30 min and permeabilized with Triton X-100 (Cat# X-100, Sigma-Aldrich, St. Luis, MO) 0.1% in TBS for 10 min. To block unspecific Fc receptor and other unspecific binding sites, our blocking solution contained: 1 ml 0.5 M EDTA pH 8.0 (Cat# 15575-038, Thermo Fisher Scientific), 100 µl gelatin from cold-water fish skin (Cat# G7765, Sigma-Aldrich), 0.1 g bovine serum albumin (BSA immunoglobulin-free, Cat# A2058, Sigma-Aldrich, or BSA fraction V, Cat# BP1605, Thermo Fisher Scientific), 100 µl horse serum (Cat# H1138, Sigma-Aldrich), 5% human serum (Cat# MT35060CI, Thermo Fisher Scientific), and 9 ml ddH_2O was used to incubate the sections for at least 1 h at room temperature or overnight at 4°C. Then the primary antibodies (MBP, anti-mouse, diluted 1:500, Cat# 5M199, BioLegend, San Diego, CA; PLP, anti-mouse, diluted 1:200, Cat# MAB388; RRID: AB_177623, Millipore) were used to treat the sections overnight at 4°C. The slides were washed several times with TBS at room temperature and incubated with the appropriate secondary antibodies conjugated for 2 h, followed by several washes in TBS. Then, tissues were mounted using Prolong Diamond Antifade Mount Medium (Cat# P36930, Thermo Fisher Scientific). Tissues were examined by confocal microscopy using an A1 Nikon with a spectral detection system (Tokyo, Japan). Analysis and quantifications of 3D reconstructions were performed using NIS Elements (Japan) and ImageJ software.

MALDI-MSI analysis

Serial sections of the unfixed human brain tissues were cut at 12 µm using a Leica CM 1860 cryostat and thaw-mounted onto stainless steel slides. After sectioning, tissues were placed in a desiccator for 15 min and then transferred to a -80°C freezer for storage. Prior to MALDI-MSI analysis, the thaw-mounted tissue sections were removed from the -80°C freezer and allowed to reach room temperature for 15 min. 1,5-Diaminonaphthalene (D21200, Sigma-Aldrich) dissolved in 70% Acetone (34850, Sigma-Aldrich) was used as a matrix for negative ion mode lipid imaging. This matrix was applied to the tissue by automated air spray deposition using the TM-sprayer (HTX Technologies LLC, Chapel Hill, NC). The nozzle temperature was set to 60°C, the flow rate was 50 µl/min, and 20 passes over the tissue were performed. MALDI-MSI analysis was performed using Q Exactive HF Hybrid Quadrupole-Orbitrap Mass Spectrometer (Thermo Fisher Scientific) equipped with an Elevated Pressure Matrix-Assisted Laser/Desorption Ionization (EP MALDI) source integrating an Nd: YAG laser (Spectroglyph LLC, Kennewick, WA). Data were acquired at 40 μm^2 lateral resolution in negative ion mode at a laser power of 7 µJ. External mass calibration was performed using calibration solutions (Cat# A39239, Thermo Fisher Scientific). The accurate mass-measured lipid peaks were identified by matching reference lipids in the LIPID MAPS and Human Metabolome Database within a ±0.002 Da mass tolerance window. Thermo RAW format data files were converted to imzML using ImageInsight software (Spectroglyph LLC, Kennewick, WA). Data visualization was performed using SciLs software (SCiLS GmbH, Bremen, Germany).

Cell Culture Methods

Cortical human fetal tissue was obtained as part of a research protocol approved by the Albert Einstein College of Medicine and collected between 2011 to 2018 (Protocol Approved for EAE). As previously described, human astrocyte cultures were prepared

(Eugenin and Berman 2007). High glucose Dulbecco's modified Eagle's medium (DMEM, Cat# 11995-065, Thermo Fisher Scientific) supplemented with 10% fetal bovine serum (FBS, Cat# S12450H, Atlanta Biologicals, Flowery Branch, GA), penicillin, and streptomycin (Cat# 15070063, Thermo Fisher Scientific) were used to grow the cells at 37°C in a humidified atmosphere with 5% CO_2. The sulfatide used was a commercial mix derived from the bovine brain, and the concentration selected was based on its lower pathological action of abnormally released lipid components at sites of injured and/or inflamed brain lesions (Jeon, Yoon et al. 2008)

HIV infection

Confluent cultures of human astrocytes were infected by incubation with HIV_{ADA} (20–50 ng/ml HIV-p24), using a previously described protocol (Eugenin, Clements et al. 2011, Valdebenito, Castellano et al. 2021). Briefly, astrocyte cultures were exposed to the virus for 24 h, the medium was removed, and astrocytes were washed extensively to eliminate the unbound virus before adding a fresh medium. The media was collected on day 7 post-inoculation.

Calcium Imaging

Human primary astrocytes are seeded in 35 mm Glass Bottom MatTek Dishes (Cat# P35G-1.5-14-C, MatTek Corporation, Ashland, MA). The confluent cells were transferred to a temperature-regulated chamber at 37°C of the confocal microscope Nikon A1 and incubated with 10 μM fluo-4 diluted in DMSO (Cat# F14201, Thermo Fisher Scientific); photometric data for $[Ca^{2+}]$ were generated by exciting cells at 488 nm and measuring emission at 516 nm every 5 sec for 20 min. An intracellular calibration was performed with each experiment by determining the fluorescence in the absence of a Ca^{2+} indicator (fluorescencemin) for 5 min and the presence of 3.6 μM ATP (Cat# A1852, Sigma-Aldrich), and 2 μM ionomycin (fluorescencemax) (Cat# I3909, Sigma-Aldrich).

The mean [Ca^{2+}] was determined from three independent plate areas and analyzed 20 cells per position.

Total mRNA isolation

Human primary astrocytes were treated with sulfatide 10 μg/ml (Cat# 24323, Cayman Chemical, Ann Arbor, MI) for 6, 12, and 24 h. This concentration was chosen according to lower pathological levels detected in non-myelinated areas of virologically suppressed HIV-infected individuals. Untreated and treated cells were harvested in TRI reagent (Cat# 93289, Sigma-Aldrich) according to the manufacturer's instructions. Cells were scratched in TRI reagent (1 ml for 60 mm well plate), and 0.2 ml of chloroform (Cat# 288306, Sigma-Aldrich) were added to the samples. After 3 min, the mixtures were transferred to 1 ml Eppendorf containing 0.5 ml pf phase-lock gel (Cat# 2302830, QuantaBio, Beverly, MA) and centrifuged at 12000 x g for 15 min at 4°C to separate the RNA (aqueous phase) from proteins (red organic phase) and DNA (interphase). The aqueous phase was transferred to a fresh tube containing 0.5 ml of isopropanol (Cat# 278475, Sigma-Aldrich). After 10 min, the samples were centrifuged at 12000 x g at 4°C for 15 min. The supernatant was removed, and 1 ml of 75% ethanol (Cat# 51976, Sigma-Aldrich) was added to the RNA pellet at the bottom of the tube. The mixture was centrifuged at 7500 x g at 4°C for 5 min. The RNA was eluted from the filter in 100 μl of DEPC-treated water (Cat# AM9938, Thermo Fisher Scientific) and warmed for 10-15 min at 60°C to fully dissolve. The RNA extract obtained was stored at -20°C until use. The concentration of each sample was calculated by spectrophotometric analysis (OD 260/280) using NanoDrop 2000 UV-Vis Spectrophotometer (Thermo Fisher Scientific).

Reverse Transcription PCR

Reverse transcription for first-strand cDNA synthesis was performed using the SuperScript III First-Strand (Cat# 18080-051, Thermo Fisher Scientific) according to the

manufacturer's instructions. 50 µM oligo (dT) was complexed with 2 µg of total RNA in a final volume of 10 µl. Samples were incubated at 65°C for 5 min and then placed on ice for at least 1 min. 10 µl of cDNA synthesis mix (containing 10x RT buffer, 2 mM MgCl2, 0.1 M DTT, 40 U/µl RNaseOUT, 200 U/ µl SuperScript III RT) was added before the use of the Thermocycler (50°C for 50 min, 85°C for 5 min) (Cat# 170-9703, BioRad, Hercules, CA). The cDNA obtained was stored at -20°C until use.

Quantitative real-time PCR (qRT-PCR)

The amplified cDNA was used to amplify and quantify GAPDH, Cx43, and ZO-1 mRNA expression by qRT-PCR using ABsolute Blue qPCR SYBR low ROX mix (Cat# AB4323A, Thermo Fisher Scientific) in a StepOnePlus Real-Time PCR system (Cat# 4376600, Thermo Fisher Scientific). The primers used correspond to human GAPDH forward: 5′-CTTGACGGTGCCATGGAATTTG-3′, GAPDH reverse: 5′-GGGTTAAGGGAAAGAGCGACC-3′; Cx43 forward: 5′-CCCCATTCGATTTTGTTCTGC-3′, Cx43 reverse: 5′-GGGTTAAGGGAAAGAGCGACC-3′; ZO-1 forward: 5′-TTTTAGGATCACCCGACGAC-3′; ZO-1 reverse: 5′-CGCCTTTGGACAAAGAGAAG-3′. The program used was denaturation for 15 min at 95°C and 40 cycles of denaturation, 30 sec at 95°C; anneal, 30 sec at 56°C; and amplification, 30 sec at 72°C. According to the CT values, expression was determined using the ΔΔCT method (Applied Biosystems, Life Technologies).

Western blotting

Human primary astrocytes untreated and treated with sulfatide for 6, 12, and 24 h were harvested in RIPA buffer (Cat# 9806, Cell Signaling, Danvers, MA) containing protease and phosphatase inhibitors (20 mM; pyrophosphate, 20 mM; NaF, 100 mM; NaVO3, 200 µM; leupeptin, 500 µg/ml; aprotinin, 40 µg/ml; soybean trypsin inhibitor, 2

mg/ml; benzamidine, 1 mg/ml; ω-aminocaproic acid, 1 mg/ml; PMSF, 3 mM; and EDTA, 20 mM) and lysed. The protein content of each cell lysate was determined using Bradford's method (Bio-Rad Labs). Samples containing 10 μg of protein were digested with 30 U of bovine intestinal alkaline phosphatase (Cat# P0114-10KU, Sigma-Aldrich) for 20 h at 4°C to eliminate the Cx43 phosphorylation and collapse all the isoforms into the non-phosphorylated isoform (Matesic, Rupp et al. 1994, Moreno, Saez et al. 1994, Mikalsen and Kaalhus 1996). Other undigested samples were used to analyze human Cx43, ZO-1, and GAPDH total protein levels. Proteins were separated in 7.5 % SDS-PAGE and transferred to a nitrocellulose membrane, incubated sequentially with a blocking solution (5% non-fat milk in Tris-buffered saline). Antibodies anti-Cx43 (anti-rabbit, dilution 1:1000, Cat# C6219, RRID:AB_476857, Sigma-Aldrich, St. Luis, MO), anti-ZO-1 (anti-rabbit, dilution 1:1000, Cat# 40-2200, RRID:AB_2533456, Thermo Fisher Scientific), anti-GAPDH (anti-rabbit, dilution 1:1000, Cat# 2118, RRID:AB_561053, Cell Signaling), and anti-rabbit IgG conjugated to HRP (dilution 1:1000, Cat# 7074, RRID:AB_2099233, Cell Signaling) were used. Antigen-antibody complexes were detected by ECL (Cat# NEL103E001EA, Perkin Elmer, Boston, MA). The resulting immunoblot signals were scanned, and densitometric analysis was performed using Image Studio Lite Ver 5.2 software. All results were normalized to the values obtained for control conditions.

Immunofluorescence

Human primary astrocytes were grown on coverslips and treated with sulfatide (resulting in a final concentration of 10 μg/ml) for 6, 12, and 24 h. Untreated and sulfatide-treated cells were fixed with 4% PFA (Cat# 15710-S, Electron Microscopy Science, Hatfield, PA) and permeabilized in 0.1% Triton (Cat# X-100, Sigma-Aldrich) for 2 min at room temperature. Cells were incubated in blocking solution (0.5 M EDTA pH 8.0; Cat# 15575-038, Thermo Fisher Scientific), 1% fish gelatin from cold water

(Cat# G7765, Sigma-Aldrich), 0.1 g albumin from bovine serum-immunoglobulin free (Thermo Fisher Scientific), 1% Horse Serum (Cat# H1138, Sigma-Aldrich), 5% human serum (Cat# 31876, Thermo Fisher Scientific), 9 ml ddH20) overnight at 4°C and then in diluted primary antibodies (anti-Cx43, anti-rabbit, dilution 1:1000, Cat# C6219, RRID:AB_476857, Sigma-Aldrich, St. Luis, MO; anti-ZO-1, anti-mouse, dilution 1:200, Cat# MABT11, RRID: AB_10616098, Millipore) overnight at 4°C. Cells were washed several times with PBS (Cat# BP665-1, Thermo Fisher Scientific) at RT and incubated with the appropriate secondary antibodies (Phalloidin 680, dilution 1:2500, Cat# A22286, Thermo Fisher Scientific) for at least 2 h at room temperature followed by several washes in PBS. Cells were then mounted using Prolong Gold anti-fade reagent (Cat# P36930, Thermo Fisher Scientific) and examined using an A1 confocal microscope with a spectral detection device (Nikon, Japan). Antibody specificity was confirmed by replacing the primary antibodies with the appropriate isotype-matched control reagent, anti-IgG2A, or the IgG fraction of normal mouse/rabbit serum (Cat# A2179, RRID: AB_257981/ Cat# A0418, RRID: AB_257885, Sigma-Aldrich).

Scrape loading assay

The functionality of GJ channels was evaluated by scrape loading using a previously published protocol [85]. In brief, 0.5% Lucifer yellow (a fixable dye permeable to GJs, 5% w/v in 150 mM LiCl; 520-Da dye, Cat# L0144, Sigma-Aldrich), and Dextran-Alexa Fluor 594 (dye not permeable to gap junctions; 10,000 k.Da., Cat# D22913, Thermo Fisher Scientific) dissolved in PBS were added to confluent primary astrocytes treated with sulfatide for 6, 12 and 24 h, and a scrape using a blade was performed. The dye solution was left on the cells for 5 min and discarded, and the plate was rinsed with PBS. Gap junctional permeability was also inhibited by adding the blocker 18-α-glycyrrhetinic acid (AGA, 50 μM in DMSO, Cat# G8503, Sigma-Aldrich) or 1-Octanol (0.5 mM, Cat# 297887, Sigma-Aldrich) for 5 min in the media before dye

permeabilization. To examine the unspecific uptake of LY from the media, plates were prepared by exposing the cells under similar conditions to the dye mixture but without scraping. The marker dye, dextran-Alexa Fluor 594, remained entrapped, thus labeling the primary loaded cells at the edge of the scrape areas. The damaged cells could pick up the dye mixture and transfer LY into the neighboring cells through functional GJ. The distance or LY diffusion from the damaged area was normalized by the distance or diffusion of the impermeable dextran-Alexa Fluor 594 and measured using the confocal microscope Nikon A1. The percentage of coupling was calculated by direct comparison to untreated cultures.

Statistical Analysis

All data were expressed as mean ± standard deviation (SD). Differences among groups were analyzed using a t-test with Welch's Correction or the Holm-Sidak method (alpha = 0.05) and 2way ANOVA Tukey's/Dunnett's/Bonferroni's multiple comparisons test. The level of significance was accepted at $p \leq 0.05$. GraphPad Prism 8 software was used for the statistical analyses performed.

RESULTS

Demographics of the samples analyzed

Table 2 summarizes the demographics of the individuals. The samples were obtained from the National NeuroAIDS Tissue Consortium (NNTC) and the NeuroBiobank. The population analyzed did not show differences among the uninfected normal and the HIV-positive groups with MND (HIV-MND) and HAD in age, except for the uninfected with Alzheimer's disease (AD) group that includes two young and two old subjects (HIV-negative, mean=45±4.7 years; HIV-positive with MND, mean=50±6.1 years; HIV-positive with HAD, mean=51±6.6 years; HIV-negative-Alzheimer's disease=

63±17.8 years; Table 2), and gender (HIV-positive=37.5% female and 62.5% male; HIV-negative=50 % female and 50% male; Table 2). The HIV-positive cohort had an average of 11.5±5.4 years living with HIV for the MND group and 9±9.6 for the HAD group. HIV-MND cohort had a mean plasma HIV RNA of 4±1.4 log copies/ml and 2.6±0.9 log copies/ml in the plasma and CSF, respectively, and an average CD4 count of 199±262.6 cells/mm^3. The HAD cohort had a mean plasma HIV RNA of 3.3±1.9 log copies/ml and 3.4±1.6 log copies/ml in the plasma and CSF, respectively, and an average CD4 count of 47.3±47.8 cells/mm^3 (see Table 2).

Myelin structure is compromised in the brain areas containing HIV reservoirs

Several laboratories using different imaging and histological techniques demonstrated that HIV-infected individuals under cART show localized damage or hyper-densities in white matter (WM) (Erten-Lyons, Woltjer et al. 2013, Behrman-Lay, Paul et al. 2016, Boerwinkle and Ances 2019). To determine whether our HIV brain tissues obtained from individuals with and without cognitive impairment (HIV-MND and HAD) had WM compromise, we analyzed the status of the myelin tracks compared to uninfected (control) and Alzheimer's disease tissues (AD). Alzheimer's brain tissues were included as a positive control for demyelination due to the severity of the selected cases. Serial sections of the prefrontal cortex were selected due to documented synaptic-dendritic damage in HIV-infected individuals (Irollo, Luchetta et al. 2021). Gross histological analysis was performed using the Luxol Blue and H&E staining (Fig. 3.1 A-H). Luxol Blue stains myelin lipoproteins in blue and the neurons in violet (Fig. 3.1 A-D). A remarkable separation between the grey and white matter was observed in brain tissues obtained from control-uninfected and HIV-MND/HAD individuals (Fig. 3.1A, B, and C). In the brain tissues obtained from individuals with severe Alzheimer's disease, WM and GM could not be delineated based on either the Luxol blue or H&E-stained images (AD, Fig. 3.1 D, and H) due to the demyelination process. Confocal and image

analysis for MBP (Fig. 3.1I-L, WM/GM interface is indicated in white lines) and PLP (Fig. 3.1M-P, WM/GM interface is indicated in white lines) indicates that both proteins were concentrated within the WM (Fig. 3.1, I and M, control). Quantification of the positive pixel versus distance from the WM/GM interface confirmed that MBP and PLP were concentrated in the WM in uninfected brains (Fig. 3.1Q and R, respectively). In brains obtained from HIV-infected individuals with MND and HAD, a reduction in MBP (Fig. 3.1J and K, quantification in Q) and PLP (Fig. 3.1N and O, quantification in R) staining were detected in the WM, interface, and the GM. The reduction in MBP and PLP staining was not associated with alterations in the numbers of cell bodies; instead, a reduction in cell processes was detected (see Fig. 3.1 J-K and N-O, respectively). Analysis of brains obtained from individuals with severe AD indicates that MBP and PLP distribution (Fig. 3.1L and P, respectively) and expression (Fig. 3.1Q and R, respectively) were reduced at the WM, interface, and GM compared to control and HIV conditions (Fig. 3.1Q and R). Overall, our data indicate that HIV infection and associated cognitive impairment compromised the distribution and expression levels of MBP and PLP.

HIV infection compromises myelin structure

To further examine the characteristic of the myelin compromise induced by HIV, we examined in more detail the structure and distribution of the myelin sheath (thickness of the myelin around the axons and the length between the Ranvier's nodes, see cartoon in Fig. 3.2A) using higher resolution confocal microscopy, 3D reconstruction, and deconvolution. To perform these analyses, tissues in two different orientations were used, sagittal and coronal, to observe cross and longitudinal axons. First, cross-sections of axons are represented as "donut" shaped MBP structures with the axon in the center (Fig. 3.2B-E). Second, longitudinal axons enable us to determine the length of the myelin sheath, including the Ranvier's node (Fig. 3.2F-I).

The analysis of cross-sections obtained from uninfected control individuals indicates that MBP staining provided a myelin sheath thickness of 5.5±1.1 μm (Fig. 3.2B). In contrast, the analysis of brain tissues obtained from HIV-infected individuals with MND or HAD and stained for MBP shows a compromised myelin sheath thickness of 4.3±0.8 μm and 3.5±1.1 μm, respectively (Fig. 3.2C and D, respectively). Analysis of brain tissues obtained from severe cases of AD shows compromised myelin thickness in the GM compared to uninfected control and HIV brain tissues (Fig. 3.2J, *$p \leq 0.0001$ compared to GM Control, 3 replicates, 4 different tissues). However, there were no differences in WM thickness among control uninfected, HIV-infected (MND or HAD), and AD tissues (Fig. 3.2J, WM). In conclusion, our MBP staining data of cross-section axons indicates that myelin thickness is reduced in HIV-infected brains to severe AD cases (Fig. 3.2J).

The analysis of coronal uninfected brain sections to observe longitudinal axon structures shows a repetitive pattern consistent with the distribution and distance of the myelin sheath separated by the Ranvier's nodes (Fig. 3.2A, F, and K, cartoon, staining, and quantification, respectively). There are no changes in the myelin length among brains of uninfected and HIV individuals with MND or HAD even when WM and GM were quantified separately (Fig. 3.2K). These data indicate that the distances between the Ranvier's nodes were constant even in HIV-infected brains. In contrast, the analysis of brains from AD individuals indicated a GM myelin length compromise compared to uninfected and HIV conditions (Fig. 3.2K, AD, *$p \leq 0.05$ compared to GM Control, 3 replicates, 3 different tissues). Overall, our data indicate that HIV infection compromises myelin structures, especially the myelin sheet's thickness.

Myelin damage is associated with the presence of viral reservoirs

A significant observation is that myelin damage was not uniform within the brain. Thus, we hypothesize that myelin damage was associated with the presence of long-

lasting HIV-infected cells, also called viral reservoirs. We performed tissue staining for HIV-DNA to demonstrate our hypothesis using a nef DNA probe, nuclei (DAPI), and MBP or PLP (Fig. 3.3). In control uninfected and AD tissues, no staining for HIV nef DNA was observed (Fig. 3.3B and N).

We identified that brain areas with compromised myelin structures were associated with the presence of cell clusters containing viral DNA in the WM and GM under MND and HAD conditions (Fig. 3.3, E-H and I-L, respectively, see dotted circles). Viral reservoirs corresponded to microglia/macrophages (Iba-1 positive cells) and astrocytes (GFAP positive cells), and the ratio of both infected cell types depends on the length of cART. The re-assessment of myelin compromise described in Fig. 3.1 and 3.2, based on the presence of HIV-DNA, indicated that 82.02 ± 11.6% of the areas with HIV-DNA were associated with decreased MBP and PLP expression and compromised myelin thickness compared to uninfected brains (Fig. 3.3, uninfected controls set to 100±26.3 A.U.). We determined that myelin compromise from HIV-DNA positive cells could reach distances up to 250±1.25 μm, suggesting a mechanism of chronic damage amplification under cART conditions. The quantification of the MBP/PLP expression around viral reservoirs (HIV- positive DNA cells and up to 250±1.25 μm around these cells, Fig. 3.3Q, white bars) indicates that myelin components were compromised more around viral reservoirs than in areas without viral reservoirs (Fig. 3.3Q, black bars, MND, white bars compared to black bars, *$p \leq 0.05$, n=3 different tissues per patient, n=16 and 8 from HIV-infected individuals). The lack of differences in myelin damage between HIV-MND and HIV-HAD also was unrelated to the numbers of HIV-nef DNA positive cells (more abundant in HAD conditions), systemic replication, CD4 counts, age, sex, cART, and years with HIV (see table 2) suggesting that even in the cART era chronic damage is still significant. In addition, there are no significant differences in MBP/PLP expression in areas without HIV-DNA or at distances over 250 μm. In conclusion, myelin compromise

is associated with the presence of viral reservoirs, and the degree of damage is maintained in HIV-MND and HAD cases.

Sulfatide is a key dysregulated lipid in HIV-associated myelin damage: a potential biomarker of HIV CNS disease

To examine further the mechanism of myelin compromise induced by HIV-infected cells, we performed an unbiased lipid screening using MALDI-MSI. Our screening indicates that sulfatide, a key lipid family involved in maintaining myelin structure, was compromised in HIV conditions. Sulfatide comprises 4-7% of all myelin lipids (Palavicini, Wang et al. 2016), plays a critical role during the myelin compaction, and remains in the compacted myelin. However, the release of sulfatides due to myelin damage promotes inflammation (Jeon, Yoon et al. 2008), oligodendrocyte survival (Shroff, Pomicter et al. 2009), and prevents axonal outgrowth (Winzeler, Mandemakers et al. 2011); but the mechanisms associated with the damage remain to be fully explored. More importantly, sulfatide species have been proposed to have strong interactions with HIV-Gp120, altering viral fusion, and HIV-associated dementia (see review by (Takahashi and Suzuki 2012)). Also, soluble sulfatide, like MBP and PLP, could generate autoreactive T cells in the patients exacerbating brain damage (Stax, Tuengel et al. 2017). Thus, we examined the expression and distribution of sulfatide in the analyzed brains by MALDI-MSI.

MALDI-MSI enables us to detect and visualize the distribution of multiple sulfatide species identified based on carbon length and saturation. Serial sections were used to perform H&E staining, and the subsequent section was used for MALDI-MSI. Analysis of different sulfatide species indicates that in control uninfected conditions, sulfatide is concentrated in the WM as expected (Han 2007) (examples of 18:0, 18:1, 22:0, 24:0, 24:1, and 26:1, as well as their hydroxylated species, are shown, Fig. 3.4 and 3.5). Shorter sulfatide species such as 18:0, 18:1, 22:0 and their hydroxylated species, as

18:0 OH, 18:1 OH, and 22:0 OH, were not altered in HIV (MND or HAD) and AD conditions (Fig. 3.4A-I and 3.5 A-I). However, the analysis of 24 carbon chain sulfatides (24:0, 24:1 and hydroxylated species, 24:0 OH and 24:1 OH) indicates an upregulation of these sulfatides (*$p \leq 0.05$ compared to control, n=4), known to be the primary sulfatides comprising mature myelin (Hirahara, Wakabayashi et al. 2017), in the WM in HIV conditions, MND and HAD. Moreover, another long-chain sulfatide, 26:1 and 26:1 OH, was not affected by HIV or AD status (Fig. 3.4 and 3.5). Surprisingly, the increased levels and specificity of the sulfatide species were similar to the changes observed in brain tissue myelin tracks from severe AD cases (Fig. 3.4 and 3.5). Further, our MALDI-MSI data indicates two critical points; first, myelin damage is specific for some sulfatide species. Second, the damage to the myelin sheath is comparable to the extensive damage observed in AD individuals. Supporting these points, structural membrane lipids like PA 39:3 or PE 40:6 were not affected by HIV infection or the cognitive impairment status, MND or HAD (Fig. 3.6, n=4 different tissues). They were expressed in the WM and GM and used as markers to delineate the tissue regions. Overall, our data indicate that HIV infection induces the dysregulation of specific sulfatide species and could provide early indicators of CNS compromise in the HIV-infected population.

Soluble sulfatide compromises the generation of calcium waves in pacemarkers astrocytes

Our data indicate that HIV infection and compromised cognition in the HIV-infected population are associated with increased sulfatide levels and myelin structural changes. However, whether soluble sulfatide can alter brain function is unknown. We hypothesize that sulfatide could participate in the bystander damage indicated above. Currently, two critical observations support a long-range or bystander-associated damage generated by HIV-infected cells: first, the association of myelin damage with HIV-infected cells, and second, the compromise of myelin integrity suggesting a long-range

electrical signaling dysfunction. Our laboratory identified gap junction channels and hemichannels as key systems to amplify bystander damage mediated by viral reservoirs by an IP_3 and calcium-mediated mechanisms even in the absence of viral replication (Eugenin and Berman 2007, Eugenin, Clements et al. 2011, Eugenin and Berman 2013, Berman, Carvallo et al. 2016, Malik, Theis et al. 2017, Gajardo-Gomez, Santibanez et al. 2020, Lutgen, Narasipura et al. 2020, Malik, Valdebenito et al. 2021, Valdebenito, Castellano et al. 2021). We determined calcium waves to measure cell-to-cell communication and bystander damage, critical mechanisms related to viral reservoirs-associated dysfunction in neighboring uninfected areas.

Human primary astrocytes were plated on Matek plates in uninfected or HIV_{ADA}-infected conditions (7 days post-infection) as we described (Eugenin and Berman 2007, Eugenin, Clements et al. 2011). Calcium imaging analysis of the primary human astrocyte cultures identified two astrocyte populations: pacemakers (with intrinsic calcium oscillations) and non-pacemakers (responders to the pacemakers). Analyzing these cell populations enables us to determine the period, amplitude, peak numbers, intensity (area under the curve), and frequency (see an example of the signaling in Fig. 3.7). Fig. 3.7A represents all the measures performed in the cultures, including the area under the curve that provides the calcium baseline (Fig. 3.7B), the number of calibrated peaks per time unit (discounting background intensity, Fig. 3.7C), the calibrated time that the peaks last during the time analyzed (period discounting background intensity, Fig. 3.7D), calibrated peak frequency (discounting background intensity, Fig. 3.7E), and the calibrated amplitude (discounting background intensity, Fig. 3.7F) (see methods for details).

Quantification of the calcium baseline or area under the curve indicates neither HIV infection nor sulfatide treatment alters the overall calcium signaling during the time analyzed in non-pacemaker (NPM) and pacemaker astrocytes (20 min post sulfatide treatment or after 7 days post-infection, Fig. 3.7B). However, the calcium peaks in

uninfected pacemaker cells were reduced by sulfatide treatment (Fig. 3.7C, *p≤0.05, n=3 independent experiments) but not in NPM cells or the pacemaker cells in HIV-infected conditions (Fig. 3.7C).

Analysis of the periods between calcium increased indicates that HIV infection reduced the total number of periods, but treatment with sulfatide recovered the number of calcium wave periods to control levels (Fig. 3.7D, *p≤0.05, n=3). No changes in periods were found in NPM cells (Fig. 3.7D). Analysis of the calibrated frequency of the calcium signals indicates no changes in uninfected or HIV-infected NPM cells and uninfected pacemaker cells (Fig. 3.7E). However, sulfatide in pacemaker cells in HIV-infected cultures reduced the calibrated frequency (Fig. 3.7E, *p≤0.0001, n=3). The analysis of the amplitude of the calcium signals in uninfected and HIV-infected cultures in the presence and absence of sulfatide indicated no changes (Fig. 3.7F).

Overall, our data indicate that sulfatide in uninfected and HIV-infected astrocytes cultures did not affect calcium signaling in NPM cells. However, sulfatide was able to compromise pacemaker cells in uninfected and HIV-infected conditions. These data indicate that HIV infection in combination with sulfatide alters the calcium signaling between the pacemaker and non-pacemaker cells (responders), compromising the coordination between both cell types.

Soluble sulfatide increases Cx43 and ZO-1 expression

Our laboratory and others identified that gap junction channels are essential to coordinate calcium waves (Nedergaard, Cooper et al. 1995, Wang, Tymianski et al. 1997, Cotrina, Lin et al. 1998, Eugenin, Gonzalez et al. 1998, Cotrina, Lin et al. 2000, Simard, Arcuino et al. 2003). Also, HIV infection of astrocytes upregulates Cx43 expression and gap junctional communication (Berman, Carvallo et al. 2016, Prevedel, Morocho et al. 2017), and blocking gap junctional communication prevents bystander damage induced by the virus (Eugenin and Berman 2007, Eugenin, Clements et al. 2011, Eugenin and

Berman 2013, Malik, Theis et al. 2017, Malik, Valdebenito et al. 2021). However, the participation of host factors such as sulfatide in regulating Cx43 channels is unknown.

We evaluated whether treating primary human astrocyte cultures with soluble sulfatide (10 μg/ml) altered Cx43 and ZO-1 expression using qRT-PCR and Western Blot analysis (Fig. 3.8). Sulfatide treatment of uninfected astrocyte cultures increased Cx43 mRNA expression in all the cultures analyzed (from different individuals) at different time points (6, 12 or 24 h) (Fig. 3.8A, 6.16 ± 3.39 folds at the peak of Cx43 mRNA, *$p \leq 0.05$ at peak upregulation analyzed, n=5).

Western blot analysis of astrocyte cultures indicates that sulfatide increased the Cx43 protein levels at all the time points analyzed, 6, 12, and 24 h (Fig. 3.8B, Cx43 and GAPDH as a loading control). However, there are no changes in the phosphorylation ratio of the protein, including non-phosphorylated, phosphorylated isoform 1 (P1), phosphorylated isoform 2 (P2), and phosphorylated isoform 3 (P3), and hyperphosphorylated (HP, not shown). To demonstrate that the total Cx43 was increased over the phosphorylation, the lysates were incubated with alkaline phosphatase (AP) to eliminate any protein phosphorylation (Fig. 3.8B and D). The quantification of total unphosphorylated Cx43 protein confirmed our previous data that sulfatide increased the total amount of Cx43. The quantification of the Cx43 protein upregulation indicates an increase of the total amount, Cx43 2.10±0.62, and digested Cx43, 1.30±0.28 (Fig. 3.8C and D, respectively. *$p \leq 0.05$ at peak upregulation analyzed, n=5 different astrocyte cultures from different individuals).

A critical partner of Cx43 at the plasma membrane is the adaptor protein, ZO-1 (Thevenin, Margraf et al. 2017). Notably, ZO-1 interaction regulates GJ's dynamic turnover maintaining GJ channels in the plasma membrane in a functional state. When ZO-1 separates from Cxs, it induces GJs closure and transitioning for endocytosis (Thevenin, Kowal et al. 2013, Thevenin, Margraf et al. 2017). qRT-PCR analysis for ZO-1 and GAPDH mRNA demonstrated that sulfatide treatment also upregulates ZO-1

mRNA compared to untreated astrocytes (Fig. 3.8E, *p≤0.05 timepoints at peak expression analyzed, n=4). Furthermore, Western blot analysis indicated that sulfatide treatment increased ZO-1 protein (Fig. 3.8F, *p≤0.05 at peaks expression analyzed, n=3). These results suggest that extracellular or soluble sulfatide upregulates Cx43 and ZO-1 expression, both critical components of calcium waves coordination and cell-to-cell communication.

Soluble sulfatide induces the maintenance of Cx43 at the plasma membrane

Untreated control and sulfatide-treated cultures were analyzed by confocal and image analysis for Cx43, ZO-1, actin (phalloidin), and nuclei (DAPI). 3D reconstructions indicate that Cx43 and ZO-1 are localized at the plasma membrane and internal vesicular stores in control conditions (Fig. 3.9A). Sulfatide treatment for 6, 12, or 24 h increased Cx43 and ZO-1 staining determined by the numbers of positive pixels (Fig. 3.9B, quantification in 3.9C, *p≤0.05 at peak expression analyzed, n=3), in agreement with our mRNA and protein data (Fig. 3.9A-F). Analysis of specific ROI, plasma membrane, GJ plaques, and intracellular vesicles indicates an upregulation in each compartment. Colocalization analysis between Cx43 and ZO-1 was performed using Pearson's colocalization (Dunn, Kamocka et al. 2011). In control, untreated conditions, most Cx43 colocalized with ZO-1, but sulfatide treatment increased the colocalization of both proteins (Fig. 3.9D, *p≤0.05 at peak expression analyzed, n=3). Overall, soluble sulfatide increased the expression and maintained the channels and the interacting proteins on the membrane, suggesting that releasing sulfatide from myelin tracks can profoundly affect gap junctional communication. Our data on neuroHIV indicates that gap junctions are essential for spreading toxicity and apoptosis even in the cART era; thus, the release of sulfatide can further increase the radius of damage.

Soluble sulfatide enhanced gap junctional communication

We performed scrape loading-dye transfer assay experiments to determine whether the changes in calcium, Cx43/ZO-1 expression, and localization resulted in functional changes in gap junctional communication (Fig. 3.10A, cartoon). Briefly, a monolayer of astrocytes was scratched in the presence of two dyes, Lucifer yellow LY, which crosses gap junctions, and dextran, which does not cross gap junctions due to its size. LY, but not dextran, is taken up for the damaged cells and diffused by gap junction into the intact neighboring cells (Nodin, Nilsson et al. 2005).

In control untreated conditions, LY, but not dextran, diffused up to 1400 μm, indicating a strong gap junctional communication (Fig. 3.10B and H correspond to the quantification of LY intensity). The preincubation of the cultures with 18α-glycyrrhetinic acid (AGA, 50 μM) or Octanol (OCT, 500 μM), two well-known gap junction blockers, prevented the diffusion of LY (Fig. 3.10C and D, *$p \leq 0.05$, n=3). Sulfatide treatment did not increased the LY diffusion distance but induced a higher LY intensity than control conditions (Fig. 3.10E and G, quantification of LY intensity, *$p \leq 0.05$, n=3). Pre-application of AGA or OCT in sulfatide-treated cultures prevented the LY diffusion and decreased LY intensity in response to the treatment reducing them to 500 and 600 μm, respectively (Fig. 3.10F and G, and H for the quantification, #$p \leq 0.05$, n=3). Overall, our data indicate that sulfatide increased gap junctional communication in astrocytes, even in the absence of HIV components, supporting the hypothesis that sulfatide release in HIV-infected tissues due to the presence of viral reservoirs enhances cell-to-cell communication.

Table 2: Patient information for the analyzed brain tissue samples

Nº.	HIV-HAND	Age	Gender	Plasma VL (log copies/ml)	CD4 (cell/mm^3)	CSF VL (log copies/ml)	cART	Years with HIV
1	NA	51	M	NA	NP	NA	NA	NA
2	NA	46	M	NA	NP	NA	NA	NA
3	NA	40	F	NA	NP	NA	NA	NA
4	NA	43	M	NA	NP	NA	NA	NA
5	HIV + MND	54	M	5.88	18	3.27	3TC; TFV; SQV; RTV	13
6	HIV + MND	54	F	2.6	211	1.7	3TC; D4T; NVP; FTV	10
7	HIV + MND	41	F	4.09	566	1.89	DLV; D4T; 3TC	5
8	HIV + MND	49	M	3.32	1	3.36	KTA; CBV; EFV; ABC	18
9	HIV + HAD	58	M	5.7	5	3.14	D4T; ZDV; 3TC; KTA	23
10	HIV + HAD	47	F	2.6	98	4.34	RTV; KTA; ZDV; 3TC	2
11	HIV + HAD	44	F	3.54	78	4.88	RTV; IDV; D4T; 3TC	4
12	HIV + HAD	55	F	1.3	8	1.3	TMC; TFV; RGV; FTC	7
13	NA - AD	54	M	NA	NP	NA	NA	NA
14	NA - AD	45	F	NA	NP	NA	NA	NA
15	NA - AD	71	F	NA	NP	NA	NA	NA
16	NA - AD	85	F	NA	NP	NA	NA	NA

Information for all 16 individual donors of brain tissue is provided, including HIV and cognitive status, age, gender, plasma viral load (log cells/ml), CD4 counts (cells/mm^3), CSF viral load (log cells/ml), cART treatment description, and years were living with HIV. NA: not applicable; NP: not present; CS: cognitive status; AD: Alzheimer's Disease; 3TC: epivir; KTA: anile heads; TFV: tenofovir; SQV: saquinavir; RTV:

ritonavir; DLV: delavirdine; D4T: stavudine; NVP: Nevirapine; FTV: Fortovase; CBV: combivir; IDV: indinavir; EVF: efavirenz; ABC: abacavir; ZDV: zidovudine; TMC: etravirine; RGV: raltegravir; FTC: emtricitabine.

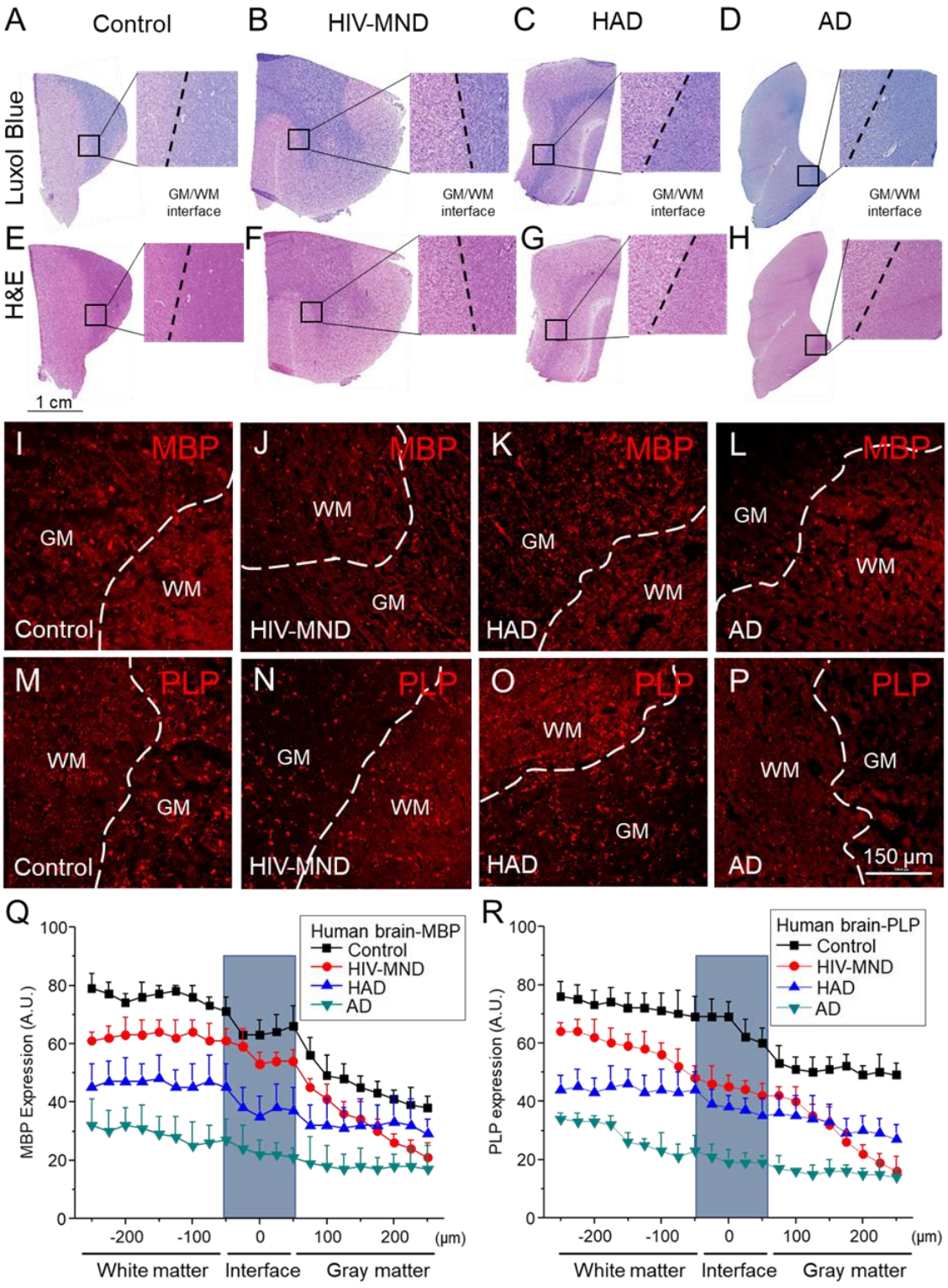

Figure 3.1. Human prefrontal cortex tissue samples obtained from HIV-infected individuals with MND and HAD show a decreased expression of myelin structural proteins than control uninfected tissues

Human prefrontal cortex obtained from control uninfected, HIV-infected with MND (HIV-MND), HAD, or Alzheimer's Disease (AD, used as a positive control) patients were analyzed by histologic and immunofluorescence staining for MBP and PLP. (A-D) Representative images of Luxol Blue stained tissues for all the conditions analyzed, the inset corresponds to the amplification shows the interface area between the WM and GM. (E-H) Representative images of H&E-stained tissues for all the conditions analyzed, the inset corresponded to the amplification shows the interface area between the WM and GM. (I-L) Distribution of MBP at the WM/GM interface (the white line indicates the interface). (M-P) Distribution of PLP at the interface (the white curve indicates the interface). (Q) Quantification of the total pixels per area for MBP staining in control (black curve), HIV- MND (red curve), HAD (blue curve), and AD (green curve) human brain tissues for MBP in the closer WM and GM to the interface (200 μm); data points were analyzed by 2-way ANOVA multiple comparison test (n=3). (R) Quantification of the total pixels per area for PLP in control (black curve), HIV- MND (red curve), HAD (blue curve), and AD (green curve) human brain tissues for PLP in the closer WM and GM to the interface (200 μm); data points were analyzed by 2-way ANOVA multiple comparison test (n=3). Overall, our data indicate that HIV infection compromises the WM/GM interface for decreased expression of key myelin-related proteins, MBP and PLP.

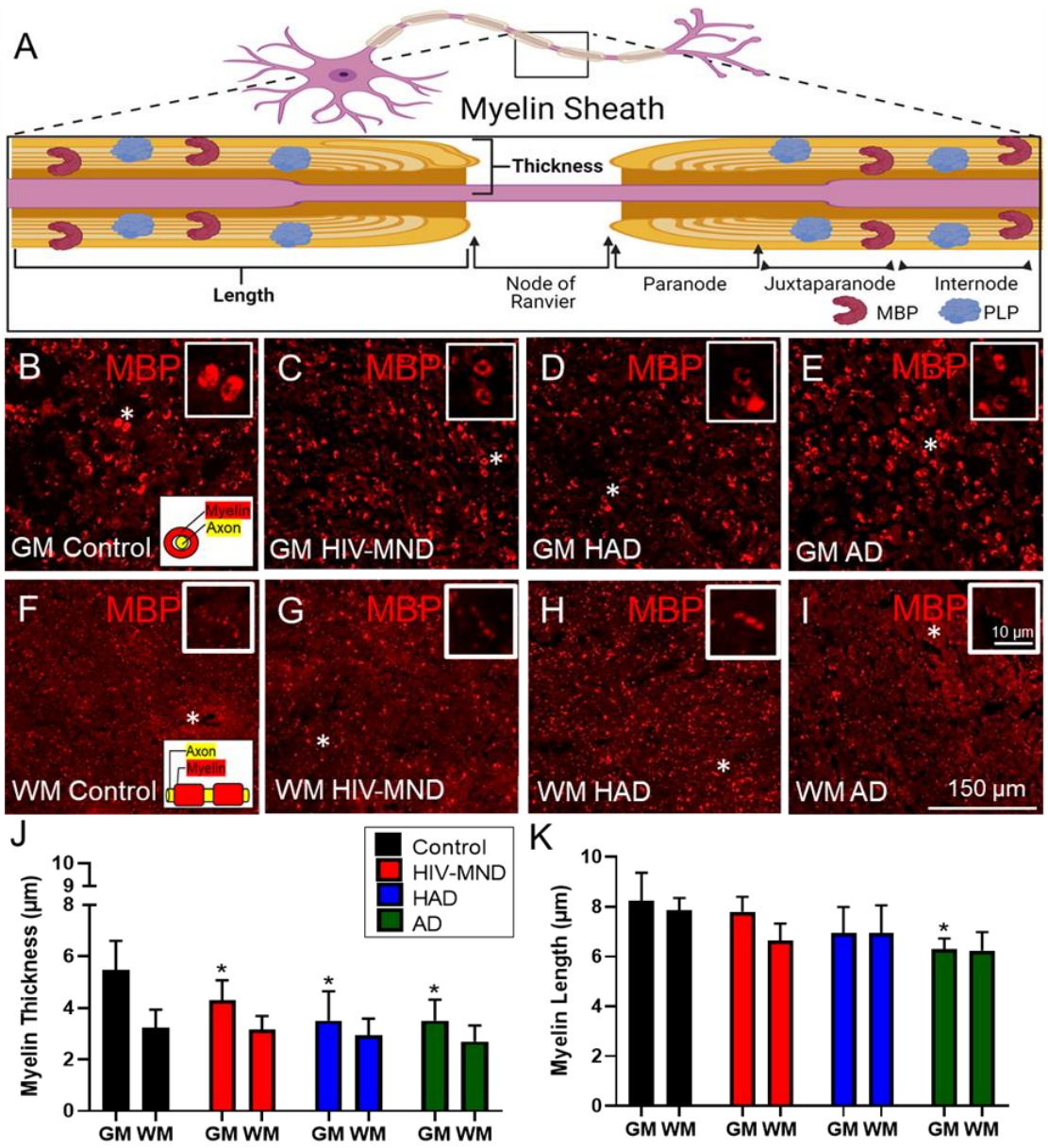

Figure 3.2. Human prefrontal cortex tissues obtained from HIV-infected individuals with HIV-MND and HAD show a decreased myelin thickness and compromised organization

Human prefrontal cortex isolated from control uninfected, HIV-infected with MND (HIV-MND) and HAD, and Alzheimer's Disease (AD) patients, used as a positive control, were analyzed by immunofluorescence staining for MBP. (A) The cartoon shows the structure of the myelin sheath and the distribution of our selected proteins, MBP and PLP. (B-E) Distribution of MBP in the GM of human brain tissues to analyze myelin thickness (star indicates magnification at the right corner). (F-I) Distribution of MBP in the WM of human brain tissues to analyze myelin length (star indicates magnification at the right corner). (J) Quantification of the myelin thickness in µm in the WM and GM of

control (black bars), HIV- MND (red bars), HAD (blue bars), and AD (green bars) human brain tissues; data points were analyzed by 2-way ANOVA multiple comparison test (*$p \leq 0.0001$ compared to GM Control). (K-J) Quantification of the myelin length in μm in the WM and GM of control (black bars), HIV- MND (red bars), HAD (blue bars), and AD (green bars) human brain tissues; data points were analyzed by 2-way ANOVA multiple comparison test (*$p \leq 0.05$ compared to GM Control; n=3).

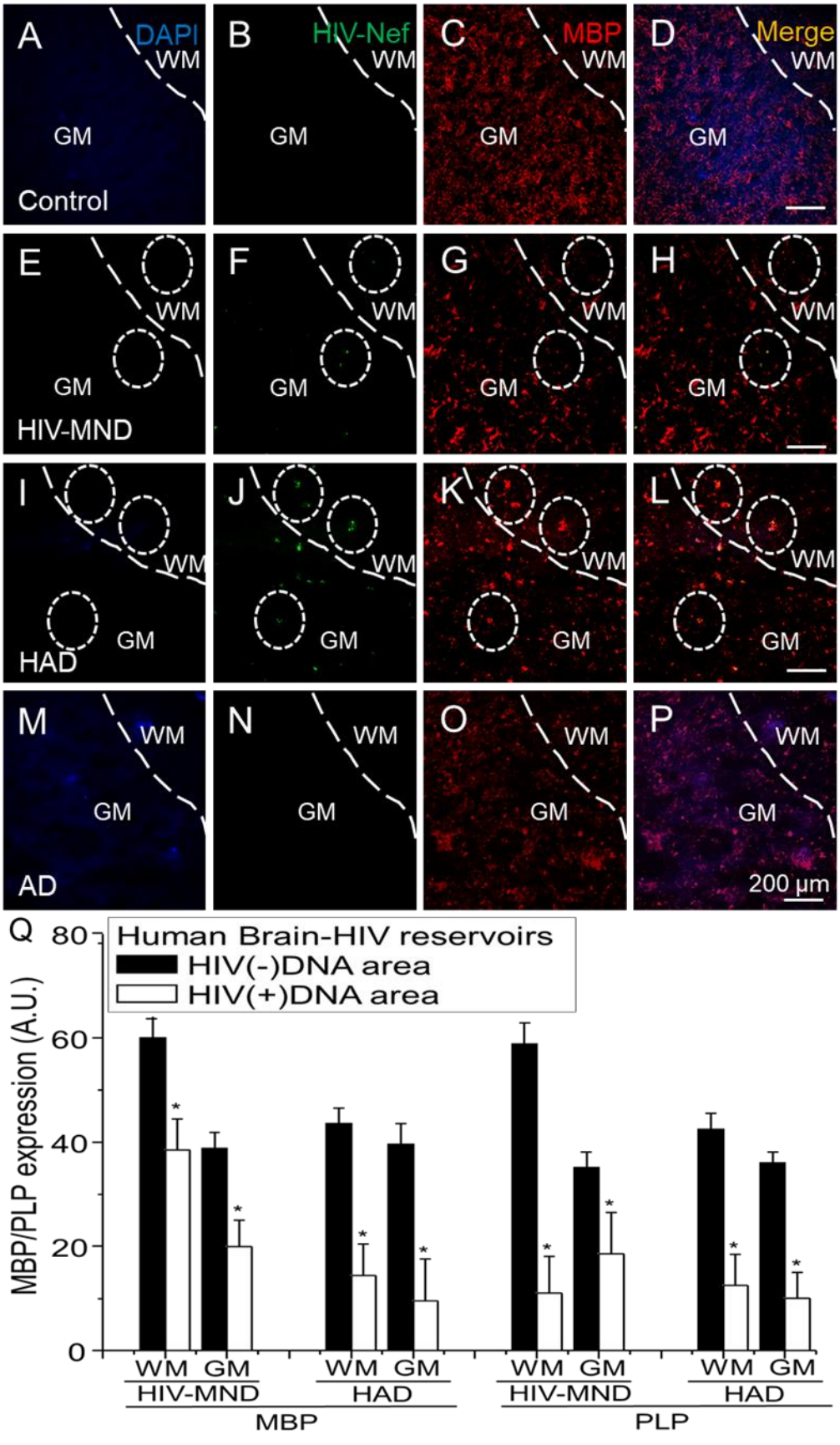
A
DAPI
WM
GM
Control
B
HIV-Nef
C
MBP
D
Merge
E
F
G
H
HIV-MND
I
J
K
L
HAD
M
N
O
P
AD
200 μm
Q
Human Brain-HIV reservoirs
HIV(-)DNA area
HIV(+)DNA area
MBP/PLP expression (A.U.)
0
20
40
60
80
WM GM
HIV-MND
HAD
MBP
PLP

Figure 3.3. Myelin structures are compromised in areas with HIV reservoirs

The human prefrontal cortex was obtained from control uninfected, HIV-infected with MND (HIV-MND) and HAD, and Alzheimer's Disease (AD) patients, used as a positive control, and analyzed by immunofluorescence staining for DAPI (blue), HIV DNA for nef (green), and MBP (red). DAPI staining was reduced to appreciate the HIV DNA signal. (A-D) correspond to a representative analysis of control uninfected brains. (E-H) Correspond to representative staining of an HIV-infected individual with MND and positive HIV DNA cells. (I-J) Correspond to a representative analysis of brains obtained from HIV-infected individuals with HAD. (M-P) Correspond to a representative example of uninfected Alzheimer's disease (AD) brains. Circles in each picture represent areas with HV DNA positive cells. (Q) Quantification of the total pixels of MBP/PLP per area unit in the absence (HIV(-)DNA area, black bars) and presence of viral reservoirs (HIV(+)DNA area, white bars). The Student's t-test analyzed data points with Welch's Correction for significance (*$p \leq 0.05$ compared to HIV(-)DNA area; n=3 different individuals).

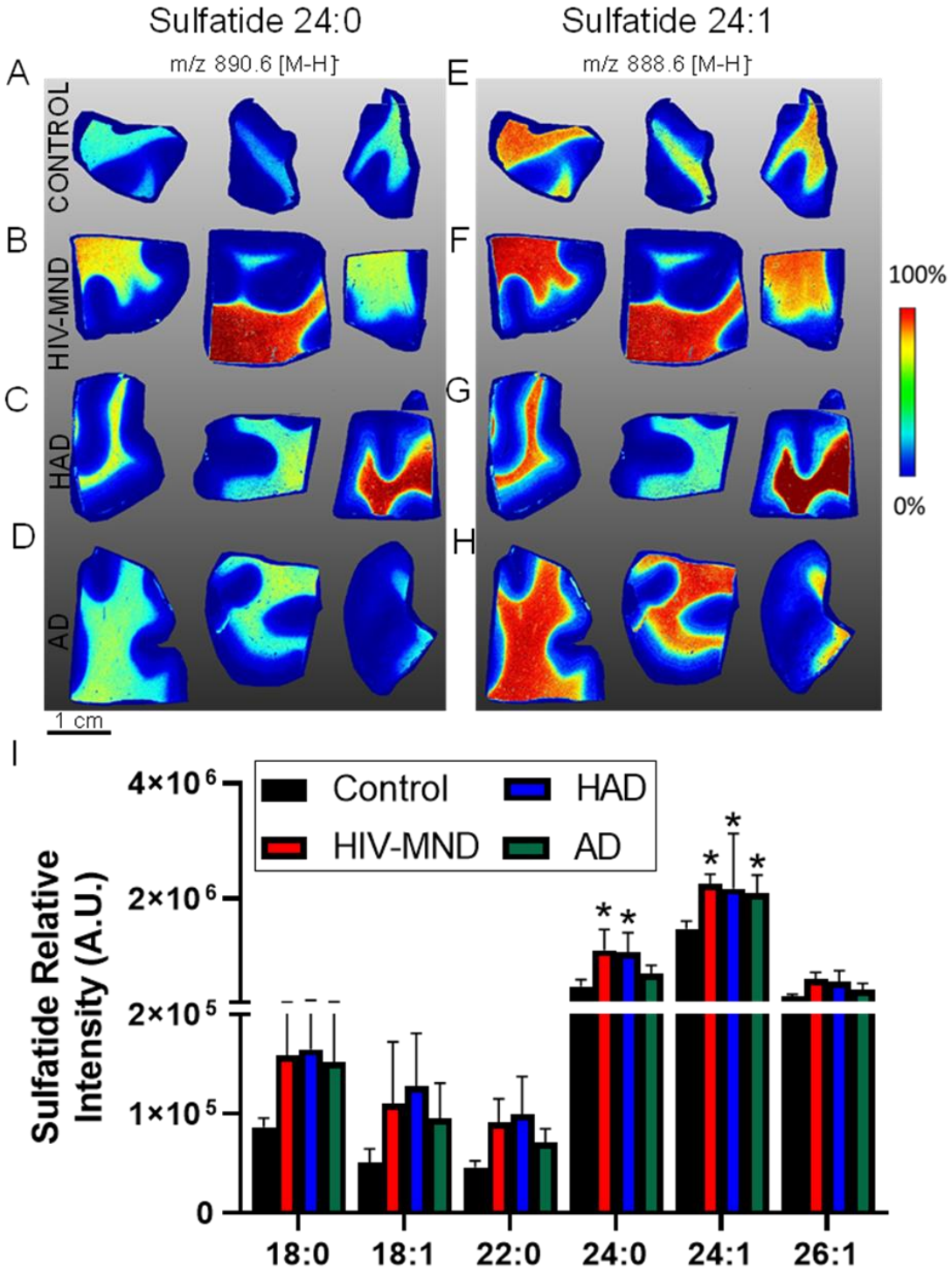

Figure 3.4. Sulfatide 24:0 and 24:1 species are upregulated in HIV-MND and HAD, similarly to severe AD cases.

The human frontal cortex of uninfected (Control), HIV-infected with MND (HIV-MND), HIV-infected with HAD (HAD), and AD patients were analyzed by MALDI-MSI

analyzed. (A-D) Representative MALDI MSI images of uninfected control, HIV-MND, HAD and AD brains for sulfatide 24:0 (n=4, three representative brains are shown). (E-H) Representative MALDI-MSI images for sulfatide 24:1 (n=4, three representative brains are shown). Statistically-significant differences were not observed for 18:0, 18:1, 22:0, and 26:1 sulfatide (See Fig. 3.5) for hydroxylated sulfatide species). All sulfatide species analyzed were highly concentrated in the WM. Sulfatides 24:0 and 24:1, known to be present in adult myelin, are significantly increased in neuroHIV conditions. Note that sulfatide compromise was similar to severe AD cases, suggesting that damage in HIV in some cases can be comparable to severe AD cases. The gradient intensity scale expresses relative intensity. In contrast, PA and PE (Fig. 3.6) were not affected and were used as markers for the WM and GM, respectively. Analysis of the hydroxylated sulfatide species was performed similarly to the sulfatide species described in the current figure (Fig. 3.5). (I) Quantification of the WM ROI lipid signal intensity for sulfatide 18:0, 18:1, 22:0, 24:0, 24:1 and 26:1 in control (black bars), HIV-MND (red bars), HIV-HAD (blue bars), and AD (green bars) conditions. Data points were analyzed by 2way ANOVA Dunnett's multiple comparisons test for significance (*$p \leq 0.05$ compared to Control; n=4).

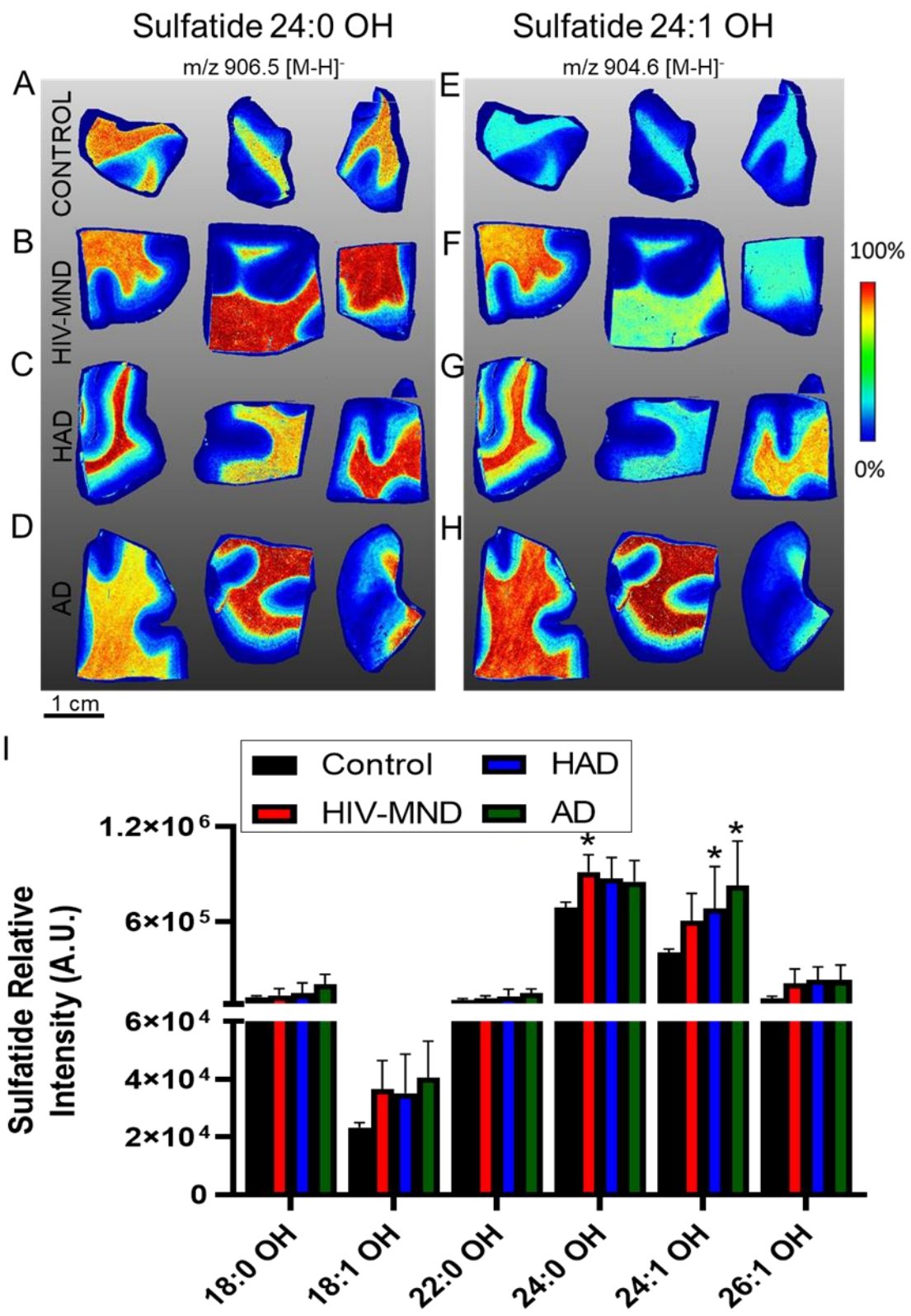

Figure 3.5. Hydroxylated sulfatides show specific changes during progressive HIV neurodegeneration

The human frontal cortex of uninfected (Control), HIV-infected with MND (HIV-MND), HIV-infected with HAD (HAD), and AD patients. (A-D) Representative MALDI MSI images for sulfatide 24:0 OH. (E-H) Representative MALDI MSI images for sulfatide 24:1 OH. In addition, sulfatide 18:0 OH, 18:1 OH, 22:0 OH, 24:0 OH, 24:1 OH, and 26:1 OH were determined. All sulfatides were localized in the WM. Sulfatide 24:0 OH and 24:1 are present in the adult myelin and significantly increase in neuroHIV conditions. (I) Represent the quantification of the sulfatide relative expression in the WM ROI for all the conditions (n=3 presented of a total of n=4 different individuals). Student's t-test with Welch's Correction for significance, *$p \leq 0.05$). The gradient intensity scale expresses relative intensity.

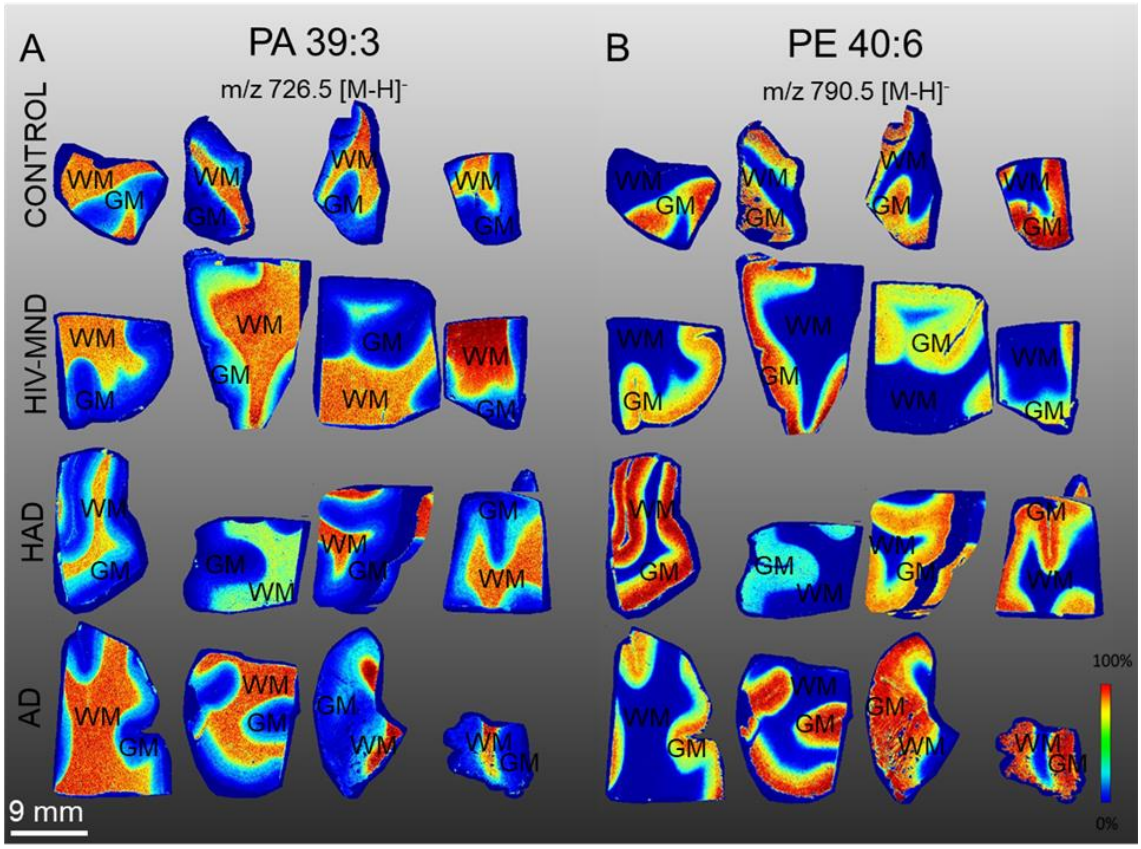

Figure 3.6. Phosphatidic acid (PA) and phosphatidylethanolamine (PE) levels and distribution are not affected in HIV or AD conditions compared to control uninfected brains

The human frontal cortex of uninfected (Control), HIV-infected with MND (HIV-MND), HIV-infected with HAD (HAD), and AD patients. (A) MALDI MSI images for PA 39:3 and (B) PE 40:6. PA 39:3 and PE 40:6 signals were localized at the WM and GM, respectively, as expected. Thus, they were used as WM and GM markers. The gradient intensity scale expresses relative intensity. n=16 different individuals were analyzed.

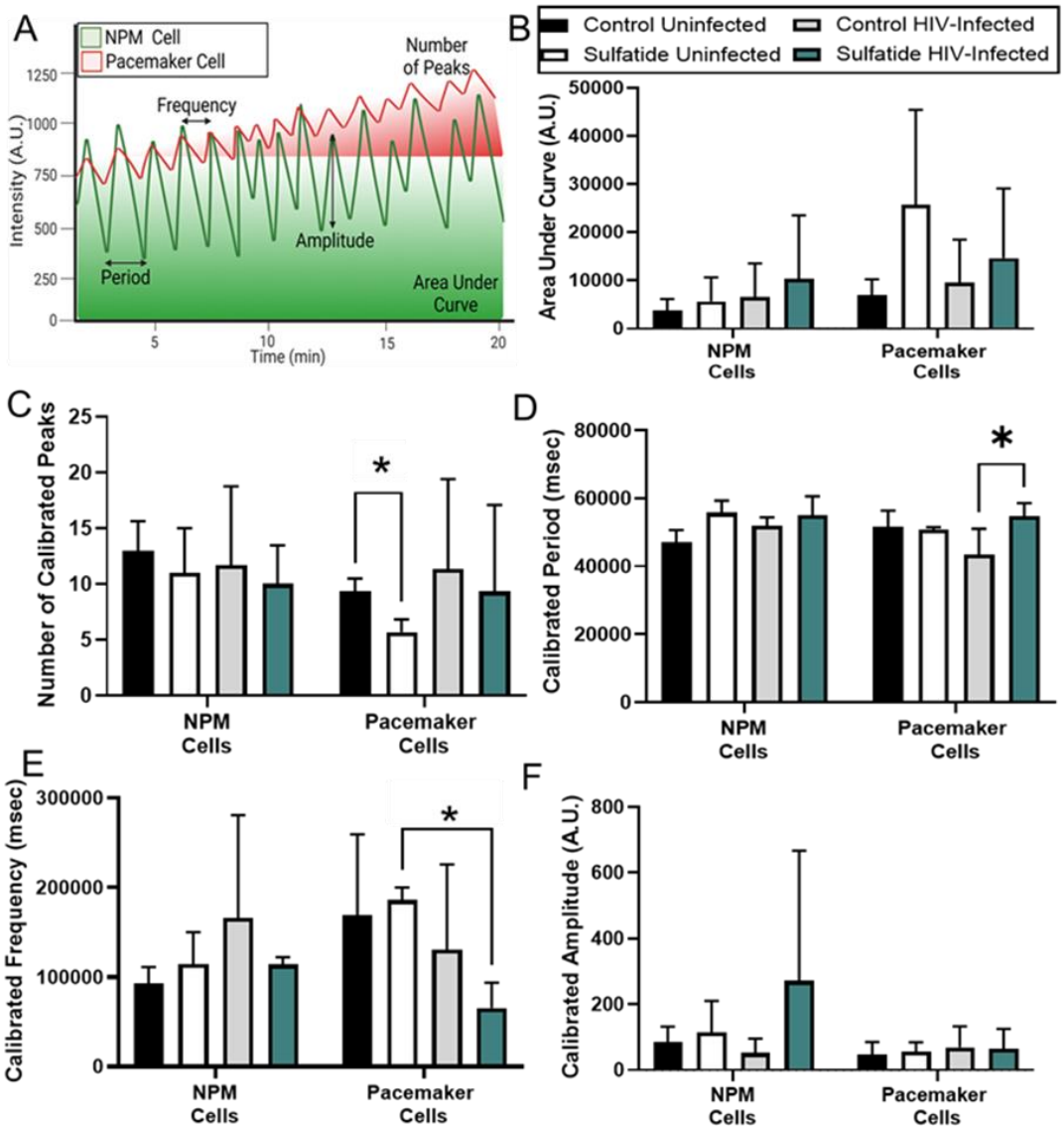

Figure 3.7. Soluble sulfatide compromise calcium waves in astrocyte pacemaker cells

Human primary astrocytes were infected with HIV_{ADA} (20–50 ng/ml HIV-p24) for 7 days and treated with 10 μg/ml sulfatide. After infection, cells were treated with 10 μM fluo-4 to perform calcium imaging for 20 min (still pictures collected every 5 sec) in three different areas of the plate. (A) Graphical presentation of a typical recording to identify non-pacemaker (NPM) and pacemaker cells. Quantification for the NPM and Pacemaker Cells Control Uninfected (black bars), Sulfatide Uninfected (white bars), HIV-infected (gray bars), Sulfatide HIV-Infected (green bars) of (B) area under the curve; (C) number of the total peaks; (D) the period of each calcium waves; (E) frequency of the calcium waves; and (F) the amplitude of the calcium waves. Data points were analyzed by 2-way ANOVA multiple comparison test (*$p \leq 0.05$ compared to pacemaker cells Control Uninfected; n=3 different cultures of different individuals).

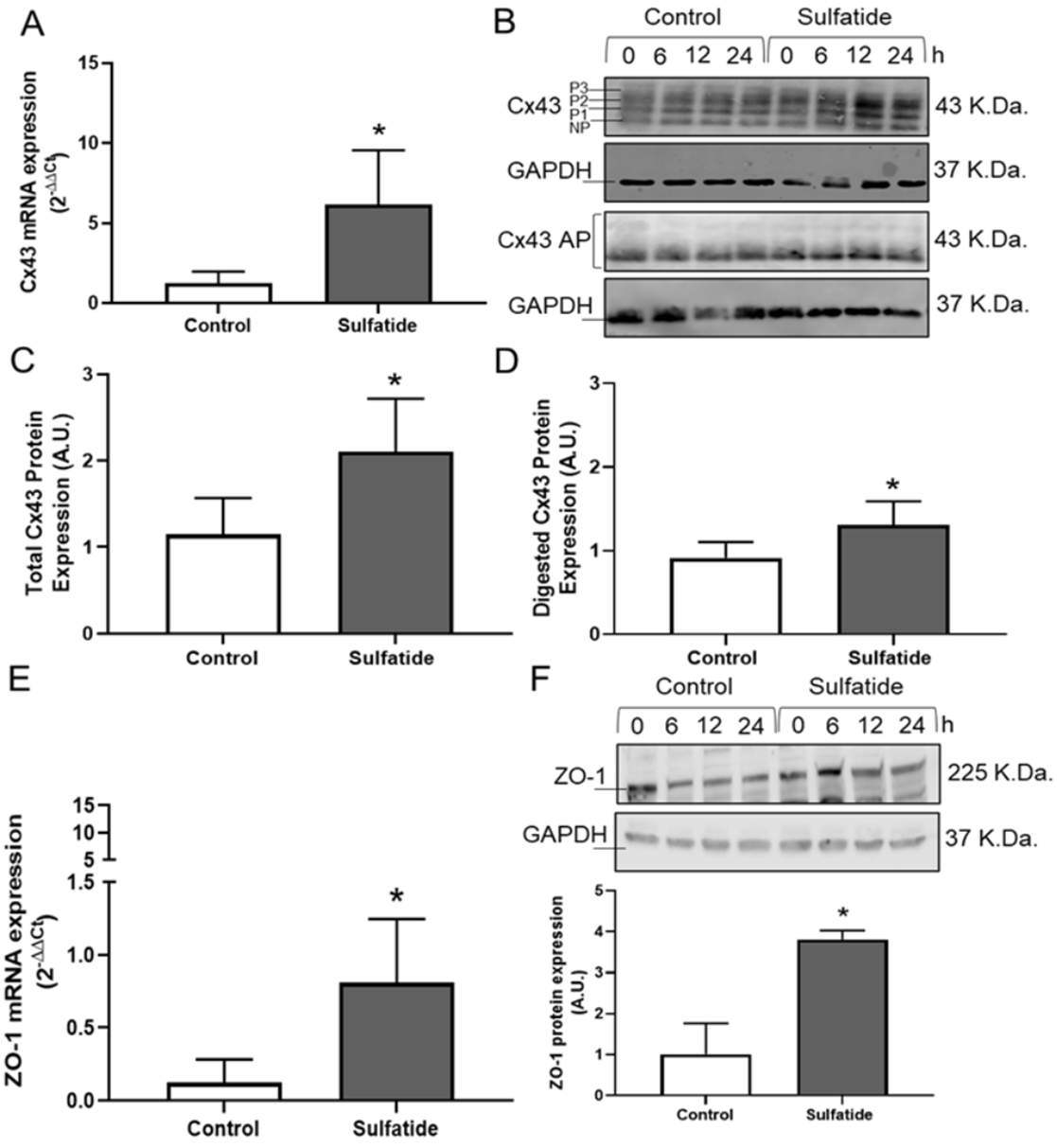

Figure 3.8. Soluble sulfatide upregulates Cx43 and ZO-1 expression in human primary astrocytes

Human primary astrocytes were treated with 10 µg/ml of sulfatide for 6, 12, and 24 h; Cx43 and ZO-1 mRNA and protein expression were analyzed. In all experiments, sulfatide treatment increased the expression of Cx43 and ZO-1 mRNA and protein at different time points, probably due to the inter-donor variability of human primary astrocytes. Thus, the maximal peak was considered to calculate the data. (A) qRT-PCR for Cx43 and GAPDH mRNA using untreated (control, white bar) and sulfatide treated (gray bar) astrocyte cultures. Sulfatide treatment increased Cx43 mRNA expression; data points for Cx43 were analyzed by Student's t-test with Welch's Correction for significance (*$p \leq 0.05$, n=5). (B) Representative immunoblotting for Cx43

(phosphorylated and unphosphorylated isoforms, P3, P2, P1, and NP) and GAPDH in control and sulfatide-treated human astrocytes for 6, 12, 24 and 48 h. The lysates were divided into two equal portions; one was treated with bovine intestinal alkaline phosphatase (AP) to assess the Cx43 total amount versus phosphorylation. (C) Western blot quantification for total Cx43 using the protein lysates of untreated (control) and sulfatide-treated astrocyte cultures. Sulfatide treatment increased total Cx43 protein expression; data points for Cx43 normalized by GAPDH were analyzed by Student's t-test with Welch's Correction for significance (*$p \leq 0.05$, n=5). (D) Western blot quantification for Cx43 using untreated (control) protein lysates and sulfatide-treated astrocyte cultures digested with bovine intestinal AP. Sulfatide treatment increased total Cx43 protein expression (phosphorylated and unphosphorylated); data points for Cx43 normalized by GAPDH were analyzed by Student's t-test with Welch's Correction for significance (*$p \leq 0.05$, n=5). (E) qRT-PCR for ZO-1 (a Cx43 partner at the plasma membrane) and GAPDH mRNA using untreated (control) and sulfatide-treated astrocyte cultures. Sulfatide treatment increased ZO-1 mRNA expression; data points for ZO-1 distributed normally were analyzed by Student's t-test with Welch's Correction for significance (*$p \leq 0.05$, n= 5). (F) Immunoblotting and Western blot densitometry band quantification for ZO-1 in control and sulfatide-treated human astrocytes for 6, 12, and 24 h. As a loading control, GAPDH was used. Sulfatide treatment increased ZO-1 protein expression. Data points for ZO-1 normalized by GAPDH were analyzed by Student's t-test with Welch's Correction for significance (*$p \leq 0.05$, n=5).

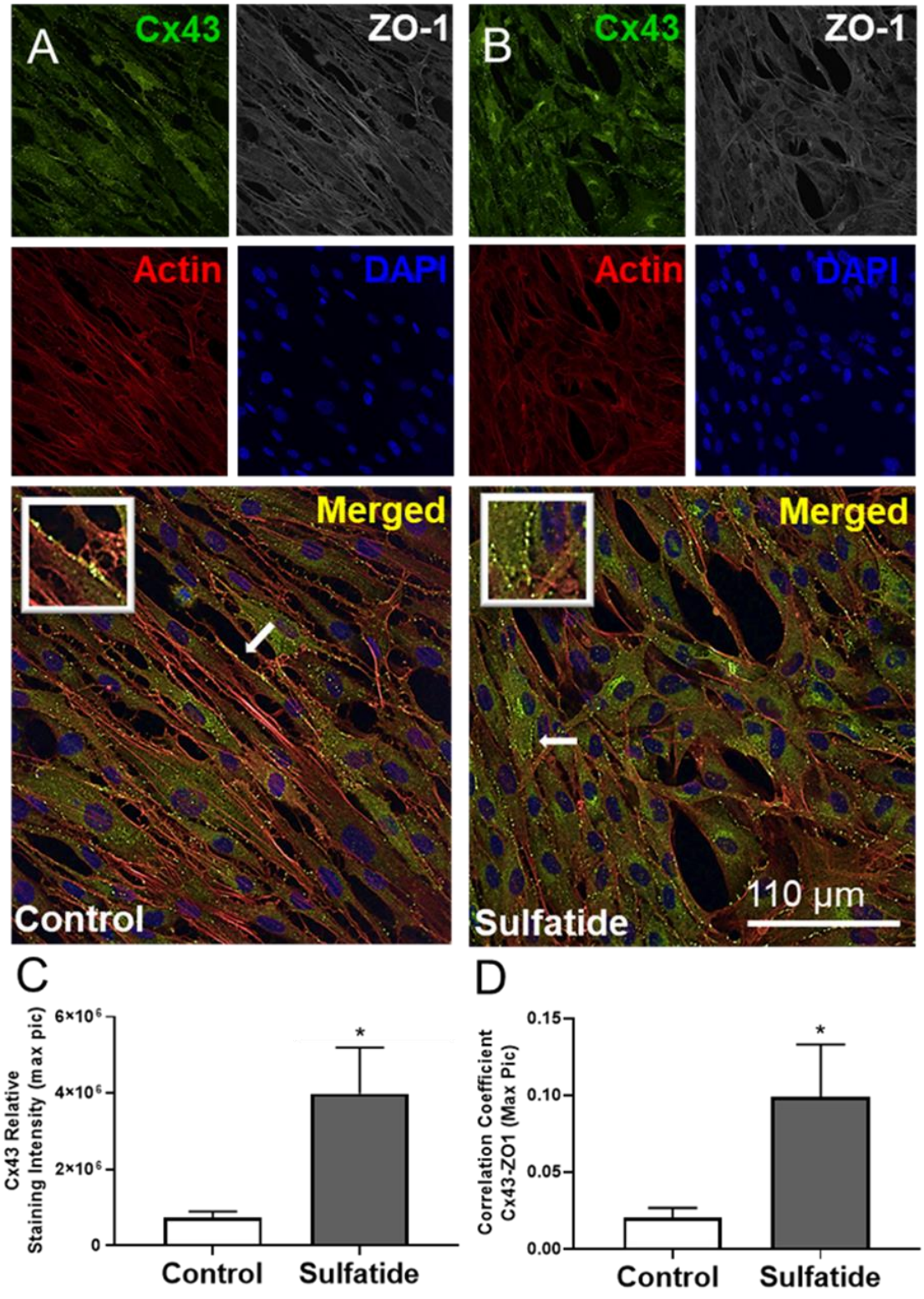

Figure 3.9. Soluble sulfatide increases Cx43-containing gap junctions at the plasma membrane in human primary astrocytes

Human primary astrocytes were treated with 10 μg/ml of sulfatide for 6, 12, and 24 h; expression and distribution of Cx43-containing channels were analyzed by confocal microscopy. In all experiments, sulfatide treatment increased the expression and distribution of Cx43 but at different time points, which may be due to the inter-donor variability of human primary astrocytes. Thus, the maximal peak was considered to calculate the data. Astrocytes were stained for Cx43 (Alexa 488, green staining), ZO-1 (Alexa 647, white staining), Phalloidin (Alexa Texas red, red staining), and the nucleus (DAPI, blue staining) in untreated (control) and sulfatide-treated conditions. (A) Correspond to control astrocytes cultures. The inset indicates the plasma membrane colocalization between Cx43 and ZO-1. (B) Corresponding to the sulfatide-treated astrocytes, the inset indicates the increased expression and localization of Cx43 and ZO-1 at the plasma membrane. The last panel represents the merge of all colors. Arrows indicate the area in the inset. Bar: 110 μm. (C) Quantification of the total pixel number for Cx43 at the maximal peak of expression induced by Sulfatide (gray bar) compared to untreated conditions (control, white bar). Data points for Cx43 were analyzed by Student's t-test with Welch's Correction for significance (*$p \leq 0.05$, n=3). (D) Quantification of the colocalization of Cx43 and ZO-1 in untreated (control) and sulfatide-treated conditions. Data points for Cx43 and ZO-1 colocalization were analyzed by Student's t-test with the Holm-Sidak method (alpha=0.05) for significance.

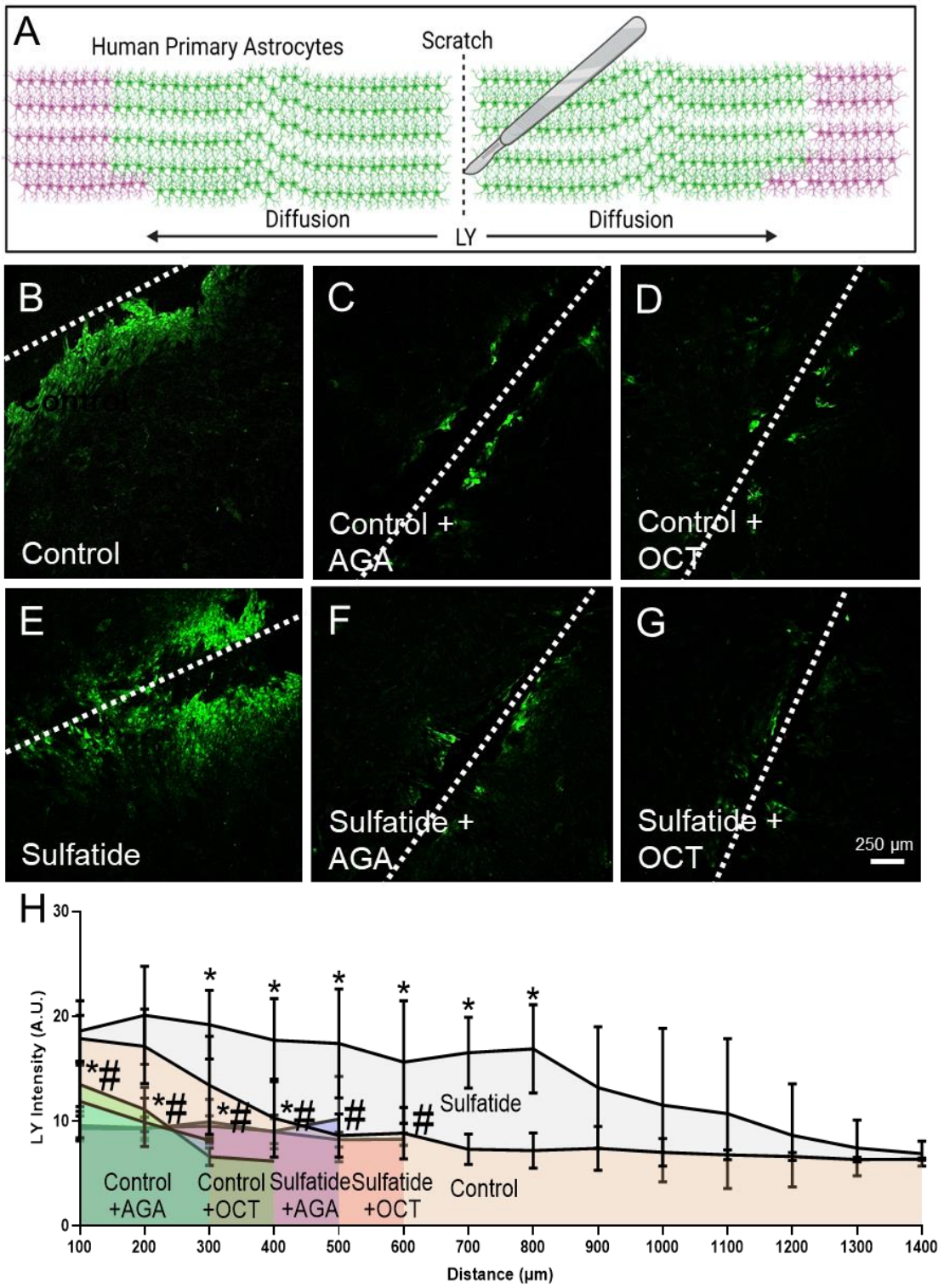

Figure 3.10. Soluble sulfatide increases gap junctional communication in human primary astrocytes

Human primary astrocytes were treated with 10 µg/ml of sulfatide for 6, 12, and 24h and the scrape loading assay was performed to evaluate gap junctional communication. (A)

Graphical presentation of the scrape loading assay. (B and E) Representative fluorescent image for Lucifer Yellow (LY) in untreated (control) and sulfatide-treated conditions. The white line represents the scratch site. Bar: 250 μm. (C-D-F-G) Representative fluorescent images for Lucifer Yellow (LY) in control and sulfatide treated conditions in the presence of two well know gap junction blockers, 18α-glycyrrhetinic acid (AGA) or Octanol (OCT). The white line represents the scratch site. (H) Quantification of the distance migrated in μm by LY from the injury site. Normalization was performed using dextran-Alexa Fluor 594 (dye not permeable to gap junctions). Treatment of human primary astrocytes with sulfatide (gray wave) resulted in increased LY intensity compared to untreated (control, beige wave) conditions. Multiple t-tests analyzed LY intensity vs. diffusion data points with the Holm-Sidak method (alpha=0.05) for statistical significance (n=7). LY diffusion was GJ dependent, as pre-incubation of untreated (control) astrocytes with AGA (green curve) or OCT (dark green curve) prevented the diffusion of LY, and the staining was captured primarily by the cells in the scrape area. Pre-incubation of sulfatide-treated astrocytes with AGA (pink curve) or OCT (orange curve) prevented the diffusion of LY, and the staining was retained primarily by the cells in the scrape area. Multiple t-tests for LY diffusion vs. intensity analyzed data points with the Holm-Sidak method (alpha=0.05) compared to control *$p \leq 0.05$ and sulfatide #$p \leq 0.05$.

DISCUSSION

Our data demonstrated that viral reservoirs mediate chronic HIV-associated CNS damage even in the current cART era, especially in myelin-rich areas compromising its structure and integrity. The presence of viral reservoirs results in increased sulfatide levels that compromise gap junctional communication and associated calcium signaling, both essential components of proper brain function. Thus, we propose that increased sulfatide levels are a key mediator of CNS damage in the HIV-infected population and could be a potential biomarker of early or chronic stages of HIV CNS dysfunction.

Using human brain tissues, we identified that specific sulfatide (24:0, 24:1 and their hydroxylated species) was upregulated in HIV-infected individuals with MND, HAD, and Alzheimer's cases. Long-chain sulfatides 24:0 and 24:1 are the major species present in mature myelin. Shorter chain sulfatides with 16 to 22 carbon non-hydroxylated and hydroxylated fatty acids play a crucial role in oligodendrocytes maturation; thus, they modulate their expression in the premature myelin stages (Hirahara, Wakabayashi et al. 2017). Our findings showed significant changes for the long-chain 24:0 and 24:1 sulfatide (hydroxy fatty acid to non-hydroxy fatty acid species) in WM of the HIV-infected population with mild and severe cognitive impairment. These sulfatide species are important for maintaining and functioning myelin sheath structure (Hirahara, Wakabayashi et al. 2017). Therefore, their altered metabolism correlates with a direct compromise of mature myelin structure observed for the HIV-MND and HAD conditions analyzed and for AD cases.

Interestingly, sulfatide dysregulation observed within the WM of HIV-MND and HAD-affected individuals was not correlating with PA/PE expression and distribution, indicating a lack of uniform cell damage/destruction within these tissues. Myelin structural protein compromise observed in the immediate surrounding area of HIV reservoirs indicates a specific mechanism of dysregulation induced by latent HIV-

infected cells. Thus, we propose that damage could be spread from viral reservoirs and compromise myelin integrity even without systemic viral replication. The concentric mechanisms of damage associated with viral reservoirs indicate that tissue reservoirs can generate chronic damage in the absence of viral replication, and novel mechanisms of amplification of damage need to be considered to reduce the devastating consequences of NeuroHIV.

Further, utilizing mild/severe AD cases as a positive control of brain damage provided several important points in the analysis of brains obtained from HIV-infected individuals. First, some of the damage can reach myelin compromise severity observed in AD cases; second, HIV damage can be expanded from viral reservoirs into neighboring uninfected areas of the brain, suggesting a unique mechanism of amplification independent of systemic viral replication; third, the HIV-mediated damage and sulfatide dysregulation can provide a unique mechanism of myelin compromise that may contribute to the motor abnormalities observed in the HIV-infected population.

Our data demonstrate that viral reservoirs are associated with significant bystander damage to large brain areas. As described by several groups, smaller cortical volumes, thinner cortical thickness, and poorer cognitive function are associated with the appearance of WM hyperdensities (Sanford, Fernandez Cruz et al. 2017, Strain, Burdo et al. 2017, Cooley, Paul et al. 2021). But the nature of these hyperdensities is unknown. Neurobiological changes have been reported to occur soon after initial HIV infection and worsen in the absence of cART, resulting in early signs of cognitive deficits (Cole, Caan et al. 2018, Sanford, Ances et al. 2018, Sanford, Fellows et al. 2018). Later, during chronic infection with cART, the total numbers of individuals with the cognitive disorder remain equal to the early infection events. However, the cases of HAD have decreased into more mild forms of cognitive impairment. In these cases, cognitive impairment is independent of systemic viral replication and immune reconstitution (Saylor, Dickens et al. 2016). Our data also indicate that myelin compromise was not associated with age,

gender, systemic HIV replication (plasma and CSF), CD4 counts, cART regimen, and reported years with HIV, suggesting that ongoing brain damage in the HIV-infected population is dependent on viral reservoirs and unknown mechanisms of toxicity.

A potential mechanism of toxicity in the HIV-infected population due to the upregulation of sulfatide and mild myelin compromise could be the immune detection of these self-antigens. Research in neurodegenerative disorders, including HIV and multiple sclerosis (MS), supports this idea, indicating that the immune system can recognize myelin components as foreign antigens and establish a strong immune response. We demonstrated that low levels of soluble MBP induce microglia/macrophage activation resulting in cytokine and chemokine release (D'Aversa, Eugenin et al. 2013). These data indicate that mild myelin damage also contributes to the amplification of damage by immune activation. In addition, sulfatide in immune cells helps lymphocyte homing and increases monocyte differentiation and adhesion (Yang, Lee et al. 2011, Kim, Han et al. 2020, Williams, Chen et al. 2020). Also, natural killer cells, innate-like T cells, could recognize lipid antigens, including sulfatide, by a CD1-dependent mechanism to elicit a strong immune response (Samygina, Popov et al. 2011, Patel, Pellicci et al. 2012, Stax, Tuengel et al. 2017). CD1 sulfatide presentation to type II natural killer cells and T cells results in regulation of the T helper 1 (Th1), Th2, and Th17 immune responses, and they could participate in autoimmune diseases (Dasgupta and Kumar 2016), indicating a potential autoimmune role for the free sulfatide increase we observed to be induced by HIV. Long-chain sulfatides are more efficient in natural killer cell activation, and the generation of soluble sulfatide has been described in autoimmune hepatitis and experimental autoimmune encephalomyelitis involving an L-selectin-dependent mechanism (Kanter, Narayana et al. 2006, Sebode, Wigger et al. 2019). Soluble sulfatide also has coagulation properties by binding fibrinogen, laminins, thrombospondin, and selectin in platelets (Kyogashima, Onaya et al. 1998, Kyogashima 2004, Inoue, Taguchi et al. 2010). Also, sulfatide has been proposed to be a biomarker of carcinoma (Takahashi

and Suzuki 2012), viral replication (Takahashi, Ito et al. 2012, Takahashi, Takaguchi et al. 2013, Takahashi and Suzuki 2015), and tuberculosis (Dos Santos, Lovero et al. 2020), suggesting that sulfatide plays a key role in several pathogenic and genetic conditions. These conditions have been described in HIV-infected individuals and probably contribute to viral reservoir survival and chronic inflammation.

Although astrocytes are considered non-excitable cells, their activation results from variations in cytosolic calcium and voltage-gated channels (Cornell-Bell, Finkbeiner et al. 1990, Sontheimer 1994, Sontheimer, Fernandez-Marques et al. 1994). Normally, these calcium signals in astrocytes respond to the synaptic activity and regulate the release and uptake of gliotransmitters such as ATP, TNF-α, or D-serine, which further modulate neuronal synapses and BBB function by a lipid-dependent mechanism (Zonta, Angulo et al. 2003, Zonta, Sebelin et al. 2003, Takano, Tian et al. 2006, Wang, Lou et al. 2006). The close association between calcium signaling in astrocytes is essential for pre- and post-synapse function by modulating neuronal synchronization and firing patterns (Perea and Araque 2005, Perea and Araque 2005). Our findings sustain that sulfatide compromised the triggering of calcium waves could have significant consequences on neuronal activity, BBB integrity, and blood flow control. All these mechanisms need further examination, especially for myelin components, due to their importance in HIV as well as traumatic brain injury (TBI) and MS.

Astrocytic calcium signals relay in several key components, pacemaker cells, IP_3R activation, and diffusion of calcium and IP_3 *via* gap junctions, both IP_3R and gap junctions are highly enriched in astrocytes (Newman 2001, Giaume, Naus et al. 2021). Our data in HIV-infected astrocytes indicate that HIV infection and latency decreased IP_3 degradation in infected cells to enable diffusion by gap junctions into surrounding uninfected cells. In HIV-infected astrocytes, the high levels of IP_3 do not result in calcium overload because Nef protein binds to the IP_3R_1 preventing its proper activation and subsequent apoptosis. However, in surrounding uninfected cells but communicated

by gap junction, Nef is not present and diffused IP_3 can trigger a calcium response. (Eugenin, Clements et al. 2011, Malik, Valdebenito et al. 2021, Valdebenito, Castellano et al. 2021). Cx43 stability and gap junction maintenance in HIV-infected astrocytes are depended on residual HIV-Tat protein expression in glial reservoirs (Eugenin and Berman 2007, Eugenin, Clements et al. 2011, Eugenin and Berman 2013, Berman, Carvallo et al. 2016, Malik, Theis et al. 2017, Gajardo-Gomez, Santibanez et al. 2020, D'Amico, Valdebenito et al. 2021, Malik, Valdebenito et al. 2021, Valdebenito, Castellano et al. 2021). Our data *in vivo* and *in vitro* indicate that latent HIV-infected astrocytes use gap junctions and IP_3 to amplify apoptosis and toxicity into neighboring uninfected cells (endothelial, neurons, and astrocytes) (Eugenin, Clements et al. 2011, Berman, Carvallo et al. 2016, Malik, Theis et al. 2017, Malik, Valdebenito et al. 2021). HIV-latent infected cells were resistant to apoptosis and toxicity by a mechanism that prevents the proper IP_3 and IP_3R signaling on the endoplasmic reticulum membrane and loss of interactions with the mitochondria (Malik, Valdebenito et al. 2021). Normally, all these components work together to signal and prevent toxicity. But how important could be astrocyte infection and dysregulated signaling in the HIV-infected population? A single astrocyte can communicate or enwrap hundreds of synapses (Ventura and Harris 1999, Mestre, Cerquido et al. 2017, Mestre, Inacio et al. 2017), but also astrocytes/astrocyte interaction and their calcium waves are essential to coordinate blood flow, BBB permeability, and the gliovascular unit to provide and exclude material to neurons/glia cells (Lin, Weigel et al. 1998, Cotrina, Lin et al. 2000, Simard, Arcuino et al. 2003, Wang, Lou et al. 2006). Thus, the potential implications of HIV, sulfatide, and calcium waves dysregulation are significant. HIV-infected cells could amplify toxicity to neighboring uninfected cells, as observed in our data in myelinic areas. Here, we propose that local myelin compromise further contributes to local inflammation and neuronal dysfunction associated with the presence and altered signaling provided by viral reservoirs. Another component of the bystander toxicity observed in HIV-infected

individuals is the high ATP concentration in the circulation that can predict cognitive decline (Velasquez, Prevedel et al. 2020). Extracellular ATP is one of the more powerful inflammatory stimuli and a key player in calcium cell-to-cell signaling by amplifying the calcium waves (Koizumi 2010, De Bock, Decrock et al. 2014, Pacholko, Wotton et al. 2020). We identified that ATP secretion is mediated by Cxs and Pannexin hemichannels used by HIV-infected cells to amplify local inflammation (Gajardo-Gomez, Santibanez et al. 2020, Velasquez, Prevedel et al. 2020, D'Amico, Valdebenito et al. 2021). Normally, Cxs/Panx-1 hemichannels are in a close stage, but upon acute or chronic infection, both become open, resulting in the release of ATP and several lipids through the channel pore (Malik, Theis et al. 2017, Gajardo-Gomez, Santibanez et al. 2020, D'Amico, Valdebenito et al. 2021, Gorska, Donoso et al. 2021). However, the potential therapeutic role of ATP, Cxs/Panx-1 channels, purinergic receptors (ATP receptors), and their interaction with gap junctional communication in HIV is only recently explored and will provide critical tools to understand the long/chronic term HIV pathogenesis but also the development of additional treatments to prevent of reducing the devastating consequences of HIV in the CNS.

In addition, our finding that free sulfatide levels are increased within the WM of neuroHIV-affected individuals and that free sulfatide can promote gap-junction controlled cell-to-cell communication identifies a potential host-directed therapeutic target to control HIV-induced bystander damage. Indeed, therapeutic modulation of specific lipid-related pathways has successfully prevented or reduced inflammatory diseases (Nakamura and Murayama 2014, Holzlechner, Eugenin et al. 2019, Darios, Mochel et al. 2020). Now, we are proposing a similar approach to chronic HIV.

Our data that CNS damage is associated with viral reservoirs provides a unique mechanism of bystander damage associated with sulfatide and gap junctional communication. Currently, the best described viral reservoirs are resting $CD4^+$ T lymphocytes, but in the brain, the main reservoirs are microglia/macrophages and a small

astrocyte population (Bruner, Hosmane et al. 2015, Churchill, Deeks et al. 2016). However, the brain is “insulated” due to the presence of the BBB, and it has been proposed that the sequences of the virus in the brain had different evolution than in other tissues (Woldemeskel, Kwaa et al. 2020, Blazkova, Gao et al. 2021, Sonti, Sharma et al. 2021). In agreement, it has been shown that rebounding HIV is genetically different from circulating viral reservoirs suggesting that viruses came from other tissues and cell types, including the brain (Lorenzo-Redondo, Fryer et al. 2016, Salemi and Rife 2016, Bandera, Gori et al. 2019, Blazkova, Gao et al. 2021). Thus, examining the different kinds of viral reservoirs and the mechanisms of bystander damage is essential to understanding and treating the cognitive decline observed in at least 50% of the HIV-infected individuals under cART.

CHAPTER 4 – PENDING DATA: CHARACTERIZATION OF CX43-ASSOCIATED BINDING PROTEINS AFTER SULFATIDE TREATMENT BY PROTEOMICS, IDENTIFICATION OF ASTROCYTES POPULATIONS SUSCEPTIBLE TO HIV INFECTION BY SCRNASEQ, AND LIPID DYSREGULATION OF HIV-INFECTED ASTROCYTES ANALYZED BY MSI

D'Amico Daniela[1,2]; Ajasin David O.[1]; Fox Howard S.[3], Prideaux Brendan[1]; Eugenin Eliseo A.[1]

[1]University of Texas Medical Branch (UTMB), Department of Neuroscience, Cell Biology and Anatomy, Galveston, TX, USA

[2]University of Palermo (UniPa), Department of Biomedicine, Neuroscience and Advanced Diagnostics, Palermo, Italy

[3]University of Nebraska Medical Center, Department of Neurological Sciences, Omaha, NE, USA

This work was funded by The National Institute of Mental Health grant, MH096625, MH128028, the National Institute of Neurological Disorders and Stroke, NS105584, and UTMB internal funding (to E.A.E).

INTRODUCTION

This chapter aims to introduce three major experiments that need to be completed in the future: first, proteomics of Cx43 interacting proteins using Hela cells stably transfected with Connexin43-CFP (Hela-Cx43-CFP) in the presence and absence of sulfatide; second, single-cell RNA sequencing (scRNAseq) of human primary astrocyte cultures knocking-down for Cx43 to identify astrocyte populations that are inclined to HIV infection or undergo bystander apoptosis; and lastly, mass spectrometry imaging (MSI) to analyze lipid dysregulation in primary cultures of HIV-infected astrocytes.

Proteomics is a large-scale study for identifying and quantifying proteomes, including a set of proteins synthesized in an organism, system, or biological context. Proteomics reflects the underlying transcriptome, so it can expand transcriptomics data to directly identify the proteins that are up- or down-regulated in specific conditions and investigate the related pathways (Aslam, Basit et al. 2017). Previous transcriptomics and proteomics results from our laboratory (data not shown) supported lipid alteration in HIV-infected astrocytes, mostly related to the upregulation of ceramide-related enzymes. Transcriptomic analysis of 7 days of HIV-infected astrocytes showed that HIV infection increased levels of glucosylceramidase, galactosyltransferase, and ceramide synthase, which are enzymes critically involved in ceramide and sulfatide synthesis. In addition, proteomics data from 21 days of HIV-infected astrocytes confirmed glucosylceramidase and galactosyltransferase up-regulation, suggesting sulfatide accumulation. This result correlates with our MALDI-MSI data presented in Chapter 3 showing higher sulfatide (24:0, 24:1, 24:0 OH, and 24:1 OH) relative abundance in the brain, specifically in the white matter of HIV-infected individuals under cART and with mild and severe cognitive impairment (see Table 2, Chapter 3). Since we have proposed sulfatide as a potential biomarker or target of HAND, that improves Cx43 mRNA and protein expression, as

well as cell-to-cell communication in primary astrocytes, our interest is to identify the Cx43 interacting proteins and associated molecular pathways through proteomics.

Single-cell RNA sequencing has revolutionized the transcriptome field reaching variations at a single-cell resolution (Slovin, Carissimo et al. 2021). In Chapter 2, we identified that only a small population of astrocytes are latent HIV-infected and synthesize a residual amount of HIV mRNA and viral proteins inducing CNS bystander damage. Thus, using scRNAseq we intend to identify and diversify astrocyte populations prone to HIV infection and becoming CNS viral reservoirs or to undergoing the bystander toxic effects mediated by the closer glial reservoirs. Five populations were identified across the adult brain. These astrocytes exhibit different spatial positions, molecular, and functional properties (John Lin, Yu et al. 2017, Khakh and Deneen 2019, Batiuk, Martirosyan et al. 2020). To select specific transcriptomic profiles of the HIV-infected astrocytes that upregulate Cx43 to enhance HIV bystander damage in the brain (Berman, Carvallo et al. 2016), we propose to analyze human primary astrocytes knocking-down for Cx43 and HIV-infected for 21 days. Hence, scRNAseq is crucial to investigating astrocyte heterogeneity in neuroHIV. This objective is part of our group collaboration with Dr. Fox Howard (University of Nebraska Medical Center).

Cellular spatial details about altered lipid metabolism in HIV-infected astrocytes are missing. In HIV-infected astrocytes, inter-organelle/lipid/second messenger interactions are essential for the survival mechanism and apoptosis of surrounding uninfected cells (Malik, Valdebenito et al. 2021). Therefore, we decided to analyze lipid dysregulation in primary cultures of astrocytes uninfected and HIV-infected using MSI in positive or negative analysis mode. This approach must be compatible with complementary imaging techniques to identify the HIV DNA-positive cells in the same cell layer.

MATERIALS AND METHODS

Cell Culture Methods

Hela cells stably transfected with Cx43-CFP were grown with high glucose Dulbecco's modified Eagle's medium (DMEM, Cat# 11995-065, Thermo Fisher Scientific, Waltham, MA) supplemented with 10% fetal bovine serum (FBS, Cat# S12450H, Atlanta Biologicals, Flowery Branch, GA), 2 mM Geneticin (Cat# 10131-027, Thermo Fisher Scientific, Waltham, MA), penicillin, and streptomycin (Cat# 15070063, Thermo Fisher Scientific, Waltham, MA) at 37 °C in a humidified atmosphere with 5% CO_2.

Cortical human fetal tissue was obtained as part of a research protocol approved by the Albert Einstein College of Medicine and collected between 2011 to 2018. The preparation of human astrocyte cultures was performed as previously described (Eugenin and Berman, 2007). High glucose Dulbecco's modified Eagle's medium (DMEM, Cat# 11995-065, Thermo Fisher Scientific, Waltham, MA) supplemented with 10% fetal bovine serum (FBS, Cat# S12450H, Atlanta Biologicals, Flowery Branch, GA), penicillin, and streptomycin (Cat# 15070063, Thermo Fisher Scientific, Waltham, MA) were used to grow the cells at 37°C in a humidified atmosphere with 5% CO_2.

HIV infection

Confluent cultures of human astrocytes were infected by incubation with HIV_{ADA} (20–50 ng/ml HIV-p24) for 21 days, using a previously described protocol (Eugenin, Clements et al. 2011, Valdebenito, Castellano et al. 2021). Briefly, astrocyte cultures were exposed to the virus for 24 h, the medium was removed, and astrocytes were washed extensively to eliminate the unbound virus before adding a fresh medium supplemented with only 2% fetal bovine serum (FBS, Cat# S12450H, Atlanta

Biologicals, Flowery Branch, GA), penicillin, and streptomycin (Cat# 15070063, Thermo Fisher Scientific, Waltham, MA) to avoid over proliferation.

Cx43 immunoprecipitation

Immunoprecipitation analysis was performed for Cx43 as described in Fig. 4.1. Hela cells stably transfected with Cx43-CFP were treated with sulfatide (10 μg/ml) for 24 h. Cells were homogenized with RIPA buffer containing protease and phosphatase inhibitors and sonicated using 5 pulses of 30 sec on and 30 sec off in a Microtip (Misonix, Inc, Microson XL-2000). Samples were pre-cleared with protein G plus agarose (Cat# sc-2002, Santa Cruz Biotechnology, Dallas, TX) and immunoprecipitated using Cx43 antibody (Cat# C6219, Sigma-Aldrich, St. Luis, MO). These samples were sent to Creative Proteomics (Shirley, NY) for identifying and quantifying using a high-resolution mass spectrometry platform coupled with nanoflow UPLC to select proteins with a fold-change cutoff above 1.5 or below 1/1.5 (n=2 technical replicates).

Proteomics for proteins associated with Cx43

The bead samples from untreated and sulfatide-treated cultures of Hela cells stably transfected with Cx43-CFP were resuspended in 40 μl of 1× electrophoresis sample buffer, boiled for 15 min and run on 12% separating gel for 20 min at 80 kV and 30 min at 120 kV. The SDS-PAGE gel was stained with Coomassie Brilliant Blue and each gel band was cut to be subjected to protein precipitation using cold acetone and centrifuged at 12,000 rpm. Later, 50 mM ammonium bicarbonate was added, and the protein solution was transferred into Microcon devices YM-10 (Millipore). The device was centrifuged at 12,000 rpm at 4°C for 10 min. Subsequently, 200 μl of 50 mM ammonium bicarbonate was added to the concentrate followed by centrifugation and repeated once. After being reduced by 10 mM DL-dithiothreitol at 56°C for 1 h and alkylated by 20 mM odoacetamide at room temperature in the dark for 1 h, the device was centrifuged at 12,000 rpm at 4°C for 10 min and washed once with 50 mM

ammonium bicarbonate. 100 µl of 50 mM ammonium bicarbonate and free trypsin were added into the protein solution at a ratio of 1:50, and the obtained solution was incubated at 37°C overnight. Finally, the device was centrifuged at 12,000 rpm at 4°C for 10 min. 100 µl of 50 mM ammonium bicarbonate was added into the device and centrifuged, and then repeated once. The extracted peptides were lyophilized to near dryness and resuspended in 2-20 µl of 0.1% formic acid before LC-MS/MS analysis. These samples were analyzed and quantified on Obitrap Q Exactive HF mass spectrometer coupled with an Ultimate 3000 nano UHPLC system. The detected peptides were analyzed and searched against human protein database using Maxquant. The parameters were set as follows: the protein modifications were carbamidomethylation (fixed) and oxidation (variable); the enzyme specificity was set to trypsin; the maximum missed cleavages were set to 2; the precursor ion mass tolerance was set to 10 ppm, and MS/MS tolerance was 0.6 Da. Pathways analysis Creative Proteomics identified 455 proteins that bind to Cx43 after sulfatide treatment. These proteins were classified into 13 families (Fig. 4.2) according to their function and location described in the GeneCards human gene database. Only the up-regulated recycling transport, mitochondrial and membrane-related proteins after sulfatide stimulation were run for the Ingenuity Pathway Analysis (IPA) to build molecular networks of each experimental system (Fig. 4.3).

Lentiviral transduction

To knockdown Cx43, human primary astrocytes were transduced with Cx43-targeted shRNA lentiviral particle (Cat# TL312771V, OriGene, Rockville, MA) and negative control shRNA lentiviral particle (Cat# TR30021V, OriGene, Rockville, MA) with manufacturer recommended protocol. Briefly, cells were seeded in 60 mm plate. Cx43-targeted shRNA lentiviral particle (100 ng/ml) was added into the cells and incubated at 37°C with atmospheric CO_2 overnight. After three days, transduced astrocytes were selected with puromycin (Cat# A1113802, Thermo Fisher Scientific,

Waltham, MA). shRNA-transduced cells were harvested to evaluate the expression of Cx43 by western blot and qRT-PCR. 37°C with 5% CO_2.

MALDI-MSI analysis

Human primary astrocytes were plated onto Corning® alkaline earth boro-aluminosilicate glasses (CB-90IN-S111, Delta Technologies, Loveland, CO) coated with Poly-D-Lysine solution (1.0 mg/mL, A-003-E, Millipore Sigma, St. Luis, MO), inside of a silicon ring. After 24h, they were infected with HIV_{ADA} (20-50 ng/ml HIV-p24). At day 21, the medium was removed, and astrocytes were washed and scanned at the digital slide scanner NanoZoomer (C13210-04, Hamamatsu, Bridgewater, NJ). Different matrixes can be applied for negative and positive ion mode lipid imaging as described in Chapter 3 and 5. Briefly, matrix was applied to the cell layer by automated air spray deposition using the TM-sprayer (HTX Technologies LLC, Chapel Hill, NC). The nozzle temperature was set to 60°C, the flow rate was 40 µL/min, and 20 passes over the cell layer were performed. MALDI-MSI analysis was performed using Q Exactive HF Hybrid Quadrupole-Orbitrap Mass Spectrometer (Thermo Fisher Scientific) equipped with an Elevated Pressure Matrix-Assisted Laser/Desorption Ionization (EP MALDI) source integrating an Nd: YAG laser (Spectroglyph LLC, Kennewick, WA). Data were acquired at 10, 15, or 20 μm^2 lateral resolution in negative/positive ion mode at a laser power of 7 µJ. External mass calibration was performed using calibration solutions (A39239, Thermo Fisher Scientific). The accurate mass-measured lipid peaks were identified by matching reference lipids in the LIPID MAPS and Human Metabolome Database within a ±0.002 Da mass tolerance window. Thermo RAW format data files were converted to imzML using ImageInsight software (Spectroglyph LLC, Kennewick, WA). Data visualization was performed using SciLs software (SCiLS GmbH, Bremen, Germany).

Immunofluorescence

Matrix can be removed by washing the cellular layer into the slide 3 times with methanol (Cat# A456-4, Thermo Fisher Scientific, Waltham, MA)/PBS (Cat# BP665-1, Thermo Fisher Scientific, Waltham, MA) solution (7:3 v/v). Antigen retrieval was performed by incubating the cell layer in a commercial antigen retrieval solution (Cat# S1700, Agilent Dako, Santa Clara, CA) for 30 min at close to 80°C water-bath. The slide was removed from the bath and then allowed to cool down in 1X TBS (Cat# BP2471-1, Thermo Fisher Scientific, Waltham, MA) and permeabilized in 0.1% Triton (Cat# X-100, Sigma-Aldrich, St. Luis, MO) for 2 min at RT. Unspecific antibody binding sites were blocked by incubating the cells with freshly prepared blocking solution (0.5 M EDTA pH 8.0; Cat# 15575-038, Thermo Fisher Scientific, Waltham, MA), 1% Fish gelatin from cold water (Cat# G7765, Sigma-Aldrich, St. Luis, MO), 0.1 g Albumin from bovine serum-immunoglobulin free (Thermo Fisher Scientific, Waltham, MA), 1% Horse Serum (Cat# H1138, Sigma-Aldrich, St. Luis, MO), 5% human serum (Cat# 31876, Thermo Fisher Scientific, Waltham, MA), 9 ml ddH20) for 2 h at RT in a humidity chamber. The primary antibodies (anti-GFAP, anti-rabbit, dilution 1:100, Cat# SAB4501162, RRID: AB_10746077, Sigma-Aldrich, St. Luis, MO) were added to the samples diluted in blocking solution and incubated at 4°C overnight. Cells were washed with TBS at RT several times and incubated with the appropriate secondary antibodies (Alexa anti-rabbit 488, dilution 1:500, Cat# A32723, Thermo Fisher Scientific, Waltham, MA) for at least 2 h at RT followed by several washes in TBS. The slides were then mounted using Prolong Gold anti-fade reagent (Cat# P36930, Thermo Fisher Scientific, Waltham, MA) and examined using an A1 confocal microscope (Nikon, Japan).

CURRENT RESULTS

Soluble sulfatide changes the molecular interactions of Cx43

As sulfatide can regulate mRNA and protein Cx43 expression, we used Hela cells stably transfected with Cx43-CFP treated with 10 μg/ml sulfatide for 24 h to pull-down Cx43 using G PLUS Agarose beads. Thus, we confirmed the presence of Cx43 in the beads by the SDS-page. Fig. 4.1 is a graphical representation of the protocol performed. These beads were processed and analyzed by Nano LC-MS/MS for proteomics. Proteomics analysis revealed 455 proteins. Comparing the control sample obtained from the coimmunoprecipitation of Cx43 in Hela cells stably transfected with Cx43-CFP and the sulfatide sample obtained from the same cells treated with sulfatide for 24 h, 263 proteins that bind to Cx43 were highlighted, 95 were upregulated and 168 downregulated. We classified the highlighted proteins of each experimental system into 13 families (ribosomal, metabolic, secreted, Golgi apparatus, endoplasmic reticulum, mitochondrial, recycling transport, ubiquitin, and membrane-related proteins, plus unknown proteins) according to their role and physiological compartments provided by GeneCards information and literature data. We show an illustration integrating all of these in Fig. 4.2. Nuclear, membrane nuclear, and mRNA-related proteins were excluded for the following analysis because they do not bind to Cx43; their detection was an experimental artifact due to the mechanical disruption of the nuclear membrane during the processing of the samples. Thus, we focused on the plasma membrane, mitochondria (Rodriguez-Sinovas, Ruiz-Meana et al. 2018), and transport compartments (Thomas, Jordan et al. 2005), where Cx43 is predominantly located (see Table 3). Focusing our analysis on the transport proteins that directly or indirectly bind to Cx43, sulfatide upregulated proteins related to myosins such as Myosin Light Chain 1 (MYOFTA, MYO1B, MYO1C) and proteins involved in vesicular fusion and trafficking like the Rabs membrane-bound proteins (RAB2A, RAB1A) and the N-Ethylmaleimide Sensitive Factor (NSF).

Parallelly, tubulin (Tubulin Alpha 1c TUBA1C, Tubulin Beta Class I TUBB, Tubulin Beta 4B Class IVb TUBB4B, Tubulin Folding Cofactor A TFCA) and cytoskeletal organized proteins such as Leucine-Rich Pentatricopeptide Repeat Containing (LRPPRC) and Dynein Cytoplasmic 1 Heavy Chain 1 (DYNC1H1) were downregulated. Subsequently, we analyzed the mitochondrial proteins highlighting upregulated proteins related to apoptosis (such as Apoptosis-Inducing Factor Mitochondria Associated 1 (AIFM1)), to chaperon (such as Heat Shock Protein Family A Member 9 (HSPA9)), and the mitochondrial transmembrane electron transport (such as Voltage-Dependent Anion Channel 1/2 (VDAC1/2)). ATP synthesis (ATP Synthase F1 Subunit Alpha ATP5A, ATP Synthase F1 Subunit Beta ATP5B, ATP Synthase Membrane Subunit G ATP5L, ATP Synthase Subunit O ATP5PO, Carbamoyl-Phosphate Synthase 1 CPS1) and fatty acid metabolism (Hydroxyacyl-CoA Dehydrogenase Trifunctional Multienzyme Complex Subunit Alpha HADHA and Hydroxyacyl-CoA Dehydrogenase Trifunctional Multienzyme Complex Subunit Beta HADHB) related proteins were downregulated in the mitochondria, suggesting that several sources of energy can be used by these cells. Finally, we analyzed the plasma membrane proteins. Specifically, sulfatide induced upregulation of proteins that regulate the cellular membrane organization and stability such as actin (ACTN1/4), annexin (ANXA1/5), and spectrin (SPTAN1, SPTBN). Sulfatide upregulated Peptidylprolyl Isomerase A (PPIA), which is necessary to form infectious HIV virions and Protein Phosphatase 1 Catalytic Subunit Alpha (PPP1CA) that is involved in HIV viral transcription, suggesting a mechanistic link between Cx43, sulfatide, and HIV-infection. Furthermore, the observed upregulation of thioredoxin (TXN), which plays a key role in the reversible S-nitrosylation of cysteine residues in target proteins, suggests that TXN may S-nitrosylate Cx43 to maintain open Cx43 hemichannels. Cytoskeleton-related proteins (Cytoskeleton Associated Protein 4 CKAP4, Ezrin EZR) were downregulated in sulfatide conditions. Subsequently, only the up-regulated recycling transport, mitochondrial, and membrane-related proteins after

sulfatide stimulation were run for the Ingenuity Pathway Analysis (IPA) to build molecular networks of our experimental system (Fig. 4.3). Ingenuity pathway analysis for sulfatide provided 4 top canonical pathways including integrin-linked kinase signaling, actin cytoskeleton signaling, remodeling of epithelial adherent junctions, and EIF2 signaling. They were represented as network overlapping in Fig. 4.3. This analysis was limited to n=2 technical replicates and a single time point of sulfatide treatment (24 h).

Transduction decreases the cell proliferation rate in human primary astrocytes

Human primary astrocytes transduced with Cx43 shRNA and infected with HIV_{ADA} for 21 days were used to identify a specific class of astrocytes infected by HIV. Fig. 4.4 is a graphical representation of the protocol performed. This shRNA construct (Cx43 shRNA lentivirus) was designed against multiple splice variants at the Cx43 gene locus. Scramble shRNA lentivirus was used as internal control. Cells were later selected with puromycin. Western Blot and qRT-PCR recommended to evaluate the silencing effect of the shRNA construct 72 h post-transfection were not performed. We observed a decrease in cell proliferation, even in the cells transduced with the scrambled shRNA used as a control.

MALDI-MSI lipidomics analysis for HIV-infected astrocytes is compatible with the following staining

Human primary astrocytes infected with HIV_{ADA} for 21 days were used to identify altered lipid metabolism in HIV-positive and neighboring uninfected cells. Fig. 4.5 is a graphical representation of the protocol performed. Cells plated, HIV-infected, and matrix sprayed were used to perform MALDI-MSI at different lateral resolutions (10, 15, and 20 μm^2) to detect lipid relative expression at the cellular spatial details (Fig. 4.5). Matrix was removed with methanol washes without compromising molecular integrities or inducing cellular detachment from the slide. A test staining for GFAP (a marker of

astrocytes) demonstrated that the signal in the area that goes through the MSI laser is lower than the signal coming from the closer areas but still significant for proper cell and organelle identification by microscopy.

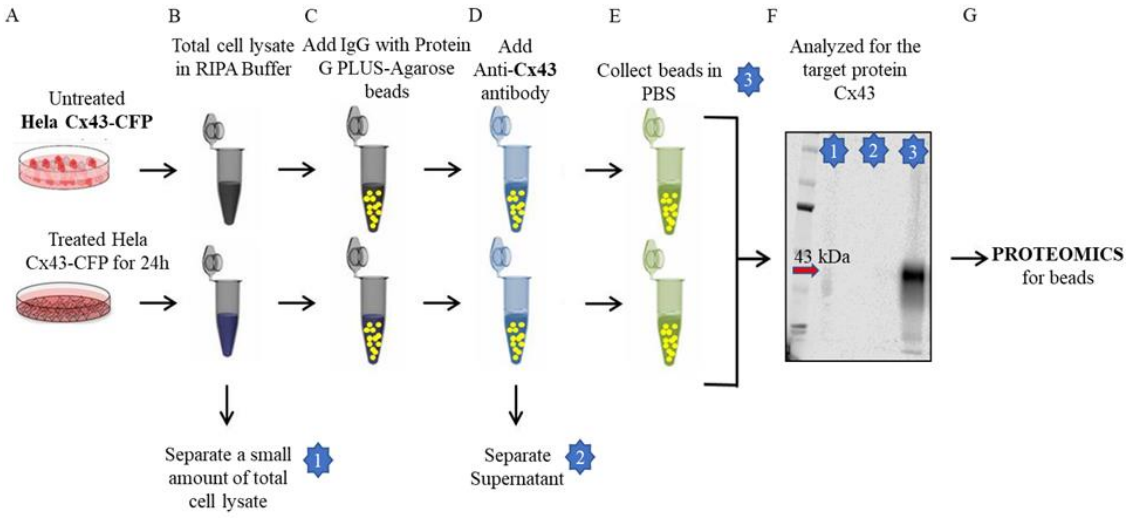

Figure 4.1. Summary of the immunoprecipitation protocol used to pull-down Cx43 for proteomics analysis

(A) Hela cells stably transfected with Cx43-CFP were plated and treated with 10 ng/ml sulfatide for 24 hours. (B) Untreated and treated cells were scratched with RIPA buffer to obtain the total cell lysates. A small amount of total cell lysate was isolated to be analyzed by SDS-page. (C) The total lysates were complemented with IgG and Protein G PLUS-Agarose beads to prevent non-specific binding. (D) Antibody against Cx43 was added to pull-down Cx43 and the related binding proteins. (E) The beads binding Cx43, and related interacting proteins were collected and dissolved in PBS. (F) SDS-page analyzed the total lysate, supernatant, and beads for Cx43. The band at 43 k.Da. representing Cx43 was strongly detected in the beads sample (3). (G) Beads were analyzed for proteomics.

Figure 4.2. Schematic representation of all the Cx43 binding proteins detected after sulfatide treatment, coimmunoprecipitation, and subsequent proteomics

Proteins binding to Cx43 were immunoprecipitated from Hela stably transfected Cx43-CFP cells treated with sulfatide for 24 hours. Proteins were classified in 13 families (nuclear, nuclear membrane, mRNA, ribosomal, metabolic, secreted, Golgi apparatus, endoplasmic reticulum, mitochondrial, recycling-transport, ubiquitin, and plasma membrane-related proteins, plus unknown proteins), according to their functional role and to their location described in GeneCards human gene database and literature data. Nuclear, membrane nuclear, and mRNA-related proteins (in the frame) were excluded because they do not physiologically bind to Cx43. Their detection was due to the mechanical disruption of the nuclear membrane during the procced of the samples. Downregulated proteins are indicated in red and upregulated in blue.

Table 3. Summary of the recycling-transport, mitochondrial, and plasma membrane-related proteins binding to Cx43 after sulfatide treatment for 24 h, following Cx43 coimmunoprecipitation, and subsequent proteomics.

Cx43 binding proteins					
Recycling-Transport		**Mitochondrial**		**Plasma Membrane**	
Down-Regulated	**Up-Regulated**	**Down-Regulated**	**Up-Regulated**	**Down-Regulated**	**Up-Regulated**
ACTA 1	B2M	ATAD3B	AIFM1	BASP1	ACTN1
ACTB	CAPZA1	ATP5PO	HSPA9	CKAP4	ACTN4
ACTR2B	MYH10	ATP5A	VDAC1	CTTN	ANXA1
ACTR3	MYL12A	ATP5B	VDAC2	EZR	ANXA5
ANXA2	MYO1B	ATP5L		IQGAP1	CFL1
ANXA4	MYO1C	CPS1		GNB2L1	DBN 1
ARPC2	NSF	HADHA		LMNB2	DSG1
ATP6V1A	PPIA	HADHB		LMO7	DSP
CAPZB	RAB1A	HMGCL		MSN	ESYT1
CKAP4	RAB2A	TUFM		PHB2	FLNB
CLTC	S100A11			SLC3A2	FSCN1
DYNC1H1	SERPINB1			STOM	PLEC
FLNA	TXN			TLN1	PPIA
FLOT1	YWHAB			VCL	PPP1CA
GDI2	YWHAZ				SPTAN1
ITGB1					SPTBN 1
LRPPRC					TXN
MYH9					
PLIN3					
RAB6					
SERPINH1					
SLC3A2					
TBCA					
TPM4					
TFRC					
TUBA1C					
TUBB					
TUBB4B					
VAT1					
YWHAG					
YWHAQ					
YWHAZ					

Downregulated proteins are shown in red; upregulated proteins are shown in blue.

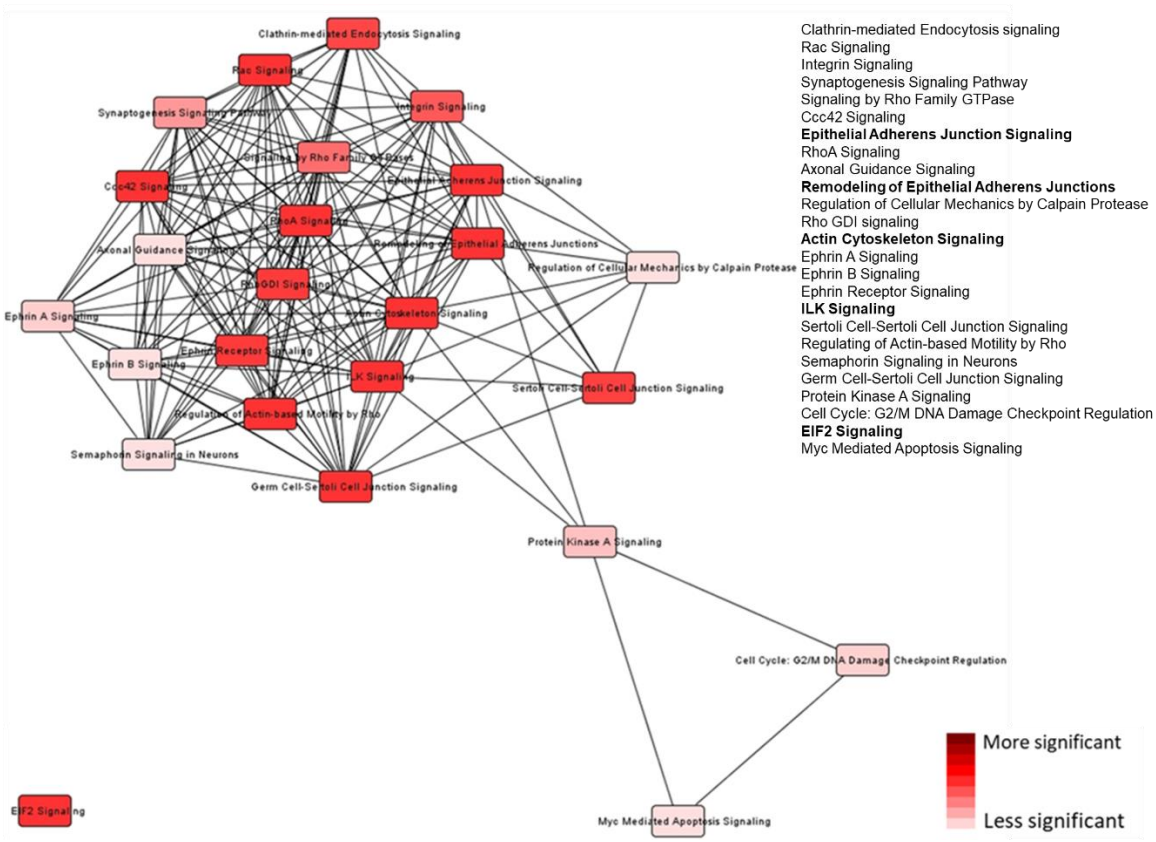

Figure 4.3. IPA network overlapping of the canonical pathways triggered by the upregulated recycling-transport, mitochondrial, and membrane-related proteins after sulfatide treatment

Proteins binding to Cx43 were immunoprecipitated from Hela stably transfected Cx43-CFP cells treated with sulfatide for 24 hours and analyzed by proteomics. The up-regulated proteins related to the recycling-transport, the mitochondrial and the membrane pathways were selected to build a specific molecular network using the Ingenuity Pathway Analysis software. The network overlapping showed the canonical pathways identified in our experimental system. Each pathway was indicated as a single "node" colored proportionally to the Fisher's Exact Test p-value; color intensity reflects average scaled expression. A line connecting two pathways when at least one data set molecule was common between them. Results suggest that the top canonical pathways include integrin-linked kinase (ILK) signaling, actin cytoskeleton signaling, remodeling of epithelial adherent junctions and EIF2 signaling. These pathways are involved in cellular morphology, assembly, organization, and movement. Future studies will examine the role of these proteins in the pathogenesis of HIV or neuroHIV.

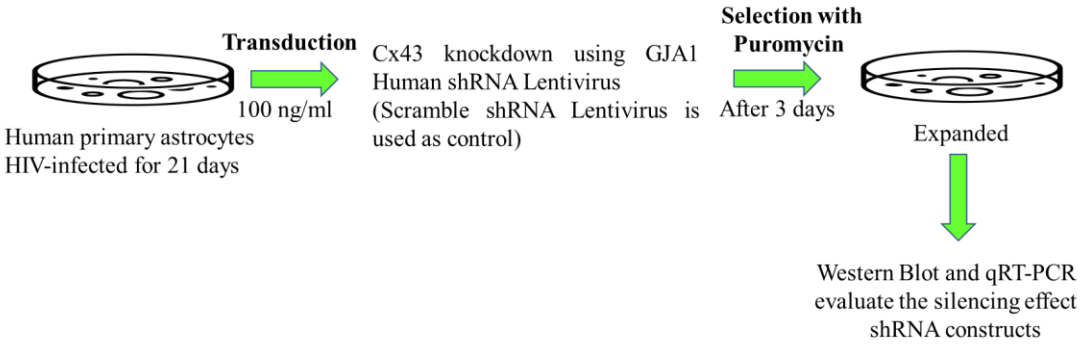

Figure 4.4. Schematic representation of Cx43 knockdown in HIV-infected human primary astrocytes

Human primary astrocytes were plated in a 60 mm plate, HIV_{ADA}-infected for 21 days, and transduced with Cx43-targeted shRNA lentiviral particle and negative control shRNA lentiviral particle as a control. Cx43 knocking down astrocytes were selected with puromycin for 3 days. After expansion, the silencing effect of the shRNA constructs must be tested by Western blotting and qRT-PCR.

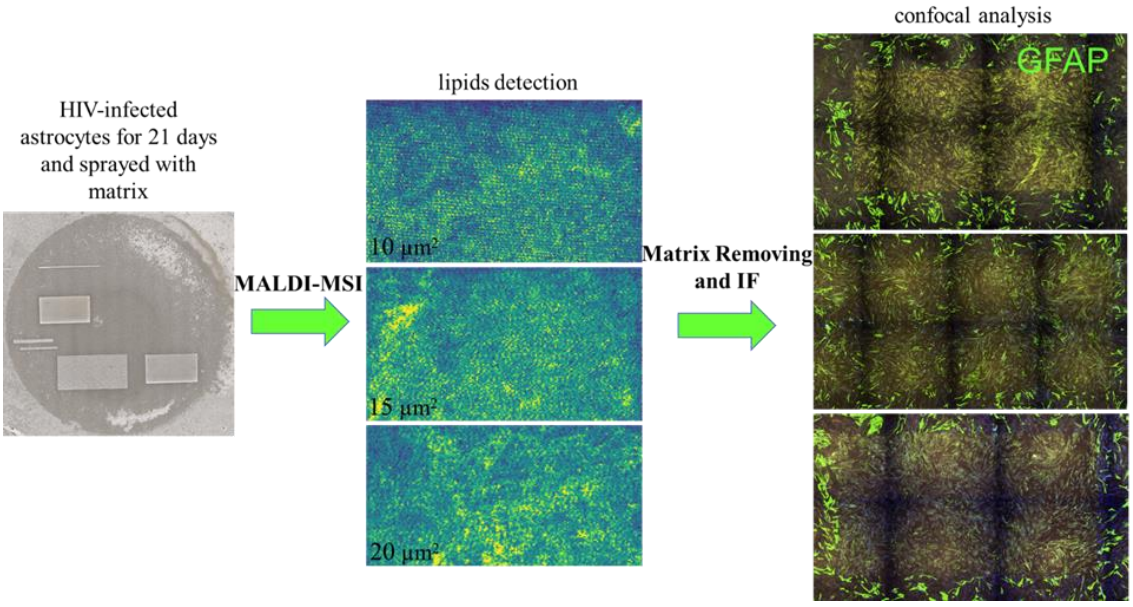

Figure 4.5. Schematic representation of lipidomics approach and complementary imaging of HIV-infected human primary astrocytes

Human primary astrocytes were plated inside a silicon ring, HIV_{ADA}-infected for 21 days, and matrix sprayed to perform MALDI-MSI at different lateral resolutions (10, 15, and 20 μm^2). Three rectangles were selected for MSI at the aforementioned lateral resolutions and resulting extracted ion images for phosphatidylcholine 36:1 are shown in the second panel. Matrix was removed and immunofluorescence for GFAP (a marker of astrocytes) was performed. GFAP positive signal was stronger in the area not irradiated by the laser; MSI laser areas showed lower GFAP signal but still sufficient to identify astrocytes.

DISCUSSION

Soluble sulfatide enhances Cx43 expression and cell-to-cell communication in human primary astrocytes. Several Cx43 partners can support Cx43 cellular coupling such as Connexin Interacting Protein of 75 k.Da. (CIP75) (Kopanic, Schlingmann et al. 2015), actin and protein kinase A (PKA)-binding protein Ezrin (Wall, Otey et al. 2007, Pidoux, Gerbaud et al. 2014, Dukic, Gerbaud et al. 2018, Sorgen, Trease et al. 2018), β-tubulin (Francis, Xu et al. 2011), Src kinase (Li, Spagnol et al. 2014), β-catenin (Talaveron, Matarredona et al. 2020), and debrin (DBN) (Butkevich, Hulsmann et al. 2004, Ambrosi, Ren et al. 2016); other proteins need to be investigated. Thus, we pulled-down Cx43 in Hela cells stably transfected with Cx43-CFP and treated with sulfatide for 24 h to perform proteomics analysis and investigate proteins that directly or indirectly bind to Cx43. Proteomics analysis provided a number of proteins that we divided into 13 families. We focused our attention on the recycling transport, mitochondria, and plasma membrane compartments to find specific correlations between sulfatide and cell-to-cell communication or sulfatide and mitochondrial metabolism. Analysis of the transport proteins induced by sulfatide and binding to Cx43 revealed an active vesicular transport, essential for the forward trafficking toward the plasma membrane and Cx43 recycling process. In addition, within the plasma membrane proteins that interact with Cx43 in the sulfatide-treated cells, peptidyl-prolyl isomerase A (PPIA) and peptidyl-prolyl isomerase A catalytic subunit α (PPP1CA) were identified. These proteins play a crucial role in the formation of infectious HIV virions and the viral transcription (An, Wang et al. 2007, Nekhai, Jerebtsova et al. 2007), supporting our association between viral reservoirs, bystander damage and lipid dysregulation investigated in Chapter 2 and 3. Sulfatide also upregulated TXN, which may induce S-nitrosylation of Cx43 on cysteine 271 to maintain open and functional Cx43 hemichannels (Retamal, Cortes et al. 2006, Straub, Billaud et al. 2011). Analyzing the mitochondrial proteins, we discovered that sulfatide induces

upregulation of Cx43 binding proteins related to fatty acid, glucose, and glutamate/glutamine synthesis.

The ingenuity pathway analysis for the upregulated proteins of recycling transport, mitochondria, and plasma membrane compartments highlighted pathways involved in cellular morphology, assembly, organization, and movement that further justify sulfatide contribution to cell-to-cell communication. The same proteomics analysis must be repeated investigating sulfatide effects at different time points and translated to HIV-infected astrocytes.

Human primary astrocytes need to be investigated to highlight the transcriptomic profile that characterize the astrocyte populations able to survive HIV infection (Eugenin, Clements et al. 2011, Eugenin and Berman 2013, Berman, Carvallo et al. 2016, Malik, Theis et al. 2017, Gorska, Donoso et al. 2021, Malik, Valdebenito et al. 2021, Valdebenito, Castellano et al. 2021) Transduced HIV-infected astrocytes with Cx43 shRNA lentivirus showed a significant decrease in cell proliferation, which was also observed in the same cells transduced with the scrambled shRNA lentivirus used as a control. Thus, we are in the process of optimizing sample preparation and troubleshooting Cx43 knowing down step before to perform scRNAseq analysis.

In correlation, latent HIV-infected astrocyte populations may be characterized by a specific lipidomic profile. To assess this, we must be able to resolve lipid signals within infected and neighboring uninfected cells. We demonstrated that merging complementary information from MALDI MSI assessment and confocal microscopy analysis is suitable within the same cell layer. Future work will focus on testing different matrices, improving lateral resolution, and running MALDI in positive and negative modes to cover all ionizable lipid species to improve our lipidomic analysis. To improve sensitivity and resolution, we plan to perform MALDI-2 MSI, a laser-based post-ionization method providing a signal increase of up to two or three orders of magnitude (as detailed in Chapter 5) (Gonzalez-Dominguez, Garcia-Barrera et al. 2014, Niehaus, Soltwisch et al.

2019). Subsequent staining will include DAPI to identify nuclei, GFAP as astrocyte marker, HIV DNA probe for the nef DNA sequence, and Alu-repeats probe as control of host DNA (Alu) to identify the astrocyte HIV-integrated DNA positive. Even though some of the approaches may appear naïve or ambitious, the nature and differentiation of immune, glial, and neuronal cells in the human brain are currently unknown. The proposed approaches can provide essential information about brain development, differentiation, and compromise in the current cART era.

Overall, the proposed approaches include high throughput and innovative analyses for the characterization of cell-to-cell heterogeneities at a molecular level for the neuroHIV and other diseases.

CHAPTER 5 – THE USE OF MALDI-2 MASS SPECTROMETRY IMAGING TO DETECT TRIGLYCERIDES IN AD MOUSE BRAIN

D'Amico Daniela[1,2], Marcatti M.[3], Fracassi A.[3],Taglialatela G.[3], Eugenin Eliseo A.[1], Prideaux Brendan [1],

[1]University of Texas Medical Branch (UTMB), Department of Neuroscience, Cell Biology and Anatomy, Galveston, TX, USA

[2]University of Palermo (UniPa), Department of Biomedicine, Neuroscience and Advanced Diagnostics, Palermo, Italy

[3]University of Texas Medical Branch (UTMB), Department of Neurology, Galveston, TX, USA.

This work was funded by The National Institute of Mental Health grant, MH096625, MH128028, the National Institute of Neurological Disorders and Stroke, NS105584, and UTMB internal funding (to E.A.E and to B.P.).

Adapted paper: D'Amico D., Marcatti M., Fracassi A., Taglialatela G., Eugenin E. A., Prideaux B. "MALDI-2 MSI Enhances Analytical Sensitivity for Triacylglycerides in Brain Tissue from an Alzheimer Mouse Model". In preparation.

INTRODUCTION

In recent years, the role of lipids has been identified as a key research focus in the study of neurological disorders. Abnormal lipid metabolism has been shown to contribute to the pathogenesis of several neurodegenerative diseases (Adibhatla and Hatcher 2008). In addition, neurological damage and lipid dysregulation occurring due to infectious etiology has been demonstrated for multiple pathogens including HIV (Bandaru, Mielke et al. 2013), Zika (Zhou, Chi et al. 2019), and Tick-Borne encephalitis (Du, Mi et al. 2021).

Neutral storage lipids have been previously shown to be dysregulated in multiple neurodegenerative disorders (Teixeira, Maciel et al. 2021). The most abundant neutral storage lipids are triacylglycerides (TAGs) and cholesteryl esters (CEs), which are typically present as lipid droplets (LDs) within tissues and cells. TAGs are comprised of three fatty acids tails esterified with a glycerol head group and may contain more than 900 different fatty acid compositions and combinations. CEs are formed by the esterification of cholesterol with long-chain fatty acids (typically C:16-C:22 in length).

The dysregulation of lipid metabolism, including aberrant accumulation of LDs, has been proposed to contribute to the development of amyotrophic lateral sclerosis (Kassan, Herms et al. 2013) and PD (Girard, Jollivet et al. 2021) pathologies. Accumulation of lipids within glial cells was even noted in the earliest AD's patient (Alzheimer, Stelzmann et al. 1995) and the role of lipid droplets within AD pathogenesis is a current research focus of particular interest (Farmer, Walsh et al. 2020, Yin 2022).

The 3xTg mouse model recapitulates similarities with the AD brain pathology observed in humans, and both amyloid beta plaques and neurofibrillary tangles become progressively present upon advanced age (Oddo, Caccamo et al. 2003). In addition, metabolic changes due to degradation of cholinergic and dopaminergic systems are recapitulated in this model (Guzman-Ramos, Osorio-Gomez et al. 2012, Moreno-Castilla,

Rodriguez-Duran et al. 2016), as well as neutral and membrane lipid alterations (Gonzalez de San Roman, Llorente-Ovejero et al. 2021). The 3xTg model has been used in multiple previous studies to investigate progressive metabolic and lipid dysfunction (Esteve, Jones et al. 2017, Kaya, Brinet et al. 2017, Chen, Hu et al. 2022). Lipid droplet accumulation in the 3xTg AD's mouse model was shown to precede the formation of the neuropathological hallmark amyloid plaques and neurofibrillary tangles (Hamilton, Dufresne et al. 2015). Using Matrix-Assisted Laser Desorption Ionization Mass Spectrometry Imaging (MALDI-MSI) and Liquid Chromatography Tandem Mass Spectrometry (LC-MS/MS), 12 distinct triglycerides were observed to accumulate within the tissues of the 3xTg AD mice versus wild-type control. Detailed localization by MALDI-MSI indicated that the accumulation of these TAGs was limited to the subventricular region of the brain. The authors also showed that free cholesterol concentrations did not change in the 3xTg mouse model versus wild-type control. However, the abundance and distribution of the esterified form of cholesterol (the form known to accumulate within lipid droplets) has not been elucidated within these regions of the brain. Hence there is a need for imaging techniques with improved sensitivity to detect and visualize the distribution of all neutral lipid classes within brain tissues from animal models and clinical samples to elucidate their role within neurodegenerative disease pathogenesis.

MALDI-MSI is a powerful and selective technique for detecting and visualizing lipid distributions within biological tissues. In MALDI-MSI, thin tissue sections are coated with a UV absorbing matrix applied in solution or as a dry application by sublimation (Gemperline, Rawson et al. 2014, Huizing, Ellis et al. 2019). A UV laser is used to ablate the tissue surface generating gas phase ions that are analyzed in the mass spectrometer. Mass spectra are acquired at each position the laser is fired and 2D ion maps can be plotted for any detected ions (peaks) in each spectrum.

A major limiting factor for the application of MALDI-MSI to study analytes within biological tissues is the sensitivity to detect molecules due to their low abundance or difficulty in generating ions that can be detected by the mass spectrometer. Moreover, as spatial resolution capabilities improve *via* the incorporation of lasers with smaller spot diameters or the use of laser oversampling, less material is ablated per laser acquisition meaning far fewer ions are produced and requiring more sensitive detection. Another issue with ion generation during MALDI-MSI is that upon irradiation with the laser, mostly neutral ions are desorbed rather than the charged ions capable of being detected by the mass spectrometer. It is estimated that the ratio of ions yielded per neutral molecule is below $1x10^{-6}$ (Tsai, Lee et al. 2013). Hence, only the most abundant or easily ionized molecules are detected. It is for this reason that most research into lipid classes in brain diseases by MALDI-MSI has concentrated upon the highly abundant and easily ionizable membrane lipids such as phosphatidylcholine and phosphatidylethanolamine (Shanta, Choi et al. 2012, Sparvero, Amoscato et al. 2012, Hong, Kang et al. 2016). Yet, there are lipid classes present at low abundance and with poor ionizing capabilities such as signaling and storage lipids that play crucial roles in neurological disease pathogenesis (Bruce, Zsombok et al. 2017).

Improved MALDI-MSI methods are urgently required to facilitate the analyses of these lipid species. A recently introduced approach for enhancing MALDI-MSI sensitivity is the incorporation of laser induced post-ionization known as MALDI-2 (Soltwisch, Kettling et al. 2015). In MALDI-2, a second pulsed UV post-ionization laser is aligned parallel to, and 200-400 μm above the tissue surface, and it is used to induce a secondary ionization of the ion plume following initial MALDI ionization. The precise mechanisms of MALDI-2 ionization are still being investigated. Current hypotheses include resonance-enhanced two-photon ionization (REMPI) (Potthoff, Minte et al. 2022) in which ionization of the matrix molecules is achieved by the post-ionization laser and proton transfer to or from neutral analyte molecules (M) in subsequent collisions to yield

the observed $[M + H]^+$ or $[M – H]^–$ species. This is supported by the increased presence of protonated analyte ions in comparison to metal cation species (such as $[M + Na]^+$ or $[M + K]^+$). A proposed mechanism for the generation of the metal cation adducts also detected during MALDI-2 is photodissociation of neutral matrix crystals during laser post-ionization (Potthoff, Dreisewerd et al. 2020).

Using MALDI-2, significantly more neutral molecules within the ion plume are ionized leading to ion yield increases of 2 orders of magnitudes or greater for small molecule analytes including lipids (Bowman, Bogie et al. 2020, Soltwisch, Heijs et al. 2020), carbohydrates (Heijs, Potthoff et al. 2020), drugs (Barre, Paine et al. 2019), and peptides (McMillen, Gutierrez et al. 2021). Lipid classes that have been shown to have the greatest increase in sensitivity include triacylglycerides (TAGs), cholesteryl esters (CEs), and hexosylceramides (HexCers) (Bowman, Bogie et al. 2020, McMillen, Fincher et al. 2020, Soltwisch, Heijs et al. 2020). Furthermore, the use of MALDI-2 enables lipid species that traditionally are only detected in negative ionization mode to be detectable using positive ionization mode including phosphatidylinositols (PI), phosphatidylethanolamines (PE), and free fatty acid (FFAs).

In the present study, MALDI-2 MSI was applied to examine neutral lipid distribution within brain tissue from the 3xTg AD mouse model at mid and advanced age timepoints and in comparison to age-matched wild-type controls. Our aim was to evaluate sensitivity gains offered by MALDI-2 MSI and assess the suitability of the technique for future neutral lipid imaging applications in neurogenerative disease research such as HAND.

MATERIALS AND METHODS

Mouse brain tissue sections

Male and female 3xTg-AD transgenic mice were purchased from Jackson Labs (Bar Harbor, ME) and maintained through a breeding program at UTMB (Bourne,

Natarajan et al. 2019). Brains were collected from 3 male mice at either 5 months or 17 months age and immediately frozen in liquid nitrogen vapor as previously described (Prideaux, Dartois et al. 2011). Control brains were collected from wild-type control B6J mice at 5-6 months of age.

Fresh frozen mouse brain tissues were cut in 10 µm thick serial sections (coronal sections) using a Leica CM1850 cryostat (Buffalo Grove, IL) and thaw-mounted onto Corning® alkaline earth boro-aluminosilicate glasses (CB-90IN-S111, Delta Technologies, Loveland, CO) coated with Poly-D-Lysine solution (1.0 mg/ml, Cat# A-003-E, Millipore Sigma, St. Luis, MO). The coated slides were prepared adding enough Poly-D-Lysine solution to cover the entire surface. After 12 h, the slides were rinsed with distillated water, dried at RT and stored at 4°C. After sectioning, slides containing tissue sections were placed in a desiccator for 15 min. Once desiccated, the slides were placed individually in zipper sealed plastic bags and transferred to the -80°C freezer for storage.

MALDI-1 MSI and MALDI-2 MSI

Prior to MALDI-MSI analysis, the bagged slides were removed from the -80°C freezer and allowed to reach room temperature for 15 min before the bags were opened. 2,4,6-Trihydroxyacetophenone (THAP, Cat# 91928, Sigma-Aldrich, St. Luis, MO) dissolved in 1:1 ethanol/cyclohexane (Cat# 611050040, and Cat# 22919M1, Thermo Fisher Scientific, Waltham, MA) at 10 mg/ml was used as the MALDI matrix. The matrix was applied to the tissue sections by automated airspray deposition using a TM-Sprayer (HTX Technologies LLC, Chapel Hill, NC). The nozzle temperature was set to 50°C and 20 passes over the tissue were performed at a flow rate of 40 ml/min. MALDI-MSI analysis was performed using a Q-Exactive HF Hybrid quadrupole Orbitrap mass spectrometer (Thermo Fisher Scientific, Walt ham, MA) equipped with a MALDI/ESI injector elevated pressure source incorporating a primary Nd:YAG laser and post-ionization 266 nm solid state laser (Crylas FQSS 266-200). For MALDI-MSI data

acquisition, the Crylas was not enabled, and data was acquired with the Explorer laser pulse energy of 5 µJ and 1000Hz repetition rate. For MALDI-2 MSI acquisition, both the CryLas and Explorer lasers were operated at 30Hz repetition rate, with a delay time of ~20nsec and an Explorer pulse energy of 5 µJ. External mass calibration was performed using calibration solutions (Cat# A3929, Thermo Fisher Scientific, Waltham, MA). Lockmass was enabled for the protonated ion of THAP at *m/z* 169.0. Depending on the experiment, spectra were acquired at 10-30 µm lateral resolution in positive ion acquisition mode. Total acquisition times were between 6-12 h. The accurate mass measured lipid peaks were identified by matching reference lipids in the Human metabolome database (www. https://hmdb.ca/) and Lipid Maps database (https://www.lipidmaps.org/) with Database within a ±0.002 Da mass tolerance window. Thermo RAW format data files were converted to imzML using ImageInsight software (Spectroglyph LLC, Kennewick, WA). Data visualization was performed using SciLs software (SCiLS GmbH, Bremen, Germany).

For the MALDI-MSI sensitivity analyses, TAG 46:3 (18:1/18:1/18:1) (Cat# 26871, Cayman Chemical, Ann Arbor, MI, USA), 46:6 (18:2/18:2/18:2) (Cat# 26951, Cayman Chemical, Ann Arbor, MI, USA), and 46:9 (18:3/18:3/18:3) (Cat# 10009825, Cayman Chemical, Ann Arbor, MI, USA) were solubilized in a solvent mixture comprising methanol and water (9:1 ratio, Cat# A454SK-4 and Cat# W5-1, Thermo Fisher Scientific, Waltham, MA) heated to 50°C to produce a final stock concentration of 10 mg/ml. One µl of each standard solution was deposited onto mouse brain tissue sections collected from a 3-month-old wild-type mouse used for a previous unrelated study. Matrix was applied to the tissue as described above. MALDI-1 MSI was performed using Explorer pulse energy of 5 µJ and laser repetition rate of either 30Hz or 1000Hz. MALDI-2 MSI was performed with CryLaser and Explorer lasers operated at 30 Hz repetition rate, with a delay time of ~20nsec and an Explorer pulse energy of 5 µJ. The Y offset function within the MALDI-injector software was set to 0 for the first

acquisition (MALDI-1 30Hz), 20 for the second acquisition (MALDI-1 1000 Hz) and 40 for the final acquisition (MALDI-2 30 Hz). The lateral resolution was set to 60 µm for each acquisition ensuring there was no overlap of the irradiated laser region in each acquisition as the measured elliptical laser spot diameter of the Explorer laser is 12x15 µm. MS images for the spotted standards were produced using SciLs software (SCiLS GmbH, Bremen, Germany). Quantification of the ion signals was performed from the raw data files using Thermo Xcalibur Qual Browser. The mean ion signal for each TAG ion adduct was calculated from three acquisition rows per spot (50-70 data points per row).

Immunofluorescence

THAP matrix was removed washing the sections 3 times with Methanol (Cat# A456-4, Thermo Fisher Scientific, Waltham, MA)/PBS (Cat# BP665-1, Thermo Fisher Scientific, Waltham, MA) solution (7:3 v/v). Antigen retrieval was performed by incubating slides sections in commercial antigen retrieval solution (Cat# S1700, Agilent Dako, Santa Clara, CA) for 30 min at close to 80 °C water-bath. Slides were removed from the bath and then allowed to cool down in 1X TBS (Cat# BP2471-1, Thermo Fisher Scientific, Waltham, MA) and permeabilized in 0.1% Triton (Cat# X-100, Sigma-Aldrich, St. Luis, MO) for 2 min at RT. Unspecific antibody binding sites were blocked by incubating the tissues with freshly prepared blocking solution (0.5 M EDTA pH 8.0; Cat# 15575-038, Thermo Fisher Scientific, Waltham, MA), 1% Fish gelatin from cold water (Cat# G7765, Sigma-Aldrich, St. Luis, MO), 0.1 g Albumin from bovine serum-immunoglobulin free (Thermo Fisher Scientific, Waltham, MA), 1% Horse Serum (Cat# H1138, Sigma-Aldrich, St. Luis, MO), 5% human serum (Cat# 31876, Thermo Fisher Scientific, Waltham, MA), 9 ml ddH20) for 2 h at RT in a humidity chamber. The primary antibodies (anti-GFAP, anti-rabbit, dilution 1:100, Cat# SAB4501162, RRID: AB_10746077, Sigma-Aldrich, St. Luis, MO; anti-Iba-1, anti-goat, dilution 1:100, Cat# ab5076, RRID: AB_2224402, Abcam, Cambridge, UK; anti-MAP2, anti-chicken,

dilution 1:100, Cat# ab5392, RRID: AB_2138153, Abcam, Cambridge, UK) were added to the samples diluted in blocking solution and incubated at 4°C overnight. Cells were washed several times with TBS at RT and incubated with the appropriate secondary antibodies (Alexa anti-rabbit 647, dilution 1:500, Cat# A21443, Thermo Fisher Scientific, Waltham, MA; Alexa anti-goat 688, dilution 1:500, Cat# A32814, Thermo Fisher Scientific, Waltham, MA; Alexa anti-chicken 568, dilution 1:500, Cat# A11041, Thermo Fisher Scientific, Waltham, MA;) for at least 2 h at RT followed by several washes in TBS. The slides were then mounted using Prolong Gold anti-fade reagent (Cat# P36930, Thermo Fisher Scientific, Waltham, MA) and examined using an A1 confocal microscope (Nikon, Japan). Specificity was confirmed by the secondary antibodies only. Coverslip removal and hematoxylin and eosin (H&E) staining was performed by the University of Texas Medical Branch Histopathology Core facility.

Statistical analyses

Statistical analyses were performed using Prism 5.0 software (GraphPad Software, Inc., San Diego, CA). Two-way ANOVA tests were used to calculate the statistical differences between lipid contents of animal brain tissues. To control for multiple comparisons, probability values of $p \leq 0.05$ were considered statistically significant based on the Tukey's approach.

RESULTS

MALDI-2 increases the sensitivity of TAG analysis when spiked onto brain tissue sections

Initial method development to assess the sensitivity of MALDI-2 in comparison to traditional MALDI (MALDI-1) was focused on optimizing a standardized matrix application that would be used for both methods. Next, we evaluated the sensitivity of

MALDI-1 and MALDI-2 to detect TAG species with increasing numbers of unsaturation (presence of double bonds in the tree present esterified fatty acids) spiked onto control mouse brain tissue sections. 1 ml of a 10 mg/ml solution of one of three different triglycerides with increasing levels of unsaturation, 54:3 (containing three oleic acids), 54:6 (containing three linoleic acids), and 54:9 (containing three alpha-linolenic acids) was pipetted onto different regions of the tissue and MALDI-1 or MALDI-2 MSI was conducted using the Y offset function available in the acquisition software (Fig. 5.1A). The use of offset acquisition on the exact same spiked tissue minimizes potential variables ensuring observed differences are not due to poor pipetting reproducibility. Significantly higher signals were detected for all three TAGs when using MALDI-2 in comparison to MALDI-1 even when the highest MALDI-1 laser repetition rate was utilized (1000 Hz) (Fig. 5.1A). The overall increase in ion signal for MALDI-2 protonated, sodium, and potassium cations combined was 4-8 fold (Fig. 5.1E, **$p \leq 0.01$, ****$p \leq 0.0001$, n=3). Interestingly, only MALDI-2 produced protonated TAG ions (Fig. 5.1B, C, and D, **$p \leq 0.01$, ****$p \leq 0.0001$, n=3), which agrees with previous observations that MALDI-2 promotes the formation of protonated versus metal cations (Barre, Paine et al. 2019, McMillen, Fincher et al. 2020). However, even with the increased protonated ion production by MALDI-2, the protonated ions were at least 20-fold lower than the potassium cation (the most abundant ion produced for all TAGs investigated) (Fig. 5.1 B, C, and D, **$p \leq 0.01$, ****$p \leq 0.0001$, n=3). A previous study investigating the increased sensitivity of MALDI-2 for analyzing drugs within tissues, showed that increasing the laser repetition rate for MALDI-1 could restore the difference in sensitivity between the two techniques (Barre, Paine et al. 2019). However, in this study increasing repetition rate to the maximum (1kHz) only offered a moderate increase in sensitivity of 1.5-2-fold versus 30Hz for the three TAGs analyzed. This was still observed to be 3-6 fold lower than the ion intensities detected using MALDI-2. Moreover, increasing the repetition rate has the potential to induce increased irradiation damage to the tissue due to the increased

number of laser shots hitting the surface. Overall, our data shows that MALDI-2 significantly increases the sensitivity of TAG analysis within spiked brain tissue sections indicating its suitability for application to analyze TAG and neutral lipid dysregulations within tissues even when the lipids are present at low abundance.

Triglycerides accumulate within the subventricular zone in 3xTg mice

We next applied the optimized MALDI-2 method to visualize the distribution of triglycerides within coronal mouse brain sections from 3xTg AD model mice and age matched wild-type controls. Histological (oil red) images and representative MALDI-2 MSI images from 5-month wild-type (5m ctrl), 5-month 3xTg (5m 3x TG), and 17-month 3xTg (17 3x TG) are shown in Fig. 5.2. Progressive hippocampal atrophy was observed in the 17m mouse brain in comparison to the 5m and no hippocampal damage was observed in the 5m wild-type (H&E data not shown). We used a phosphatidylcholine cell membrane marker of grey matter (PC 34:1 $[M+H]^+$ *m/z* 760.6, Fig. 5.2B) to visualize cortex integrity. No clear compromise in cortex integrity was observed either through general loss of membrane phospholipid signal or localized regions of increased or decreased PC metabolism (Fig. 5.2B). Phosphatidylcholine marker of myelin/white matter was used to assess morphological and structural changes in white matter (PC 36:1 $[M+H]^+$ *m/z* 788.6, Fig. 5.2C). No noticeable thinning of the corpus callosum was observed in this study in contrast to what has been reported in moderate and advanced clinical AD's disease (Yamauchi, Fukuyama et al. 2000). When MALDI-2 MS ion maps for the TAG 54:3 were generated, very little signal was observed within the coronal brain sections from wild-type mice (Fig. 5.2D). However, in both the 5m and 17m 3xTg mice brains, heterogenous TAG 54:3 signal was clearly detected, and when viewed in the context of the myelin and grey mater tissue markers, appeared to be localized to the regions at the immediate border of the lateral ventricles (merge in Fig. 5.2E).

In matching oil red-stained serial tissue sections, lipid droplets were observed to be present within the tissue bordering the ventricles and mainly within the ependymal cells lining the ventricles (Fig. 5.2A). The lipid droplets were only present in the 5m and 17m 3xTg mice and not the wild-type 5m control in agreement with the MALDI-2 MS distributions of TAG 54:3 (Fig. 5.2A and D). As the two primary lipid species that comprise lipid droplets are TAGs and cholesteryl esters (CEs), we also interrogated the acquired datasets for the any detected CE lipids (Fig. 5.2F). MALDI-2 has recently been demonstrated to be a sensitive method for CE analysis (Bowman, Bogie et al. 2020). The only CE lipid detected within the mouse brain sections from the 3xTg mice was cholesteryl oleate (CE 18:1 $[M+K]^+$ *m/z* 689.6) (Fig. 5.2F). CE 18:1 signal did not colocalize with either the TAG signal or the presence of lipid droplets and was only weakly detected. Hence, we have shown that the neutral lipid composition of lipid droplets accumulating with the SVZ in the 3xTg mice are comprised of TAG and not CE.

The severity of brain morphology alterations was noticeably varied between mice, even when the mice were compared within the same age group. MALDI-2 MS images of TAG 54:3, H&E images from the same brain tissue sections after matrix removal, and oil red-stained adjacent tissue sections from the 17m 3xTg mice are shown in Fig. 5.3. When comparing 3xTg mice from the 17m age group, the observed morphological changes ranged from mild ventricle enlargement (mouse 2) to moderate enlargement (mouse 1) and ultimately, extremely severe ventricular enlargement with advanced hippocampal atrophy (mouse 3, as evidenced by the absence of hippocampal tissue within the sampled brain section) (Fig. 5.3A). MALDI-2 MSI analysis of the localization of TAG 54:3 within the tissue sections, revealed a consistent distribution of TAG despite the severity of morphological damage (Fig. 5.3B). The strongest TAG signal was observed within the upper “ridge” of the tissue bordering the ventricle and was typically present throughout the length of the ridge (the most severe example is present in mouse 3, Fig. 5.3B). As noted previously, the TAG signal strongly colocalized with the presence of lipid droplets

detected by oil red staining (Fig. 5.3C, select lipid droplets indicated by the arrows). Less TAG signal was observed in the lower tissue areas bordering the ventricle even though the tissues appeared morphologically similar, with a clear bordering ependymal cell layer present in both. In agreement with the MALDI-2 MSI TAG distribution data, lipid droplets were also not present within these lower ventricle bordering regions (Fig. 5.3C).

MALDI-2 ionization enhances TAG imaging in 3xTg mouse brain sections

Using standards spiked onto control mouse brain, we showed that MALDI-2 was superior to MALDI-1 for sensitive imaging analysis of TAGs of varied fatty acid compositions (Fig. 5.1A). However, one aspect of the MSI process, that is not recapitulated in a tissue surface spiking study, is the ability to extract the analytes from the tissue into the matrix crystals at the surface. Therefore, our next goal was to assess the ability of the MALDI-2 approach to image multiple TAG species of varied carbon lengths and fatty acid saturation directly within the 3xTg mouse brain sections. Previous studies conducted by Hamilton *et al*, using MALDI-1 time of flight mass spectrometry imaging identified 12 different TAG species within 3xTg mouse SVZ brain regions (Hamilton, Dufresne et al. 2015) and we proposed that the increased sensitivity of the MALDI-2 MSI technique would enabled the detection of additional species in our study.

Due to the lack of chromatographic separation, MALDI-MSI is incapable of resolving true isobaric ions. Hence, in these studies we cannot resolve the precise fatty acid composition of each detected triglyceride. TAG species are identified based on accurate mass and classified based on the total number of carbons and total number of double bonds comprised of the three esterified fatty acids. Therefore, each fatty acid species identified by MSI may be comprised of many different fatty acid combinations that add up to the same number of total carbons and double bonds. For example, TAG 54:6 may be composed of three linoleic acids (18:2/18:2/18:2) or one saturated palmitic

acid, one unsaturated linoleic acid, and one polyunsaturated arachidonic acid (16:0/18:2/20:4) among many other potential combinations.

To identify all detected TAG species by MALDI-2 MSI, we drew regions of interest (ROIs) encompassing 200 μm in diameter from the border of the lateral ventricle (encompassing the subventricular zone). Peak lists from the ROI mean spectra were extracted using SCiLS software and were cross referenced with the Lipid Maps database. $[M+K]^+$ TAGs within a mass tolerance window of 3 ppm were assigned to matching spectral peaks. The TAG species putatively identified due to accurate mass matching are shown in Table 4 along with their theoretical and acquired m/z values. In total 30 putative TAG species were identified. Extracted ion images were plotted for each of the 30 identified TAG species (as an example, images for all TAG species 17m 3xTg mouse 1 is shown in Fig. 5.4) and all were observed to colocalize with the SVZ in agreement with TAG 54:3 distribution and the presence of lipid droplets (Fig. 5.3).

Mean relative ion signal intensities were calculated for SVZ regions of interest in 3xTg and wild-type mice using SCiLS software (Fig. 5.5A-D, *$p \leq 0.05$, **$p \leq 0.01$, ***$p \leq 0.001$, ****$p \leq 0.0001$, n=3). Only eight TAG species were detected in 5m old wild-type mice and ion abundances for each were extremely low. In TAGs containing fatty acids with 46-50 total carbons, 48:0, 48:1, 50:0, and 50:1 were detected in wild-type mice (Fig. 5.5A). However, quantification of ion signals revealed that relative abundances were 20-50-fold lower than those detected in 5-month-old 3xTg mice (Fig. 5.5A, *$p \leq 0.05$, **$p \leq 0.01$, ***$p \leq 0.001$, ****$p \leq 0.0001$, n=3). Robust ion abundances were observed in the 5m and 17m 3xTg mice for all eight TAGs and there were minimal differences between the 5m and 17m animals (only 50:1 was significantly increased in 17m in comparison to 5m, ****$p \leq 0.0001$, n=3). TAG 50:1 was the most abundant species in all mouse models and ages. In TAGs containing fatty acids with 52 total carbons, 52:1 and 52:2 were detected in wild-type mice (Fig. 5.5B). As for the shorter carbon TAGs, relative abundance was low in the wild-type mice and normalized ion

counts for 52:1 and 52:2 were 130-fold and 180-fold lower than in 5m 3xTg mice, respectively. TAG 52:2 was the most abundant species and no significant differences between 5m and 17m 3xTg mice were observed. In TAGs containing fatty acids with 54 total carbons, only 54:2 and 54:3 were detected in wild-type mice (Fig 5.5C) and their relative ion abundances were 130-fold and 8-fold lower than in 5 month 3xTg mice, respectively (Fig 5.5C, ****$p \leq 0.0001$, n=3). TAGs 54:2 and 54:3 were the most abundant species and significantly increased levels of unsaturated fatty acids were observed in the 17m 3xTg mouse than the 5m (continuing the trend observed in the 52 carbon TAGs). TAGs containing fatty acids with 56 total carbons were not detected in the 5m old wild-type SVZ (Fig. 5.5D). TAGs 56:4 and 56:5 were the most abundant in the 3xTg mice SVZ and the highly unsaturated TAGs (56:4, 56:5, and 56:6) were all present at significantly higher levels in the 17m 3xTg mice in comparison to the 5m (Fig. 5.5D). This data allowed us to determine that greater amounts of unsaturation within long carbon chain TAGs correlated with increased age in the 3xTg mouse brain. However, similar changes were not observed in shorter chain TAGs (46-50 carbon length). Overall, this data shows that TAG accumulation within the SVZ occurs early in disease pathogenesis in the 3xTg mouse model (prior to 5 months) and that increased accumulation of unsaturated TAGs is progressive as the mice age.

MALDI-2 facilitates downstream confocal microscopy of same tissue section

Using poly-lysine coated glass MALDI slides, we have demonstrated the feasibility of downstream histochemical staining and imaging on the same tissue section as prior MALDI-MSI analyses (Fig. 5.2 and 5.3). However, to accurately interpret MS images within the context of cellular composition and protein/enzyme activity, additional immunohistochemical (IHC) or immunofluorescence (IF) imaging analyses are required. As the ultimate goal of our approach is to elucidate metabolic changes occurring at the

cellular level in neurogenerative diseases, a high spatial resolution MALDI-MSI method is required that is fully compatible with downstream IHC and IF microscope imaging.

First, we compared MALDI-1 versus MALDI-2 MSI within defined regions of 5m 3xTg mouse brain sections. MALDI MSI was conducted at a lateral resolution of 20 μm as due the laser spot having a diameter of 12 x 15 μm no overlap of the laser spot would occur between adjacent positions (pixels) at this resolution (Fig. 5.6A). A laser repetition rate of 1000 Hz was used for the MALDI-1 acquisitions, due to this parameter setting producing the highest TAG signal. Following MALDI acquisition, the matrix was removed from the tissue and staining was performed using DAPI for nuclei, GFAP (astrocytes marker), and MAP-2 (neuronal marker). Immunofluorescence images acquired using confocal microscopy are shown in Fig. 5.6A. Images acquired after MALDI-2 MSI analysis had no detectable compromise of signals or presence of autofluorescence when compared to confocal images taken from areas of the tissue that did not undergo MALDI-2 MSI imaging. However, in the MALDI-1 confocal image comparisons tissue damage is readily apparent as evidenced by the induction of autofluorescence present in a grid pattern throughout the image. This finding was supported by subsequent H&E staining of the same tissue sections (Fig. 5.6B), which revealed a grid-like laser burn pattern throughout the MALDI-1 MSI tissue sections that was not present in the MALDI-2 MSI images. Next, we repeated the MALDI-2 MSI analysis at 10 μm lateral resolution to evaluate whether cellular level MSI would be compatible with confocal microscopy analysis. At this resolution, the acquired pixels are smaller than the laser spot diameter resulting in “oversampling” (Bowman, Bogie et al. 2020). As shown in Fig. 5.6A, no compromise of labeling or image quality is observed in brain section regions in which MALDI-2 MSI was performed in comparison with non-laser irradiated areas. Hence, laser irradiation of the tissue section during MALDI-2 MSI acquisition is compatible with antibody labeling and microscopy.

Another stage in the MALDI-2 MSI process with the potential to negatively affect IF confocal microscopy analysis is the application of the MALDI matrix during sample preparation. To assess this, we compared downstream IF in adjacent 3xTg mouse brain sections with and without MALDI-2 MSI acquisition (Fig. 5.7). As shown in Fig. 5.7A, signal intensities for DAPI, GFAP, or MAP-2 did not appear to be compromised in the MALDI-2 MSI tissue in comparison to tissue sections that did not undergo the MALDI-2 samples preparation process. In addition, upon inspection of subsequent H&E staining in the same tissue sections, no tissue damage was observed in the MALDI-2 tissues. With this data, we have demonstrated that MALDI-2 MSI acquisition is superior to MALDI-1 in limiting laser-induced tissue damage that compromises IF analysis. Moreover, we have also shown that our MALDI-2 methods produce equivalent IF image quality to that acquired in adjacent fresh-frozen tissue sections. Hence, confirming the approach is suitable for high spatial resolution MSI, IF, and H&E within a single tissue section, enabling cellular level imaging of lipids and metabolites with markers of cell type, enzymatic pathways, and morphology.

Table 4. List of identified TAG lipids within the SVG of 3xTg mouse brain sections based on accurate mass measurements.

TAG	Theoretical m/z	Acquired m/z	Difference (ppm)
46:0	817.6682	817.6683	0.1
48:0	845.6695	845.7002	0.8
48:1	845.6838	843.6844	0.7
50:0	873.7308	873.7322	1.6
50:1	871.7151	871.7159	0.9
50:2	869.6995	869.7002	0.8
50:3	867.6838	867.6849	1.3
52:0	901.7621	901.7634	1.4
52:1	899.7464	899.7481	1.9
52:2	897.7308	897.7315	0.8
52:3	895.7151	895.7159	0.9
52:4	893.6995	893.7001	0.7
52:5	891.6838	891.6850	1.6
52:6	889.6682	889.6700	2.0
52:7	887.6525	887.6548	2.6
54:0	929.7934	929.7947	1.4
54:1	927.7777	927.7793	1.7
54:2	925.7621	925.7631	1.1
54:3	923.7464	923.7472	0.9
54:4	921.7308	921.7315	0.8
54:5	919.7151	919.7154	0.3
54:6	917.6995	917.6998	0.3
54:7	915.6838	915.6844	0.5
56:0	957.8247	957.8281	3.5
56:1	955.8090	955.8104	1.5
56:2	953.7935	953.7947	1.4
56:3	951.7777	951.7785	0.8
56:4	949.7621	949.7631	1.1
56:5	947.7464	947.7470	0.6
56:6	945.7308	945.7314	0.6
56:7	943.7151	943.7157	0.6

Theoretical *m/z* values for each identified TAG are shown in the first column. Actual acquired peak values are shown in column 2. The ppm difference between calculated *m/z* and recorded *m/z* is shown in column 3. Peaks with an acquired *m/z* within 3ppm of the TAG theoretical value were assigned.

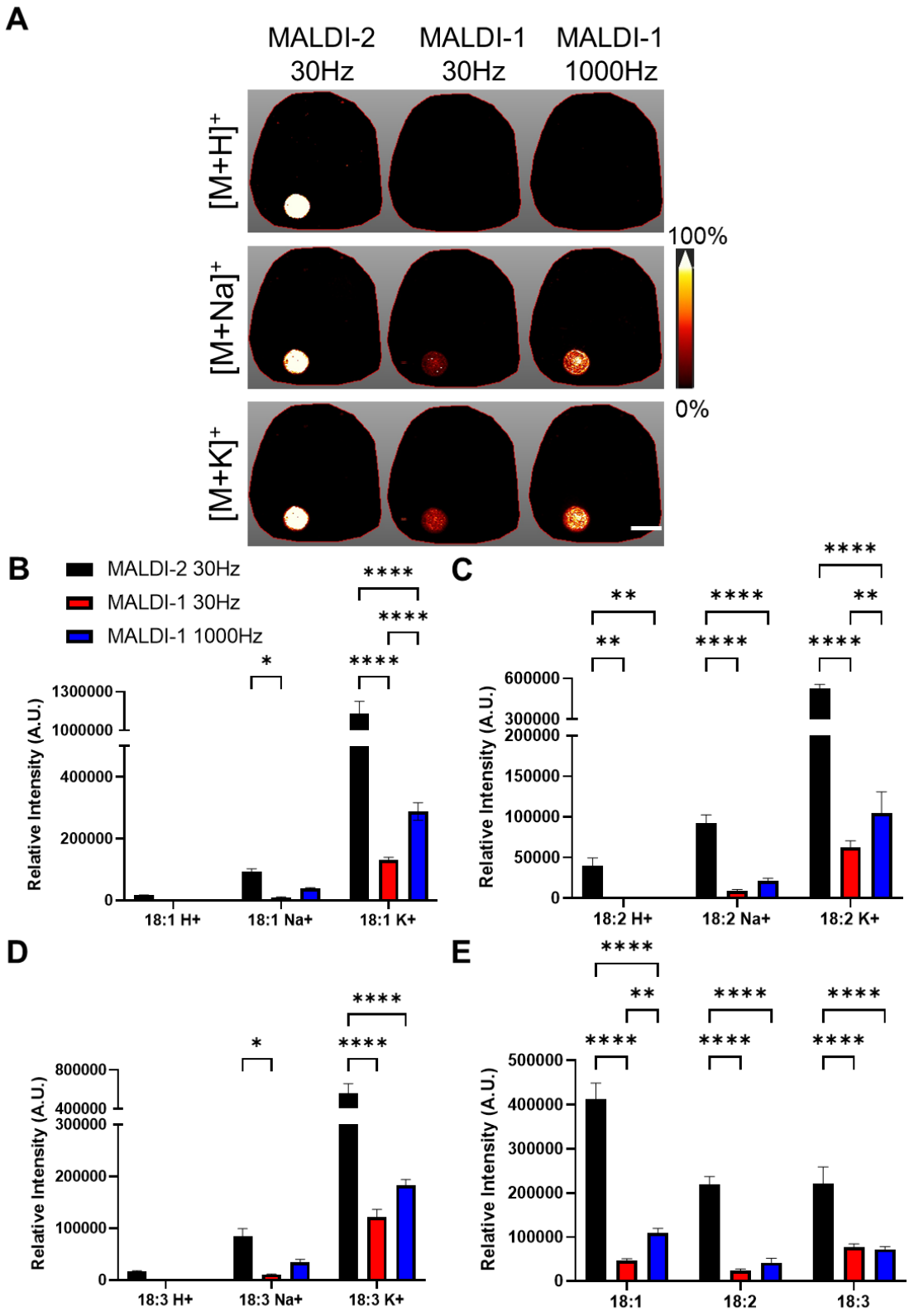

Figure 5.1. MALDI-2 MSI enhances analytical sensitivity for Triacylglycerol lipids

1 ml of a 10 mg/mL solution of 3 TAGs of differing fatty acid saturations was spiked onto control mouse brain tissue sections. (A) MALDI-MSI of TAG 54:3 (18:1/18:1/18:1) using 3 different ionization methods (MALDI-1 at low and high laser repetition rates, and MALDI-2 at its maximum available repetition rate). Extracted ion images are shown for the three major ions produced. (B) Graph showing quantification of ion signals produced for TAG 54:3. (C) Graph showing quantification of ion signals for TAG 54:6 (18:2/18:2/18:2). (D) Graph showing quantification of ion signals for TAG 54:9 (18:3/18:3/18:3). (E) Graph showing summed ion intensities ($[M+H]^+$, $[M+Na]^+$, and $[M+K]^+$). *$p \leq 0.05$, **$p \leq 0.01$, ****$p \leq 0.0001$. Scalebar = 5 mm.

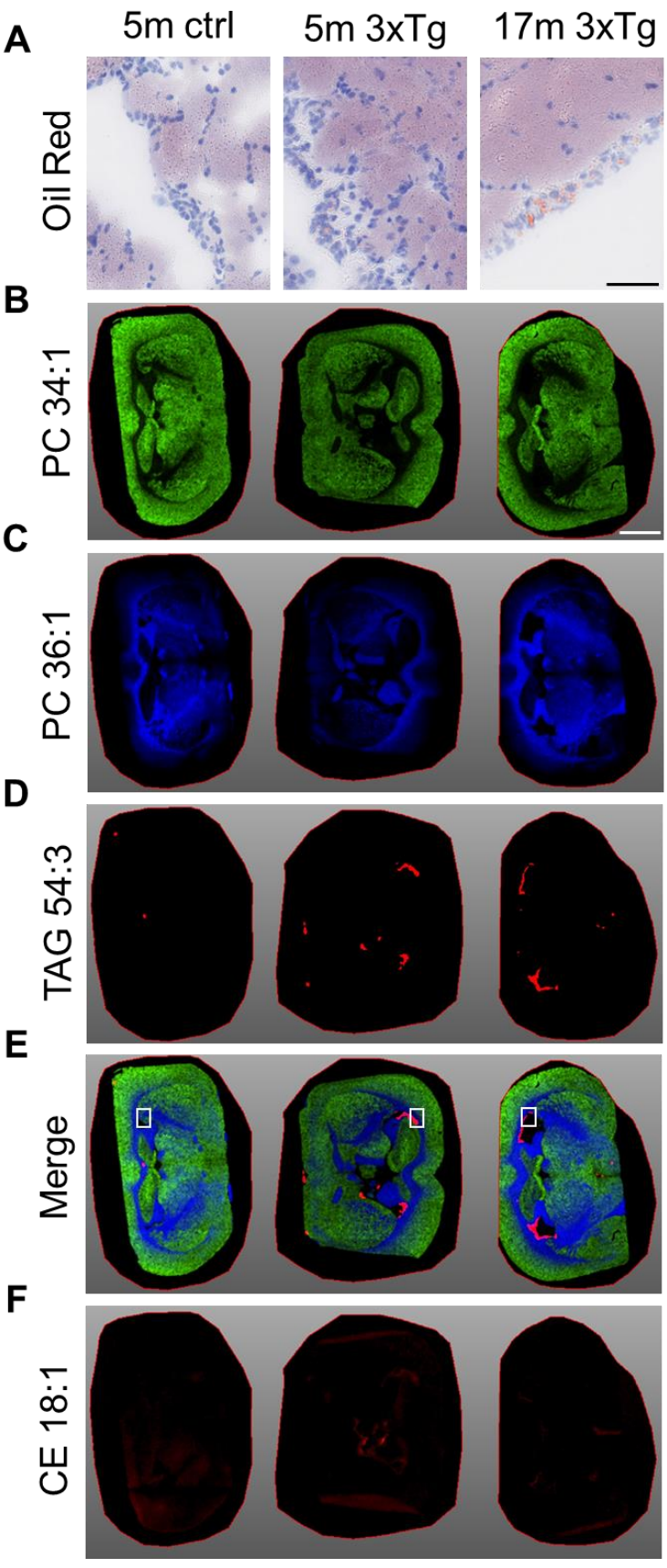
A
5m ctrl
5m 3xTg
17m 3xTg
Oil Red
B
PC 34:1
C
PC 36:1
D
TAG 54:3
E
Merge
F
CE 18:1

Figure 5.2. MALDI-2 MSI enables visualization and relative quantification of TAGs accumulating within the subventricular zone (SVZ) in 3xTg mice

MALDI-2 MSI analysis was performed on coronal brain sections from 5m wild-type, 5m 3xTg, and 17m 3xTg. Extracted ion images were produced for brain tissue markers and TAG 54:3. (A) Oil red staining of lipid droplets within the SVZ of adjacent brain tissue sections to those used for MALDI-2 MSI. (B) MALDI-2 MS image of a phosphatidylcholine marker of grey matter (PC 34:1 $[M+H]^+$ *m/z* 760.6). (C) MALDI-MS image of a phosphatidylcholine marker of myelin/white matter (PC 36:1 $[M+H]^+$ *m/z* 788.6). (D) MALDI-MS image of TAG 54:3 ($[M+K]^+$ *m/z* 923.7). (E) RGB overlay of all three markers. The white boxes delineate the regions from which the high magnification oil red images were taken. (F) MALDI-2 MS image of cholesteryl ester 18:1 ($[M+K]^+$ *m/z* 689.6). Representative MALDI-2 MS images from n=3 per condition are shown. Scalebar for all MS images = 5 mm. Scalebar for oil red images = 100 mm

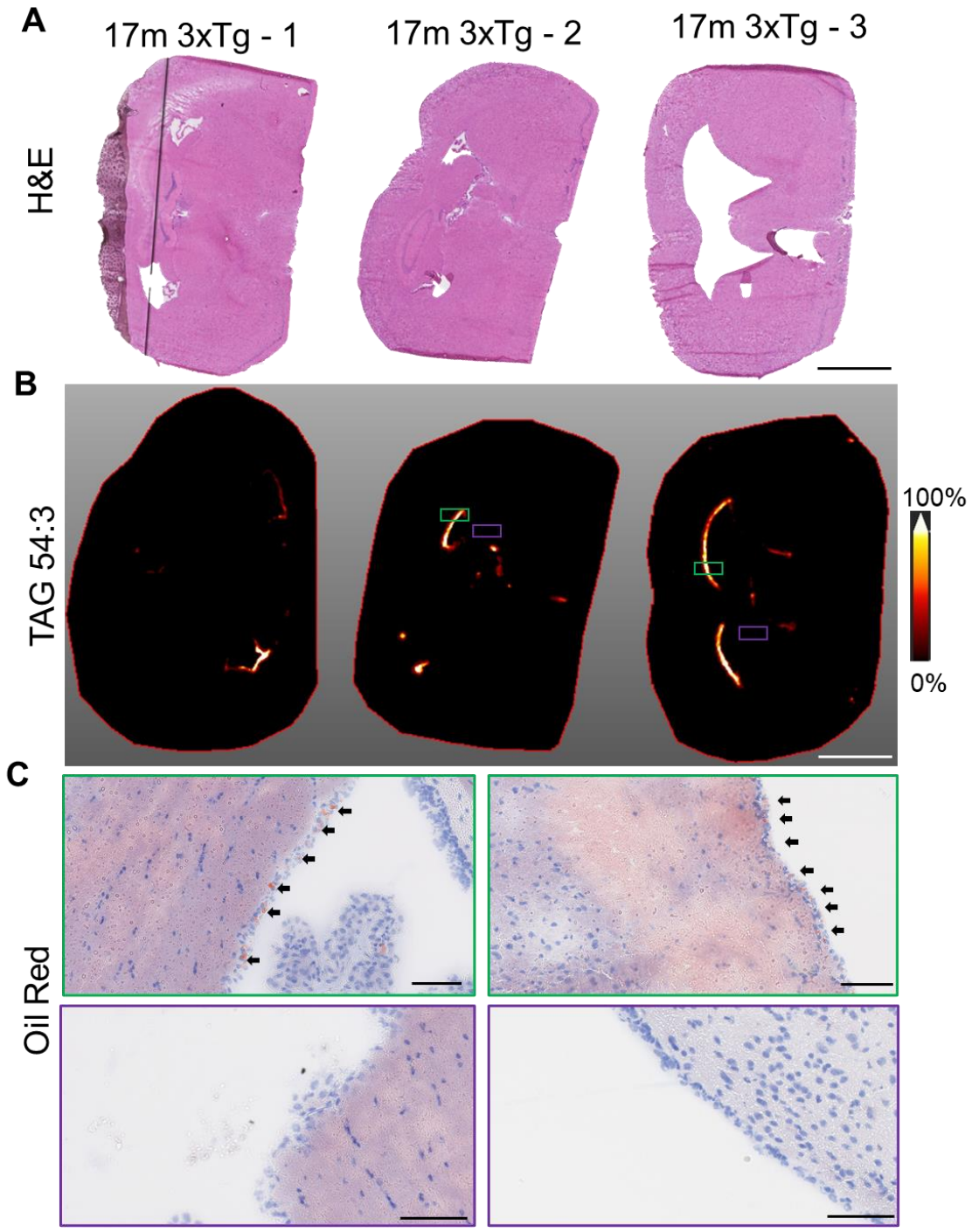

Figure 5.3. Diverse brain morphology is observed in aged 3xTg mice

(A) Images of H&E-stained coronal brain sections from 17m 3xTg mice. These images were from the exact same tissue used for prior MALDI-2 MSI analysis. Scalebar = 5 mm (B) MALDI-2 MS I for TAG 54:3 ($[M+K]^+$ *m/z* 923.7). The green and purple boxes delineate the SVZ regions magnified in adjacent oil red-stained sections in which oil droplets were present (green box) or absent (purple box). Scalebar = 5 mm (C) Magnified

SVZ regions from oil red-stained mouse brain sections adjacent to those used for MALDI-2 MSI and H&E. Regions containing lipid droplets are outlined in green, regions without the presence of lipid droplets are outlined in purple. Intact lipid droplets are indicated by the black arrowheads. Scalebar = 100 mm. All 3 17m 3xTg mice sections are shown.

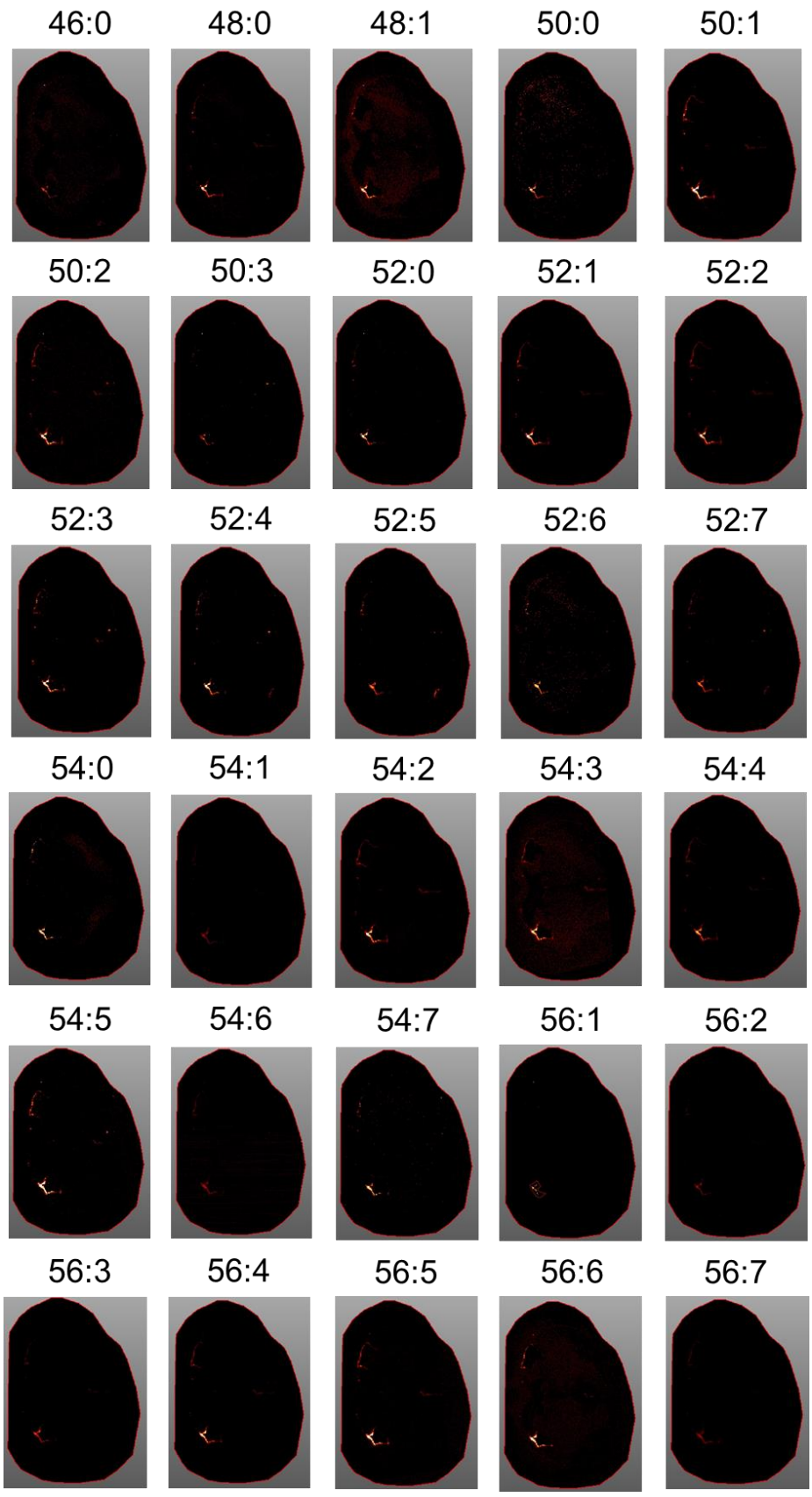
46:0
48:0
48:1
50:0
50:1
50:2
50:3
52:0
52:1
52:2
52:3
52:4
52:5
52:6
52:7
54:0
54:1
54:2
54:3
54:4
54:5
54:6
54:7
56:1
56:2
56:3
56:4
56:5
56:6
56:7

Figure 5.4. MALDI-2 MSI identified 30 different TAG species within subventricular zone (SVZ) in 3xTg mice

Extracted ion images for all 30 identified TAGs (as listed in Table 4) in a 17m 3xTg mouse-1 coronal brain section. Images are shown for TAGs identified based upon accurate mass measurement and precise colocalize with the distribution of TAG 54:3 and the confirmed presence of lipid droplets by oil red staining). Representative MALDI-2 MS images from n=3 per condition are shown. Scalebar = 5 mm

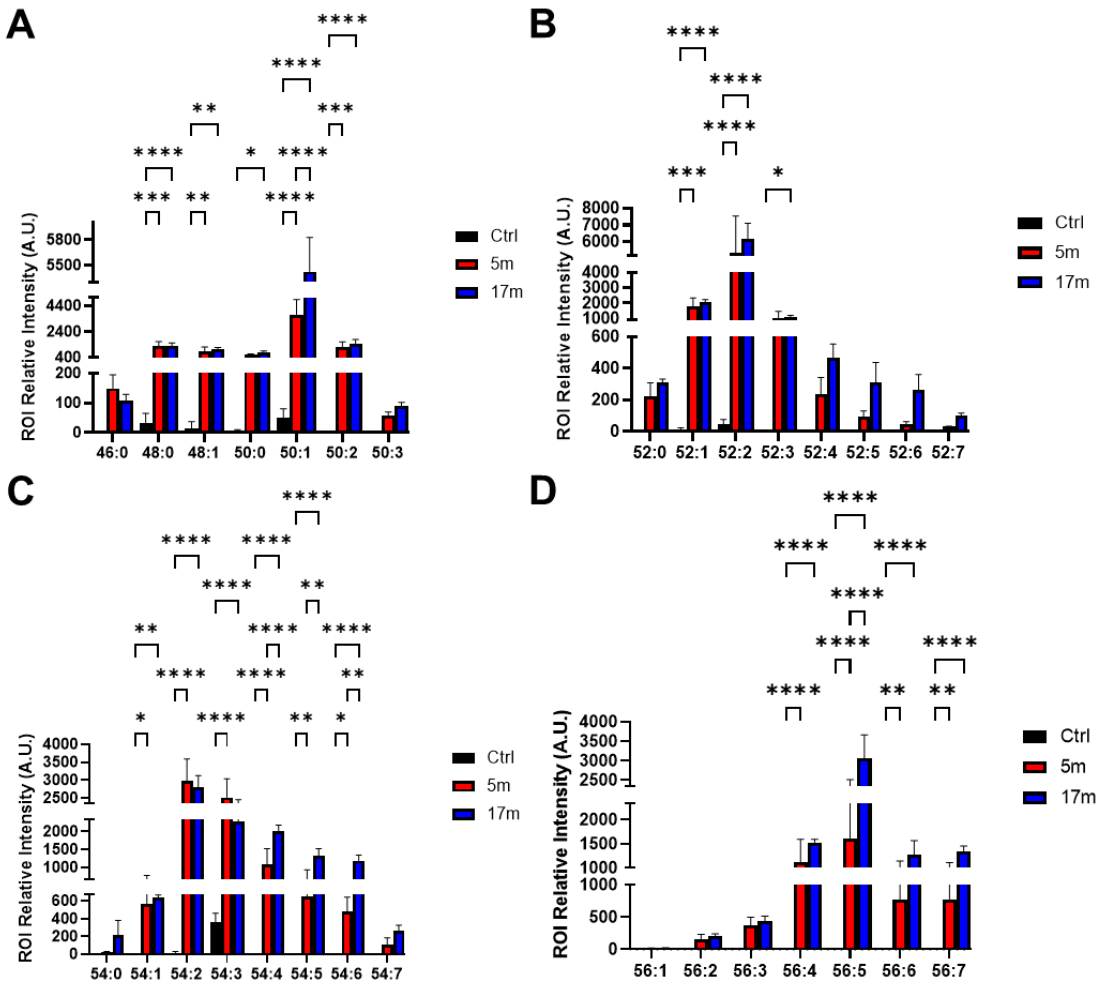

Figure 5.5. Quantification of TAG abundance within the SVZ of wild-type and 3xTg mice

Regions of interest were drawn in the SVZ of the brain right hemisphere from all three mouse conditions and the mean ion signal within was calculated using SCiLS lab software. Relative quantification comparisons were performed using 3 mice per condition (n=3), *p≤0.05, **p≤0.01, ***p≤0.001, ****p≤0.0001. Due to the high number of detected TAGs, mean intensity results were plotted on 4 graphs separated based on the total number of carbons within the esterified fatty acids. (A) Graph showing the mean intensity of TAG signal within the SVZ for TAGs containing 46-50 total fatty acid carbons. (B) Graph showing the mean intensity of TAG signal within the SVZ for TAGs containing 52 total fatty acid carbons. (C) Graph showing the mean intensity of TAG signal within the SVZ for TAGs containing 54 total fatty acid carbons. (D) Graph showing the mean intensity of TAG signal within the SVZ for TAGs containing 56 total fatty acid carbons.

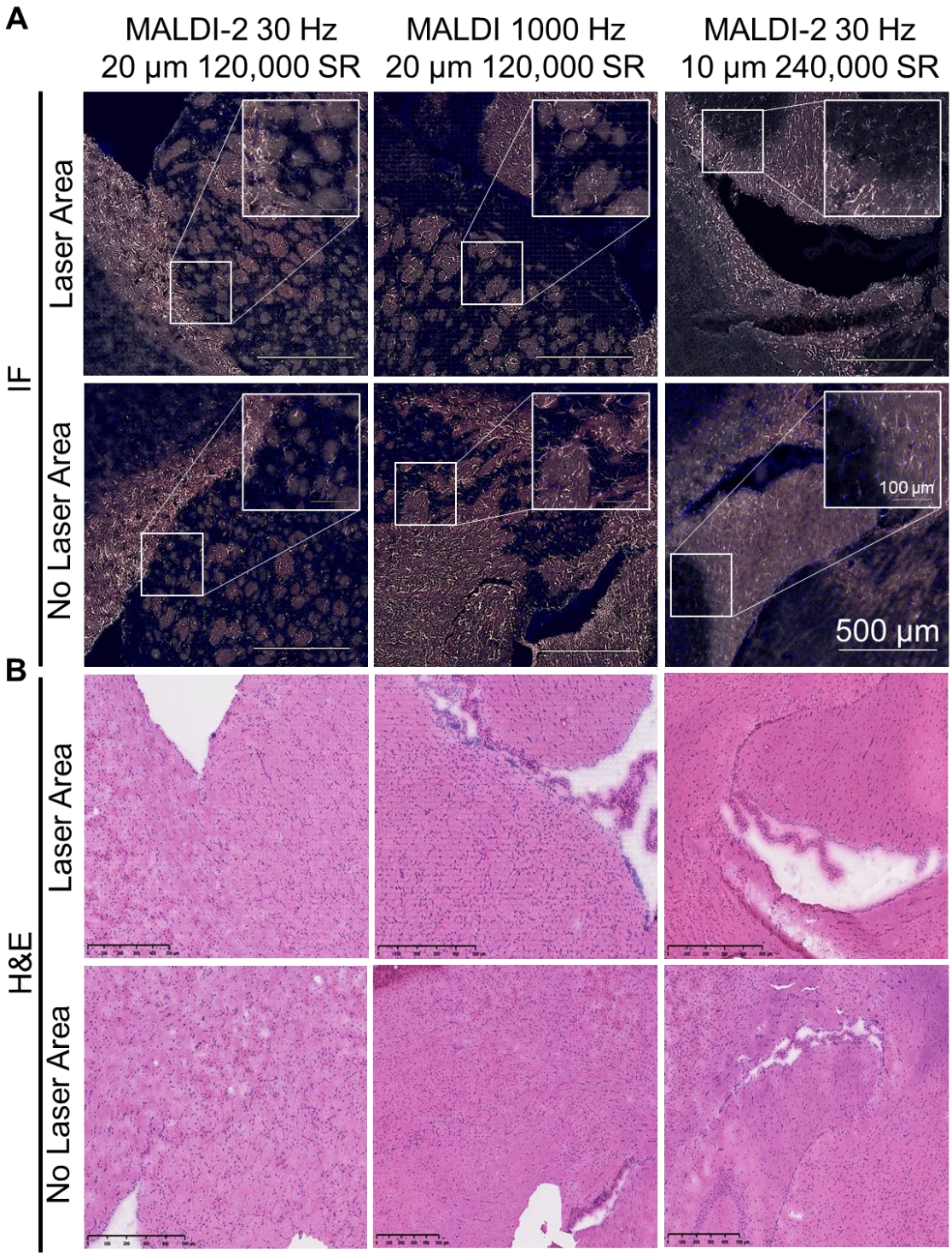

Figure 5.6. The use of MALDI-2 MSI prevents laser-induced tissue damage and is compatible with immunofluorescent imaging

Tissue sections underwent standard sample preparation for MALDI-MSI and MSI was performed on one hemisphere of the coronal mouse brain section for a 5m 3xTg mouse.

Following MALDI-1 or MALDI-2 MSI analysis of coronal mouse brain sections at high (20 μm lateral resolution) or cellular-level detail (10 μm lateral resolution), THAP matrix was removed from the tissue surface and immunofluorescence was performed to stain DAPI (blue), GFAP (astrocyte marker in white), and MAP-2 (neuron marker in red). (A) Merge of DAPI, GFAP, and MAP-2 from brain regions in which MALDI-1 (1000 Hz laser repetition rate) and MALDI-2 (30 Hz laser repetition rate, at two different lateral resolution) was performed (first row). Merge of DAPI, GFAP, and MAP-2 from matching brain regions in the hemisphere that was not analyzed by MSI are shown in the second row. (B) Images of the same tissue regions as shown in (A) after H&E-staining. Clear tissue damage and increased autofluorescence was observed in the tissue regions analyzed using MALDI-1 MSI. Scalebar = 500 mm main panel, 100 mm inset panel.

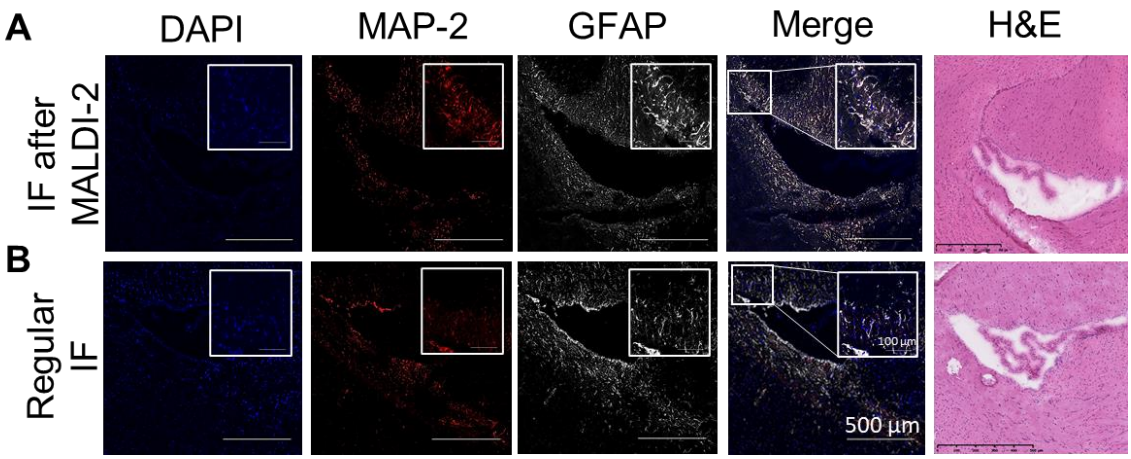

Figure 5.7. MALDI matrix application and removal steps for MALDI-2 MSI do not compromise downstream IF imaging

MALDI-2 MSI was performed as described in Fig. 5.6. Following MALDI-2 MSI analysis at 10 µm lateral resolution, THAP matrix was removed from the tissue surface and IF was performed for DAPI (blue), GFAP (astrocyte marker in white), and MAP-2 (neuron marker in red). The same confocal microscopy analysis was conducted in an adjacent tissue section using standard fresh frozen IF methods (i.e. the tissue did not undergo previous MALDI-2 MSI analysis or any of the MALDI-2 sample preparation steps). (A) Single channel and merge images for DAPI (blue), GFAP (white), and MAP-2 (red) and corresponding H&E in tissue regions following MALDI-2 MSI. (B) Single channel and merge images for DAPI (blue), GFAP (white), and MAP-2 (red) and corresponding H&E in matching fresh-frozen tissue sections without any of the MALDI-2 sample preparation steps. No compromises in signal intensity, autofluorescence, or image quality were observed. Scalebar = 500 µm main panel, 100 µm inset panel.

DISCUSSION

The use of laser induced post-ionization (MALDI-2) MSI has been demonstrated to significantly increase the sensitivity of MALDI-MSI for many small molecule analytes, including lipids, metabolites, and drugs. In this study, we have demonstrated that MALDI-2 MSI is a highly-sensitive technique for detecting and localizing neutral lipid dysregulation within the brain tissue sections taken from a clinically-relevant murine model of progressive AD.

We evaluated the sensitivity of MALDI-2 versus MALDI-1 MSI techniques to detect and visualize TAG lipid standards spiked onto young wild-type mouse brain sections (in which endogenous TAG would not be expected to be present (Ralhan, Chang et al. 2021)). MALDI-2 increased the sensitivity of all TAG detection by 3-20-fold (depending upon the TAG species and generated ion). The main reported limitations of applying MALDI-MSI to study triglycerides in biological tissues are lack of analytical sensitivity required to detect them, lack of mass resolution, and accuracy capabilities to resolve TAG ions from endogenous tissue-derived peaks, and lack of spatial resolving capabilities to accurately determine tissue and cellular localization (Alamri, Patterson et al. 2019). To circumvent these limitations, several approaches have been used to enhance analytical sensitivity for TAGs including the use of sputtered gold coating to enhance ionization (sodium-doped gold-assisted LDI IMS) (Dufresne, Masson et al. 2016) and silicon nanopost array (NAPA) substrates that selectively ionize TAGs (Fincher, Korte et al. 2020). However, the MALDI-2 approach requires no additional sample preparation steps than regular MALDI, negating additional time, and cost requirements in addition to significantly increasing the analytical sensitivity. Regarding ion formation, potassium adduct TAGs were the most abundant ions detected for all TAG species when either MALDI-1 or MALDI-2 was used. Previous studies applying MALDI to detect triglycerides in olive oil samples found that the TAGs were primarily present as sodium

adducts (Kubo, Satoh et al. 2013, Kuo, Kuei et al. 2019) and to date most applications of MALDI analysis to the study of triglycerides have been in agriculture and food science. This study is the first to report the detection of protonated TAG ions by MALDI-MSI, which we hypothesize to be due to the known ability of MALDI-2 to promote the generate protonated ion species.

After optimizing and evaluating the MALDI-2 MSI approach on TAG-spiked tissue sections, we then applied the technique to visualize neutral lipid dysregulation in brain tissue collected from 3xTg AD mouse models and age-matched wild-type controls. When visualizing TAG 54:3 distributions within the brain tissues, very low signals were observed in 5m wild-type mice, whereas high signal intensities were observed for both 5m and 17m old 3xTg mice. The observed TAG signal in the 3xTg mice was localized to the border of the lateral ventricles, which were enlarged in this model. Only one cholesteryl ester lipid was detected within 3xTg mouse brain. However, the signal intensity was low and did not colocalize with the distribution of TAG. Oil red staining performed on adjacent tissue sections revealed the presence of lipid droplets within the subventricular zone at the border of the lateral ventricles. This distribution of lipid droplets perfectly colocalized with the MALDI-2 MSI distributions of TAG, confirming that the neutral lipids accumulating within the 3xTg brains were TAGs and not CE. Previous studies by Hamilton *et al* identified that TAGs accumulate within the SVZ of 3xTg mice and brain tissues collected from AD patients (Hamilton, Dufresne et al. 2015). However, CE was not investigated and therefore this is the first study to demonstrate that the neutral lipid droplet composition is exclusively TAG.

As mentioned previously, the sensitivity of traditional MALDI MSI is a primary limiting factor for detecting TAGs in biological tissues. Previous investigations using sodium-doped gold-assisted MALDI to evaluate TAG lipid dysregulation within 3xTg mouse and clinical AD brain tissues revealed the presence of 12 different TAG species (Hamilton, Dufresne et al. 2015). Using MALDI-2 MSI we identified 30 different TAG

species that were present within the SVZ of 3xTg mouse and colocalized with the presence of lipid droplets. Moreover, in the aforementioned study oleic acid (monounsaturated) containing TAGs were identified as the major species present within the SVZ. In this study, we detected multiple polyunsaturated TAGs with up to seven total unsaturation across all esterified fatty acids. As the sensitivity of TAG detection by MALDI MSI decreases in correlation with increasing carbon length and number of saturations, these longer carbon and polyunsaturated TAGs may not have been detected in the previous study using a less sensitive approach. Interestingly, no significant difference was observed in the accumulation of shorter carbon TAGs with lower numbers of unsaturation between 5m and 17m 3xTg mice, indicating that the initial accumulation occurs early (prior to 5m of age). Select longer carbon chain TAGs (>54) and TAGs containing more four or more unsaturations were observed to be significantly increased in the 17m 3xTg mice versus the 5m. Thus, the degree of unsaturation and carbon length of TAGs in this mouse model correlates with progressive disease development.

The localization of TAG within the SVZ is of particular striking due to it being one of only two regions where neurogenesis persists in the postnatal brain (Doetsch, Caille et al. 1999). The SVZ lines the wall of the lateral ventricles and is composed of neural stem cells which have the capability to differentiate into various CNS lineages (Doetsch, Garcia-Verdugo et al. 1999). The highest TAG signal was observed to colocalize with the ependymal cell layer at the outer edge of the SVZ and with the presence of lipid droplets. Ependymal cells are glial cells that act as a barrier between the brain parenchyma and the cerebrospinal fluid. They play crucial roles in brain metabolism, maintaining CSF homeostasis, and waste elimination (Ralhan, Chang et al. 2021). Fatty acid metabolism is known to be high within ependymal cells and lipid droplets accumulate within the cells even under healthy conditions with increasing age (Capilla-Gonzalez, Cebrian-Silla et al. 2014, Farmer, Walsh et al. 2020). One limitation of this study is the lack of age matched wild-type mice for the 17m 3xTg mouse TAG

data, precluding comparison to the expected increased TAG levels occurring due to nonpathogenic advanced age.

A detailed and mechanistic interpretation of TAG accumulation within the SVG of 3xTg mice is beyond the scope of this work. However, future studies could focus on longitudinal analysis of TAG dysregulation very early in AD progression and correlate this with neurocognitive impairment as working and memory deficits have been reported to occur as early as 2 months of age in this mouse model (Stevens and Brown 2015).

One major advantage of the MALDI-2 MSI technique is the ability to conduct downstream antibody labeling and IF microscopy imaging on the same tissue section as used for MSI. We demonstrated that the MALDI-2 approach induced less tissue damage and produced higher quality images for cell and nuclear markers than was achieved using MALDI-1. The ability to perform these analyses on the same tissue section enables precise, cellular level colocalization of TAG and IF images.

Further limitations of the study include the use of only male 3xTg mice. Due to the known sexual dimorphism in pathogenesis between male and female 3xTg mice (Dennison, Ricciardi et al. 2021), the study would need to be repeated using age matched female mice before conclusions could be extrapolated to the female population. In addition, due to the inability of MALDI-MSI to identify the specific fatty acid chains of the detected TAGs, the presence of specific fatty acids implicated in inflammation such as arachidonic acid and docosahexaenoic acid cannot be confirmed. In future studies, we propose to use laser capture microdissection to isolate the SVZ of 3xTg mice and use liquid chromatography mass spectrometry (LC-MS/MS) to identify the specific fatty acid composition of the TAGs as previously described for drug and metabolite quantification in tissues (Zimmerman, Blanc et al. 2018).

In addition to AD, lipid droplet formation and accumulation has been implicated in the pathogenesis of multiple neurodegenerative disorders including Parkinson's disease (Cole, Murphy et al. 2002), Huntington's disease (Martinez-Vicente, Talloczy et

al. 2010), amyotrophic lateral sclerosis (Bailey, Koster et al. 2015), and hereditary spastic paraplegia (Arribat, Grepper et al. 2020). Furthermore, lipid dysregulation is a key pathological feature of infectious neurological diseases including HIV (Bandaru, Mielke et al. 2013, Castellano, Prevedel et al. 2019), meningitis (Czepiel, Gdula-Argasinska et al. 2019), and Zika (Zhou, Chi et al. 2019). Therefore, the developed MALDI-2 MSI techniques have great potential value for elucidating mechanisms behind the molecular pathogenesis of these debilitating diseases.

In summary, the optimized MALDI-2 MSI approach enables high spatial resolution images of TAGs to be determined within coronal brain sections from 3xTg mice. This approach, that combines lipidomic MALDI-2 MSI assessment, immunofluorescence analysis, and histological staining for morphological evaluation, is significant for a direct colocalization of lipid/metabolite with protein signals at the single-cell spatial resolution. This characterization will be translated to other neurodegenerative diseases, including HAND, in order to elucidate potential targets for new pharmacological therapies.

CHAPTER 6– CONCLUSION AND FUTURE DIRECTIONS

HIV infection is a major public health concern, affecting 38 million people worldwide (https://www.who.int/news-room/fact-sheets/detail/hiv-aids). HIV infection is now considered a chronic and manageable disease. The existing drugs to the treat HIV-infected population are not a cure even if they induce immune reconstitution (Perdomo-Celis, Taborda et al. 2019, Jilg, Garcia-Broncano et al. 2020). Most HIV-infected patients under cART that show a normal CD4 count, a low to undetectable viral load, and an increased life-expectancy, develop symptoms of accelerated aging, including HIV-associated neurocognitive disorder (HAND) (Saylor, Dickens et al. 2016). It is a spectrum of motor and behavioral/psychosocial dysfunctions (Saylor, Dickens et al. 2016). According to the cohort studies of the CNS HIV Anti-Retroviral Therapy Effects Research (CHARTER), the prevalence of HAND in the current cART era is 47%: 33% of patients exhibited asymptomatic neurocognitive impairment (ANI), 12% mild neurocognitive disorder (MND), and only 2% HIV-associated dementia (HAD) (Heaton, Clifford et al. 2010, Sacktor, Skolasky et al. 2016, Rosenthal and Tyor 2019, Vastag, Fira-Mladinescu et al. 2022). HAND diagnosing and management is not fully standardized such that statistical evaluation about the different types of HAND can differ (Wang, Liu et al. 2020, Vastag, Fira-Mladinescu et al. 2022). Cognitive impairment occurs due to early CNS infection before cART administration, the presence of viral reservoirs, and the aging of the HIV-infected population. Viral reservoirs are resident cells harboring integrated and replication-competent provirus within host cellular DNA; they cannot be targeted by the immune natural or engineered system and cART (Churchill, Deeks et al. 2016).

Long-term cART has shifted HAND to the milder forms, but it has maintained the same frequency in the HIV-infected population (Heaton, Clifford et al. 2010).

Importantly, the mechanisms by which HIV induces HAND in the current cART era are unknown.

The most demanding barrier to cure HIV infection is the presence of viral reservoirs in different anatomical compartments, including the brain (Svicher, Ceccherini-Silberstein et al. 2014, Churchill, Deeks et al. 2016, Siliciano and Siliciano 2018, Wang, Simonetti et al. 2018, De Scheerder, Vrancken et al. 2019, Abdel-Mohsen, Richman et al. 2020, Chaillon, Gianella et al. 2020, Lutgen, Narasipura et al. 2020). Upon cART interruption or for viral blips that can take place during cART administration, HIV can rebound from all the anatomical compartments in which viral reservoirs are resident (Sorstedt, Nilsson et al. 2016, De Scheerder, Vrancken et al. 2019, De-Scheerder, Depelseneer et al. 2020, Fujinaga and Cary 2020, Suzuki, Levert et al. 2021).

Currently, there is not a reliable method to detect viral reservoirs, and there is still open the scientific debate concerning the cell type in which the HIV genome is integrated and the size of these cells (Falcinelli, Ceriani et al. 2019). The mechanisms related to neuroHIV need to be fully investigated. Thus, this thesis tried to deal with these three major problems.

As we extensively described in the general introduction and Chapter 2, there are no consistent methods to detect viral reservoirs, especially in the tissues. In this thesis, we outlined a microscopy strategy that can be used for the reliable identification, localization, and quantification of viral reservoirs in the tissues and the blood of HIV-infected individuals. This methodology is based on a multi-probe and antigen detection system using a DNA probe targeting the HIV-Nef sequence, an mRNA probe targeting HIV gag-pol mRNA, and detecting HIV proteins and cellular markers using the traditional antibody-based technology. Our approach is very innovative because it can detect circulating or tissue-associated viral reservoirs and enables the identification of HIV-integrated DNA, HIV mRNA, and several viral proteins in a single analysis. To

consider the HIV DNA Nef probe a positive signal, it needs to colocalize with the Alu-repeats probe and DAPI, which we used as nuclear markers (correlation coefficient≥0.8). Instead, the viral mRNA signal does not colocalize with DAPI and Alu-repeats due to the different subcellular distribution. A similar selection for specificity was used for HIV viral proteins. For this analysis, we used human brain tissues provided by National NeuroAIDS Tissue Consortium (NNTC) and NeuroBioBank collected from uninfected (control and Alzheimers's disease) and HIV-infected patients. Infected patients were under cART for long a time showing undetectable, low, or high viral load; encephalitic patients were not virally suppressed with cART or under monotherapy (see Table 1, Chapter 2). Through our strategy, we confirmed that the brain is a sanctuary site for viral reservoirs (Balcom, Roda et al. 2019) and that a small population of microglia/macrophage and a smaller population of astrocytes are the major reservoirs within the brain (Li, Henderson et al. 2016, Clayton, Garcia et al. 2017) in the pre- and current cART era. Only a few of the microglia/macrophages and astrocytes in the brain were infected with HIV, suggesting that an unknown mechanism of selection is used for specific niches within the brain that have a higher susceptibility to HIV infection. Among the HIV-DNA positive cells, only 1/3 of them were HIV RNA positive, and a few (~1/3) of these double-positive cells synthetized viral proteins. Literature data regarding the pre-cART era indicated that the percentage of macrophages and astrocytes with HIV-integrated DNA is higher than our analysis (Churchill, Wesselingh et al. 2009). Through our system, we identified that cART induces a reduction in the viral reservoir pools. Specifically, myeloid and glial reservoirs undergo a distinct cART effect; the amount of astrocyte reservoirs is not altered by the different degrees of systemic replication compared to macrophage/microglia that proportionally decrease in high, low, and undetectable viral load conditions. However, cART cannot completely inhibit HIV-mRNA production and HIV protein synthesis. The low number of viral reservoirs we detected in the brain cannot directly explain the cognitive decline and the structural

damage detected in HIV-infected patients. We demonstrated that viral reservoirs synthesize p24, Gp120, Nef, Vpr, and Tat proteins, but not Integrase, which are released and taken up by neighboring uninfected cells even during cART administration. Several laboratories using animal models such as humanized mouse models and non-human primates (Hanna, Kay et al. 1998, Nesbit and Schwartz 2002, Hansen, Vieville et al. 2009, Yamada, Yoshikawa et al. 2015) have shown a consistent synthesis of HIV proteins that is not representative of what we observed in human brain tissues, where HIV proteins synthesis is not systemic but localized. The basal synthesis of HIV proteins can validate the theory of HIV protein neurotoxicity that has been discussed for many years and implicates HIV proteins in the progression of neuroHIV (Wallace 2006, Kovalevich and Langford 2012, Mocchetti, Bachis et al. 2012). Thus, we demonstrated that viral reservoirs contribute to the bystander damage by secretion of HIV proteins that reach limited but considerable distances (μm range) into the brain.

The brain of HIV-infected population virally suppressed with cART also exhibited significant structural changes, such as the decrease in gray matter volume and the presence of hyper-densities in the white matter (Su, Wit et al. 2016, Eggers, Arendt et al. 2017, Strain, Burdo et al. 2017, Underwood, Cole et al. 2017, van Zoest, Underwood et al. 2017, Sanford, Strain et al. 2019).

In this thesis we associated the presence of viral reservoirs in the brain with a local myelin sheath compromise. Myelin structural impairment by HIV infection involves myelin structural proteins and lipids. We demonstrated *in vitro* that sulfatide, the major structural lipid in the myelin, compromised gap junctional communication and calcium waves, correlating with CNS damage and cognitive decline observed in the HIV-infected population under cART.

Since the clinical settings that enable the partitioning of HAND in ANI and MND are still debated in the scientific community (Nightingale, Winston et al. 2014, Saylor, Dickens et al. 2016), we divided our analysis in mild and severe forms of HAND (HIV-

MND and HAD). We included uninfected patients not affected by neurodegenerative diseases and affected by AD as controls. AD brains were used as a positive control for demyelination, defects in the biosynthesis of myelin lipids, and cognitive decline (see Table 2, Chapter 3) (Papuc and Rejdak 2020). Our findings demonstrated that HIV infection and associated cognitive impairment reduced the expression of myelin structural proteins (MBP and PLP) in the cell processes, but only mildly compared to AD pathogenesis. Genome-wide microarray analysis of HIV-infected frontal cortex tissues from patients virally suppressed with cART and developing HAND revealed down-regulated MBP mRNA levels (Borjabad, Morgello et al. 2011, Borjabad and Volsky 2012), as well as RNA sequencing of HIV-humanized mice brain showed decrease transcripts for MBP and PLP (Li, Gorantla et al. 2017, Jensen, Roth et al. 2019). Our future experiments aim to investigate the expression of other myelin sheath structural proteins such as myelin-associated glycoprotein (MAG) and myelin oligodendrocyte glycoprotein (MOG) (Kursula 2008).

HIV-infected individuals with MND or HAD also had a significant reduction of myelin sheath thickness compared to uninfected people without cognitive decline conditions, suggesting implications for the normal neuronal circuits (Suminaite, Lyons et al. 2019). In the current cART era, subcortical white matter (WM) damage is observed in HAND and this damage correlates with demyelination, inflammation, synaptodendritic injury, and microvascular alterations (Alakkas, Ellis et al. 2019). In our analysis, a loss of myelin structural integrity was observed in neighboring uninfected areas indicating the presence of CNS damage amplification even in the absence of systemic viral replication.

A potential driving mechanism of CNS damage triggering HAND onset and pathogenesis is lipid dysregulation. Our recent data indicates that HIV-infected individuals under cART display altered circulating lipid metabolism (Velasquez, Prevedel et al. 2020). In addition, existing literature data revealed that HIV dysregulates lipids resulting in adipose accumulation in the body (Martinez, Mocroft et al. 2001,

Bernasconi, Boubaker et al. 2002) and dyslipidemia in the blood (Souza, Luzia et al. 2013, Finkelstein, Gala et al. 2015) with an elevated risk of cardiovascular diseases (Waters and Hsue 2019, Drechsler, Ayers et al. 2021).

HAND, as well as other neurodegenerative diseases, has been linked to lipid dysregulation (Bandaru, Mielke et al. 2013, Bandera, Taramasso et al. 2019, Torkzaban, Mohseni Ahooyi et al. 2020), but a comprehensive examination of structural and signaling lipids in the brain of HIV-infected individuals under cART and developing neurocognitive impairment is missing. In this thesis, we analyzed lipid distribution in the brain of HIV-infected individuals by MALDI-MSI, demonstrateing that sulfatide, a key lipid family involved in maintaining myelin structure, was compromised in HIV conditions. Sulfatide is the major lipid component of the myelin sheath (Schmitt, Castelvetri et al. 2015, Blomqvist, Zetterberg et al. 2021). In our analysis, the long carbon chain sulfatides (24:0, 24:1 and hydroxylated species, 24:0 OH and 24:1 OH) showed a significant upregulation in the WM of HIV-infected individuals with milder and severe cognitive impairment. Sulfatide species with various fatty acid chains have different roles in the myelin sheath structure; short-chain sulfatides with 16 to 22 carbon non-hydroxylated and hydroxylated fatty acids support myelin development; instead, long-chain sulfatides with 24 carbon non-hydroxylated and hydroxylated fatty acids are predominant in the adult brain and support myelin sheath maintenance (Hirahara, Wakabayashi et al. 2017). Other neurodegenerative diseases showed significant changes in lipid distribution and CNS structural damage (Hussain, Anwar et al. 2020). If sulfatide expression in HAND conditions is compared to Alzheimer's (AD) and Parkinson's diseases (PD), sulfatide increases in the white matter of HIV-infected patients with cognitive decline rather than in the grey matter as observed in PD's patients (Cheng, Xu et al. 2003) or being reduced in both grey and white matter as observed in AD condition (Han, D et al. 2002). Thus, a neuroHIV specific mechanism characterizes sulfatide dysregulation and mild myelin structural compromise. This process may involve the

immune detection of sulfatide as self-antigens to trigger the chronic inflammation observed in the brain of HIV-infected individuals under cART and affected by HAND. Literature data indicate sulfatide is a lipid antigen, which can stimulate a strong immune response (Kanter, Narayana et al. 2006, Samygina, Popov et al. 2011, Yang, Lee et al. 2011, Patel, Pellicci et al. 2012, Fuss, Joshi et al. 2014, Dasgupta and Kumar 2016, Stax, Tuengel et al. 2017, Sebode, Wigger et al. 2019, Kim, Han et al. 2020, Williams, Chen et al. 2020). Thus, our future directions aim to highlight sulfatide as a biomarker of HIV-associated cognitive impairment, inflammation, and bystander damage triggered by the persistence of viral reservoirs in the brain. We intend to expand our research to larger clinical cohorts and HIV animal models (non-human primates and humanized mice/rats), and also include sulfatide precursors such as galactosylceramide and ceramide to identify and quantify autoantigens and elucidate new HIV pathogenic mechanisms through the isolation of the areas of the viral reservoirs by Laser Capture Microdissection (LCM). Many restrictions affect the use of HIV animal models in our project, especially the persistent HIV reservoir in the brain and their excessive synthesis of viral proteins. However, HIV animal models can be useful to reduce the variance of human demographic factors in investigating the CNS lipid disorder (Saylor, Dickens et al. 2016, Marsden 2020). In the future, analysis of multiple lipid markers, rather than a single lipid, could be necessary for improving the diagnostic accuracy and prognostic evaluation of HAND. Galactosylceramide family, the direct precursor of sulfatide, also participate in myelin structure maintenance and differentiation (Reza, Ugorski et al. 2021), and it is recognized as the binding molecule of the HIV-1 surface envelope glycoprotein gp120 (Cook, Fantini et al. 1994). In addition, ceramide is the backbone of all the sphingolipids, it is a key regulator of brain homeostasis and is altered in neurodegenerative diseases (Mencarelli and Martinez-Martinez 2013, Castro, Prieto et al. 2014, Hussain, Anwar et al. 2020).

Regarding the functional significance of soluble sulfatide in the context of CNS damage, one of the key finding of our laboratory is that HIV uses a cell-to-cell communication system, gap junction channels and hemichannels, to amplify the bystander damage mediated by viral reservoirs through IP_3 and calcium signaling (Eugenin, King et al. 2007, Eugenin, Clements et al. 2011, Roberts, Eugenin et al. 2012, Eugenin and Berman 2013, Berman, Carvallo et al. 2016, Malik, Theis et al. 2017, Gajardo-Gomez, Santibanez et al. 2020, Lutgen, Narasipura et al. 2020, Velasquez, Prevedel et al. 2020, Gorska, Donoso et al. 2021, Malik, Valdebenito et al. 2021, Valdebenito, Castellano et al. 2021). Hence, we have investigated soluble sulfatide effects on human primary astrocytes. Soluble sulfatide compromised the triggering of calcium waves in the astrocyte pacemaker cells, affecting the coordination between the pacemaker and non-pacemaker cells. The propagation of calcium waves between the astrocytes is principally mediated *via* Cx43 gap junctions (Scemes, Dermietzel et al. 1998), whose expression is upregulated by HIV-Tat in the glial reservoirs to induce bystander apoptosis into the neighboring uninfected cells (Eugenin and Berman 2007, Eugenin, Clements et al. 2011, Eugenin and Berman 2013, Berman, Carvallo et al. 2016, Malik, Theis et al. 2017, Gajardo-Gomez, Santibanez et al. 2020, D'Amico, Valdebenito et al. 2021, Malik, Valdebenito et al. 2021, Valdebenito, Castellano et al. 2021). In this thesis, we demonstrated that soluble sulfatide increased Cx43 mRNA and protein levels in human primary astrocytes. Soluble sulfatide also up-regulated ZO-1 mRNA and protein, which regulates Cx43 GJ's dynamic turnover including the forward trafficking of Cx43 toward the plasma membrane to be opened and in functional conformation (Thevenin, Kowal et al. 2013, Thevenin, Margraf et al. 2017). Soluble sulfatide further increased gap junctional communication, suggesting that it can increase the radius of damage arising from the glial reservoirs. Hela cells were used as a stable system for Cx43 expression to study its binding proteins after sulfatide stimulation by coimmunoprecipitation and subsequent proteomics. Preliminary proteomics data revealed

that sulfatide regulated three important families of proteins related to recycling-transport, mitochondria, and cellular membrane. Within the recycling-transport proteins, we identified proteins binding to Cx43, involved in an active vesicular transport such as myosin and rab proteins. Mitochondrial proteins binding Cx43 and upregulated by sulfatide were related to glucose and glutamate/glutamine synthesis. Future experiments aim to demonstrate the direct interaction of Cx43 with these specific metabolic enzymes in the mitochondria. In addition, we found a potential specific proteomic profile for Cx43 in the plasma membrane that stabilizes Cx43 open and functional conformation that needs to be confirmed in additional experiments. We chose Hela cells to perform this analysis because they represent a simple model, future studies intend to characterize Cx43 binding proteins in human primary astrocytes treated with sulfatide and HIV-infected. Pending experiments also aim to knock-down Cx43 in HIV-infected astrocytes to identify the populations susceptible to HIV infection or bystander damage by single-cell RNA sequencing. Other pending experiments aim to analyze lipid dysregulation in primary cultures of astrocytes uninfected and HIV-infected using MALDI-2 MSI, to improve the sensitivity and the spatial resolution of the lipid analysis.

To improve our lipidomics assay at the cellular level spatial detail, we developed a MALDI-2 MSI method to image triglycerides and cholesteryl esters that are not easily ionized using regular MALDI-MSI. We analyzed triglyceride and cholesteryl ester expression in the brain of 5- and 17-month-old 3xTg mouse model for the pathological mechanisms of AD and age-matched wild-type control B6J mice. Using MALDI-2 MSI, we identified more than 30 triglyceride species in the brain of 3xTg mice four-fold higher than we detected with regular MALDI-MSI. Triglyceride species, detected in the brain of 3xTg mice, mostly localized within the ependymal cells lining the ventricle and adjacent tissue areas, and their expression was age and AD pathogenesis dependent. Our approach is groundbreaking because it combines highly innovative lipidomic MALDI-2 MSI assessment, immunofluorescence analysis for cellular markers, and histological staining

for morphological evaluation in the same tissue section. This is critical because it enables a direct co-localization of lipid/metabolite with protein signals at the single-cell spatial resolution. For future studies, we intend to associate a spatial transcriptomics analysis to have a complete map of lipid metabolism and related gene activity in the same tissue sample (Dries, Chen et al. 2021, Rao, Barkley et al. 2021). This will enable a full and multi-omics characterization of dysregulated pathways in several neurodegenerative diseases and elucidate potential targets for novel therapeutic approaches.

HAND is not an age-related and progressive neuropathology like AD. A critical obstacle to study HAND pathologic mechanisms in the HIV-infected population is the possibility that reestablish the motor/cognitive functions. Typically, HAND remains stable during effective cART, but in rare instances can be resolved completely or progress to severe forms of HAND (Sacktor, Skolasky et al. 2016). Thus, translating our multi-omics characterization of dysregulated pathways and finding specific combined biomarkers for the distinct stages of HAND are clinically relevant to improve the everyday functioning of the HIV-infected population under cART.

Overall, there are major contributions to the HIV field presented in this thesis.

First, we have optimized a high throughput technique to identify, localize, and quantify viral reservoirs in the tissues and the blood.

Second, we identify that small populations of microglia/macrophages and smaller astrocyte population are CNS viral reservoirs in the pre- and the current cART era.

Third, HIV brain reservoirs are rare, heterogeneously distributed in the brain, and organized in small clusters.

Fourth, HIV brain reservoirs produce residual viral mRNAs and proteins despite cART long-term administration. We demonstrated that HIV-p24, Gp120, Nef, Vpr, and Tat proteins are synthesized by myeloid and glial reservoirs, released, and taken up by neighboring uninfected cells to amplify the brain damage observed in the HIV-infected population.

Fifth, viral reservoir-induced damage includes myelin structural protein and lipid changes. We identified that HIV-infected patients under cART with mild and severe cognitive impairment have lower expression of MBP and PLP proteins in the brain, and their myelin structure is reduced in thickness. These patients also showed an increased expression of certain species of sulfatide, suggesting amplification of damage controlled by viral proteins through a lipid-mediated mechanism.

Sixth, we identified that sulfatide increases cell-to-cell communication *in vitro* by upregulating Cx43 GJ, which are essential components to spread bystander damage.

Seventh, we developed a MALDI-2 MSI method to detect triglycerides and cholesteryl esters associated with histochemical analyses in the AD mouse brain, useful to investigate other neurocognitive disorders, including HAND.

Although CNS damage in HIV-infected individuals under cART is multifactorial we provided specific tools and unique data that describe a mechanism of bystander damage in HAND. Based on our untargeted lipidomic analyses, we proposed sulfatide as a potential biomarker or a molecular target for preventing or curing neurocognitive disorders that affect HIV aviremic population. There are many gaps of knowledge that need to be adressed to elucidate HAND pathogenesis. Our multi-faceted approach utilizing viral reservoirs identification and quantification, myelin structural impairment, and lipid dysregulation can be clinically relevant for developing drugs that prevent or alleviate the motor and behavioral/psychosocial dysfunctions that distress a good portion of the HIV-infected population under cART.

References

Abbas, W. and G. Herbein (2012). "Molecular Understanding of HIV-1 Latency." Adv Virol **2012**: 574967.

Abdel-Mohsen, M., D. Richman, R. F. Siliciano, M. C. Nussenzweig, B. J. Howell, J. Martinez-Picado, N. Chomont, K. J. Bar, X. G. Yu, M. Lichterfeld, J. Alcami, D. Hazuda, F. Bushman, J. D. Siliciano, M. R. Betts, A. M. Spivak, V. Planelles, B. H. Hahn, D. M. Smith, Y. C. Ho, M. J. Buzon, C. Gaebler, M. Paiardini, Q. Li, J. D. Estes, T. J. Hope, J. Kostman, K. Mounzer, M. Caskey, L. Fox, I. Frank, J. L. Riley, P. Tebas, L. J. Montaner and B.-H. D. C. t. C. H.-. infection (2020). "Recommendations for measuring HIV reservoir size in cure-directed clinical trials." Nat Med **26**(9): 1339-1350.

Abdulle, S., A. Mellgren, B. J. Brew, P. Cinque, L. Hagberg, R. W. Price, L. Rosengren and M. Gisslen (2007). "CSF neurofilament protein (NFL) -- a marker of active HIV-related neurodegeneration." J Neurol **254**(8): 1026-1032.

Abramov, A. Y., M. Ionov, E. Pavlov and M. R. Duchen (2011). "Membrane cholesterol content plays a key role in the neurotoxicity of beta-amyloid: implications for Alzheimer's disease." Aging Cell **10**(4): 595-603.

Abreu, C., E. N. Shirk, S. E. Queen, J. L. Mankowski, L. Gama and J. E. Clements (2019). "A Quantitative Approach to SIV Functional Latency in Brain Macrophages." J Neuroimmune Pharmacol **14**(1): 23-32.

Adibhatla, R. M. and J. F. Hatcher (2007). "Role of Lipids in Brain Injury and Diseases." Future Lipidol **2**(4): 403-422.

Adibhatla, R. M. and J. F. Hatcher (2008). "Altered lipid metabolism in brain injury and disorders." Subcell Biochem **49**: 241-268.

Adiele, R. C. and C. A. Adiele (2019). "Metabolic defects in multiple sclerosis." Mitochondrion **44**: 7-14.

Adu-Gyamfi, C., D. Savulescu, L. Mikhathani, K. Otwombe, N. Salazar-Austin, R. Chaisson, N. Martinson, J. George and M. Suchard (2021). "Plasma Kynurenine-to-Tryptophan Ratio, a Highly Sensitive Blood-Based Diagnostic Tool for Tuberculosis in Pregnant Women Living With Human Immunodeficiency Virus (HIV)." Clin Infect Dis **73**(6): 1027-1036.

Adu-Gyamfi, C. G., T. Snyman, C. J. Hoffmann, N. A. Martinson, R. E. Chaisson, J. A. George and M. S. Suchard (2017). "Plasma Indoleamine 2, 3-Dioxygenase, a Biomarker for Tuberculosis in Human Immunodeficiency Virus-Infected Patients." Clin Infect Dis **65**(8): 1356-1358.

Adu-Gyamfi, C. G., T. Snyman, L. Makhathini, K. Otwombe, F. Darboe, A. Penn-Nicholson, M. Fisher, D. Savulescu, C. Hoffmann, R. Chaisson, N. Martinson, T. J. Scriba, J. A. George and M. S. Suchard (2020). "Diagnostic accuracy of plasma kynurenine/tryptophan ratio, measured by enzyme-linked immunosorbent assay, for pulmonary tuberculosis." Int J Infect Dis **99**: 441-448.

Agar, N. Y., H. W. Yang, R. S. Carroll, P. M. Black and J. N. Agar (2007). "Matrix solution fixation: histology-compatible tissue preparation for MALDI mass spectrometry imaging." Anal Chem **79**(19): 7416-7423.

Aggarwal, S., L. Yurlova and M. Simons (2011). "Central nervous system myelin: structure, synthesis and assembly." Trends Cell Biol **21**(10): 585-593.

Ajasin, D. and E. A. Eugenin (2020). "HIV-1 Tat: Role in Bystander Toxicity." Frontiers in cellular and infection microbiology **10**: 61.

Al-Harthi, L. (2012). "Interplay between Wnt/beta-catenin signaling and HIV: virologic and biologic consequences in the CNS." J Neuroimmune Pharmacol **7**(4): 731-739.

Al-Harti, L., J. Joseph and A. Nath (2018). "Astrocytes as an HIV CNS reservoir: highlights and reflections of an NIMH-sponsored symposium." Journal of neurovirology **24**(6): 665-669.

Alakkas, A., R. J. Ellis, C. W. Watson, A. Umlauf, R. K. Heaton, S. Letendre, A. Collier, C. Marra, D. B. Clifford, B. Gelman, N. Sacktor, S. Morgello, D. Simpson, J. A. McCutchan, A. Kallianpur, S. Gianella, T. Marcotte, I. Grant, C. Fennema-Notestine and C. Group (2019). "White matter damage, neuroinflammation, and neuronal integrity in HAND." J Neurovirol **25**(1): 32-41.

Alamri, H., N. H. Patterson, E. Yang, P. Zoroquiain, A. Lazaris, P. Chaurand and P. Metrakos (2019). "Mapping the triglyceride distribution in NAFLD human liver by MALDI imaging mass spectrometry reveals molecular differences in micro and macro steatosis." Anal Bioanal Chem **411**(4): 885-894.

Alzheimer, A., R. A. Stelzmann, H. N. Schnitzlein and F. R. Murtagh (1995). "An English translation of Alzheimer's 1907 paper, "Uber eine eigenartige Erkankung der Hirnrinde"." Clin Anat **8**(6): 429-431.

Ambrosi, C., C. Ren, G. Spagnol, G. Cavin, A. Cone, E. E. Grintsevich, G. E. Sosinsky and P. L. Sorgen (2016). "Connexin43 Forms Supramolecular Complexes through Non-Overlapping Binding Sites for Drebrin, Tubulin, and ZO-1." PLoS One **11**(6): e0157073.

Amtul, Z., M. Uhrig, R. F. Rozmahel and K. Beyreuther (2011). "Structural insight into the differential effects of omega-3 and omega-6 fatty acids on the production of Abeta peptides and amyloid plaques." J Biol Chem **286**(8): 6100-6107.

An, P., L. H. Wang, H. Hutcheson-Dilks, G. Nelson, S. Donfield, J. J. Goedert, C. R. Rinaldo, S. Buchbinder, G. D. Kirk, S. J. O'Brien and C. A. Winkler (2007). "Regulatory polymorphisms in the cyclophilin A gene, PPIA, accelerate progression to AIDS." PLoS Pathog **3**(6): e88.

Ances, B. M., M. Ortega, F. Vaida, J. Heaps and R. Paul (2012). "Independent effects of HIV, aging, and HAART on brain volumetric measures." J Acquir Immune Defic Syndr **59**(5): 469-477.

Andersen, A. B., I. Law, K. S. Krabbe, H. Bruunsgaard, S. R. Ostrowski, H. Ullum, L. Hojgaard, A. Lebech, J. Gerstoft and A. Kjaer (2010). "Cerebral FDG-PET scanning abnormalities in optimally treated HIV patients." J Neuroinflammation **7**: 13.

Anderson, A. M., J. L. Lennox, M. M. Mulligan, D. W. Loring, H. Zetterberg, K. Blennow, C. Kessing, R. Koneru, K. Easley and W. R. Tyor (2017). "Cerebrospinal fluid interferon alpha levels correlate with neurocognitive impairment in ambulatory HIV-Infected individuals." J Neurovirol **23**(1): 106-112.

Anderson, E. M. and F. Maldarelli (2018). "The role of integration and clonal expansion in HIV infection: live long and prosper." Retrovirology **15**(1): 71.

Ando, S., Y. Tanaka, Y. Toyoda and K. Kon (2003). "Turnover of myelin lipids in aging brain." Neurochem Res **28**(1): 5-13.

Andreasson, K. (2010). "Emerging roles of PGE2 receptors in models of neurological disease." Prostaglandins Other Lipid Mediat **91**(3-4): 104-112.

Andrieu-Abadie, N., V. Gouaze, R. Salvayre and T. Levade (2001). "Ceramide in apoptosis signaling: relationship with oxidative stress." Free Radic Biol Med **31**(6): 717-728.

Ann, H. W., S. Jun, N. Y. Shin, S. Han, J. Y. Ahn, M. Y. Ahn, Y. D. Jeon, I. Y. Jung, M. H. Kim, W. Y. Jeong, N. S. Ku, J. M. Kim, D. M. Smith and J. Y. Choi (2016). "Characteristics of Resting-State Functional Connectivity in HIV-Associated Neurocognitive Disorder." PLoS One **11**(4): e0153493.

Antinori, A., G. Arendt, J. T. Becker, B. J. Brew, D. A. Byrd, M. Cherner, D. B. Clifford, P. Cinque, L. G. Epstein, K. Goodkin, M. Gisslen, I. Grant, R. K. Heaton, J. Joseph, K. Marder, C. M. Marra, J. C. McArthur, M. Nunn, R. W. Price, L. Pulliam, K. R. Robertson, N. Sacktor, V. Valcour and V. E. Wojna (2007). "Updated research nosology for HIV-associated neurocognitive disorders." Neurology **69**(18): 1789-1799.

Archibald, S. L., J. A. McCutchan, C. Sanders, T. Wolfson, T. L. Jernigan, R. J. Ellis, B. M. Ances, A. C. Collier, J. C. McArthur, S. Morgello, D. M. Simpson, C. Marra, B. B. Gelman, D. B. Clifford, I. Grant, C. Fennema-Notestine and C. Group (2014). "Brain

morphometric correlates of metabolic variables in HIV: the CHARTER study." J Neurovirol **20**(6): 603-611.

Archin, N. M., J. L. Kirchherr, J. A. Sung, G. Clutton, K. Sholtis, Y. Xu, B. Allard, E. Stuelke, A. D. Kashuba, J. D. Kuruc, J. Eron, C. L. Gay, N. Goonetilleke and D. M. Margolis (2017). "Interval dosing with the HDAC inhibitor vorinostat effectively reverses HIV latency." J Clin Invest **127**(8): 3126-3135.

Archin, N. M., A. L. Liberty, A. D. Kashuba, S. K. Choudhary, J. D. Kuruc, A. M. Crooks, D. C. Parker, E. M. Anderson, M. F. Kearney, M. C. Strain, D. D. Richman, M. G. Hudgens, R. J. Bosch, J. M. Coffin, J. J. Eron, D. J. Hazuda and D. M. Margolis (2012). "Administration of vorinostat disrupts HIV-1 latency in patients on antiretroviral therapy." Nature **487**(7408): 482-485.

Ariazi, J., A. Benowitz, V. De Biasi, M. L. Den Boer, S. Cherqui, H. Cui, N. Douillet, E. A. Eugenin, D. Favre, S. Goodman, K. Gousset, D. Hanein, D. I. Israel, S. Kimura, R. B. Kirkpatrick, N. Kuhn, C. Jeong, E. Lou, R. Mailliard, S. Maio, G. Okafo, M. Osswald, J. Pasquier, R. Polak, G. Pradel, B. de Rooij, P. Schaeffer, V. A. Skeberdis, I. F. Smith, A. Tanveer, N. Volkmann, Z. Wu and C. Zurzolo (2017). "Tunneling Nanotubes and Gap Junctions-Their Role in Long-Range Intercellular Communication during Development, Health, and Disease Conditions." Front Mol Neurosci **10**: 333.

Arribat, Y., D. Grepper, S. Lagarrigue, T. Qi, S. Cohen and F. Amati (2020). "Spastin mutations impair coordination between lipid droplet dispersion and reticulum." PLoS Genet **16**(4): e1008665.

Arts, E. J. and D. J. Hazuda (2012). "HIV-1 antiretroviral drug therapy." Cold Spring Harb Perspect Med **2**(4): a007161.

Asamitsu, K., K. Fujinaga and T. Okamoto (2018). "HIV Tat/P-TEFb Interaction: A Potential Target for Novel Anti-HIV Therapies." Molecules **23**(4).

Ashburner, J. and K. J. Friston (2000). "Voxel-based morphometry--the methods." Neuroimage **11**(6 Pt 1): 805-821.

Aslam, B., M. Basit, M. A. Nisar, M. Khurshid and M. H. Rasool (2017). "Proteomics: Technologies and Their Applications." J Chromatogr Sci **55**(2): 182-196.

Athenstaedt, K. and G. Daum (2006). "The life cycle of neutral lipids: synthesis, storage and degradation." Cell Mol Life Sci **63**(12): 1355-1369.

Bachis, A., S. A. Aden, R. L. Nosheny, P. M. Andrews and I. Mocchetti (2006). "Axonal transport of human immunodeficiency virus type 1 envelope protein glycoprotein 120 is found in association with neuronal apoptosis." The Journal of neuroscience : the official journal of the Society for Neuroscience **26**(25): 6771-6780.

Bailey, A. P., G. Koster, C. Guillermier, E. M. Hirst, J. I. MacRae, C. P. Lechene, A. D. Postle and A. P. Gould (2015). "Antioxidant Role for Lipid Droplets in a Stem Cell Niche of Drosophila." Cell **163**(2): 340-353.

Bairwa, D., V. Kumar, S. Vyas, B. K. Das, A. K. Srivastava, R. M. Pandey, S. K. Sharma, N. R. Jagannathan and S. Sinha (2016). "Case control study: magnetic resonance spectroscopy of brain in HIV infected patients." BMC Neurol **16**: 99.

Balcom, E. F., W. C. Roda, E. A. Cohen, M. Y. Li and C. Power (2019). "HIV-1 persistence in the central nervous system: viral and host determinants during antiretroviral therapy." Curr Opin Virol **38**: 54-62.

Bandaru, V. V., M. M. Mielke, N. Sacktor, J. C. McArthur, I. Grant, S. Letendre, L. Chang, V. Wojna, C. Pardo, P. Calabresi, S. Munsaka and N. J. Haughey (2013). "A lipid storage-like disorder contributes to cognitive decline in HIV-infected subjects." Neurology **81**(17): 1492-1499.

Bandera, A., A. Gori, M. Clerici and M. Sironi (2019). "Phylogenies in ART: HIV reservoirs, HIV latency and drug resistance." Curr Opin Pharmacol **48**: 24-32.

Bandera, A., L. Taramasso, G. Bozzi, A. Muscatello, J. A. Robinson, T. H. Burdo and A. Gori (2019). "HIV-Associated Neurocognitive Impairment in the Modern ART Era: Are We Close to Discovering Reliable Biomarkers in the Setting of Virological Suppression?" Front Aging Neurosci **11**: 187.

Bar, K. J., E. Coronado, T. Hensley-McBain, M. A. O'Connor, J. M. Osborn, C. Miller, T. M. Gott, S. Wangari, N. Iwayama, C. Y. Ahrens, J. Smedley, C. Moats, R. M. Lynch, E. K. Haddad, N. L. Haigwood, D. H. Fuller, G. M. Shaw, N. R. Klatt and J. A. Manuzak (2019). "Simian-Human Immunodeficiency Virus SHIV.CH505 Infection of Rhesus Macaques Results in Persistent Viral Replication and Induces Intestinal Immunopathology." Journal of virology **93**(18).

Barat, C., A. Proust, A. Deshiere, M. Leboeuf, J. Drouin and M. J. Tremblay (2018). "Astrocytes sustain long-term productive HIV-1 infection without establishment of reactivable viral latency." Glia **66**(7): 1363-1381.

Barre-Sinoussi, F., J. C. Chermann, F. Rey, M. T. Nugeyre, S. Chamaret, J. Gruest, C. Dauguet, C. Axler-Blin, F. Vezinet-Brun, C. Rouzioux, W. Rozenbaum and L. Montagnier (1983). "Isolation of a T-lymphotropic retrovirus from a patient at risk for acquired immune deficiency syndrome (AIDS)." Science **220**(4599): 868-871.

Barre, F. P. Y., M. R. L. Paine, B. Flinders, A. J. Trevitt, P. D. Kelly, R. Ait-Belkacem, J. P. Garcia, L. B. Creemers, J. Stauber, R. J. Vreeken, B. Cillero-Pastor, S. R. Ellis and R. M. A. Heeren (2019). "Enhanced Sensitivity Using MALDI Imaging Coupled with Laser Postionization (MALDI-2) for Pharmaceutical Research." Anal Chem **91**(16): 10840-10848.

Bartke, N. and Y. A. Hannun (2009). "Bioactive sphingolipids: metabolism and function." J Lipid Res **50 Suppl**: S91-96.

Baslow, M. H. (2003). "N-acetylaspartate in the vertebrate brain: metabolism and function." Neurochem Res **28**(6): 941-953.

Batiuk, M. Y., A. Martirosyan, J. Wahis, F. de Vin, C. Marneffe, C. Kusserow, J. Koeppen, J. F. Viana, J. F. Oliveira, T. Voet, C. P. Ponting, T. G. Belgard and M. G. Holt (2020). "Identification of region-specific astrocyte subtypes at single cell resolution." Nat Commun **11**(1): 1220.

Behrman-Lay, A. M., R. H. Paul, J. Heaps-Woodruff, L. M. Baker, C. Usher and B. M. Ances (2016). "Human immunodeficiency virus has similar effects on brain volumetrics and cognition in males and females." J Neurovirol **22**(1): 93-103.

Bellingan, G. J., H. Caldwell, S. E. Howie, I. Dransfield and C. Haslett (1996). "In vivo fate of the inflammatory macrophage during the resolution of inflammation: inflammatory macrophages do not die locally, but emigrate to the draining lymph nodes." J Immunol **157**(6): 2577-2585.

Berghoff, S. A., L. Spieth, T. Sun, L. Hosang, C. Depp, A. O. Sasmita, M. H. Vasileva, P. Scholz, Y. Zhao, D. Krueger-Burg, S. Wichert, E. R. Brown, K. Michail, K. A. Nave, S. Bonn, F. Odoardi, M. Rossner, T. Ischebeck, J. M. Edgar and G. Saher (2021). "Neuronal cholesterol synthesis is essential for repair of chronically demyelinated lesions in mice." Cell Rep **37**(4): 109889.

Berman, J. W., L. Carvallo, C. M. Buckner, A. Luers, L. Prevedel, M. V. Bennett and E. A. Eugenin (2016). "HIV-tat alters Connexin43 expression and trafficking in human astrocytes: role in NeuroAIDS." J Neuroinflammation **13**(1): 54.

Bernasconi, E., K. Boubaker, C. Junghans, M. Flepp, H. J. Furrer, A. Haensel, B. Hirschel, K. Boggian, J. P. Chave, M. Opravil, R. Weber, M. Rickenbach, A. Telenti and H. I. V. C. S. Swiss (2002). "Abnormalities of body fat distribution in HIV-infected persons treated with antiretroviral drugs: The Swiss HIV Cohort Study." J Acquir Immune Defic Syndr **31**(1): 50-55.

Bernhard, W., K. Barreto, A. Saunders, M. S. Dahabieh, P. Johnson and I. Sadowski (2011). "The Suv39H1 methyltransferase inhibitor chaetocin causes induction of integrated HIV-1 without producing a T cell response." FEBS Lett **585**(22): 3549-3554.

Berry, K. A., J. A. Hankin, R. M. Barkley, J. M. Spraggins, R. M. Caprioli and R. C. Murphy (2011). "MALDI imaging of lipid biochemistry in tissues by mass spectrometry." Chem Rev **111**(10): 6491-6512.

Besnard, E., S. Hakre, M. Kampmann, H. W. Lim, N. N. Hosmane, A. Martin, M. C. Bassik, E. Verschueren, E. Battivelli, J. Chan, J. P. Svensson, A. Gramatica, R. J.

Conrad, M. Ott, W. C. Greene, N. J. Krogan, R. F. Siliciano, J. S. Weissman and E. Verdin (2016). "The mTOR Complex Controls HIV Latency." Cell Host Microbe **20**(6): 785-797.

Bhandari, D. R., M. Schott, A. Rompp, A. Vilcinskas and B. Spengler (2015). "Metabolite localization by atmospheric pressure high-resolution scanning microprobe matrix-assisted laser desorption/ionization mass spectrometry imaging in whole-body sections and individual organs of the rove beetle Paederus riparius." Anal Bioanal Chem **407**(8): 2189-2201.

Biddison, W. E., D. D. Taub, W. W. Cruikshank, D. M. Center, E. W. Connor and K. Honma (1997). "Chemokine and matrix metalloproteinase secretion by myelin proteolipid protein-specific CD8+ T cells: potential roles in inflammation." J Immunol **158**(7): 3046-3053.

Billah, M. M. and J. C. Anthes (1990). "The regulation and cellular functions of phosphatidylcholine hydrolysis." Biochem J **269**(2): 281-291.

Bishop, W. R. and R. M. Bell (1988). "Functions of diacylglycerol in glycerolipid metabolism, signal transduction and cellular transformation." Oncogene Res **2**(3): 205-218.

Blanc, L., A. Lenaerts, V. Dartois and B. Prideaux (2018). "Visualization of Mycobacterial Biomarkers and Tuberculosis Drugs in Infected Tissue by MALDI-MS Imaging." Anal Chem **90**(10): 6275-6282.

Blankson, J. N., D. Persaud and R. F. Siliciano (2002). "The challenge of viral reservoirs in HIV-1 infection." Annu Rev Med **53**: 557-593.

Blazkova, J., F. Gao, M. H. Marichannegowda, J. S. Justement, V. Shi, E. J. Whitehead, R. F. Schneck, E. D. Huiting, K. Gittens, M. Cottrell, E. Benko, C. Kovacs, J. Lack, M. C. Sneller, S. Moir, A. S. Fauci and T. W. Chun (2021). "Distinct mechanisms of long-term virologic control in two HIV-infected individuals after treatment interruption of anti-retroviral therapy." Nat Med **27**(11): 1893-1898.

Blokhuis, C., H. Mutsaerts, S. Cohen, H. J. Scherpbier, M. W. A. Caan, C. Majoie, T. W. Kuijpers, P. Reiss, F. Wit and D. Pajkrt (2017). "Higher subcortical and white matter cerebral blood flow in perinatally HIV-infected children." Medicine (Baltimore) **96**(7): e5891.

Blomqvist, M., H. Zetterberg, K. Blennow and J. E. Mansson (2021). "Sulfatide in health and disease. The evaluation of sulfatide in cerebrospinal fluid as a possible biomarker for neurodegeneration." Mol Cell Neurosci **116**: 103670.

Boerwinkle, A. and B. M. Ances (2019). "Molecular Imaging of Neuroinflammation in HIV." J Neuroimmune Pharmacol **14**(1): 9-15.

Boggs, J. M. (2006). "Myelin basic protein: a multifunctional protein." Cell Mol Life Sci **63**(17): 1945-1961.

Boggs, J. M., G. Rangaraj, Y. M. Heng, Y. Liu and G. Harauz (2011). "Myelin basic protein binds microtubules to a membrane surface and to actin filaments in vitro: effect of phosphorylation and deimination." Biochim Biophys Acta **1808**(3): 761-773.

Borjabad, A., S. Morgello, W. Chao, S. Y. Kim, A. I. Brooks, J. Murray, M. J. Potash and D. J. Volsky (2011). "Significant effects of antiretroviral therapy on global gene expression in brain tissues of patients with HIV-1-associated neurocognitive disorders." PLoS Pathog **7**(9): e1002213.

Borjabad, A. and D. J. Volsky (2012). "Common transcriptional signatures in brain tissue from patients with HIV-associated neurocognitive disorders, Alzheimer's disease, and Multiple Sclerosis." J Neuroimmune Pharmacol **7**(4): 914-926.

Boros, J., N. Arnoult, V. Stroobant, J. F. Collet and A. Decottignies (2014). "Polycomb repressive complex 2 and H3K27me3 cooperate with H3K9 methylation to maintain heterochromatin protein 1alpha at chromatin." Mol Cell Biol **34**(19): 3662-3674.

Borroni, M. V., A. S. Valles and F. J. Barrantes (2016). "The lipid habitats of neurotransmitter receptors in brain." Biochim Biophys Acta **1858**(11): 2662-2670.

Bourne, K. Z., C. Natarajan, C. X. M. Perez, B. Tumurbaatar, G. Taglialatela and B. Krishnan (2019). "Suppressing aberrant phospholipase D1 signaling in 3xTg Alzheimer's disease mouse model promotes synaptic resilience." Sci Rep **9**(1): 18342.

Bowerman, B., P. O. Brown, J. M. Bishop and H. E. Varmus (1989). "A nucleoprotein complex mediates the integration of retroviral DNA." Genes Dev **3**(4): 469-478.

Bowman, A. P., J. F. J. Bogie, J. J. A. Hendriks, M. Haidar, M. Belov, R. M. A. Heeren and S. R. Ellis (2020). "Evaluation of lipid coverage and high spatial resolution MALDI-imaging capabilities of oversampling combined with laser post-ionisation." Anal Bioanal Chem **412**(10): 2277-2289.

Bozzi, G., F. R. Simonetti, S. A. Watters, E. M. Anderson, M. Gouzoulis, M. F. Kearney, P. Rote, C. Lange, W. Shao, R. Gorelick, B. Fullmer, S. Kumar, S. Wank, S. Hewitt, D. E. Kleiner, J. Hattori, M. J. Bale, S. Hill, J. Bell, C. Rehm, Z. Grossman, R. Yarchoan, T. Uldrick and F. Maldarelli (2019). "No evidence of ongoing HIV replication or compartmentalization in tissues during combination antiretroviral therapy: Implications for HIV eradication." Sci Adv **5**(9): eaav2045.

Bracq, L., M. Xie, S. Benichou and J. Bouchet (2018). "Mechanisms for Cell-to-Cell Transmission of HIV-1." Front Immunol **9**: 260.

Bratton, D. L. and P. M. Henson (2008). "Apoptotic cell recognition: will the real phosphatidylserine receptor(s) please stand up?" Curr Biol **18**(2): R76-79.

Brier, M. R., Q. Wu, A. B. Tanenbaum, E. T. Westerhaus, E. D. Kharasch and B. M. Ances (2015). "Effect of HAART on Brain Organization and Function in HIV-Negative Subjects." J Neuroimmune Pharmacol **10**(4): 517-521.

Bruce, K. D., A. Zsombok and R. H. Eckel (2017). "Lipid Processing in the Brain: A Key Regulator of Systemic Metabolism." Front Endocrinol (Lausanne) **8**: 60.

Bruner, K. M., N. N. Hosmane and R. F. Siliciano (2015). "Towards an HIV-1 cure: measuring the latent reservoir." Trends Microbiol **23**(4): 192-203.

Bruner, K. M., A. J. Murray, R. A. Pollack, M. G. Soliman, S. B. Laskey, A. A. Capoferri, J. Lai, M. C. Strain, S. M. Lada, R. Hoh, Y. C. Ho, D. D. Richman, S. G. Deeks, J. D. Siliciano and R. F. Siliciano (2016). "Defective proviruses rapidly accumulate during acute HIV-1 infection." Nat Med **22**(9): 1043-1049.

Bruner, K. M., Z. Wang, F. R. Simonetti, A. M. Bender, K. J. Kwon, S. Sengupta, E. J. Fray, S. A. Beg, A. A. R. Antar, K. M. Jenike, L. N. Bertagnolli, A. A. Capoferri, J. T. Kufera, A. Timmons, C. Nobles, J. Gregg, N. Wada, Y. C. Ho, H. Zhang, J. B. Margolick, J. N. Blankson, S. G. Deeks, F. D. Bushman, J. D. Siliciano, G. M. Laird and R. F. Siliciano (2019). "A quantitative approach for measuring the reservoir of latent HIV-1 proviruses." Nature **566**(7742): 120-125.

Buchberger, A. R., K. DeLaney, J. Johnson and L. Li (2018). "Mass Spectrometry Imaging: A Review of Emerging Advancements and Future Insights." Anal Chem **90**(1): 240-265.

Budin, I., T. de Rond, Y. Chen, L. J. G. Chan, C. J. Petzold and J. D. Keasling (2018). "Viscous control of cellular respiration by membrane lipid composition." Science **362**(6419): 1186-1189.

Burdo, T. H., M. R. Lentz, P. Autissier, A. Krishnan, E. Halpern, S. Letendre, E. S. Rosenberg, R. J. Ellis and K. C. Williams (2011). "Soluble CD163 made by monocyte/macrophages is a novel marker of HIV activity in early and chronic infection prior to and after anti-retroviral therapy." J Infect Dis **204**(1): 154-163.

Burdo, T. H., A. Weiffenbach, S. P. Woods, S. Letendre, R. J. Ellis and K. C. Williams (2013). "Elevated sCD163 in plasma but not cerebrospinal fluid is a marker of neurocognitive impairment in HIV infection." AIDS **27**(9): 1387-1395.

Burlacu, R., A. Umlauf, T. D. Marcotte, B. Soontornniyomkij, C. C. Diaconu, A. Bulacu-Talnariu, A. Temereanca, S. M. Ruta, S. Letendre, L. Ene and C. L. Achim (2020). "Plasma CXCL10 correlates with HAND in HIV-infected women." J Neurovirol **26**(1): 23-31.

Bush, S. and D. M. Tebit (2015). "HIV-1 Group O Origin, Evolution, Pathogenesis, and Treatment: Unraveling the Complexity of an Outlier 25 Years Later." AIDS Rev **17**(3): 147-158.

Butkevich, E., S. Hulsmann, D. Wenzel, T. Shirao, R. Duden and I. Majoul (2004). "Drebrin is a novel connexin-43 binding partner that links gap junctions to the submembrane cytoskeleton." Curr Biol **14**(8): 650-658.

Byrd, D. A., R. P. Fellows, S. Morgello, D. Franklin, R. K. Heaton, R. Deutsch, J. H. Atkinson, D. B. Clifford, A. C. Collier, C. M. Marra, B. Gelman, J. A. McCutchan, N. A. Duarte, D. M. Simpson, J. McArthur, I. Grant and C. Group (2011). "Neurocognitive impact of substance use in HIV infection." J Acquir Immune Defic Syndr **58**(2): 154-162.

Campbell, E. M. and T. J. Hope (2015). "HIV-1 capsid: the multifaceted key player in HIV-1 infection." Nat Rev Microbiol **13**(8): 471-483.

Cantres-Rosario, Y., M. Plaud-Valentin, Y. Gerena, R. L. Skolasky, V. Wojna and L. M. Melendez (2013). "Cathepsin B and cystatin B in HIV-seropositive women are associated with infection and HIV-1-associated neurocognitive disorders." AIDS **27**(3): 347-356.

Capilla-Gonzalez, V., A. Cebrian-Silla, H. Guerrero-Cazares, J. M. Garcia-Verdugo and A. Quinones-Hinojosa (2014). "Age-related changes in astrocytic and ependymal cells of the subventricular zone." Glia **62**(5): 790-803.

Cary, D. C., K. Fujinaga and B. M. Peterlin (2016). "Molecular mechanisms of HIV latency." J Clin Invest **126**(2): 448-454.

Cassol, E., V. Misra, S. Morgello and D. Gabuzda (2013). "Applications and limitations of inflammatory biomarkers for studies on neurocognitive impairment in HIV infection." J Neuroimmune Pharmacol **8**(5): 1087-1097.

Castellano, P. and E. A. Eugenin (2014). "Regulation of gap junction channels by infectious agents and inflammation in the CNS." Front Cell Neurosci **8**: 122.

Castellano, P., L. Prevedel and E. A. Eugenin (2017). "HIV-infected macrophages and microglia that survive acute infection become viral reservoirs by a mechanism involving Bim." Sci Rep **7**(1): 12866.

Castellano, P., L. Prevedel and E. A. Eugenin (2017). "HIV-infected macrophages and microglia that survive acute infection become viral reservoirs by a mechanism involving Bim." Scientific reports **7**(1): 12866.

Castellano, P., L. Prevedel, S. Valdebenito and E. A. Eugenin (2019). "HIV infection and latency induce a unique metabolic signature in human macrophages." Sci Rep **9**(1): 3941.
Castro, B. M., M. Prieto and L. C. Silva (2014). "Ceramide: a simple sphingolipid with unique biophysical properties." Prog Lipid Res **54**: 53-67.

Centlivre, M., N. Legrand, S. Klamer, Y. P. Liu, K. Jasmijn von Eije, M. Bohne, E. S. Rijnstra, K. Weijer, B. Blom, C. Voermans, H. Spits and B. Berkhout (2013). "Preclinical in vivo evaluation of the safety of a multi-shRNA-based gene therapy against HIV-1." Mol Ther Nucleic Acids **2**: e120.

Chaganti, J. and B. J. Brew (2021). "MR spectroscopy in HIV associated neurocognitive disorder in the era of cART: a review." AIDS Res Ther **18**(1): 65.

Chaganti, J. R., A. Heinecke, T. M. Gates, K. J. Moffat and B. J. Brew (2017). "Functional Connectivity in Virally Suppressed Patients with HIV-Associated Neurocognitive Disorder: A Resting-State Analysis." AJNR Am J Neuroradiol **38**(8): 1623-1629.

Chaillon, A., S. Gianella, S. Dellicour, S. A. Rawlings, T. E. Schlub, M. F. De Oliveira, C. Ignacio, M. Porrachia, B. Vrancken and D. M. Smith (2020). "HIV persists throughout deep tissues with repopulation from multiple anatomical sources." J Clin Invest **130**(4): 1699-1712.

Chan, J. K. and W. C. Greene (2011). "NF-kappaB/Rel: agonist and antagonist roles in HIV-1 latency." Curr Opin HIV AIDS **6**(1): 12-18.

Chang, L. and D. K. Shukla (2018). "Imaging studies of the HIV-infected brain." Handb Clin Neurol **152**: 229-264.

Chang, L., G. J. Wang, N. D. Volkow, T. Ernst, F. Telang, J. Logan and J. S. Fowler (2008). "Decreased brain dopamine transporters are related to cognitive deficits in HIV patients with or without cocaine abuse." Neuroimage **42**(2): 869-878.

Chauhan, A. (2015). "Enigma of HIV-1 latent infection in astrocytes: an in-vitro study using protein kinase C agonist as a latency reversing agent." Microbes Infect **17**(9): 651-659.

Chauvin, M. and D. Sauce (2022). "Mechanisms of immune aging in HIV." Clin Sci (Lond) **136**(1): 61-80.

Checkley, M. A., B. G. Luttge and E. O. Freed (2011). "HIV-1 envelope glycoprotein biosynthesis, trafficking, and incorporation." J Mol Biol **410**(4): 582-608.

Chen, Y., D. Hu, L. Zhao, W. Tang and B. Li (2022). "Unraveling metabolic alterations in transgenic mouse model of Alzheimer's disease using MALDI MS imaging with 4-aminocinnoline-3-carboxamide matrix." Anal Chim Acta **1192**: 339337.

Cheney, L., H. Guzik, F. P. Macaluso, F. Macian, A. M. Cuervo and J. W. Berman (2020). "HIV Nef and Antiretroviral Therapy Have an Inhibitory Effect on Autophagy in Human Astrocytes that May Contribute to HIV-Associated Neurocognitive Disorders." Cells **9**(6).

Cheng, H., J. Xu, D. W. McKeel, Jr. and X. Han (2003). "Specificity and potential mechanism of sulfatide deficiency in Alzheimer's disease: an electrospray ionization mass spectrometric study." Cell Mol Biol (Noisy-le-grand) **49**(5): 809-818.

Chiang, K., T. L. Sung and A. P. Rice (2012). "Regulation of cyclin T1 and HIV-1 Replication by microRNAs in resting CD4+ T lymphocytes." J Virol **86**(6): 3244-3252.

Chompre, G., E. Cruz, L. Maldonado, V. Rivera-Amill, J. T. Porter and R. J. Noel, Jr. (2013). "Astrocytic expression of HIV-1 Nef impairs spatial and recognition memory." Neurobiology of disease **49**: 128-136.

Chrast, R., G. Saher, K. A. Nave and M. H. Verheijen (2011). "Lipid metabolism in myelinating glial cells: lessons from human inherited disorders and mouse models." J Lipid Res **52**(3): 419-434.

Chughtai, K. and R. M. Heeren (2010). "Mass spectrometric imaging for biomedical tissue analysis." Chem Rev **110**(5): 3237-3277.

Churchill, M. J., S. G. Deeks, D. M. Margolis, R. F. Siliciano and R. Swanstrom (2016). "HIV reservoirs: what, where and how to target them." Nat Rev Microbiol **14**(1): 55-60.

Churchill, M. J., S. L. Wesselingh, D. Cowley, C. A. Pardo, J. C. McArthur, B. J. Brew and P. R. Gorry (2009). "Extensive astrocyte infection is prominent in human immunodeficiency virus-associated dementia." Ann Neurol **66**(2): 253-258.

Clark, E., B. Nava and M. Caputi (2017). "Tat is a multifunctional viral protein that modulates cellular gene expression and functions." Oncotarget **8**(16): 27569-27581.

Claypool, S. M. (2009). "Cardiolipin, a critical determinant of mitochondrial carrier protein assembly and function." Biochim Biophys Acta **1788**(10): 2059-2068.

Clayton, K. L., J. V. Garcia, J. E. Clements and B. D. Walker (2017). "HIV Infection of Macrophages: Implications for Pathogenesis and Cure." Pathog Immun **2**(2): 179-192.

Clifford, D. B. and B. M. Ances (2013). "HIV-associated neurocognitive disorder." Lancet Infect Dis **13**(11): 976-986.

Coffin, J. and R. Swanstrom (2013). "HIV pathogenesis: dynamics and genetics of viral populations and infected cells." Cold Spring Harb Perspect Med **3**(1): a012526.

Cohen, M. S., G. M. Shaw, A. J. McMichael and B. F. Haynes (2011). "Acute HIV-1 Infection." N Engl J Med **364**(20): 1943-1954.

Cohn, L. B., N. Chomont and S. G. Deeks (2020). "The Biology of the HIV-1 Latent Reservoir and Implications for Cure Strategies." Cell Host Microbe **27**(4): 519-530.

Cole, J. H., M. W. A. Caan, J. Underwood, D. De Francesco, R. A. van Zoest, F. Wit, H. Mutsaerts, R. Leech, G. J. Geurtsen, P. Portegies, C. Majoie, M. F. Schim van der Loeff, C. A. Sabin, P. Reiss, A. Winston, D. J. Sharp and A. C. Comorbidity in Relations to (2018). "No Evidence for Accelerated Aging-Related Brain Pathology in Treated Human Immunodeficiency Virus: Longitudinal Neuroimaging Results From the Comorbidity in Relation to AIDS (COBRA) Project." Clin Infect Dis **66**(12): 1899-1909.

Cole, N. B., D. D. Murphy, T. Grider, S. Rueter, D. Brasaemle and R. L. Nussbaum (2002). "Lipid droplet binding and oligomerization properties of the Parkinson's disease protein alpha-synuclein." J Biol Chem **277**(8): 6344-6352.

Connolly, C. G., A. Bischoff-Grethe, S. J. Jordan, S. P. Woods, R. J. Ellis, M. P. Paulus, I. Grant and A. R. C. G. Translational Methamphetamine (2014). "Altered functional response to risky choice in HIV infection." PLoS One **9**(10): e111583.

Cook, D. G., J. Fantini, S. L. Spitalnik and F. Gonzalez-Scarano (1994). "Binding of human immunodeficiency virus type I (HIV-1) gp120 to galactosylceramide (GalCer): relationship to the V3 loop." Virology **201**(2): 206-214.

Cooley, S. A., R. H. Paul, J. F. Strain, A. Boerwinkle, C. Kilgore and B. M. Ances (2021). "Effects of anticholinergic medication use on brain integrity in persons living with HIV and persons without HIV." AIDS **35**(3): 381-391.

Cornell-Bell, A. H., S. M. Finkbeiner, M. S. Cooper and S. J. Smith (1990). "Glutamate induces calcium waves in cultured astrocytes: long-range glial signaling." Science **247**(4941): 470-473.

Correa, D. G., N. Zimmermann, T. M. Doring, N. V. Wilner, S. C. Leite, R. F. Cabral, R. P. Fonseca, P. R. Bahia and E. L. Gasparetto (2015). "Diffusion tensor MR imaging of white matter integrity in HIV-positive patients with planning deficit." Neuroradiology **57**(5): 475-482.

Cosenza, M. A., M. L. Zhao, Q. Si and S. C. Lee (2002). "Human brain parenchymal microglia express CD14 and CD45 and are productively infected by HIV-1 in HIV-1 encephalitis." Brain Pathol **12**(4): 442-455.

Cotrina, M. L., J. H. Lin, J. C. Lopez-Garcia, C. C. Naus and M. Nedergaard (2000). "ATP-mediated glia signaling." J Neurosci **20**(8): 2835-2844.

Cotrina, M. L., J. H. Lin and M. Nedergaard (1998). "Cytoskeletal assembly and ATP release regulate astrocytic calcium signaling." J Neurosci **18**(21): 8794-8804.

Couttas, T. A., N. Kain, B. Daniels, X. Y. Lim, C. Shepherd, J. Kril, R. Pickford, H. Li, B. Garner and A. S. Don (2014). "Loss of the neuroprotective factor Sphingosine 1-phosphate early in Alzheimer's disease pathogenesis." Acta Neuropathol Commun **2**: 9.

Craigie, R. and F. D. Bushman (2012). "HIV DNA integration." Cold Spring Harb Perspect Med **2**(7): a006890.

Cribbs, S. K., K. Crothers and A. Morris (2019). "Pathogenesis of HIV-related lung disease: Immunity, infection, and inflammation." Physiol Rev.

Czepiel, J., J. Gdula-Argasinska, G. Biesiada, B. Bystrowska, A. Jurczyszyn, W. Perucki, K. Sroczynska, A. Zajac, T. Librowski and A. Garlicki (2019). "Fatty acids and selected endocannabinoids content in cerebrospinal fluids from patients with neuroinfections." Metab Brain Dis **34**(1): 331-339.

D'Amico, D., S. Valdebenito and E. A. Eugenin (2021). "The role of Pannexin-1 channels and extracellular ATP in the pathogenesis of the human immunodeficiency virus." Purinergic Signal **17**(4): 563-576.

D'Aversa, T. G., E. A. Eugenin, L. Lopez and J. W. Berman (2013). "Myelin basic protein induces inflammatory mediators from primary human endothelial cells and blood-brain barrier disruption: implications for the pathogenesis of multiple sclerosis." Neuropathol Appl Neurobiol **39**(3): 270-283.

Dahabieh, M. S., E. Battivelli and E. Verdin (2015). "Understanding HIV latency: the road to an HIV cure." Annu Rev Med **66**: 407-421.

Darios, F., F. Mochel and G. Stevanin (2020). "Lipids in the Physiopathology of Hereditary Spastic Paraplegias." Front Neurosci **14**: 74.

Dasgupta, S. and V. Kumar (2016). "Type II NKT cells: a distinct CD1d-restricted immune regulatory NKT cell subset." Immunogenetics **68**(8): 665-676.

Datta, P. K., S. Deshmane, K. Khalili, S. Merali, J. C. Gordon, C. Fecchio and C. A. Barrero (2016). "Glutamate metabolism in HIV-1 infected macrophages: Role of HIV-1 Vpr." Cell cycle **15**(17): 2288-2298.

Dayton, A. I. (2004). "Within you, without you: HIV-1 Rev and RNA export." Retrovirology **1**: 35.

De-Scheerder, M. A., B. Depelseneer, L. Vandekerckhove and W. Trypsteen (2020). "Evolution of Experimental Design and Research Techniques in HIV-1 Reservoir Studies: A Systematic Review." AIDS Rev **22**(1): 16-24.

de Almeida, S. M., C. E. Ribeiro, I. Rotta, M. Piovesan, B. Tang, F. Vaida, S. M. Raboni, S. Letendre, M. Potter, M. S. Batistela Fernandes, R. J. Ellis and H. I. V. N. R. C. Group (2018). "Biomarkers of neuronal injury and amyloid metabolism in the cerebrospinal fluid of patients infected with HIV-1 subtypes B and C." J Neurovirol **24**(1): 28-40.

de Almeida, S. M., I. Rotta, Y. Jiang, X. Li, S. M. Raboni, C. E. Ribeiro, D. Smith, M. Potter, F. Vaida, S. Letendre, R. J. Ellis and H. Group (2016). "Biomarkers of chemotaxis and inflammation in cerebrospinal fluid and serum in individuals with HIV-1 subtype C versus B." J Neurovirol **22**(6): 715-724.

de Almeida, S. M., I. Rotta, C. E. Ribeiro, M. F. Oliveira, A. Chaillon, A. P. de Pereira, A. P. Cunha, M. Zonta, J. F. Bents, S. M. Raboni, D. Smith, S. Letendre and R. J. Ellis (2017). "Dynamic of CSF and serum biomarkers in HIV-1 subtype C encephalitis with CNS genetic compartmentalization-case study." J Neurovirol **23**(3): 460-473.

De Bock, M., E. Decrock, N. Wang, M. Bol, M. Vinken, G. Bultynck and L. Leybaert (2014). "The dual face of connexin-based astroglial Ca(2+) communication: a key player in brain physiology and a prime target in pathology." Biochim Biophys Acta **1843**(10): 2211-2232.

De Scheerder, M. A., B. Vrancken, S. Dellicour, T. Schlub, E. Lee, W. Shao, S. Rutsaert, C. Verhofstede, T. Kerre, T. Malfait, D. Hemelsoet, M. Coppens, A. Dhondt, D. De Looze, F. Vermassen, P. Lemey, S. Palmer and L. Vandekerckhove (2019). "HIV Rebound Is Predominantly Fueled by Genetically Identical Viral Expansions from Diverse Reservoirs." Cell Host Microbe **26**(3): 347-358 e347.

Deere, J. D., R. C. Kauffman, E. Cannavo, J. Higgins, A. Villalobos, L. Adamson, R. F. Schinazi, P. A. Luciw and T. W. North (2014). "Analysis of multiply spliced transcripts in lymphoid tissue reservoirs of rhesus macaques infected with RT-SHIV during HAART." PLoS One **9**(2): e87914.

Dennison, J. L., N. R. Ricciardi, I. Lohse, C. H. Volmar and C. Wahlestedt (2021). "Sexual Dimorphism in the 3xTg-AD Mouse Model and Its Impact on Pre-Clinical Research." J Alzheimers Dis **80**(1): 41-52.

Denton, P. W., O. S. Sogaard and M. Tolstrup (2019). "Impacts of HIV Cure Interventions on Viral Reservoirs in Tissues." Front Microbiol **10**: 1956.

Di Cio, F., S. Minosse, E. Picchi, F. Di Giuliano, L. Sarmati, E. Teti, M. Andreoni, R. Floris, M. Guerrisi, F. Garaci and N. Toschi (2021). "Whole-brain white matter network reorganization in HIV." Annu Int Conf IEEE Eng Med Biol Soc **2021**: 3830-3833.

Di Paolo, G. and P. De Camilli (2006). "Phosphoinositides in cell regulation and membrane dynamics." Nature **443**(7112): 651-657.

Do, T., G. Murphy, L. A. Earl, G. Q. Del Prete, G. Grandinetti, G. H. Li, J. D. Estes, P. Rao, C. M. Trubey, J. Thomas, J. Spector, D. Bliss, A. Nath, J. D. Lifson and S. Subramaniam (2014). "Three-dimensional imaging of HIV-1 virological synapses reveals membrane architectures involved in virus transmission." J Virol **88**(18): 10327-10339.

Doetsch, F., I. Caille, D. A. Lim, J. M. Garcia-Verdugo and A. Alvarez-Buylla (1999). "Subventricular zone astrocytes are neural stem cells in the adult mammalian brain." Cell **97**(6): 703-716.

Doetsch, F., J. M. Garcia-Verdugo and A. Alvarez-Buylla (1999). "Regeneration of a germinal layer in the adult mammalian brain." Proc Natl Acad Sci U S A **96**(20): 11619-11624.

Doitsh, G., N. L. Galloway, X. Geng, Z. Yang, K. M. Monroe, O. Zepeda, P. W. Hunt, H. Hatano, S. Sowinski, I. Munoz-Arias and W. C. Greene (2014). "Cell death by pyroptosis drives CD4 T-cell depletion in HIV-1 infection." Nature **505**(7484): 509-514.

Dos Santos, D. C. M., K. L. Lovero, C. M. Schmidt, A. Barros, A. P. Quintanilha, A. P. Barbosa, M. V. S. Pone, S. M. Pone, J. M. Araujo, C. de Paula Martins, E. M. Cosme, T. R. Dourado de Oliveira, A. L. Miceli, M. L. Vieira, A. Queiroz, L. G. Coca Velarde, A. Kritski, M. de Fatima Pombo March, S. Maria de Azevedo Sias, A. C. C. Sant, L. W. Riley and C. A. Araujo Cardoso (2020). "Serological biomarkers for monitoring response to treatment of pulmonary and extrapulmonary tuberculosis in children and adolescents." Tuberculosis (Edinb) **123**: 101960.

Dowhan, W., H. Vitrac and M. Bogdanov (2019). "Lipid-Assisted Membrane Protein Folding and Topogenesis." Protein J **38**(3): 274-288.

Drechsler, H., C. Ayers, J. Cutrell, R. Arasaratnam and R. Bedimo (2021). "Consistent use of lipid lowering therapy in HIV infection is associated with low mortality." BMC Infect Dis **21**(1): 150.

Dries, R., J. Chen, N. Del Rossi, M. M. Khan, A. Sistig and G. C. Yuan (2021). "Advances in spatial transcriptomic data analysis." Genome Res **31**(10): 1706-1718.

Du Pasquier, R. A., S. Jilek, M. Kalubi, S. Yerly, C. A. Fux, C. Gutmann, A. Cusini, H. F. Gunthard, M. Cavassini, P. L. Vernazza and H. I. V. C. S. Swiss (2013). "Marked increase of the astrocytic marker S100B in the cerebrospinal fluid of HIV-infected patients on LPV/r-monotherapy." AIDS **27**(2): 203-210.

Du, Y., Z. Mi, Y. Xie, D. Lu, H. Zheng, H. Sun, M. Zhang and Y. Niu (2021). "Insights into the molecular basis of tick-borne encephalitis from multiplatform metabolomics." PLoS Negl Trop Dis **15**(3): e0009172.

Dufourc, E. J. (2008). "Sterols and membrane dynamics." J Chem Biol **1**(1-4): 63-77.

Dufresne, M., J. F. Masson and P. Chaurand (2016). "Sodium-Doped Gold-Assisted Laser Desorption Ionization for Enhanced Imaging Mass Spectrometry of Triacylglycerols from Thin Tissue Sections." Anal Chem **88**(11): 6018-6025.

Dukic, A. R., P. Gerbaud, J. Guibourdenche, B. Thiede, K. Tasken and G. Pidoux (2018). "Ezrin-anchored PKA phosphorylates serine 369 and 373 on connexin 43 to enhance gap junction assembly, communication, and cell fusion." Biochem J **475**(2): 455-476.

Duncan, I. D. and A. B. Radcliff (2016). "Inherited and acquired disorders of myelin: The underlying myelin pathology." Exp Neurol **283**(Pt B): 452-475.

Dunn, K. W., M. M. Kamocka and J. H. McDonald (2011). "A practical guide to evaluating colocalization in biological microscopy." Am J Physiol Cell Physiol **300**(4): C723-742.

Dupree, J. L. and A. D. Pomicter (2010). "Myelin, DIGs, and membrane rafts in the central nervous system." Prostaglandins Other Lipid Mediat **91**(3-4): 118-129.
Eckhardt, M. (2008). "The role and metabolism of sulfatide in the nervous system." Mol Neurobiol **37**(2-3): 93-103.

Eggers, C., G. Arendt, K. Hahn, I. W. Husstedt, M. Maschke, E. Neuen-Jacob, M. Obermann, T. Rosenkranz, E. Schielke, E. Straube and A. u. N.-I. German Association of Neuro (2017). "HIV-1-associated neurocognitive disorder: epidemiology, pathogenesis, diagnosis, and treatment." J Neurol **264**(8): 1715-1727.

Elliott, J. H., F. Wightman, A. Solomon, K. Ghneim, J. Ahlers, M. J. Cameron, M. Z. Smith, T. Spelman, J. McMahon, P. Velayudham, G. Brown, J. Roney, J. Watson, M. H. Prince, J. F. Hoy, N. Chomont, R. Fromentin, F. A. Procopio, J. Zeidan, S. Palmer, L. Odevall, R. W. Johnstone, B. P. Martin, E. Sinclair, S. G. Deeks, D. J. Hazuda, P. U. Cameron, R. P. Sekaly and S. R. Lewin (2014). "Activation of HIV transcription with short-course vorinostat in HIV-infected patients on suppressive antiretroviral therapy." PLoS Pathog **10**(10): e1004473.

Ellis, R., D. Langford and E. Masliah (2007). "HIV and antiretroviral therapy in the brain: neuronal injury and repair." Nat Rev Neurosci **8**(1): 33-44.

Engelman, A., K. Mizuuchi and R. Craigie (1991). "HIV-1 DNA integration: mechanism of viral DNA cleavage and DNA strand transfer." Cell **67**(6): 1211-1221.

Eriksson, S., E. H. Graf, V. Dahl, M. C. Strain, S. A. Yukl, E. S. Lysenko, R. J. Bosch, J. Lai, S. Chioma, F. Emad, M. Abdel-Mohsen, R. Hoh, F. Hecht, P. Hunt, M. Somsouk, J. Wong, R. Johnston, R. F. Siliciano, D. D. Richman, U. O'Doherty, S. Palmer, S. G. Deeks and J. D. Siliciano (2013). "Comparative analysis of measures of viral reservoirs in HIV-1 eradication studies." PLoS Pathog **9**(2): e1003174.

Erten-Lyons, D., R. Woltjer, J. Kaye, N. Mattek, H. H. Dodge, S. Green, H. Tran, D. B. Howieson, K. Wild and L. C. Silbert (2013). "Neuropathologic basis of white matter hyperintensity accumulation with advanced age." Neurology **81**(11): 977-983.

Escota, G. V., J. A. O'Halloran, W. G. Powderly and R. M. Presti (2018). "Understanding mechanisms to promote successful aging in persons living with HIV." Int J Infect Dis **66**: 56-64.

Esteve, C., E. A. Jones, D. B. Kell, H. Boutin and L. A. McDonnell (2017). "Mass spectrometry imaging shows major derangements in neurogranin and in purine metabolism in the triple-knockout 3xTg Alzheimer mouse model." Biochim Biophys Acta Proteins Proteom **1865**(7): 747-754.

Eugenin, E. A. (2014). "Role of connexin/pannexin containing channels in infectious diseases." FEBS letters **588**(8): 1389-1395.

Eugenin, E. A. (2014). "Role of connexin/pannexin containing channels in infectious diseases." FEBS Lett **588**(8): 1389-1395.

Eugenin, E. A. (2019). "Role of cell-to-cell communication in cancer: New features, insights, and directions." Cancer Rep (Hoboken) **2**(6): e1228.

Eugenin, E. A., D. Basilio, J. C. Saez, J. A. Orellana, C. S. Raine, F. Bukauskas, M. V. Bennett and J. W. Berman (2012). "The role of gap junction channels during physiologic and pathologic conditions of the human central nervous system." J Neuroimmune Pharmacol **7**(3): 499-518.

Eugenin, E. A., D. Basilio, J. C. Saez, J. A. Orellana, C. S. Raine, F. Bukauskas, M. V. Bennett and J. W. Berman (2012). "The role of gap junction channels during physiologic and pathologic conditions of the human central nervous system." Journal of neuroimmune pharmacology : the official journal of the Society on NeuroImmune Pharmacology **7**(3): 499-518.

Eugenin, E. A. and J. W. Berman (2007). "Gap junctions mediate human immunodeficiency virus-bystander killing in astrocytes." J Neurosci **27**(47): 12844-12850.

Eugenin, E. A. and J. W. Berman (2013). "Cytochrome C dysregulation induced by HIV infection of astrocytes results in bystander apoptosis of uninfected astrocytes by an IP3 and calcium-dependent mechanism." J Neurochem **127**(5): 644-651.

Eugenin, E. A. and J. W. Berman (2013). "Cytochrome C dysregulation induced by HIV infection of astrocytes results in bystander apoptosis of uninfected astrocytes by an IP3 and calcium-dependent mechanism." Journal of neurochemistry **127**(5): 644-651.

Eugenin, E. A., J. E. Clements, M. C. Zink and J. W. Berman (2011). "Human immunodeficiency virus infection of human astrocytes disrupts blood-brain barrier integrity by a gap junction-dependent mechanism." J Neurosci **31**(26): 9456-9465.

Eugenin, E. A., J. E. Clements, M. C. Zink and J. W. Berman (2011). "Human immunodeficiency virus infection of human astrocytes disrupts blood-brain barrier integrity by a gap junction-dependent mechanism." The Journal of neuroscience : the official journal of the Society for Neuroscience **31**(26): 9456-9465.

Eugenin, E. A., T. G. D'Aversa, L. Lopez, T. M. Calderon and J. W. Berman (2003). "MCP-1 (CCL2) protects human neurons and astrocytes from NMDA or HIV-tat-induced apoptosis." Journal of neurochemistry **85**(5): 1299-1311.

Eugenin, E. A., P. J. Gaskill and J. W. Berman (2009). "Tunneling nanotubes (TNT): A potential mechanism for intercellular HIV trafficking." Commun Integr Biol **2**(3): 243-244.

Eugenin, E. A., H. Gonzalez, C. G. Saez and J. C. Saez (1998). "Gap junctional communication coordinates vasopressin-induced glycogenolysis in rat hepatocytes." Am J Physiol **274**(6): G1109-1116.

Eugenin, E. A., J. E. King, A. Nath, T. M. Calderon, R. S. Zukin, M. V. Bennett and J. W. Berman (2007). "HIV-tat induces formation of an LRP-PSD-95- NMDAR-nNOS complex that promotes apoptosis in neurons and astrocytes." Proc Natl Acad Sci U S A **104**(9): 3438-3443.

Eugenin, E. A., K. Osiecki, L. Lopez, H. Goldstein, T. M. Calderon and J. W. Berman (2006). "CCL2/monocyte chemoattractant protein-1 mediates enhanced transmigration of human immunodeficiency virus (HIV)-infected leukocytes across the blood-brain barrier: a potential mechanism of HIV-CNS invasion and NeuroAIDS." J Neurosci **26**(4): 1098-1106.

Evans, D. T. and G. Silvestri (2013). "Nonhuman primate models in AIDS research." Current opinion in HIV and AIDS **8**(4): 255-261.

Fabelo, N., V. Martin, G. Santpere, R. Marin, L. Torrent, I. Ferrer and M. Diaz (2011). "Severe alterations in lipid composition of frontal cortex lipid rafts from Parkinson's disease and incidental Parkinson's disease." Mol Med **17**(9-10): 1107-1118.

Fadeel, B. and D. Xue (2009). "The ins and outs of phospholipid asymmetry in the plasma membrane: roles in health and disease." Crit Rev Biochem Mol Biol **44**(5): 264-277.

Fahy, E., D. Cotter, M. Sud and S. Subramaniam (2011). "Lipid classification, structures and tools." Biochim Biophys Acta **1811**(11): 637-647.

Fahy, E., S. Subramaniam, H. A. Brown, C. K. Glass, A. H. Merrill, Jr., R. C. Murphy, C. R. Raetz, D. W. Russell, Y. Seyama, W. Shaw, T. Shimizu, F. Spener, G. van Meer, M. S. VanNieuwenhze, S. H. White, J. L. Witztum and E. A. Dennis (2005). "A comprehensive classification system for lipids." J Lipid Res **46**(5): 839-861.

Falcinelli, S. D., C. Ceriani, D. M. Margolis and N. M. Archin (2019). "New Frontiers in Measuring and Characterizing the HIV Reservoir." Front Microbiol **10**: 2878.

Farhadian, S., P. Patel and S. Spudich (2017). "Neurological Complications of HIV Infection." Curr Infect Dis Rep **19**(12): 50.

Farmer, B. C., A. E. Walsh, J. C. Kluemper and L. A. Johnson (2020). "Lipid Droplets in Neurodegenerative Disorders." Front Neurosci **14**: 742.

Farooqui, A. A., L. A. Horrocks and T. Farooqui (2007). "Modulation of inflammation in brain: a matter of fat." J Neurochem **101**(3): 577-599.

Fauci, A. S. and R. C. Desrosiers (1997). Pathogenesis of HIV and SIV. Retroviruses. J. M. Coffin, S. H. Hughes and H. E. Varmus. Cold Spring Harbor (NY).

Fields, J., W. Dumaop, S. Eleuteri, S. Campos, E. Serger, M. Trejo, K. Kosberg, A. Adame, B. Spencer, E. Rockenstein, J. J. He and E. Masliah (2015). "HIV-1 Tat alters neuronal autophagy by modulating autophagosome fusion to the lysosome: implications for HIV-associated neurocognitive disorders." The Journal of neuroscience : the official journal of the Society for Neuroscience **35**(5): 1921-1938.

Fincher, J. A., A. R. Korte, J. E. Dyer, S. Yadavilli, N. J. Morris, D. R. Jones, V. K. Shanmugam, R. K. Pirlo and A. Vertes (2020). "Mass spectrometry imaging of triglycerides in biological tissues by laser desorption ionization from silicon nanopost arrays." J Mass Spectrom **55**(4): e4443.

Finkelstein, J. L., P. Gala, R. Rochford, M. J. Glesby and S. Mehta (2015). "HIV/AIDS and lipodystrophy: implications for clinical management in resource-limited settings." J Int AIDS Soc **18**: 19033.

Finzi, D., M. Hermankova, T. Pierson, L. M. Carruth, C. Buck, R. E. Chaisson, T. C. Quinn, K. Chadwick, J. Margolick, R. Brookmeyer, J. Gallant, M. Markowitz, D. D. Ho, D. D. Richman and R. F. Siliciano (1997). "Identification of a reservoir for HIV-1 in patients on highly active antiretroviral therapy." Science **278**(5341): 1295-1300.

Flirski, M. and T. Sobow (2005). "Biochemical markers and risk factors of Alzheimer's disease." Curr Alzheimer Res **2**(1): 47-64.

Folch-Pi, J. (1972). "Proteolipids." Adv Exp Med Biol **32**(0): 171-199.

Fox, M. D. and M. E. Raichle (2007). "Spontaneous fluctuations in brain activity observed with functional magnetic resonance imaging." Nat Rev Neurosci **8**(9): 700-711.

Francis, R., X. Xu, H. Park, C. J. Wei, S. Chang, B. Chatterjee and C. Lo (2011). "Connexin43 modulates cell polarity and directional cell migration by regulating microtubule dynamics." PLoS One **6**(10): e26379.

Freed, E. O. (1998). "HIV-1 gag proteins: diverse functions in the virus life cycle." Virology **251**(1): 1-15.

Freed, E. O., E. L. Delwart, G. L. Buchschacher, Jr. and A. T. Panganiban (1992). "A mutation in the human immunodeficiency virus type 1 transmembrane glycoprotein gp41 dominantly interferes with fusion and infectivity." Proc Natl Acad Sci U S A **89**(1): 70-74.

Freed, E. O. and A. J. Mouland (2006). "The cell biology of HIV-1 and other retroviruses." Retrovirology **3**: 77.

Freeman, K. P., A. E. Castro and C. E. Kautz (1986). "Unusual characteristics of a parvovirus isolated from a clinically ill steer." Vet Microbiol **11**(1-2): 61-68.

Freen-van Heeren, J. J. (2021). "Addressing HIV-1 latency with Flow-FISH: Finding, characterizing and targeting HIV-1 infected cells." Cytometry A **99**(9): 861-865.

Frid, K., O. Einstein, Y. Friedman-Levi, O. Binyamin, T. Ben-Hur and R. Gabizon (2015). "Aggregation of MBP in chronic demyelination." Ann Clin Transl Neurol **2**(7): 711-721.

Frisardi, V., F. Panza, D. Seripa, T. Farooqui and A. A. Farooqui (2011). "Glycerophospholipids and glycerophospholipid-derived lipid mediators: a complex meshwork in Alzheimer's disease pathology." Prog Lipid Res **50**(4): 313-330.

Fujinaga, K. and D. C. Cary (2020). "Experimental Systems for Measuring HIV Latency and Reactivation." Viruses **12**(11).

Fulton, D., P. M. Paez and A. T. Campagnoni (2010). "The multiple roles of myelin protein genes during the development of the oligodendrocyte." ASN Neuro **2**(1): e00027.

Fuss, I. J., B. Joshi, Z. Yang, H. Degheidy, S. Fichtner-Feigl, H. de Souza, F. Rieder, F. Scaldaferri, A. Schirbel, M. Scarpa, G. West, C. Yi, L. Xu, P. Leland, M. Yao, P. Mannon, R. K. Puri, C. Fiocchi and W. Strober (2014). "IL-13Ralpha2-bearing, type II NKT cells reactive to sulfatide self-antigen populate the mucosa of ulcerative colitis." Gut **63**(11): 1728-1736.

Gaebler, C., S. D. Falcinelli, E. Stoffel, J. Read, R. Murtagh, T. Y. Oliveira, V. Ramos, J. C. C. Lorenzi, J. Kirchherr, K. S. James, B. Allard, C. Baker, J. D. Kuruc, M. Caskey, N. M. Archin, R. F. Siliciano, D. M. Margolis and M. C. Nussenzweig (2021). "Sequence Evaluation and Comparative Analysis of Novel Assays for Intact Proviral HIV-1 DNA." J Virol **95**(6).

Gajardo-Gomez, R., C. A. Santibanez, V. C. Labra, G. I. Gomez, E. A. Eugenin and J. A. Orellana (2020). "HIV gp120 Protein Increases the Function of Connexin 43

Hemichannels and Pannexin-1 Channels in Astrocytes: Repercussions on Astroglial Function." Int J Mol Sci **21**(7).

Galloway, N. L., G. Doitsh, K. M. Monroe, Z. Yang, I. Munoz-Arias, D. N. Levy and W. C. Greene (2015). "Cell-to-Cell Transmission of HIV-1 Is Required to Trigger Pyroptotic Death of Lymphoid-Tissue-Derived CD4 T Cells." Cell Rep **12**(10): 1555-1563.

Galvagnion, C., A. K. Buell, G. Meisl, T. C. Michaels, M. Vendruscolo, T. P. Knowles and C. M. Dobson (2015). "Lipid vesicles trigger alpha-synuclein aggregation by stimulating primary nucleation." Nat Chem Biol **11**(3): 229-234.

Ganor, Y., F. Real, A. Sennepin, C. A. Dutertre, L. Prevedel, L. Xu, D. Tudor, B. Charmeteau, A. Couedel-Courteille, S. Marion, A. R. Zenak, J. P. Jourdain, Z. Zhou, A. Schmitt, C. Capron, E. A. Eugenin, R. Cheynier, M. Revol, S. Cristofari, A. Hosmalin and M. Bomsel (2019). "HIV-1 reservoirs in urethral macrophages of patients under suppressive antiretroviral therapy." Nat Microbiol **4**(4): 633-644.

Gelpi, M., H. J. Hartling, P. M. Ueland, H. Ullum, M. Troseid and S. D. Nielsen (2017). "Tryptophan catabolism and immune activation in primary and chronic HIV infection." BMC Infect Dis **17**(1): 349.

Gemperline, E., S. Rawson and L. Li (2014). "Optimization and comparison of multiple MALDI matrix application methods for small molecule mass spectrometric imaging." Anal Chem **86**(20): 10030-10035.

German Advisory Committee Blood, S. A. o. P. T. b. B. (2016). "Human Immunodeficiency Virus (HIV)." Transfus Med Hemother **43**(3): 203-222.

Giaume, C., C. C. Naus, J. C. Saez and L. Leybaert (2021). "Glial Connexins and Pannexins in the Healthy and Diseased Brain." Physiol Rev **101**(1): 93-145.

Gill, M. S. A., S. S. Hassan and N. Ahemad (2019). "Evolution of HIV-1 reverse transcriptase and integrase dual inhibitors: Recent advances and developments." European journal of medicinal chemistry **179**: 423-448.

Girard, V., F. Jollivet, O. Knittelfelder, M. Celle, J. N. Arsac, G. Chatelain, D. M. Van den Brink, T. Baron, A. Shevchenko, R. P. Kuhnlein, N. Davoust and B. Mollereau (2021). "Abnormal accumulation of lipid droplets in neurons induces the conversion of alpha-Synuclein to proteolytic resistant forms in a Drosophila model of Parkinson's disease." PLoS Genet **17**(11): e1009921.

Gisslen, M., R. W. Price, U. Andreasson, N. Norgren, S. Nilsson, L. Hagberg, D. Fuchs, S. Spudich, K. Blennow and H. Zetterberg (2016). "Plasma Concentration of the Neurofilament Light Protein (NFL) is a Biomarker of CNS Injury in HIV Infection: A Cross-Sectional Study." EBioMedicine **3**: 135-140.

Glatz, J. F. (2015). "Lipids and lipid binding proteins: a perfect match." Prostaglandins Leukot Essent Fatty Acids **93**: 45-49.

Gonzalez-Dominguez, R., T. Garcia-Barrera and J. L. Gomez-Ariza (2014). "Combination of metabolomic and phospholipid-profiling approaches for the study of Alzheimer's disease." J Proteomics **104**: 37-47.

Gonzalez de San Roman, E., A. Llorente-Ovejero, J. Martinez-Gardeazabal, M. Moreno-Rodriguez, L. Gimenez-Llort, I. Manuel and R. Rodriguez-Puertas (2021). "Modulation of Neurolipid Signaling and Specific Lipid Species in the Triple Transgenic Mouse Model of Alzheimer's Disease." Int J Mol Sci **22**(22).

Good, C. D., J. Ashburner and R. S. Frackowiak (2001). "Computational neuroanatomy: new perspectives for neuroradiology." Rev Neurol (Paris) **157**(8-9 Pt 1): 797-806.

Gorska, A. M., M. Donoso, S. Valdebenito, B. Prideaux, S. Queen, E. Scemes, J. Clements and E. Eugenin (2021). "Human immunodeficiency virus-1/simian immunodeficiency virus infection induces opening of pannexin-1 channels resulting in neuronal synaptic compromise: A novel therapeutic opportunity to prevent NeuroHIV." J Neurochem.

Gorska, A. M., M. Donoso, S. Valdebenito, B. Prideaux, S. Queen, E. Scemes, J. Clements and E. Eugenin (2021). "Human immunodeficiency virus-1/simian immunodeficiency virus infection induces opening of pannexin-1 channels resulting in neuronal synaptic compromise: A novel therapeutic opportunity to prevent NeuroHIV." J Neurochem **158**(2): 500-521.

Goto-Inoue, N., T. Hayasaka, N. Zaima and M. Setou (2011). "Imaging mass spectrometry for lipidomics." Biochim Biophys Acta **1811**(11): 961-969.

Gottlieb, M. S., R. Schroff, H. M. Schanker, J. D. Weisman, P. T. Fan, R. A. Wolf and A. Saxon (1981). "Pneumocystis carinii pneumonia and mucosal candidiasis in previously healthy homosexual men: evidence of a new acquired cellular immunodeficiency." N Engl J Med **305**(24): 1425-1431.

Graf, E. H. and U. O'Doherty (2013). "Quantitation of integrated proviral DNA in viral reservoirs." Curr Opin HIV AIDS **8**(2): 100-105.

Greer, J. M., E. Trifilieff and M. P. Pender (2020). "Correlation Between Anti-Myelin Proteolipid Protein (PLP) Antibodies and Disease Severity in Multiple Sclerosis Patients With PLP Response-Permissive HLA Types." Front Immunol **11**: 1891.

Grennan, J. T., M. R. Loutfy, D. Su, P. R. Harrigan, C. Cooper, M. Klein, N. Machouf, J. S. Montaner, S. Rourke, C. Tsoukas, B. Hogg, J. Raboud and C. Collaboration (2012). "Magnitude of virologic blips is associated with a higher risk for virologic rebound in HIV-infected individuals: a recurrent events analysis." J Infect Dis **205**(8): 1230-1238.

Griffin, D. E., S. L. Wesselingh and J. C. McArthur (1994). "Elevated central nervous system prostaglandins in human immunodeficiency virus-associated dementia." Ann Neurol **35**(5): 592-597.

Guha, D., S. S. Mukerji, S. Chettimada, V. Misra, D. R. Lorenz, S. Morgello and D. Gabuzda (2019). "Cerebrospinal fluid extracellular vesicles and neurofilament light protein as biomarkers of central nervous system injury in HIV-infected patients on antiretroviral therapy." AIDS **33**(4): 615-625.

Gupta, R. K., S. Abdul-Jawad, L. E. McCoy, H. P. Mok, D. Peppa, M. Salgado, J. Martinez-Picado, M. Nijhuis, A. M. J. Wensing, H. Lee, P. Grant, E. Nastouli, J. Lambert, M. Pace, F. Salasc, C. Monit, A. J. Innes, L. Muir, L. Waters, J. Frater, A. M. L. Lever, S. G. Edwards, I. H. Gabriel and E. Olavarria (2019). "HIV-1 remission following CCR5Delta32/Delta32 haematopoietic stem-cell transplantation." Nature **568**(7751): 244-248.

Guzman-Ramos, K., D. Osorio-Gomez, P. Moreno-Castilla and F. Bermudez-Rattoni (2012). "Post-acquisition release of glutamate and norepinephrine in the amygdala is involved in taste-aversion memory consolidation." Learn Mem **19**(6): 231-238.

Hallpike, J. F. and C. W. Adams (1969). "Proteolysis and myelin breakdown: a review of recent histochemical and biochemical studies." Histochem J **1**(6): 559-578.

Hamilton, L. K., M. Dufresne, S. E. Joppe, S. Petryszyn, A. Aumont, F. Calon, F. Barnabe-Heider, A. Furtos, M. Parent, P. Chaurand and K. J. Fernandes (2015). "Aberrant Lipid Metabolism in the Forebrain Niche Suppresses Adult Neural Stem Cell Proliferation in an Animal Model of Alzheimer's Disease." Cell Stem Cell **17**(4): 397-411.

Hammoud, D. A., C. J. Endres, A. R. Chander, T. R. Guilarte, D. F. Wong, N. C. Sacktor, J. C. McArthur and M. G. Pomper (2005). "Imaging glial cell activation with [11C]-R-PK11195 in patients with AIDS." J Neurovirol **11**(4): 346-355.

Han, X. (2007). "Potential mechanisms contributing to sulfatide depletion at the earliest clinically recognizable stage of Alzheimer's disease: a tale of shotgun lipidomics." J Neurochem **103 Suppl 1**: 171-179.

Han, X., M. H. D, D. W. McKeel, Jr., J. Kelley and J. C. Morris (2002). "Substantial sulfatide deficiency and ceramide elevation in very early Alzheimer's disease: potential role in disease pathogenesis." J Neurochem **82**(4): 809-818.

Han, X. and R. W. Gross (2003). "Global analyses of cellular lipidomes directly from crude extracts of biological samples by ESI mass spectrometry: a bridge to lipidomics." J Lipid Res **44**(6): 1071-1079.

Hanna, Z., D. G. Kay, N. Rebai, A. Guimond, S. Jothy and P. Jolicoeur (1998). "Nef harbors a major determinant of pathogenicity for an AIDS-like disease induced by HIV-1 in transgenic mice." Cell **95**(2): 163-175.

Hannun, Y. A. and L. M. Obeid (1995). "Ceramide: an intracellular signal for apoptosis." Trends Biochem Sci **20**(2): 73-77.

Hannun, Y. A. and L. M. Obeid (2008). "Principles of bioactive lipid signalling: lessons from sphingolipids." Nat Rev Mol Cell Biol **9**(2): 139-150.

Hansen, S. G., C. Vieville, N. Whizin, L. Coyne-Johnson, D. C. Siess, D. D. Drummond, A. W. Legasse, M. K. Axthelm, K. Oswald, C. M. Trubey, M. Piatak, Jr., J. D. Lifson, J. A. Nelson, M. A. Jarvis and L. J. Picker (2009). "Effector memory T cell responses are associated with protection of rhesus monkeys from mucosal simian immunodeficiency virus challenge." Nat Med **15**(3): 293-299.

Harezlak, J., S. Buchthal, M. Taylor, G. Schifitto, J. Zhong, E. Daar, J. Alger, E. Singer, T. Campbell, C. Yiannoutsos, R. Cohen, B. Navia and H. I. V. N. Consortium (2011). "Persistence of HIV-associated cognitive impairment, inflammation, and neuronal injury in era of highly active antiretroviral treatment." AIDS **25**(5): 625-633.

Harris, A. L. (2001). "Emerging issues of connexin channels: biophysics fills the gap." Q Rev Biophys **34**(3): 325-472.

Harris, A. L. (2007). "Connexin channel permeability to cytoplasmic molecules." Prog Biophys Mol Biol **94**(1-2): 120-143.

Harris, J. L., I. Y. Choi and W. M. Brooks (2015). "Probing astrocyte metabolism in vivo: proton magnetic resonance spectroscopy in the injured and aging brain." Front Aging Neurosci **7**: 202.

Harrison, S. C. (2008). "Viral membrane fusion." Nat Struct Mol Biol **15**(7): 690-698.
Hartline, D. K. and D. R. Colman (2007). "Rapid conduction and the evolution of giant axons and myelinated fibers." Curr Biol **17**(1): R29-35.

Hategan, A., E. Masliah and A. Nath (2019). "HIV and Alzheimer's disease: complex interactions of HIV-Tat with amyloid beta peptide and Tau protein." Journal of neurovirology **25**(5): 648-660.

Haughey, N. J., R. G. Cutler, A. Tamara, J. C. McArthur, D. L. Vargas, C. A. Pardo, J. Turchan, A. Nath and M. P. Mattson (2004). "Perturbation of sphingolipid metabolism and ceramide production in HIV-dementia." Ann Neurol **55**(2): 257-267.

Hayasaka, T., N. Goto-Inoue, N. Zaima, Y. Kimura and M. Setou (2009). "Organ-specific distributions of lysophosphatidylcholine and triacylglycerol in mouse embryo." Lipids **44**(9): 837-848.

Hayasaka, T., N. Goto-Inoue, N. Zaima, K. Shrivas, Y. Kashiwagi, M. Yamamoto, M. Nakamoto and M. Setou (2010). "Imaging mass spectrometry with silver nanoparticles reveals the distribution of fatty acids in mouse retinal sections." J Am Soc Mass Spectrom **21**(8): 1446-1454.

Hazleton, J. E., J. W. Berman and E. A. Eugenin (2010). "Novel mechanisms of central nervous system damage in HIV infection." HIV AIDS (Auckl) **2**: 39-49.

He, X., Y. Huang, B. Li, C. X. Gong and E. H. Schuchman (2010). "Deregulation of sphingolipid metabolism in Alzheimer's disease." Neurobiol Aging **31**(3): 398-408.

Heaton, R. K., D. B. Clifford, D. R. Franklin, Jr., S. P. Woods, C. Ake, F. Vaida, R. J. Ellis, S. L. Letendre, T. D. Marcotte, J. H. Atkinson, M. Rivera-Mindt, O. R. Vigil, M. J. Taylor, A. C. Collier, C. M. Marra, B. B. Gelman, J. C. McArthur, S. Morgello, D. M. Simpson, J. A. McCutchan, I. Abramson, A. Gamst, C. Fennema-Notestine, T. L. Jernigan, J. Wong and I. Grant (2010). "HIV-associated neurocognitive disorders persist in the era of potent antiretroviral therapy: CHARTER Study." Neurology **75**(23): 2087-2096.

Heaton, R. K., D. B. Clifford, D. R. Franklin, Jr., S. P. Woods, C. Ake, F. Vaida, R. J. Ellis, S. L. Letendre, T. D. Marcotte, J. H. Atkinson, M. Rivera-Mindt, O. R. Vigil, M. J. Taylor, A. C. Collier, C. M. Marra, B. B. Gelman, J. C. McArthur, S. Morgello, D. M. Simpson, J. A. McCutchan, I. Abramson, A. Gamst, C. Fennema-Notestine, T. L. Jernigan, J. Wong, I. Grant and C. Group (2010). "HIV-associated neurocognitive disorders persist in the era of potent antiretroviral therapy: CHARTER Study." Neurology **75**(23): 2087-2096.

Heijs, B., A. Potthoff, J. Soltwisch and K. Dreisewerd (2020). "MALDI-2 for the Enhanced Analysis of N-Linked Glycans by Mass Spectrometry Imaging." Anal Chem **92**(20): 13904-13911.

Hemelaar, J. (2012). "The origin and diversity of the HIV-1 pandemic." Trends Mol Med **18**(3): 182-192.

Henderson, L. J., T. P. Johnson, B. R. Smith, L. B. Reoma, U. A. Santamaria, M. Bachani, C. Demarino, R. A. Barclay, J. Snow, N. Sacktor, J. McArthur, S. Letendre, J. Steiner, F. Kashanchi and A. Nath (2019). "Presence of Tat and transactivation response element in spinal fluid despite antiretroviral therapy." AIDS **33 Suppl 2**: S145-S157.

Henderson, L. J., L. B. Reoma, J. A. Kovacs and A. Nath (2020). "Advances toward Curing HIV-1 Infection in Tissue Reservoirs." J Virol **94**(3).

Hiener, B., B. A. Horsburgh, J. S. Eden, K. Barton, T. E. Schlub, E. Lee, S. von Stockenstrom, L. Odevall, J. M. Milush, T. Liegler, E. Sinclair, R. Hoh, E. A. Boritz, D. Douek, R. Fromentin, N. Chomont, S. G. Deeks, F. M. Hecht and S. Palmer (2017).

"Identification of Genetically Intact HIV-1 Proviruses in Specific CD4(+) T Cells from Effectively Treated Participants." Cell Rep **21**(3): 813-822.

Hirahara, Y., T. Wakabayashi, T. Mori, T. Koike, I. Yao, M. Tsuda, K. Honke, H. Gotoh, K. Ono and H. Yamada (2017). "Sulfatide species with various fatty acid chains in oligodendrocytes at different developmental stages determined by imaging mass spectrometry." J Neurochem **140**(3): 435-450.

Hoffmann, T. and P. C. Dorrestein (2015). "Homogeneous matrix deposition on dried agar for MALDI imaging mass spectrometry of microbial cultures." J Am Soc Mass Spectrom **26**(11): 1959-1962.

Holman, A. G., M. E. Mefford, N. O'Connor and D. Gabuzda (2010). "HIVBrainSeqDB: a database of annotated HIV envelope sequences from brain and other anatomical sites." AIDS Res Ther **7**: 43.

Holzlechner, M., E. Eugenin and B. Prideaux (2019). "Mass spectrometry imaging to detect lipid biomarkers and disease signatures in cancer." Cancer Rep (Hoboken) **2**(6): e1229.

Hong, J. H., J. W. Kang, D. K. Kim, S. H. Baik, K. H. Kim, S. R. Shanta, J. H. Jung, I. Mook-Jung and K. P. Kim (2016). "Global changes of phospholipids identified by MALDI imaging mass spectrometry in a mouse model of Alzheimer's disease." J Lipid Res **57**(1): 36-45.

Honke, K. (2013). "Biosynthesis and biological function of sulfoglycolipids." Proc Jpn Acad Ser B Phys Biol Sci **89**(4): 129-138.

Hooijmans, C. R. and A. J. Kiliaan (2008). "Fatty acids, lipid metabolism and Alzheimer pathology." Eur J Pharmacol **585**(1): 176-196.

Hosmane, N. N., K. J. Kwon, K. M. Bruner, A. A. Capoferri, S. Beg, D. I. Rosenbloom, B. F. Keele, Y. C. Ho, J. D. Siliciano and R. F. Siliciano (2017). "Proliferation of latently infected CD4(+) T cells carrying replication-competent HIV-1: Potential role in latent reservoir dynamics." The Journal of experimental medicine **214**(4): 959-972.

Howdle, G. C., Y. Quide, M. S. Kassem, K. Johnson, C. D. Rae, B. J. Brew and L. A. Cysique (2020). "Brain amyloid in virally suppressed HIV-associated neurocognitive disorder." Neurol Neuroimmunol Neuroinflamm **7**(4).

Hu, W. S. and S. H. Hughes (2012). "HIV-1 reverse transcription." Cold Spring Harb Perspect Med **2**(10).

Hu, Y., I. Doudevski, D. Wood, M. Moscarello, C. Husted, C. Genain, J. A. Zasadzinski and J. Israelachvili (2004). "Synergistic interactions of lipids and myelin basic protein." Proc Natl Acad Sci U S A **101**(37): 13466-13471.

Huang, Y., L. Zhao, B. Jia, L. Wu, Y. Li, N. Curthoys and J. C. Zheng (2011). "Glutaminase dysregulation in HIV-1-infected human microglia mediates neurotoxicity: relevant to HIV-1-associated neurocognitive disorders." The Journal of neuroscience : the official journal of the Society for Neuroscience **31**(42): 15195-15204.

Huizing, L. R. S., S. R. Ellis, B. Beulen, F. P. Y. Barre, P. B. Kwant, R. J. Vreeken and R. M. A. Heeren (2019). "Development and evaluation of matrix application techniques for high throughput mass spectrometry imaging of tissues in the clinic." Clin Mass Spectrom **12**: 7-15.

Huntemer-Silveira, A., N. Patil, M. A. Brickner and A. M. Parr (2020). "Strategies for Oligodendrocyte and Myelin Repair in Traumatic CNS Injury." Front Cell Neurosci **14**: 619707.

Hussain, G., H. Anwar, A. Rasul, A. Imran, M. Qasim, S. Zafar, M. Imran, S. K. S. Kamran, N. Aziz, A. Razzaq, W. Ahmad, A. Shabbir, J. Iqbal, S. M. Baig, M. Ali, J. L. Gonzalez de Aguilar, T. Sun, A. Muhammad and A. Muhammad Umair (2020). "Lipids as biomarkers of brain disorders." Crit Rev Food Sci Nutr **60**(3): 351-374.

Hutter, G., D. Nowak, M. Mossner, S. Ganepola, A. Mussig, K. Allers, T. Schneider, J. Hofmann, C. Kucherer, O. Blau, I. W. Blau, W. K. Hofmann and E. Thiel (2009). "Long-term control of HIV by CCR5 Delta32/Delta32 stem-cell transplantation." N Engl J Med **360**(7): 692-698.

Imai, K., H. Togami and T. Okamoto (2010). "Involvement of histone H3 lysine 9 (H3K9) methyltransferase G9a in the maintenance of HIV-1 latency and its reactivation by BIX01294." J Biol Chem **285**(22): 16538-16545.

Inoue, T., I. Taguchi, S. Abe, G. Li, R. Hu, T. Nakajima, A. Hara, T. Aoyama, R. Kannagi, M. Kyogashima and K. Node (2010). "Sulfatides are associated with neointimal thickening after vascular injury." Atherosclerosis **211**(1): 291-296.

Irollo, E., J. Luchetta, C. Ho, B. Nash and O. Meucci (2021). "Mechanisms of neuronal dysfunction in HIV-associated neurocognitive disorders." Cell Mol Life Sci **78**(9): 4283-4303.

Isaac, G., Z. Pernber, V. Gieselmann, E. Hansson, J. Bergquist and J. E. Mansson (2006). "Sulfatide with short fatty acid dominates in astrocytes and neurons." FEBS J **273**(8): 1782-1790.

Ishizuka, I. (1997). "Chemistry and functional distribution of sulfoglycolipids." Prog Lipid Res **36**(4): 245-319.

Itokazu, Y., J. Wang and R. K. Yu (2018). "Gangliosides in Nerve Cell Specification." Prog Mol Biol Transl Sci **156**: 241-263.

Jackson, S. N., K. Baldwin, L. Muller, V. M. Womack, J. A. Schultz, C. Balaban and A. S. Woods (2014). "Imaging of lipids in rat heart by MALDI-MS with silver nanoparticles." Anal Bioanal Chem **406**(5): 1377-1386.

Jadlowsky, J. K., J. Y. Wong, A. C. Graham, C. Dobrowolski, R. L. Devor, M. D. Adams, K. Fujinaga and J. Karn (2014). "Negative elongation factor is required for the maintenance of proviral latency but does not induce promoter-proximal pausing of RNA polymerase II on the HIV long terminal repeat." Mol Cell Biol **34**(11): 1911-1928.

Jaeger, L. B. and A. Nath (2012). "Modeling HIV-associated neurocognitive disorders in mice: new approaches in the changing face of HIV neuropathogenesis." Dis Model Mech **5**(3): 313-322.

Jayappa, K. D., Z. Ao and X. Yao (2012). "The HIV-1 passage from cytoplasm to nucleus: the process involving a complex exchange between the components of HIV-1 and cellular machinery to access nucleus and successful integration." Int J Biochem Mol Biol **3**(1): 70-85.

Jenkins, G. M. and M. A. Frohman (2005). "Phospholipase D: a lipid centric review." Cell Mol Life Sci **62**(19-20): 2305-2316.

Jensen, B. K., H. Monnerie, M. V. Mannell, P. J. Gannon, C. A. Espinoza, M. A. Erickson, A. J. Bruce-Keller, B. B. Gelman, L. A. Briand, R. C. Pierce, K. L. Jordan-Sciutto and J. B. Grinspan (2015). "Altered Oligodendrocyte Maturation and Myelin Maintenance: The Role of Antiretrovirals in HIV-Associated Neurocognitive Disorders." J Neuropathol Exp Neurol **74**(11): 1093-1118.

Jensen, B. K., L. M. Roth, J. B. Grinspan and K. L. Jordan-Sciutto (2019). "White matter loss and oligodendrocyte dysfunction in HIV: A consequence of the infection, the antiretroviral therapy or both?" Brain Res **1724**: 146397.

Jeon, S. B., H. J. Yoon, S. H. Park, I. H. Kim and E. J. Park (2008). "Sulfatide, a major lipid component of myelin sheath, activates inflammatory responses as an endogenous stimulator in brain-resident immune cells." J Immunol **181**(11): 8077-8087.

Jernigan, T. L., S. L. Archibald, C. Fennema-Notestine, M. J. Taylor, R. J. Theilmann, M. D. Julaton, R. J. Notestine, T. Wolfson, S. L. Letendre, R. J. Ellis, R. K. Heaton, A. C. Gamst, D. R. Franklin, Jr., D. B. Clifford, A. C. Collier, B. B. Gelman, C. Marra, J. C. McArthur, J. A. McCutchan, S. Morgello, D. M. Simpson and I. Grant (2011). "Clinical factors related to brain structure in HIV: the CHARTER study." Journal of neurovirology **17**(3): 248-257.

Jessen Krut, J., T. Mellberg, R. W. Price, L. Hagberg, D. Fuchs, L. Rosengren, S. Nilsson, H. Zetterberg and M. Gisslen (2014). "Biomarker evidence of axonal injury in neuroasymptomatic HIV-1 patients." PLoS One **9**(2): e88591.

Jiang, C., X. Lian, C. Gao, X. Sun, K. B. Einkauf, J. M. Chevalier, S. M. Y. Chen, S. Hua, B. Rhee, K. Chang, J. E. Blackmer, M. Osborn, M. J. Peluso, R. Hoh, M. Somsouk, J. Milush, L. N. Bertagnolli, S. E. Sweet, J. A. Varriale, P. D. Burbelo, T. W. Chun, G. M. Laird, E. Serrao, A. N. Engelman, M. Carrington, R. F. Siliciano, J. M. Siliciano, S. G. Deeks, B. D. Walker, M. Lichterfeld and X. G. Yu (2020). "Distinct viral reservoirs in individuals with spontaneous control of HIV-1." Nature **585**(7824): 261-267.

Jiang, G. and S. Dandekar (2015). "Targeting NF-kappaB signaling with protein kinase C agonists as an emerging strategy for combating HIV latency." AIDS Res Hum Retroviruses **31**(1): 4-12.

Jiang, G., D. Nguyen, N. M. Archin, S. A. Yukl, G. Mendez-Lagares, Y. Tang, M. M. Elsheikh, G. R. Thompson, 3rd, D. J. Hartigan-O'Connor, D. M. Margolis, J. K. Wong and S. Dandekar (2018). "HIV latency is reversed by ACSS2-driven histone crotonylation." J Clin Invest **128**(3): 1190-1198.

Jilg, N., P. Garcia-Broncano, M. Peluso, F. P. Segal, R. J. Bosch, C. Roberts-Toler, S. M. Y. Chen, C. N. Van Dam, M. C. Keefer, D. R. Kuritzkes, A. L. Landay, S. Deeks, X. G. Yu, P. E. Sax, J. Z. Li and A. C. T. G. A. S. Team (2020). "Maintenance of Viral Suppression in Human Immunodeficiency Virus Controllers Despite Waning T-Cell Responses During Antiretroviral Therapy." J Infect Dis **222**(11): 1837-1842.

John Lin, C. C., K. Yu, A. Hatcher, T. W. Huang, H. K. Lee, J. Carlson, M. C. Weston, F. Chen, Y. Zhang, W. Zhu, C. A. Mohila, N. Ahmed, A. J. Patel, B. R. Arenkiel, J. L. Noebels, C. J. Creighton and B. Deneen (2017). "Identification of diverse astrocyte populations and their malignant analogs." Nat Neurosci **20**(3): 396-405.

Jones, R. B. and B. D. Walker (2016). "HIV-specific CD8(+) T cells and HIV eradication." J Clin Invest **126**(2): 455-463.

Jonsson, M., H. Zetterberg, E. van Straaten, K. Lind, S. Syversen, A. Edman, K. Blennow, L. Rosengren, L. Pantoni, D. Inzitari and A. Wallin (2010). "Cerebrospinal fluid biomarkers of white matter lesions - cross-sectional results from the LADIS study." Eur J Neurol **17**(3): 377-382.

Jumare, J., C. Akolo, N. Ndembi, S. Bwala, P. Alabi, K. Okwuasaba, R. Adebiyi, A. Umlauf, M. Cherner, A. Abimiku, M. Charurat, W. A. Blattner and W. Royal, 3rd (2020). "Elevated Plasma Levels of sCD14 and MCP-1 Are Associated With HIV Associated Neurocognitive Disorders Among Antiretroviral-Naive Individuals in Nigeria." J Acquir Immune Defic Syndr **84**(2): 196-202.

Justice, A., L. Sullivan, D. Fiellin and T. Veterans Aging Cohort Study Project (2010). "HIV/AIDS, comorbidity, and alcohol: can we make a difference?" Alcohol Res Health **33**(3): 258-266.

Kallianpur, A. R., H. Gittleman, S. Letendre, R. Ellis, J. S. Barnholtz-Sloan, W. S. Bush, R. Heaton, D. C. Samuels, D. R. Franklin, Jr., D. Rosario-Cookson, D. B. Clifford, A. C. Collier, B. Gelman, C. M. Marra, J. C. McArthur, J. A. McCutchan, S. Morgello, I. Grant, D. Simpson, J. R. Connor, T. Hulgan and C. S. Group (2019). "Cerebrospinal Fluid Ceruloplasmin, Haptoglobin, and Vascular Endothelial Growth Factor Are Associated with Neurocognitive Impairment in Adults with HIV Infection." Mol Neurobiol **56**(5): 3808-3818.

Kanmogne, G. D., R. C. Kennedy and P. Grammas (2002). "HIV-1 gp120 proteins and gp160 peptides are toxic to brain endothelial cells and neurons: possible pathway for HIV entry into the brain and HIV-associated dementia." J Neuropathol Exp Neurol **61**(11): 992-1000.

Kanter, J. L., S. Narayana, P. P. Ho, I. Catz, K. G. Warren, R. A. Sobel, L. Steinman and W. H. Robinson (2006). "Lipid microarrays identify key mediators of autoimmune brain inflammation." Nat Med **12**(1): 138-143.

Karas, M. and R. Kruger (2003). "Ion formation in MALDI: the cluster ionization mechanism." Chem Rev **103**(2): 427-440.

Karn, J. and C. M. Stoltzfus (2012). "Transcriptional and posttranscriptional regulation of HIV-1 gene expression." Cold Spring Harb Perspect Med **2**(2): a006916.

Kasparov, S. (2016). "Are Astrocytes the Pressure-Reservoirs of Lactate in the Brain?" Cell Metab **23**(1): 1-2.

Kassan, A., A. Herms, A. Fernandez-Vidal, M. Bosch, N. L. Schieber, B. J. Reddy, A. Fajardo, M. Gelabert-Baldrich, F. Tebar, C. Enrich, S. P. Gross, R. G. Parton and A. Pol (2013). "Acyl-CoA synthetase 3 promotes lipid droplet biogenesis in ER microdomains." J Cell Biol **203**(6): 985-1001.

Kaya, I., D. Brinet, W. Michno, S. Syvanen, D. Sehlin, H. Zetterberg, K. Blennow and J. Hanrieder (2017). "Delineating Amyloid Plaque Associated Neuronal Sphingolipids in Transgenic Alzheimer's Disease Mice (tgArcSwe) Using MALDI Imaging Mass Spectrometry." ACS Chem Neurosci **8**(2): 347-355.

Kearns, A., J. Gordon, T. H. Burdo and X. Qin (2017). "HIV-1-Associated Atherosclerosis: Unraveling the Missing Link." J Am Coll Cardiol **69**(25): 3084-3098.

Kehn-Hall, K., I. Guendel, L. Carpio, L. Skaltsounis, L. Meijer, L. Al-Harthi, J. P. Steiner, A. Nath, O. Kutsch and F. Kashanchi (2011). "Inhibition of Tat-mediated HIV-1 replication and neurotoxicity by novel GSK3-beta inhibitors." Virology **415**(1): 56-68.

Kelesidis, T. and J. S. Currier (2014). "Dyslipidemia and cardiovascular risk in human immunodeficiency virus infection." Endocrinol Metab Clin North Am **43**(3): 665-684.

Kessing, C. F., C. C. Nixon, C. Li, P. Tsai, H. Takata, G. Mousseau, P. T. Ho, J. B. Honeycutt, M. Fallahi, L. Trautmann, J. V. Garcia and S. T. Valente (2017). "In Vivo Suppression of HIV Rebound by Didehydro-Cortistatin A, a "Block-and-Lock" Strategy for HIV-1 Treatment." Cell Rep **21**(3): 600-611.

Khakh, B. S. and B. Deneen (2019). "The Emerging Nature of Astrocyte Diversity." Annu Rev Neurosci **42**: 187-207.

Kielian, T. (2008). "Glial connexins and gap junctions in CNS inflammation and disease." J Neurochem **106**(3): 1000-1016.

Kim, H. G., K. C. Kim, T. Y. Roh, J. Park, K. M. Jung, J. S. Lee, S. Y. Choi, S. S. Kim and B. S. Choi (2011). "Gene silencing in HIV-1 latency by polycomb repressive group." Virol J **8**: 179.

Kim, H. S., M. Han, I. H. Park, C. H. Park, M. S. Kwak and J. S. Shin (2020). "Sulfatide Inhibits HMGB1 Secretion by Hindering Toll-Like Receptor 4 Localization Within Lipid Rafts." Front Immunol **11**: 1305.

Kim, M., N. N. Hosmane, C. K. Bullen, A. Capoferri, H. C. Yang, J. D. Siliciano and R. F. Siliciano (2014). "A primary CD4(+) T cell model of HIV-1 latency established after activation through the T cell receptor and subsequent return to quiescence." Nat Protoc **9**(12): 2755-2770.

Kim, Y., J. L. Anderson and S. R. Lewin (2018). "Getting the "Kill" into "Shock and Kill": Strategies to Eliminate Latent HIV." Cell Host Microbe **23**(1): 14-26.

Kim, Y. K., U. Mbonye, J. Hokello and J. Karn (2011). "T-cell receptor signaling enhances transcriptional elongation from latent HIV proviruses by activating P-TEFb through an ERK-dependent pathway." J Mol Biol **410**(5): 896-916.

Klaver, B. and B. Berkhout (1994). "Comparison of 5' and 3' long terminal repeat promoter function in human immunodeficiency virus." J Virol **68**(6): 3830-3840.

Knochenmuss, R. and L. V. Zhigilei (2010). "Molecular dynamics simulations of MALDI: laser fluence and pulse width dependence of plume characteristics and consequences for matrix and analyte ionization." J Mass Spectrom **45**(4): 333-346.

Ko, A., G. Kang, J. B. Hattler, H. I. Galadima, J. Zhang, Q. Li and W. K. Kim (2019). "Macrophages but not Astrocytes Harbor HIV DNA in the Brains of HIV-1-Infected Aviremic Individuals on Suppressive Antiretroviral Therapy." J Neuroimmune Pharmacol **14**(1): 110-119.

Kogan, M. and J. Rappaport (2011). "HIV-1 accessory protein Vpr: relevance in the pathogenesis of HIV and potential for therapeutic intervention." Retrovirology **8**: 25.

Koizumi, S. (2010). "Synchronization of Ca2+ oscillations: involvement of ATP release in astrocytes." FEBS J **277**(2): 286-292.

Kolter, T. (2012). "Ganglioside biochemistry." ISRN Biochem **2012**: 506160.

Koneru, P. C., A. C. Francis, N. Deng, S. V. Rebensburg, A. C. Hoyte, J. Lindenberger, D. Adu-Ampratwum, R. C. Larue, M. F. Wempe, A. N. Engelman, D. Lyumkis, J. R. Fuchs, R. M. Levy, G. B. Melikyan and M. Kvaratskhelia (2019). "HIV-1 integrase tetramers are the antiviral target of pyridine-based allosteric integrase inhibitors." eLife **8**.

Kopanic, J. L., B. Schlingmann, M. Koval, A. F. Lau, P. L. Sorgen and V. F. Su (2015). "Degradation of gap junction connexins is regulated by the interaction with Cx43-interacting protein of 75 kDa (CIP75)." Biochem J **466**(3): 571-585.

Kosicek, M. and S. Hecimovic (2013). "Phospholipids and Alzheimer's disease: alterations, mechanisms and potential biomarkers." Int J Mol Sci **14**(1): 1310-1322.

Kovalevich, J. and D. Langford (2012). "Neuronal toxicity in HIV CNS disease." Future Virol **7**(7): 687-698.

Krasnopolsky, S., A. Kuzmina and R. Taube (2020). "Genome-wide CRISPR knockout screen identifies ZNF304 as a silencer of HIV transcription that promotes viral latency." PLoS Pathog **16**(9): e1008834.

Kubo, A., T. Satoh, Y. Itoh, M. Hashimoto, J. Tamura and R. B. Cody (2013). "Structural analysis of triacylglycerols by using a MALDI-TOF/TOF system with monoisotopic precursor selection." J Am Soc Mass Spectrom **24**(5): 684-689.

Kumar, A., G. Darcis, C. Van Lint and G. Herbein (2015). "Epigenetic control of HIV-1 post integration latency: implications for therapy." Clin Epigenetics **7**: 103.

Kuo, T. H., M. S. Kuei, Y. Hsiao, H. H. Chung, C. C. Hsu and H. J. Chen (2019). "Matrix-Assisted Laser Desorption/Ionization Mass Spectrometry Typings of Edible Oils through Spectral Networking of Triacylglycerol Fingerprints." ACS Omega **4**(13): 15734-15741.

Kursula, P. (2008). "Structural properties of proteins specific to the myelin sheath." Amino Acids **34**(2): 175-185.

Kwong, P. D., R. Wyatt, J. Robinson, R. W. Sweet, J. Sodroski and W. A. Hendrickson (1998). "Structure of an HIV gp120 envelope glycoprotein in complex with the CD4 receptor and a neutralizing human antibody." Nature **393**(6686): 648-659.

Kyogashima, M. (2004). "The role of sulfatide in thrombogenesis and haemostasis." Arch Biochem Biophys **426**(2): 157-162.

Kyogashima, M., J. Onaya, A. Hara and T. Taketomi (1998). "Sulfatide can markedly enhance thrombogenesis in rat deep vein thrombosis model." Glycoconj J **15**(9): 915-922.

Lafeuillade, A. and M. Stevenson (2011). "The search for a cure for persistent HIV reservoirs." AIDS Rev **13**(2): 63-66.

Lamers, S. L., R. Rose, E. Maidji, M. Agsalda-Garcia, D. J. Nolan, G. B. Fogel, M. Salemi, D. L. Garcia, P. Bracci, W. Yong, D. Commins, J. Said, N. Khanlou, C. H. Hinkin, M. V. Sueiras, G. Mathisen, S. Donovan, B. Shiramizu, C. A. Stoddart, M. S. McGrath and E. J. Singer (2016). "HIV DNA Is Frequently Present within Pathologic Tissues Evaluated at Autopsy from Combined Antiretroviral Therapy-Treated Patients with Undetectable Viral Loads." J Virol **90**(20): 8968-8983.

Landgraf, R. R., M. C. Prieto Conaway, T. J. Garrett, P. W. Stacpoole and R. A. Yost (2009). "Imaging of lipids in spinal cord using intermediate pressure matrix-assisted laser desorption-linear ion trap/Orbitrap MS." Anal Chem **81**(20): 8488-8495.

Langer, S., X. Yin, A. Diaz, A. J. Portillo, D. E. Gordon, U. H. Rogers, J. M. Marlett, N. J. Krogan, J. A. T. Young, L. Pache and S. K. Chanda (2020). "The E3 Ubiquitin-Protein Ligase Cullin 3 Regulates HIV-1 Transcription." Cells **9**(9).

Larder, B. A., G. Darby and D. D. Richman (1989). "HIV with reduced sensitivity to zidovudine (AZT) isolated during prolonged therapy." Science **243**(4899): 1731-1734.
Lassmann, H. (2018). "Multiple Sclerosis Pathology." Cold Spring Harb Perspect Med **8**(3).

Lassmann, H. and W. F. Hickey (1993). "Radiation bone marrow chimeras as a tool to study microglia turnover in normal brain and inflammation." Clin Neuropathol **12**(5): 284-285.

Lee, C. H., P. Olson and R. M. Evans (2003). "Minireview: lipid metabolism, metabolic diseases, and peroxisome proliferator-activated receptors." Endocrinology **144**(6): 2201-2207.

Leite, S. C., D. G. Correa, T. M. Doring, T. T. Kubo, T. M. Netto, R. Ferracini, N. Ventura, P. R. Bahia and E. L. Gasparetto (2013). "Diffusion tensor MRI evaluation of the corona radiata, cingulate gyri, and corpus callosum in HIV patients." J Magn Reson Imaging **38**(6): 1488-1493.

Lemp, G. F., S. F. Payne, G. W. Rutherford, N. A. Hessol, W. Winkelstein, Jr., J. A. Wiley, A. R. Moss, R. E. Chaisson, R. T. Chen, D. W. Feigal, Jr. and et al. (1990). "Projections of AIDS morbidity and mortality in San Francisco." JAMA **263**(11): 1497-1501.

Lenasi, T., X. Contreras and B. M. Peterlin (2008). "Transcriptional interference antagonizes proviral gene expression to promote HIV latency." Cell Host Microbe **4**(2): 123-133.

Leopold, J., Y. Popkova, K. M. Engel and J. Schiller (2018). "Recent Developments of Useful MALDI Matrices for the Mass Spectrometric Characterization of Lipids." Biomolecules **8**(4).

Li, B., Y. Zhang, J. Ge, K. Liu and P. Li (2018). "Sample preparation for mass spectrometry imaging of leaf tissues: a case study on analyte delocalization." Anal Bioanal Chem **410**(28): 7449-7456.

Li, C., G. Mousseau and S. T. Valente (2019). "Tat inhibition by didehydro-Cortistatin A promotes heterochromatin formation at the HIV-1 long terminal repeat." Epigenetics Chromatin **12**(1): 23.

Li, G., R. Hu, J. Gu and H. Z. Wu (2015). "Relationship between carotid artery atherosclerosis and sulfatide in hypertensive patients." Genet Mol Res **14**(2): 4840-4846.

Li, G. H., L. Henderson and A. Nath (2016). "Astrocytes as an HIV Reservoir: Mechanism of HIV Infection." Curr HIV Res **14**(5): 373-381.

Li, H., G. Spagnol, N. Naslavsky, S. Caplan and P. L. Sorgen (2014). "TC-PTP directly interacts with connexin43 to regulate gap junction intercellular communication." J Cell Sci **127**(Pt 15): 3269-3279.

Li, P., P. Kaiser, H. W. Lampiris, P. Kim, S. A. Yukl, D. V. Havlir, W. C. Greene and J. K. Wong (2016). "Stimulating the RIG-I pathway to kill cells in the latent HIV reservoir following viral reactivation." Nat Med **22**(7): 807-811.

Li, W., S. Gorantla, H. E. Gendelman and L. Y. Poluektova (2017). "Systemic HIV-1 infection produces a unique glial footprint in humanized mouse brains." Dis Model Mech **10**(12): 1489-1502.

Lin, A., B. D. Ross, K. Harris and W. Wong (2005). "Efficacy of proton magnetic resonance spectroscopy in neurological diagnosis and neurotherapeutic decision making." NeuroRx **2**(2): 197-214.

Lin, J. H., H. Weigel, M. L. Cotrina, S. Liu, E. Bueno, A. J. Hansen, T. W. Hansen, S. Goldman and M. Nedergaard (1998). "Gap-junction-mediated propagation and amplification of cell injury." Nat Neurosci **1**(6): 494-500.

Lingwood, D. and K. Simons (2010). "Lipid rafts as a membrane-organizing principle." Science **327**(5961): 46-50.

Liu, H., E. Xu, J. Liu and H. Xiong (2016). "Oligodendrocyte Injury and Pathogenesis of HIV-1-Associated Neurocognitive Disorders." Brain Sci **6**(3).

Liu, Y., H. Liu, B. O. Kim, V. H. Gattone, J. Li, A. Nath, J. Blum and J. J. He (2004). "CD4-independent infection of astrocytes by human immunodeficiency virus type 1: requirement for the human mannose receptor." J Virol **78**(8): 4120-4133.

Lorenzo-Redondo, R., H. R. Fryer, T. Bedford, E. Y. Kim, J. Archer, S. L. K. Pond, Y. S. Chung, S. Penugonda, J. Chipman, C. V. Fletcher, T. W. Schacker, M. H. Malim, A. Rambaut, A. T. Haase, A. R. McLean and S. M. Wolinsky (2016). "Persistent HIV-1 replication maintains the tissue reservoir during therapy." Nature **530**(7588): 51-56.

Lourenco, T., J. Paes de Faria, C. A. Bippes, J. Maia, J. A. Lopes-da-Silva, J. B. Relvas and M. Graos (2016). "Modulation of oligodendrocyte differentiation and maturation by combined biochemical and mechanical cues." Sci Rep **6**: 21563.

Luoma, A. M., C. D. Castro, T. Mayassi, L. A. Bembinster, L. Bai, D. Picard, B. Anderson, L. Scharf, J. E. Kung, L. V. Sibener, P. B. Savage, B. Jabri, A. Bendelac and E. J. Adams (2013). "Crystal structure of Vdelta1 T cell receptor in complex with CD1d-sulfatide shows MHC-like recognition of a self-lipid by human gammadelta T cells." Immunity **39**(6): 1032-1042.

Lusic, M., B. Marini, H. Ali, B. Lucic, R. Luzzati and M. Giacca (2013). "Proximity to PML nuclear bodies regulates HIV-1 latency in CD4+ T cells." Cell Host Microbe **13**(6): 665-677.

Lutgen, V., S. D. Narasipura, H. J. Barbian, M. Richards, J. Wallace, R. Razmpour, T. Buzhdygan, S. H. Ramirez, L. Prevedel, E. A. Eugenin and L. Al-Harthi (2020). "HIV infects astrocytes in vivo and egresses from the brain to the periphery." PLoS Pathog **16**(6): e1008381.

Lyons, J. L., H. Uno, P. Ancuta, A. Kamat, D. J. Moore, E. J. Singer, S. Morgello and D. Gabuzda (2011). "Plasma sCD14 is a biomarker associated with impaired neurocognitive test performance in attention and learning domains in HIV infection." J Acquir Immune Defic Syndr **57**(5): 371-379.

Macedo, A. B., C. L. Novis and A. Bosque (2019). "Targeting Cellular and Tissue HIV Reservoirs With Toll-Like Receptor Agonists." Front Immunol **10**: 2450.

Mahboobi, S. H., A. A. Javanpour and M. R. Mofrad (2015). "The interaction of RNA helicase DDX3 with HIV-1 Rev-CRM1-RanGTP complex during the HIV replication cycle." PLoS One **10**(2): e0112969.

Maier, O., D. Hoekstra and W. Baron (2008). "Polarity development in oligodendrocytes: sorting and trafficking of myelin components." J Mol Neurosci **35**(1): 35-53.

Malik, S., M. Theis and E. A. Eugenin (2017). "Connexin43 Containing Gap Junction Channels Facilitate HIV Bystander Toxicity: Implications in NeuroHIV." Front Mol Neurosci **10**: 404.

Malik, S., S. Valdebenito, D. D'Amico, B. Prideaux and E. A. Eugenin (2021). "HIV infection of astrocytes compromises inter-organelle interactions and inositol phosphate metabolism: A potential mechanism of bystander damage and viral reservoir survival." Prog Neurobiol **206**: 102157.

Mamik, M. K., S. Banerjee, T. F. Walseth, R. Hirte, L. Tang, K. Borgmann and A. Ghorpade (2011). "HIV-1 and IL-1beta regulate astrocytic CD38 through mitogen-activated protein kinases and nuclear factor-kappaB signaling mechanisms." J Neuroinflammation **8**: 145.

Marangon, D., M. Boccazzi, D. Lecca and M. Fumagalli (2020). "Regulation of Oligodendrocyte Functions: Targeting Lipid Metabolism and Extracellular Matrix for Myelin Repair." J Clin Med **9**(2).

Marban, C., F. Forouzanfar, A. Ait-Ammar, F. Fahmi, H. El Mekdad, F. Daouad, O. Rohr and C. Schwartz (2016). "Targeting the Brain Reservoirs: Toward an HIV Cure." Front Immunol **7**: 397.

Marlink, R. (1996). "Lessons from the second AIDS virus, HIV-2." AIDS **10**(7): 689-699.

Marsden, M. D. (2020). "Benefits and limitations of humanized mice in HIV persistence studies." Retrovirology **17**(1): 7.

Martin, A. R., A. M. Bender, J. Hackman, K. J. Kwon, B. A. Lynch, D. Bruno, C. Martens, S. Beg, S. S. Florman, N. Desai, D. Segev, G. M. Laird, J. D. Siliciano, T. C. Quinn, A. A. R. Tobian, C. M. Durand, R. F. Siliciano and A. D. Redd (2021). "Similar Frequency and Inducibility of Intact Human Immunodeficiency Virus-1 Proviruses in Blood and Lymph Nodes." J Infect Dis **224**(2): 258-268.

Martin, N., S. Welsch, C. Jolly, J. A. Briggs, D. Vaux and Q. J. Sattentau (2010). "Virological synapse-mediated spread of human immunodeficiency virus type 1 between T cells is sensitive to entry inhibition." J Virol **84**(7): 3516-3527.

Martinez-Vicente, M., Z. Talloczy, E. Wong, G. Tang, H. Koga, S. Kaushik, R. de Vries, E. Arias, S. Harris, D. Sulzer and A. M. Cuervo (2010). "Cargo recognition failure is responsible for inefficient autophagy in Huntington's disease." Nat Neurosci **13**(5): 567-576.

Martinez, E., A. Mocroft, M. A. Garcia-Viejo, J. B. Perez-Cuevas, J. L. Blanco, J. Mallolas, L. Bianchi, I. Conget, J. Blanch, A. Phillips and J. M. Gatell (2001). "Risk of

lipodystrophy in HIV-1-infected patients treated with protease inhibitors: a prospective cohort study." Lancet **357**(9256): 592-598.

Masini, E., L. Giannini, S. Nistri, L. Cinci, R. Mastroianni, W. Xu, S. A. Comhair, D. Li, S. Cuzzocrea, G. M. Matuschak and D. Salvemini (2008). "Ceramide: a key signaling molecule in a Guinea pig model of allergic asthmatic response and airway inflammation." J Pharmacol Exp Ther **324**(2): 548-557.

Massanella, M., C. Yek, S. M. Lada, M. Nakazawa, N. Shefa, K. Huang and D. D. Richman (2018). "Improved assays to measure and characterize the inducible HIV reservoir." EBioMedicine **36**: 113-121.

Matesic, D. F., H. L. Rupp, W. J. Bonney, R. J. Ruch and J. E. Trosko (1994). "Changes in gap-junction permeability, phosphorylation, and number mediated by phorbol ester and non-phorbol-ester tumor promoters in rat liver epithelial cells." Mol Carcinog **10**(4): 226-236.

Mbonye, U. and J. Karn (2011). "Control of HIV latency by epigenetic and non-epigenetic mechanisms." Curr HIV Res **9**(8): 554-567.

McCutchan, F. E. (2006). "Global epidemiology of HIV." J Med Virol **78 Suppl 1**: S7-S12.

McMillen, J. C., J. A. Fincher, D. R. Klein, J. M. Spraggins and R. M. Caprioli (2020). "Effect of MALDI matrices on lipid analyses of biological tissues using MALDI-2 postionization mass spectrometry." J Mass Spectrom **55**(12): e4663.

McMillen, J. C., D. B. Gutierrez, A. M. Judd, J. M. Spraggins and R. M. Caprioli (2021). "Enhancement of Tryptic Peptide Signals from Tissue Sections Using MALDI IMS Postionization (MALDI-2)." J Am Soc Mass Spectrom **32**(10): 2583-2591.

McNally, G. A. (2019). "HIV and Cancer: An Overview of AIDS-Defining and Non-AIDS-Defining Cancers in Patients With HIV." Clin J Oncol Nurs **23**(3): 327-331.

Mencarelli, C. and P. Martinez-Martinez (2013). "Ceramide function in the brain: when a slight tilt is enough." Cell Mol Life Sci **70**(2): 181-203.

Menger, R. F., W. L. Stutts, D. S. Anbukumar, J. A. Bowden, D. A. Ford and R. A. Yost (2012). "MALDI mass spectrometric imaging of cardiac tissue following myocardial infarction in a rat coronary artery ligation model." Anal Chem **84**(2): 1117-1125.

Merrill, A. H., Jr., E. M. Schmelz, D. L. Dillehay, S. Spiegel, J. A. Shayman, J. J. Schroeder, R. T. Riley, K. A. Voss and E. Wang (1997). "Sphingolipids--the enigmatic lipid class: biochemistry, physiology, and pathophysiology." Toxicol Appl Pharmacol **142**(1): 208-225.

Mestre, A. L. G., M. Cerquido, P. M. C. Inacio, S. Asgarifar, A. S. Lourenco, M. L. S. Cristiano, P. Aguiar, M. C. R. Medeiros, I. M. Araujo, J. Ventura and H. L. Gomes (2017). "Ultrasensitive gold micro-structured electrodes enabling the detection of extra-cellular long-lasting potentials in astrocytes populations." Sci Rep **7**(1): 14284.

Mestre, A. L. G., P. M. C. Inacio, Y. Elamine, S. Asgarifar, A. S. Lourenco, M. L. S. Cristiano, P. Aguiar, M. C. R. Medeiros, I. M. Araujo, J. Ventura and H. L. Gomes (2017). "Extracellular Electrophysiological Measurements of Cooperative Signals in Astrocytes Populations." Front Neural Circuits **11**: 80.

Michalski, J. P., C. Anderson, A. Beauvais, Y. De Repentigny and R. Kothary (2011). "The proteolipid protein promoter drives expression outside of the oligodendrocyte lineage during embryonic and early postnatal development." PLoS One **6**(5): e19772.

Mikalsen, S. O. and O. Kaalhus (1996). "A characterization of pervanadate, an inducer of cellular tyrosine phosphorylation and inhibitor of gap junctional intercellular communication." Biochim Biophys Acta **1290**(3): 308-318.

Mitchell, B. I., E. I. Laws and L. C. Ndhlovu (2019). "Impact of Myeloid Reservoirs in HIV Cure Trials." Curr HIV/AIDS Rep **16**(2): 129-140.

Mocchetti, I., A. Bachis and V. Avdoshina (2012). "Neurotoxicity of human immunodeficiency virus-1: viral proteins and axonal transport." Neurotox Res **21**(1): 79-89.

Mohamed, M., P. B. Barker, R. L. Skolasky and N. Sacktor (2018). "7T Brain MRS in HIV Infection: Correlation with Cognitive Impairment and Performance on Neuropsychological Tests." AJNR Am J Neuroradiol **39**(4): 704-712.

Mohamed, M. A., P. B. Barker, R. L. Skolasky, O. A. Selnes, R. T. Moxley, M. G. Pomper and N. C. Sacktor (2010). "Brain metabolism and cognitive impairment in HIV infection: a 3-T magnetic resonance spectroscopy study." Magn Reson Imaging **28**(9): 1251-1257.

Mok, H. P. and A. M. Lever (2007). "Chromatin, gene silencing and HIV latency." Genome Biol **8**(11): 228.

Montesinos, J., C. Guardia-Laguarta and E. Area-Gomez (2020). "The fat brain." Curr Opin Clin Nutr Metab Care **23**(2): 68-75.

Moranguinho, I. and S. T. Valente (2020). "Block-And-Lock: New Horizons for a Cure for HIV-1." Viruses **12**(12).

Moreno-Castilla, P., L. F. Rodriguez-Duran, K. Guzman-Ramos, A. Barcenas-Femat, M. L. Escobar and F. Bermudez-Rattoni (2016). "Dopaminergic neurotransmission

dysfunction induced by amyloid-beta transforms cortical long-term potentiation into long-term depression and produces memory impairment." Neurobiol Aging **41**: 187-199.

Moreno, A. P., J. C. Saez, G. I. Fishman and D. C. Spray (1994). "Human connexin43 gap junction channels. Regulation of unitary conductances by phosphorylation." Circ Res **74**(6): 1050-1057.

Moss, A. R. and P. Bacchetti (1989). "Natural history of HIV infection." AIDS **3**(2): 55-61.

Mourez, T., F. Simon and J. C. Plantier (2013). "Non-M variants of human immunodeficiency virus type 1." Clin Microbiol Rev **26**(3): 448-461.

Mousseau, G., C. F. Kessing, R. Fromentin, L. Trautmann, N. Chomont and S. T. Valente (2015). "The Tat Inhibitor Didehydro-Cortistatin A Prevents HIV-1 Reactivation from Latency." mBio **6**(4): e00465.

Moyano, A. L., G. Li, A. Lopez-Rosas, J. E. Mansson, R. B. van Breemen and M. I. Givogri (2014). "Distribution of C16:0, C18:0, C24:1, and C24:0 sulfatides in central nervous system lipid rafts by quantitative ultra-high-pressure liquid chromatography tandem mass spectrometry." Anal Biochem **467**: 31-39.

Nadon, N. L. and M. West (1998). "Myelin proteolipid protein: function in myelin structure is distinct from its role in oligodendrocyte development." Dev Neurosci **20**(6): 533-539.

Nakagawa, F., M. May and A. Phillips (2013). "Life expectancy living with HIV: recent estimates and future implications." Curr Opin Infect Dis **26**(1): 17-25.

Nakamura, H. and T. Murayama (2014). "Role of sphingolipids in arachidonic acid metabolism." J Pharmacol Sci **124**(3): 307-312.

Nath, A. (2002). "Human immunodeficiency virus (HIV) proteins in neuropathogenesis of HIV dementia." J Infect Dis **186 Suppl 2**: S193-198.

Nedergaard, M., A. J. Cooper and S. A. Goldman (1995). "Gap junctions are required for the propagation of spreading depression." J Neurobiol **28**(4): 433-444.

Nekhai, S., M. Jerebtsova, A. Jackson and W. Southerland (2007). "Regulation of HIV-1 transcription by protein phosphatase 1." Curr HIV Res **5**(1): 3-9.

Nesbit, C. E. and S. A. Schwartz (2002). "In vitro and animal models of human immunodeficiency virus infection of the central nervous system." Clin Diagn Lab Immunol **9**(3): 515-524.

Newman, E. A. (2001). "Propagation of intercellular calcium waves in retinal astrocytes and Muller cells." J Neurosci **21**(7): 2215-2223.

Niehaus, M., J. Soltwisch, M. E. Belov and K. Dreisewerd (2019). "Transmission-mode MALDI-2 mass spectrometry imaging of cells and tissues at subcellular resolution." Nat Methods **16**(9): 925-931.

Nightingale, S., A. Winston, S. Letendre, B. D. Michael, J. C. McArthur, S. Khoo and T. Solomon (2014). "Controversies in HIV-associated neurocognitive disorders." Lancet Neurol **13**(11): 1139-1151.

Nodin, C., M. Nilsson and F. Blomstrand (2005). "Gap junction blockage limits intercellular spreading of astrocytic apoptosis induced by metabolic depression." J Neurochem **94**(4): 1111-1123.

Novakova, L., A. K. Singh, M. Axelsson, M. Stahlman, M. Adiels, C. Malmestrom, H. Zetterberg, J. Boren, J. Lycke, S. L. Cardell and M. Blomqvist (2018). "Sulfatide isoform pattern in cerebrospinal fluid discriminates progressive MS from relapsing-remitting MS." J Neurochem **146**(3): 322-332.

O'Brien, J. S. and E. L. Sampson (1965). "Fatty acid and fatty aldehyde composition of the major brain lipids in normal human gray matter, white matter, and myelin." J Lipid Res **6**(4): 545-551.

Oddo, S., A. Caccamo, J. D. Shepherd, M. P. Murphy, T. E. Golde, R. Kayed, R. Metherate, M. P. Mattson, Y. Akbari and F. M. LaFerla (2003). "Triple-transgenic model of Alzheimer's disease with plaques and tangles: intracellular Abeta and synaptic dysfunction." Neuron **39**(3): 409-421.

Okafo, G., L. Prevedel and E. Eugenin (2017). "Tunneling nanotubes (TNT) mediate long-range gap junctional communication: Implications for HIV cell to cell spread." Sci Rep **7**(1): 16660.

Okazaki, T., A. Bielawska, R. M. Bell and Y. A. Hannun (1990). "Role of ceramide as a lipid mediator of 1 alpha,25-dihydroxyvitamin D3-induced HL-60 cell differentiation." J Biol Chem **265**(26): 15823-15831.

Okoye, A. A., R. Fromentin, H. Takata, J. H. Brehm, Y. Fukazawa, B. Randall, M. Pardons, V. Tai, J. Tang, J. Smedley, M. Axthelm, J. D. Lifson, L. J. Picker, D. Favre, L. Trautmann and N. Chomont (2022). "The ingenol-based protein kinase C agonist GSK445A is a potent inducer of HIV and SIV RNA transcription." PLoS Pathog **18**(1): e1010245.

Oliveira, M. F., A. Chaillon, M. Nakazawa, M. Vargas, S. L. Letendre, M. C. Strain, R. J. Ellis, S. Morris, S. J. Little, D. M. Smith and S. Gianella (2017). "Early Antiretroviral Therapy Is Associated with Lower HIV DNA Molecular Diversity and Lower

Inflammation in Cerebrospinal Fluid but Does Not Prevent the Establishment of Compartmentalized HIV DNA Populations." PLoS Pathog **13**(1): e1006112.

Olsen, A. S. B. and N. J. Faergeman (2017). "Sphingolipids: membrane microdomains in brain development, function and neurological diseases." Open Biol **7**(5).

Orellana, J. A., J. C. Saez, M. V. Bennett, J. W. Berman, S. Morgello and E. A. Eugenin (2014). "HIV increases the release of dickkopf-1 protein from human astrocytes by a Cx43 hemichannel-dependent mechanism." J Neurochem **128**(5): 752-763.

Orellana, J. A., J. C. Saez, M. V. Bennett, J. W. Berman, S. Morgello and E. A. Eugenin (2014). "HIV increases the release of dickkopf-1 protein from human astrocytes by a Cx43 hemichannel-dependent mechanism." Journal of neurochemistry **128**(5): 752-763.

Ozturk, T., A. Kollhoff, A. M. Anderson, J. Christina Howell, D. W. Loring, D. Waldrop-Valverde, D. Franklin, S. Letendre, W. R. Tyor and W. T. Hu (2019). "Linked CSF reduction of phosphorylated tau and IL-8 in HIV associated neurocognitive disorder." Sci Rep **9**(1): 8733.

Pacholko, A. G., C. A. Wotton and L. K. Bekar (2020). "Astrocytes-The Ultimate Effectors of Long-Range Neuromodulatory Networks?" Front Cell Neurosci **14**: 581075.

Padmapriyadarsini, C., K. Ramesh, L. Sekar, G. Ramachandran, D. Reddy, G. Narendran, S. Sekar, C. Chandrasekar, D. Anbarasu, C. Wanke and S. Swaminathan (2017). "Factors affecting high-density lipoprotein cholesterol in HIV-infected patients on nevirapine-based antiretroviral therapy." Indian J Med Res **145**(5): 641-650.

Paine, M. R. L., J. Liu, D. Huang, S. R. Ellis, D. Trede, J. H. Kobarg, R. M. A. Heeren, F. M. Fernandez and T. J. MacDonald (2019). "Three-Dimensional Mass Spectrometry Imaging Identifies Lipid Markers of Medulloblastoma Metastasis." Sci Rep **9**(1): 2205.

Pak, V., T. T. Eifler, S. Jager, N. J. Krogan, K. Fujinaga and B. M. Peterlin (2015). "CDK11 in TREX/THOC Regulates HIV mRNA 3' End Processing." Cell Host Microbe **18**(5): 560-570.

Palacios-Prado, N., G. Hoge, A. Marandykina, L. Rimkute, S. Chapuis, N. Paulauskas, V. A. Skeberdis, J. O'Brien, A. E. Pereda, M. V. Bennett and F. F. Bukauskas (2013). "Intracellular magnesium-dependent modulation of gap junction channels formed by neuronal connexin36." J Neurosci **33**(11): 4741-4753.

Palaniyar, N., J. L. Semotok, D. D. Wood, M. A. Moscarello and G. Harauz (1998). "Human proteolipid protein (PLP) mediates winding and adhesion of phospholipid membranes but prevents their fusion." Biochim Biophys Acta **1415**(1): 85-100.

Palavicini, J. P., C. Wang, L. Chen, S. Ahmar, J. D. Higuera, J. L. Dupree and X. Han (2016). "Novel molecular insights into the critical role of sulfatide in myelin maintenance/function." J Neurochem **139**(1): 40-54.

Papuc, E. and K. Rejdak (2020). "The role of myelin damage in Alzheimer's disease pathology." Arch Med Sci **16**(2): 345-351.

Park, E. S., J. H. Lee, J. H. Hong, Y. K. Park, J. W. Lee, W. J. Lee, J. W. Lee, K. P. Kim and K. H. Kim (2014). "Phosphatidylcholine alteration identified using MALDI imaging MS in HBV-infected mouse livers and virus-mediated regeneration defects." PLoS One **9**(8): e103955.

Park, J. Y., M. H. Pillinger and S. B. Abramson (2006). "Prostaglandin E2 synthesis and secretion: the role of PGE2 synthases." Clin Immunol **119**(3): 229-240.

Patel, O., D. G. Pellicci, S. Gras, M. L. Sandoval-Romero, A. P. Uldrich, T. Mallevaey, A. J. Clarke, J. Le Nours, A. Theodossis, S. L. Cardell, L. Gapin, D. I. Godfrey and J. Rossjohn (2012). "Recognition of CD1d-sulfatide mediated by a type II natural killer T cell antigen receptor." Nat Immunol **13**(9): 857-863.

Pau, A. K. and J. M. George (2014). "Antiretroviral therapy: current drugs." Infect Dis Clin North Am **28**(3): 371-402.

Paulick, M. G. and C. R. Bertozzi (2008). "The glycosylphosphatidylinositol anchor: a complex membrane-anchoring structure for proteins." Biochemistry **47**(27): 6991-7000.

Perdomo-Celis, F., N. A. Taborda and M. T. Rugeles (2019). "CD8(+) T-Cell Response to HIV Infection in the Era of Antiretroviral Therapy." Front Immunol **10**: 1896.

Perea, G. and A. Araque (2005). "Glial calcium signaling and neuron-glia communication." Cell Calcium **38**(3-4): 375-382.

Perea, G. and A. Araque (2005). "Synaptic regulation of the astrocyte calcium signal." J Neural Transm (Vienna) **112**(1): 127-135.

Perez-Santiago, J., R. D. Schrier, M. F. de Oliveira, S. Gianella, S. R. Var, T. R. Day, M. Ramirez-Gaona, J. D. Suben, B. Murrell, M. Massanella, M. Cherner, D. M. Smith, R. J. Ellis, S. L. Letendre and S. R. Mehta (2016). "Cell-free mitochondrial DNA in CSF is associated with early viral rebound, inflammation, and severity of neurocognitive deficits in HIV infection." J Neurovirol **22**(2): 191-200.

Persaud, D., H. Gay, C. Ziemniak, Y. H. Chen, M. Piatak, Jr., T. W. Chun, M. Strain, D. Richman and K. Luzuriaga (2013). "Absence of detectable HIV-1 viremia after treatment cessation in an infant." N Engl J Med **369**(19): 1828-1835.

Petravic, J., T. A. Rasmussen, S. R. Lewin, S. J. Kent and M. P. Davenport (2017). "Relationship between Measures of HIV Reactivation and Decline of the Latent Reservoir under Latency-Reversing Agents." J Virol **91**(9).

Pidoux, G., P. Gerbaud, J. Dompierre, B. Lygren, T. Solstad, D. Evain-Brion and K. Tasken (2014). "A PKA-ezrin-Cx43 signaling complex controls gap junction communication and thereby trophoblast cell fusion." J Cell Sci **127**(Pt 19): 4172-4185.

Pinzone, M. R. and U. O'Doherty (2018). "Measuring integrated HIV DNA ex vivo and in vitro provides insights about how reservoirs are formed and maintained." Retrovirology **15**(1): 22.

Pitman, M. C., J. S. Y. Lau, J. H. McMahon and S. R. Lewin (2018). "Barriers and strategies to achieve a cure for HIV." Lancet HIV **5**(6): e317-e328.

Poitelon, Y., A. M. Kopec and S. Belin (2020). "Myelin Fat Facts: An Overview of Lipids and Fatty Acid Metabolism." Cells **9**(4).

Posse de Chaves, E. and S. Sipione (2010). "Sphingolipids and gangliosides of the nervous system in membrane function and dysfunction." FEBS Lett **584**(9): 1748-1759.

Potthoff, A., K. Dreisewerd and J. Soltwisch (2020). "Detailed Characterization of the Postionization Efficiencies in MALDI-2 as a Function of Relevant Input Parameters." J Am Soc Mass Spectrom **31**(9): 1844-1853.

Potthoff, A., O. Minte, K. Dreisewerd and J. Soltwisch (2022). "Effect of the Laser Pulse Width in MALDI-2: A Comparative Study of Picosecond versus Nanosecond Wide Pulses for Laser Postionization." J Am Soc Mass Spectrom **33**(2): 315-321.

Prevedel, L., C. Morocho, M. V. L. Bennett and E. A. Eugenin (2017). "HIV-Associated Cardiovascular Disease: Role of Connexin 43." Am J Pathol **187**(9): 1960-1970.

Prevedel, L., N. Ruel, P. Castellano, C. Smith, S. Malik, C. Villeux, M. Bomsel, S. Morgello and E. A. Eugenin (2019). "Identification, Localization, and Quantification of HIV Reservoirs Using Microscopy." Curr Protoc Cell Biol **82**(1): e64.

Prideaux, B., V. Dartois, D. Staab, D. M. Weiner, A. Goh, L. E. Via, C. E. Barry, 3rd and M. Stoeckli (2011). "High-sensitivity MALDI-MRM-MS imaging of moxifloxacin distribution in tuberculosis-infected rabbit lungs and granulomatous lesions." Anal Chem **83**(6): 2112-2118.

Prideaux, B., M. S. ElNaggar, M. Zimmerman, J. M. Wiseman, X. Li and V. Dartois (2015). "Mass spectrometry imaging of levofloxacin distribution in TB-infected pulmonary lesions by MALDI-MSI and continuous liquid microjunction surface sampling." Int J Mass Spectrom **377**: 699-708.

Prideaux, B. and M. Stoeckli (2012). "Mass spectrometry imaging for drug distribution studies." J Proteomics **75**(16): 4999-5013.

Prideaux, B., L. E. Via, M. D. Zimmerman, S. Eum, J. Sarathy, P. O'Brien, C. Chen, F. Kaya, D. M. Weiner, P. Y. Chen, T. Song, M. Lee, T. S. Shim, J. S. Cho, W. Kim, S. N. Cho, K. N. Olivier, C. E. Barry, 3rd and V. Dartois (2015). "The association between sterilizing activity and drug distribution into tuberculosis lesions." Nat Med **21**(10): 1223-1227.

Procopio, F. A., R. Fromentin, D. A. Kulpa, J. H. Brehm, A. G. Bebin, M. C. Strain, D. D. Richman, U. O'Doherty, S. Palmer, F. M. Hecht, R. Hoh, R. J. Barnard, M. D. Miller, D. J. Hazuda, S. G. Deeks, R. P. Sekaly and N. Chomont (2015). "A Novel Assay to Measure the Magnitude of the Inducible Viral Reservoir in HIV-infected Individuals." EBioMedicine **2**(8): 874-883.

Raasakka, A., S. Ruskamo, J. Kowal, R. Barker, A. Baumann, A. Martel, J. Tuusa, M. Myllykoski, J. Burck, A. S. Ulrich, H. Stahlberg and P. Kursula (2017). "Membrane Association Landscape of Myelin Basic Protein Portrays Formation of the Myelin Major Dense Line." Sci Rep **7**(1): 4974.

Raghu, P., A. Joseph, H. Krishnan, P. Singh and S. Saha (2019). "Phosphoinositides: Regulators of Nervous System Function in Health and Disease." Front Mol Neurosci **12**: 208.

Ralhan, I., C. L. Chang, J. Lippincott-Schwartz and M. S. Ioannou (2021). "Lipid droplets in the nervous system." J Cell Biol **220**(7).

Ramadan, S., A. Lin and P. Stanwell (2013). "Glutamate and glutamine: a review of in vivo MRS in the human brain." NMR Biomed **26**(12): 1630-1646.

Rao, A., D. Barkley, G. S. Franca and I. Yanai (2021). "Exploring tissue architecture using spatial transcriptomics." Nature **596**(7871): 211-220.

Rasmussen, T. A. and O. S. Sogaard (2018). "Clinical Interventions in HIV Cure Research." Adv Exp Med Biol **1075**: 285-318.

Real, F., C. Capron, A. Sennepin, R. Arrigucci, A. Zhu, G. Sannier, J. Zheng, L. Xu, J. M. Masse, S. Greffe, M. Cazabat, M. Donoso, P. Delobel, J. Izopet, E. Eugenin, M. L. Gennaro, E. Rouveix, E. Cramer Borde and M. Bomsel (2020). "Platelets from HIV-infected individuals on antiretroviral drug therapy with poor CD4(+) T cell recovery can harbor replication-competent HIV despite viral suppression." Sci Transl Med **12**(535).

Retamal, M. A., C. J. Cortes, L. Reuss, M. V. Bennett and J. C. Saez (2006). "S-nitrosylation and permeation through connexin 43 hemichannels in astrocytes: induction by oxidant stress and reversal by reducing agents." Proc Natl Acad Sci U S A **103**(12): 4475-4480.

Reza, S., M. Ugorski and J. Suchanski (2021). "Glucosylceramide and galactosylceramide, small glycosphingolipids with significant impact on health and disease." Glycobiology **31**(11): 1416-1434.

Rice, A. P. (2016). "Cyclin-dependent kinases as therapeutic targets for HIV-1 infection." Expert Opin Ther Targets **20**(12): 1453-1461.

Roberts, T. K., E. A. Eugenin, L. Lopez, I. A. Romero, B. B. Weksler, P. O. Couraud and J. W. Berman (2012). "CCL2 disrupts the adherens junction: implications for neuroinflammation." Lab Invest **92**(8): 1213-1233.

Rodriguez-Sinovas, A., M. Ruiz-Meana, A. Denuc and D. Garcia-Dorado (2018). "Mitochondrial Cx43, an important component of cardiac preconditioning." Biochim Biophys Acta Biomembr **1860**(1): 174-181.

Rosenthal, J. and W. Tyor (2019). "Aging, comorbidities, and the importance of finding biomarkers for HIV-associated neurocognitive disorders." J Neurovirol **25**(5): 673-685.

Roth, M. J., P. L. Schwartzberg and S. P. Goff (1989). "Structure of the termini of DNA intermediates in the integration of retroviral DNA: dependence on IN function and terminal DNA sequence." Cell **58**(1): 47-54.

Rumbaugh, J. A. and W. Tyor (2015). "HIV-associated neurocognitive disorders: Five new things." Neurol Clin Pract **5**(3): 224-231.

Russell, R. A., J. Chojnacki, D. M. Jones, E. Johnson, T. Do, C. Eggeling, S. Padilla-Parra and Q. J. Sattentau (2017). "Astrocytes Resist HIV-1 Fusion but Engulf Infected Macrophage Material." Cell Rep **18**(6): 1473-1483.

Sacktor, N., R. L. Skolasky, E. Seaberg, C. Munro, J. T. Becker, E. Martin, A. Ragin, A. Levine and E. Miller (2016). "Prevalence of HIV-associated neurocognitive disorders in the Multicenter AIDS Cohort Study." Neurology **86**(4): 334-340.

Saher, G., B. Brugger, C. Lappe-Siefke, W. Mobius, R. Tozawa, M. C. Wehr, F. Wieland, S. Ishibashi and K. A. Nave (2005). "High cholesterol level is essential for myelin membrane growth." Nat Neurosci **8**(4): 468-475.

Saher, G. and M. Simons (2010). "Cholesterol and myelin biogenesis." Subcell Biochem **51**: 489-508.

Saher, G. and S. K. Stumpf (2015). "Cholesterol in myelin biogenesis and hypomyelinating disorders." Biochim Biophys Acta **1851**(8): 1083-1094.

Sailasuta, N., W. Ross, J. Ananworanich, T. Chalermchai, V. DeGruttola, S. Lerdlum, M. Pothisri, E. Busovaca, S. Ratto-Kim, L. Jagodzinski, S. Spudich, N. Michael, J. H. Kim,

V. Valcour and R. S. p. teams (2012). "Change in brain magnetic resonance spectroscopy after treatment during acute HIV infection." PLoS One **7**(11): e49272.

Salantes, D. B., Y. Zheng, F. Mampe, T. Srivastava, S. Beg, J. Lai, J. Z. Li, R. L. Tressler, R. A. Koup, J. Hoxie, M. Abdel-Mohsen, S. Sherrill-Mix, K. McCormick, E. T. Overton, F. D. Bushman, G. H. Learn, R. F. Siliciano, J. M. Siliciano, P. Tebas and K. J. Bar (2018). "HIV-1 latent reservoir size and diversity are stable following brief treatment interruption." J Clin Invest **128**(7): 3102-3115.

Salemi, M. and B. Rife (2016). "Phylogenetics and Phyloanatomy of HIV/SIV Intra-Host Compartments and Reservoirs: The Key Role of the Central Nervous System." Curr HIV Res **14**(2): 110-120.

Sami Saribas, A., S. Cicalese, T. M. Ahooyi, K. Khalili, S. Amini and I. K. Sariyer (2017). "HIV-1 Nef is released in extracellular vesicles derived from astrocytes: evidence for Nef-mediated neurotoxicity." Cell death & disease **8**(1): e2542.

Samygina, V. R., A. N. Popov, A. Cabo-Bilbao, B. Ochoa-Lizarralde, F. Goni-de-Cerio, X. Zhai, J. G. Molotkovsky, D. J. Patel, R. E. Brown and L. Malinina (2011). "Enhanced selectivity for sulfatide by engineered human glycolipid transfer protein." Structure **19**(11): 1644-1654.

Sanford, R., B. M. Ances, D. J. Meyerhoff, R. W. Price, D. Fuchs, H. Zetterberg, S. Spudich and D. L. Collins (2018). "Longitudinal Trajectories of Brain Volume and Cortical Thickness in Treated and Untreated Primary Human Immunodeficiency Virus Infection." Clin Infect Dis **67**(11): 1697-1704.

Sanford, R., L. K. Fellows, B. M. Ances and D. L. Collins (2018). "Association of Brain Structure Changes and Cognitive Function With Combination Antiretroviral Therapy in HIV-Positive Individuals." JAMA Neurol **75**(1): 72-79.

Sanford, R., A. L. Fernandez Cruz, S. C. Scott, N. E. Mayo, L. K. Fellows, B. M. Ances and D. L. Collins (2017). "Regionally Specific Brain Volumetric and Cortical Thickness Changes in HIV-Infected Patients in the HAART Era." J Acquir Immune Defic Syndr **74**(5): 563-570.

Sanford, R., J. Strain, M. Dadar, J. Maranzano, A. Bonnet, N. E. Mayo, S. C. Scott, L. K. Fellows, B. M. Ances and D. L. Collins (2019). "HIV infection and cerebral small vessel disease are independently associated with brain atrophy and cognitive impairment." AIDS **33**(7): 1197-1205.

Santaella, A., H. B. Kuiperij, A. van Rumund, R. A. J. Esselink, B. R. Bloem and M. M. Verbeek (2020). "Cerebrospinal fluid myelin basic protein is elevated in multiple system atrophy." Parkinsonism Relat Disord **76**: 80-84.

Sathekge, M., A. McFarren and E. Dadachova (2014). "Role of nuclear medicine in neuroHIV: PET, SPECT, and beyond." Nucl Med Commun **35**(8): 792-796.

Saylor, D., A. M. Dickens, N. Sacktor, N. Haughey, B. Slusher, M. Pletnikov, J. L. Mankowski, A. Brown, D. J. Volsky and J. C. McArthur (2016). "HIV-associated neurocognitive disorder--pathogenesis and prospects for treatment." Nat Rev Neurol **12**(4): 234-248.

Saylor, D., A. M. Dickens, N. Sacktor, N. Haughey, B. Slusher, M. Pletnikov, J. L. Mankowski, A. Brown, D. J. Volsky and J. C. McArthur (2016). "HIV-associated neurocognitive disorder - pathogenesis and prospects for treatment." Nat Rev Neurol **12**(5): 309.

Scemes, E., R. Dermietzel and D. C. Spray (1998). "Calcium waves between astrocytes from Cx43 knockout mice." Glia **24**(1): 65-73.

Scheller, C., G. Arendt, T. Nolting, C. Antke, S. Sopper, M. Maschke, M. Obermann, A. Angerer, I. W. Husstedt, F. Meisner, E. Neuen-Jacob, H. W. Muller, P. Carey, V. Ter Meulen, P. Riederer and E. Koutsilieri (2010). "Increased dopaminergic neurotransmission in therapy-naive asymptomatic HIV patients is not associated with adaptive changes at the dopaminergic synapses." J Neural Transm (Vienna) **117**(6): 699-705.

Scheri, G. C., S. N. Fard, I. Schietroma, A. Mastrangelo, C. Pinacchio, N. Giustini, S. Serafino, G. De Girolamo, E. N. Cavallari, M. Statzu, L. Laghi, A. Vullo, G. Ceccarelli, V. Vullo and G. d'Ettorre (2017). "Modulation of Tryptophan/Serotonin Pathway by Probiotic Supplementation in Human Immunodeficiency Virus-Positive Patients: Preliminary Results of a New Study Approach." Int J Tryptophan Res **10**: 1178646917710668.

Schlaepfer, E. and R. F. Speck (2011). "TLR8 activates HIV from latently infected cells of myeloid-monocytic origin directly via the MAPK pathway and from latently infected CD4+ T cells indirectly via TNF-alpha." J Immunol **186**(7): 4314-4324.

Schmitt, S., L. C. Castelvetri and M. Simons (2015). "Metabolism and functions of lipids in myelin." Biochim Biophys Acta **1851**(8): 999-1005.

Schnaar, R. L., R. Gerardy-Schahn and H. Hildebrandt (2014). "Sialic acids in the brain: gangliosides and polysialic acid in nervous system development, stability, disease, and regeneration." Physiol Rev **94**(2): 461-518.

Schober, Y., S. Guenther, B. Spengler and A. Rompp (2012). "High-resolution matrix-assisted laser desorption/ionization imaging of tryptic peptides from tissue." Rapid Commun Mass Spectrom **26**(9): 1141-1146.

Schousboe, A. and H. S. Waagepetersen (2005). "Role of astrocytes in glutamate homeostasis: implications for excitotoxicity." Neurotox Res **8**(3-4): 221-225.

Schwamborn, K. and R. M. Caprioli (2010). "Molecular imaging by mass spectrometry--looking beyond classical histology." Nat Rev Cancer **10**(9): 639-646.

Schwartz, C., S. Bouchat, C. Marban, V. Gautier, C. Van Lint, O. Rohr and V. Le Douce (2017). "On the way to find a cure: Purging latent HIV-1 reservoirs." Biochem Pharmacol **146**: 10-22.

Sebode, M., J. Wigger, P. Filpe, L. Fischer, S. Weidemann, T. Krech, C. Weiler-Normann, M. Peiseler, J. Hartl, E. Tolosa, J. Herkel, C. Schramm, A. W. Lohse and P. Arrenberg (2019). "Inflammatory Phenotype of Intrahepatic Sulfatide-Reactive Type II NKT Cells in Humans With Autoimmune Hepatitis." Front Immunol **10**: 1065.

Seeley, E. H. and R. M. Caprioli (2008). "Molecular imaging of proteins in tissues by mass spectrometry." Proc Natl Acad Sci U S A **105**(47): 18126-18131.

Sengupta, S. and R. F. Siliciano (2018). "Targeting the Latent Reservoir for HIV-1." Immunity **48**(5): 872-895.

Shan, L., K. Deng, N. S. Shroff, C. M. Durand, S. A. Rabi, H. C. Yang, H. Zhang, J. B. Margolick, J. N. Blankson and R. F. Siliciano (2012). "Stimulation of HIV-1-specific cytolytic T lymphocytes facilitates elimination of latent viral reservoir after virus reactivation." Immunity **36**(3): 491-501.

Shan, L., H. C. Yang, S. A. Rabi, H. C. Bravo, N. S. Shroff, R. A. Irizarry, H. Zhang, J. B. Margolick, J. D. Siliciano and R. F. Siliciano (2011). "Influence of host gene transcription level and orientation on HIV-1 latency in a primary-cell model." J Virol **85**(11): 5384-5393.

Shanta, S. R., C. S. Choi, J. H. Lee, C. Y. Shin, Y. J. Kim, K. H. Kim and K. P. Kim (2012). "Global changes in phospholipids identified by MALDI MS in rats with focal cerebral ischemia." J Lipid Res **53**(9): 1823-1831.

Sharp, P. M. and B. H. Hahn (2011). "Origins of HIV and the AIDS pandemic." Cold Spring Harb Perspect Med **1**(1): a006841.

Shaw, G. M. and E. Hunter (2012). "HIV transmission." Cold Spring Harb Perspect Med **2**(11).

Shen, L. and R. F. Siliciano (2008). "Viral reservoirs, residual viremia, and the potential of highly active antiretroviral therapy to eradicate HIV infection." J Allergy Clin Immunol **122**(1): 22-28.

Shi, W., L. Zhou, X. Peng, H. Ren, Q. Wang, F. Shan, Z. Zhang, L. Liu and Y. Shi (2019). "HIV-infected patients with opportunistic pulmonary infections misdiagnosed as lung cancers: the clinicoradiologic features and initial application of CT radiomics." J Thorac Dis **11**(6): 2274-2286.

Shroff, S. M., A. D. Pomicter, W. N. Chow, M. A. Fox, R. J. Colello, S. C. Henderson and J. L. Dupree (2009). "Adult CST-null mice maintain an increased number of oligodendrocytes." J Neurosci Res **87**(15): 3403-3414.

Shugars, D. C., C. T. Wild, T. K. Greenwell and T. J. Matthews (1996). "Biophysical characterization of recombinant proteins expressing the leucine zipper-like domain of the human immunodeficiency virus type 1 transmembrane protein gp41." J Virol **70**(5): 2982-2991.

Siliciano, J. D., J. Kajdas, D. Finzi, T. C. Quinn, K. Chadwick, J. B. Margolick, C. Kovacs, S. J. Gange and R. F. Siliciano (2003). "Long-term follow-up studies confirm the stability of the latent reservoir for HIV-1 in resting CD4+ T cells." Nat Med **9**(6): 727-728.

Siliciano, J. D., J. Kajdas, D. Finzi, T. C. Quinn, K. Chadwick, J. B. Margolick, C. Kovacs, S. J. Gange and R. F. Siliciano (2003). "Long-term follow-up studies confirm the stability of the latent reservoir for HIV-1 in resting CD4+ T cells." Nature medicine **9**(6): 727-728.

Siliciano, J. D. and R. F. Siliciano (2018). "Assays to Measure Latency, Reservoirs, and Reactivation." Curr Top Microbiol Immunol **417**: 23-41.

Siliciano, R. F. and W. C. Greene (2011). "HIV latency." Cold Spring Harb Perspect Med **1**(1): a007096.

Simard, M., G. Arcuino, T. Takano, Q. S. Liu and M. Nedergaard (2003). "Signaling at the gliovascular interface." J Neurosci **23**(27): 9254-9262.

Simon, F., P. Mauclere, P. Roques, I. Loussert-Ajaka, M. C. Muller-Trutwin, S. Saragosti, M. C. Georges-Courbot, F. Barre-Sinoussi and F. Brun-Vezinet (1998). "Identification of a new human immunodeficiency virus type 1 distinct from group M and group O." Nat Med **4**(9): 1032-1037.

Simons, M., E. M. Kramer, C. Thiele, W. Stoffel and J. Trotter (2000). "Assembly of myelin by association of proteolipid protein with cholesterol- and galactosylceramide-rich membrane domains." J Cell Biol **151**(1): 143-154.

Sinxadi, P. Z., S. H. Khoo and M. Boffito (2021). "Pharmacokinetic interactions of modern antiretroviral therapy." AIDS **35**(Suppl 2): S145-S151.

Slovin, S., A. Carissimo, F. Panariello, A. Grimaldi, V. Bouche, G. Gambardella and D. Cacchiarelli (2021). "Single-Cell RNA Sequencing Analysis: A Step-by-Step Overview." Methods Mol Biol **2284**: 343-365.

Smith, J. A., J. Yeung, G. D. Kao and R. Daniel (2010). "A role for the histone deacetylase HDAC4 in the life-cycle of HIV-1-based vectors." Virol J **7**: 237.

Soltwisch, J., B. Heijs, A. Koch, S. Vens-Cappell, J. Hohndorf and K. Dreisewerd (2020). "MALDI-2 on a Trapped Ion Mobility Quadrupole Time-of-Flight Instrument for Rapid Mass Spectrometry Imaging and Ion Mobility Separation of Complex Lipid Profiles." Anal Chem **92**(13): 8697-8703.

Soltwisch, J., T. W. Jaskolla and K. Dreisewerd (2013). "Color matters--material ejection and ion yields in UV-MALDI mass spectrometry as a function of laser wavelength and laser fluence." J Am Soc Mass Spectrom **24**(10): 1477-1488.

Soltwisch, J., H. Kettling, S. Vens-Cappell, M. Wiegelmann, J. Muthing and K. Dreisewerd (2015). "Mass spectrometry imaging with laser-induced postionization." Science **348**(6231): 211-215.

Sonnino, S., M. Aureli, L. Mauri, M. G. Ciampa and A. Prinetti (2015). "Membrane lipid domains in the nervous system." Front Biosci (Landmark Ed) **20**(2): 280-302.

Sontheimer, H. (1994). "Voltage-dependent ion channels in glial cells." Glia **11**(2): 156-172.

Sontheimer, H., E. Fernandez-Marques, N. Ullrich, C. A. Pappas and S. G. Waxman (1994). "Astrocyte Na+ channels are required for maintenance of Na+/K(+)-ATPase activity." J Neurosci **14**(5 Pt 1): 2464-2475.

Sonti, S., A. L. Sharma and M. Tyagi (2021). "HIV-1 persistence in the CNS: Mechanisms of latency, pathogenesis and an update on eradication strategies." Virus Res **303**: 198523.

Sorgen, P. L., A. J. Trease, G. Spagnol, M. Delmar and M. S. Nielsen (2018). "Protein(-)Protein Interactions with Connexin 43: Regulation and Function." Int J Mol Sci **19**(5).

Sorstedt, E., S. Nilsson, A. Blaxhult, M. Gisslen, L. Flamholc, A. Sonnerborg and A. Yilmaz (2016). "Viral blips during suppressive antiretroviral treatment are associated with high baseline HIV-1 RNA levels." BMC Infect Dis **16**: 305.

Souza, S. J., L. A. Luzia, S. S. Santos and P. H. Rondo (2013). "Lipid profile of HIV-infected patients in relation to antiretroviral therapy: a review." Rev Assoc Med Bras (1992) **59**(2): 186-198.

Sparvero, L. J., A. A. Amoscato, C. E. Dixon, J. B. Long, P. M. Kochanek, B. R. Pitt, H. Bayir and V. E. Kagan (2012). "Mapping of phospholipids by MALDI imaging (MALDI-MSI): realities and expectations." Chem Phys Lipids **165**(5): 545-562.

Spector, C., A. R. Mele, B. Wigdahl and M. R. Nonnemacher (2019). "Genetic variation and function of the HIV-1 Tat protein." Medical microbiology and immunology **208**(2): 131-169.

Stax, A. M., J. Tuengel, E. Girardi, N. Kitano, L. L. Allan, V. Liu, D. Zheng, W. J. Panenka, J. Guillaume, C. H. Wong, S. van Calenbergh, D. M. Zajonc and P. van den Elzen (2017). "Autoreactivity to Sulfatide by Human Invariant NKT Cells." J Immunol **199**(1): 97-106.

Stein, J., M. Storcksdieck Genannt Bonsmann and H. Streeck (2016). "Barriers to HIV Cure." HLA **88**(4): 155-163.

Stevens, L. M. and R. E. Brown (2015). "Reference and working memory deficits in the 3xTg-AD mouse between 2 and 15-months of age: a cross-sectional study." Behav Brain Res **278**: 496-505.

Stoffel, W. and A. Bosio (1997). "Myelin glycolipids and their functions." Curr Opin Neurobiol **7**(5): 654-661.

Strain, J. F., T. H. Burdo, S. K. Song, P. Sun, O. El-Ghazzawy, B. Nelson, E. Westerhaus, L. Baker, F. Vaida and B. M. Ances (2017). "Diffusion Basis Spectral Imaging Detects Ongoing Brain Inflammation in Virologically Well-Controlled HIV+ Patients." J Acquir Immune Defic Syndr **76**(4): 423-430.

Strain, M. C. and D. D. Richman (2013). "New assays for monitoring residual HIV burden in effectively treated individuals." Curr Opin HIV AIDS **8**(2): 106-110.

Straub, A. C., M. Billaud, S. R. Johnstone, A. K. Best, S. Yemen, S. T. Dwyer, R. Looft-Wilson, J. J. Lysiak, B. Gaston, L. Palmer and B. E. Isakson (2011). "Compartmentalized connexin 43 s-nitrosylation/denitrosylation regulates heterocellular communication in the vessel wall." Arterioscler Thromb Vasc Biol **31**(2): 399-407.

Su, H., Y. Cheng, S. Sravanam, S. Mathews, S. Gorantla, L. Y. Poluektova, P. K. Dash and H. E. Gendelman (2019). "Immune Activations and Viral Tissue Compartmentalization During Progressive HIV-1 Infection of Humanized Mice." Frontiers in immunology **10**: 340.

Su, T., F. W. Wit, M. W. Caan, J. Schouten, M. Prins, G. J. Geurtsen, J. H. Cole, D. J. Sharp, E. Richard, L. Reneman, P. Portegies, P. Reiss, C. B. Majoie and A. G. C. Study (2016). "White matter hyperintensities in relation to cognition in HIV-infected men with sustained suppressed viral load on combination antiretroviral therapy." AIDS **30**(15): 2329-2339.

Subczynski, W. K., M. Pasenkiewicz-Gierula, J. Widomska, L. Mainali and M. Raguz (2017). "High Cholesterol/Low Cholesterol: Effects in Biological Membranes: A Review." Cell Biochem Biophys **75**(3-4): 369-385.

Suminaite, D., D. A. Lyons and M. R. Livesey (2019). "Myelinated axon physiology and regulation of neural circuit function." Glia **67**(11): 2050-2062.

Sundquist, W. I. and H. G. Krausslich (2012). "HIV-1 assembly, budding, and maturation." Cold Spring Harb Perspect Med **2**(7): a006924.

Sunshine, H. and M. L. Iruela-Arispe (2017). "Membrane lipids and cell signaling." Curr Opin Lipidol **28**(5): 408-413.

Suzuki, K., A. Levert, J. Yeung, M. Starr, J. Cameron, R. Williams, N. Rismanto, T. Stark, D. Druery, S. Prasad, C. Ferrarini, I. Hanafi, L. P. McNally, P. Cunningham, Z. Liu, T. Ishida, C. S. Huang, V. Oswald, L. Evans, G. Symonds, B. J. Brew and J. Zaunders (2021). "HIV-1 viral blips are associated with repeated and increasingly high levels of cell-associated HIV-1 RNA transcriptional activity." AIDS **35**(13): 2095-2103.

Svensson, J., M. Blomqvist, P. Kettunen, C. Eckerstrom, M. Henricsson, M. Jonsson, M. Bjerke, J. E. Mansson and A. Wallin (2021). "Cerebrospinal Fluid Sulfatide Levels Lack Diagnostic Utility in the Subcortical Small Vessel Type of Dementia." J Alzheimers Dis **82**(2): 781-790.

Svicher, V., F. Ceccherini-Silberstein, A. Antinori, S. Aquaro and C. F. Perno (2014). "Understanding HIV compartments and reservoirs." Curr HIV/AIDS Rep **11**(2): 186-194.

Takahashi, T., K. Ito, K. Fukushima, M. Takaguchi, T. Hayakawa, Y. Suzuki and T. Suzuki (2012). "Sulfatide negatively regulates the fusion process of human parainfluenza virus type 3." J Biochem **152**(4): 373-380.

Takahashi, T. and T. Suzuki (2012). "Role of sulfatide in normal and pathological cells and tissues." J Lipid Res **53**(8): 1437-1450.

Takahashi, T. and T. Suzuki (2015). "Role of sulfatide in influenza A virus replication." Biol Pharm Bull **38**(6): 809-816.

Takahashi, T., M. Takaguchi, T. Kawakami and T. Suzuki (2013). "Sulfatide regulates caspase-3-independent apoptosis of influenza A virus through viral PB1-F2 protein." PLoS One **8**(4): e61092.

Takano, T., G. F. Tian, W. Peng, N. Lou, W. Libionka, X. Han and M. Nedergaard (2006). "Astrocyte-mediated control of cerebral blood flow." Nat Neurosci **9**(2): 260-267.

Talaveron, R., E. R. Matarredona, A. Herrera, J. M. Medina and A. Tabernero (2020). "Connexin43 Region 266-283, via Src Inhibition, Reduces Neural Progenitor Cell

Proliferation Promoted by EGF and FGF-2 and Increases Astrocytic Differentiation." Int J Mol Sci **21**(22).

Tan, M., H. Luo, S. Lee, F. Jin, J. S. Yang, E. Montellier, T. Buchou, Z. Cheng, S. Rousseaux, N. Rajagopal, Z. Lu, Z. Ye, Q. Zhu, J. Wysocka, Y. Ye, S. Khochbin, B. Ren and Y. Zhao (2011). "Identification of 67 histone marks and histone lysine crotonylation as a new type of histone modification." Cell **146**(6): 1016-1028.

Tan, N. K., D. Carrington and C. F. Pope (2018). "Verification of the Roche cobas((R)) 6800 PCR 200 microl and 500 microl protocols for the quantification of HIV-1 RNA, HBV DNA and HCV RNA and evaluation with COBAS((R)) Ampliprep/COBAS((R)) TaqMan((R)) assays." J Med Microbiol **67**(12): 1711-1717.

Taylor, B. S., H. V. Tieu, J. Jones and T. J. Wilkin (2019). "CROI 2019: advances in antiretroviral therapy." Top Antivir Med **27**(1): 50-68.

Tedaldi, E. M., N. L. Minniti and T. Fischer (2015). "HIV-associated neurocognitive disorders: the relationship of HIV infection with physical and social comorbidities." Biomed Res Int **2015**: 641913.

Teixeira, V., P. Maciel and V. Costa (2021). "Leading the way in the nervous system: Lipid Droplets as new players in health and disease." Biochim Biophys Acta Mol Cell Biol Lipids **1866**(1): 158820.

Tekeste, S. S., T. A. Wilkinson, E. M. Weiner, X. Xu, J. T. Miller, S. F. Le Grice, R. T. Clubb and S. A. Chow (2015). "Interaction between Reverse Transcriptase and Integrase Is Required for Reverse Transcription during HIV-1 Replication." J Virol **89**(23): 12058-12069.

Thevenin, A. F., T. J. Kowal, J. T. Fong, R. M. Kells, C. G. Fisher and M. M. Falk (2013). "Proteins and mechanisms regulating gap-junction assembly, internalization, and degradation." Physiology (Bethesda) **28**(2): 93-116.

Thevenin, A. F., R. A. Margraf, C. G. Fisher, R. M. Kells-Andrews and M. M. Falk (2017). "Phosphorylation regulates connexin43/ZO-1 binding and release, an important step in gap junction turnover." Mol Biol Cell **28**(25): 3595-3608.

Thomas, T., K. Jordan, J. Simek, Q. Shao, C. Jedeszko, P. Walton and D. W. Laird (2005). "Mechanisms of Cx43 and Cx26 transport to the plasma membrane and gap junction regeneration." J Cell Sci **118**(Pt 19): 4451-4462.

Thompson, K. A., C. L. Cherry, J. E. Bell and C. A. McLean (2011). "Brain cell reservoirs of latent virus in presymptomatic HIV-infected individuals." Am J Pathol **179**(4): 1623-1629.

Timilsina, U. and R. Gaur (2016). "Modulation of apoptosis and viral latency - an axis to be well understood for successful cure of human immunodeficiency virus." J Gen Virol **97**(4): 813-824.

Tomaras, G. D. and B. F. Haynes (2009). "HIV-1-specific antibody responses during acute and chronic HIV-1 infection." Curr Opin HIV AIDS **4**(5): 373-379.

Torkzaban, B., T. Mohseni Ahooyi, M. Duggan, S. Amini and K. Khalili (2020). "Cross-talk between lipid homeostasis and endoplasmic reticulum stress in neurodegeneration: Insights for HIV-1 associated neurocognitive disorders (HAND)." Neurochem Int **141**: 104880.

Trentalange, A., A. Prochet, D. Imperiale, J. Cusato, M. Tettoni, G. Nunnari, A. Barco, S. Bonora, G. Di Perri and A. Calcagno (2020). "Cerebral white matter Hyperintensities in HIV-positive patients." Brain Imaging Behav **14**(1): 10-18.

Tripathy, M. K., M. E. McManamy, B. D. Burch, N. M. Archin and D. M. Margolis (2015). "H3K27 Demethylation at the Proviral Promoter Sensitizes Latent HIV to the Effects of Vorinostat in Ex Vivo Cultures of Resting CD4+ T Cells." J Virol **89**(16): 8392-8405.

Tsai, M. T., S. Lee, I. C. Lu, K. Y. Chu, C. W. Liang, C. H. Lee, Y. T. Lee and C. K. Ni (2013). "Ion-to-neutral ratio of 2,5-dihydroxybenzoic acid in matrix-assisted laser desorption/ionization." Rapid Commun Mass Spectrom **27**(9): 955-963.

Tseng, A., C. A. Hughes, J. Wu, J. Seet and E. J. Phillips (2017). "Cobicistat Versus Ritonavir: Similar Pharmacokinetic Enhancers But Some Important Differences." Ann Pharmacother **51**(11): 1008-1022.

Turner, A. W. and D. M. Margolis (2017). "Chromatin Regulation and the Histone Code in HIV Latency." Yale J Biol Med **90**(2): 229-243.

Turner, B. G. and M. F. Summers (1999). "Structural biology of HIV." J Mol Biol **285**(1): 1-32.

Underwood, J., J. H. Cole, M. Caan, D. De Francesco, R. Leech, R. A. van Zoest, T. Su, G. J. Geurtsen, B. A. Schmand, P. Portegies, M. Prins, F. Wit, C. A. Sabin, C. Majoie, P. Reiss, A. Winston, D. J. Sharp and A. C. Comorbidity in Relation to (2017). "Gray and White Matter Abnormalities in Treated Human Immunodeficiency Virus Disease and Their Relationship to Cognitive Function." Clin Infect Dis **65**(3): 422-432.

Urbanelli, L., S. Buratta, B. Tancini, K. Sagini, F. Delo, S. Porcellati and C. Emiliani (2019). "The Role of Extracellular Vesicles in Viral Infection and Transmission." Vaccines (Basel) **7**(3).

Valcour, V. G., J. Ananworanich, M. Agsalda, N. Sailasuta, T. Chalermchai, A. Schuetz, C. Shikuma, C. Y. Liang, S. Jirajariyavej, P. Sithinamsuwan, S. Tipsuk, D. B. Clifford, R. Paul, J. L. Fletcher, M. A. Marovich, B. M. Slike, V. DeGruttola, B. Shiramizu and S. P. Team (2013). "HIV DNA reservoir increases risk for cognitive disorders in cART-naive patients." PLoS One **8**(7): e70164.

Valdebenito, S., P. Castellano, D. Ajasin and E. A. Eugenin (2021). "Astrocytes are HIV reservoirs in the brain: A cell type with poor HIV infectivity and replication but efficient cell-to-cell viral transfer." J Neurochem.

Valdebenito, S., P. Castellano, D. Ajasin and E. A. Eugenin (2021). "Astrocytes are HIV reservoirs in the brain: A cell type with poor HIV infectivity and replication but efficient cell-to-cell viral transfer." J Neurochem **158**(2): 429-443.

Vallari, A., V. Holzmayer, B. Harris, J. Yamaguchi, C. Ngansop, F. Makamche, D. Mbanya, L. Kaptue, N. Ndembi, L. Gurtler, S. Devare and C. A. Brennan (2011). "Confirmation of putative HIV-1 group P in Cameroon." J Virol **85**(3): 1403-1407.

Van Zijl, P. C. and P. B. Barker (1997). "Magnetic resonance spectroscopy and spectroscopic imaging for the study of brain metabolism." Ann N Y Acad Sci **820**: 75-96.

van Zoest, R. A., J. Underwood, D. De Francesco, C. A. Sabin, J. H. Cole, F. W. Wit, M. W. A. Caan, N. A. Kootstra, D. Fuchs, H. Zetterberg, C. Majoie, P. Portegies, A. Winston, D. J. Sharp, M. Gisslen, P. Reiss and A. C. Comorbidity in Relation to (2017). "Structural Brain Abnormalities in Successfully Treated HIV Infection: Associations With Disease and Cerebrospinal Fluid Biomarkers." J Infect Dis **217**(1): 69-81.

Vance, J. E. and R. Steenbergen (2005). "Metabolism and functions of phosphatidylserine." Prog Lipid Res **44**(4): 207-234.

Vanhamel, J., A. Bruggemans and Z. Debyser (2019). "Establishment of latent HIV-1 reservoirs: what do we really know?" J Virus Erad **5**(1): 3-9.

Vansant, G., A. Bruggemans, J. Janssens and Z. Debyser (2020). "Block-And-Lock Strategies to Cure HIV Infection." Viruses **12**(1).

Vassall, K. A., V. V. Bamm and G. Harauz (2015). "MyelStones: the executive roles of myelin basic protein in myelin assembly and destabilization in multiple sclerosis." Biochem J **472**(1): 17-32.

Vassallo, M., B. Dunais, J. Durant, H. Carsenti-Dellamonica, A. Harvey-Langton, J. Cottalorda, M. Ticchioni, M. Laffon, C. Lebrun-Frenay, P. Dellamonica and C. Pradier (2013). "Relevance of lipopolysaccharide levels in HIV-associated neurocognitive impairment: the Neuradapt study." J Neurovirol **19**(4): 376-382.

Vastag, Z., O. Fira-Mladinescu and E. C. Rosca (2022). "HIV-Associated Neurocognitive Disorder (HAND): Obstacles to Early Neuropsychological Diagnosis." Int J Gen Med **15**: 4079-4090.

Vejar, S., J. E. Oyarzun, M. A. Retamal, F. C. Ortiz and J. A. Orellana (2019). "Connexin and Pannexin-Based Channels in Oligodendrocytes: Implications in Brain Health and Disease." Front Cell Neurosci **13**: 3.

Velasquez, S., L. Prevedel, S. Valdebenito, A. M. Gorska, M. Golovko, N. Khan, J. Geiger and E. A. Eugenin (2020). "Circulating levels of ATP is a biomarker of HIV cognitive impairment." EBioMedicine **51**: 102503.

Ventura, R. and K. M. Harris (1999). "Three-dimensional relationships between hippocampal synapses and astrocytes." J Neurosci **19**(16): 6897-6906.

Vigneswaran, S., J. H. Rojas, L. Garvey, S. Taylor-Robinson and A. Winston (2015). "Differences in the variability of cerebral proton magnetic resonance spectroscopy (1H-MRS) measurements within three HIV-infected cohorts." Neuroradiol J **28**(6): 545-554.

Villanelo, F., Y. Escalona, C. Pareja-Barrueto, J. A. Garate, I. M. Skerrett and T. Perez-Acle (2017). "Accessing gap-junction channel structure-function relationships through molecular modeling and simulations." BMC Cell Biol **18**(Suppl 1): 5.

Visseaux, B., F. Damond, S. Matheron, D. Descamps and C. Charpentier (2016). "Hiv-2 molecular epidemiology." Infect Genet Evol **46**: 233-240.

Wadhwa, P., P. Jain, S. Rudrawar and H. R. A. Jadhav (2018). "Quinoline, Coumarin and Other Heterocyclic Analogs Based HIV-1 Integrase Inhibitors." Current drug discovery technologies **15**(1): 2-19.

Wagner, C. A., P. J. Roque, T. R. Mileur, D. Liggitt and J. M. Goverman (2020). "Myelin-specific CD8+ T cells exacerbate brain inflammation in CNS autoimmunity." J Clin Invest **130**(1): 203-213.

Wall, M. E., C. Otey, J. Qi and A. J. Banes (2007). "Connexin 43 is localized with actin in tenocytes." Cell Motil Cytoskeleton **64**(2): 121-130.

Wallace, D. R. (2006). "HIV neurotoxicity: potential therapeutic interventions." J Biomed Biotechnol **2006**(3): 65741.

Wallet, C., M. De Rovere, J. Van Assche, F. Daouad, S. De Wit, V. Gautier, P. W. G. Mallon, A. Marcello, C. Van Lint, O. Rohr and C. Schwartz (2019). "Microglial Cells: The Main HIV-1 Reservoir in the Brain." Front Cell Infect Microbiol **9**: 362.

Wan, J., H. Liu, J. Chu and H. Zhang (2019). "Functions and mechanisms of lysine crotonylation." J Cell Mol Med **23**(11): 7163-7169.

Wang, G. J., L. Chang, N. D. Volkow, F. Telang, J. Logan, T. Ernst and J. S. Fowler (2004). "Decreased brain dopaminergic transporters in HIV-associated dementia patients." Brain **127**(Pt 11): 2452-2458.

Wang, J., Y. Zhang, Q. Xu, J. Qiu, H. Zheng, X. Ye, Y. Xue, Y. Yin, Z. Zhang, Y. Liu, Y. Hao, Q. Wei, W. Wang, K. Mori, S. Izumo, R. Kubota, Y. Shao and H. Q. Xing (2017). "Menin mediates Tat-induced neuronal apoptosis in brain frontal cortex of SIV-infected macaques and in Tat-treated cells." Oncotarget **8**(11): 18082-18094.

Wang, K. K., Z. Yang, T. Zhu, Y. Shi, R. Rubenstein, J. A. Tyndall and G. T. Manley (2018). "An update on diagnostic and prognostic biomarkers for traumatic brain injury." Expert Rev Mol Diagn **18**(2): 165-180.

Wang, X., N. Lou, Q. Xu, G. F. Tian, W. G. Peng, X. Han, J. Kang, T. Takano and M. Nedergaard (2006). "Astrocytic Ca2+ signaling evoked by sensory stimulation in vivo." Nat Neurosci **9**(6): 816-823.

Wang, X. and H. Xu (2021). "Residual Proviral Reservoirs: A High Risk for HIV Persistence and Driving Forces for Viral Rebound after Analytical Treatment Interruption." Viruses **13**(2).

Wang, Y., M. Liu, Q. Lu, M. Farrell, J. M. Lappin, J. Shi, L. Lu and Y. Bao (2020). "Global prevalence and burden of HIV-associated neurocognitive disorder: A meta-analysis." Neurology **95**(19): e2610-e2621.

Wang, Z., F. R. Simonetti, R. F. Siliciano and G. M. Laird (2018). "Measuring replication competent HIV-1: advances and challenges in defining the latent reservoir." Retrovirology **15**(1): 21.

Wang, Z., M. Tymianski, O. T. Jones and M. Nedergaard (1997). "Impact of cytoplasmic calcium buffering on the spatial and temporal characteristics of intercellular calcium signals in astrocytes." J Neurosci **17**(19): 7359-7371.

Waters, D. D. and P. Y. Hsue (2019). "Lipid Abnormalities in Persons Living With HIV Infection." Can J Cardiol **35**(3): 249-259.

Wenzel, E. D., A. Bachis, V. Avdoshina, F. Taraballi, E. Tasciotti and I. Mocchetti (2017). "Endocytic Trafficking of HIV gp120 is Mediated by Dynamin and Plays a Role in gp120 Neurotoxicity." Journal of neuroimmune pharmacology : the official journal of the Society on NeuroImmune Pharmacology **12**(3): 492-503.

Williams, C. R., L. Chen, E. S. Sheppard, P. Chopra, J. Locklin, G. J. Boons and D. C. Krause (2020). "Distinct Mycoplasma pneumoniae Interactions with Sulfated and Sialylated Receptors." Infect Immun **88**(11).

Williams, D. W., E. A. Eugenin, T. M. Calderon and J. W. Berman (2012). "Monocyte maturation, HIV susceptibility, and transmigration across the blood brain barrier are critical in HIV neuropathogenesis." J Leukoc Biol **91**(3): 401-415.

Williams, D. W., M. Veenstra, P. J. Gaskill, S. Morgello, T. M. Calderon and J. W. Berman (2014). "Monocytes mediate HIV neuropathogenesis: mechanisms that contribute to HIV associated neurocognitive disorders." Curr HIV Res **12**(2): 85-96.

Winzeler, A. M., W. J. Mandemakers, M. Z. Sun, M. Stafford, C. T. Phillips and B. A. Barres (2011). "The lipid sulfatide is a novel myelin-associated inhibitor of CNS axon outgrowth." J Neurosci **31**(17): 6481-6492.

Woldemeskel, B. A., A. K. Kwaa and J. N. Blankson (2020). "Viral reservoirs in elite controllers of HIV-1 infection: Implications for HIV cure strategies." EBioMedicine **62**: 103118.

Wong, J. K. and S. A. Yukl (2016). "Tissue reservoirs of HIV." Curr Opin HIV AIDS **11**(4): 362-370.

Wong, L. M. and G. Jiang (2021). "NF-kappaB sub-pathways and HIV cure: A revisit." EBioMedicine **63**: 103159.

Wood, B. R. (2019). "Switching Antiretroviral Therapy in the Setting of Virologic Suppression: A Why and How-To Guide." Infect Dis Clin North Am **33**(3): 693-705.

Woods, S. P., J. D. Rippeth, A. B. Frol, J. K. Levy, E. Ryan, V. M. Soukup, C. H. Hinkin, D. Lazzaretto, M. Cherner, T. D. Marcotte, B. B. Gelman, S. Morgello, E. J. Singer, I. Grant and R. K. Heaton (2004). "Interrater reliability of clinical ratings and neurocognitive diagnoses in HIV." J Clin Exp Neuropsychol **26**(6): 759-778.

Wright, P. W., J. M. Heaps, J. S. Shimony, J. B. Thomas and B. M. Ances (2012). "The effects of HIV and combination antiretroviral therapy on white matter integrity." AIDS **26**(12): 1501-1508.

Xicota, L., F. Ichou, F. X. Lejeune, B. Colsch, A. Tenenhaus, I. Leroy, G. Fontaine, M. Lhomme, H. Bertin, M. O. Habert, S. Epelbaum, B. Dubois, F. Mochel, M. C. Potier and I. s. group (2019). "Multi-omics signature of brain amyloid deposition in asymptomatic individuals at-risk for Alzheimer's disease: The INSIGHT-preAD study." EBioMedicine **47**: 518-528.

Xu, L. and M. C. Desai (2009). "Pharmacokinetic enhancers for HIV drugs." Curr Opin Investig Drugs **10**(8): 775-786.

Yamada, E., R. Yoshikawa, Y. Nakano, N. Misawa, Y. Koyanagi and K. Sato (2015). "Impacts of humanized mouse models on the investigation of HIV-1 infection: illuminating the roles of viral accessory proteins in vivo." Viruses **7**(3): 1373-1390.

Yamauchi, H., H. Fukuyama, Y. Nagahama, Y. Katsumi, T. Hayashi, C. Oyanagi, J. Konishi and H. Shio (2000). "Comparison of the pattern of atrophy of the corpus callosum in frontotemporal dementia, progressive supranuclear palsy, and Alzheimer's disease." J Neurol Neurosurg Psychiatry **69**(5): 623-629.

Yang, H. C., S. Xing, L. Shan, K. O'Connell, J. Dinoso, A. Shen, Y. Zhou, C. K. Shrum, Y. Han, J. O. Liu, H. Zhang, J. B. Margolick and R. F. Siliciano (2009). "Small-molecule screening using a human primary cell model of HIV latency identifies compounds that reverse latency without cellular activation." J Clin Invest **119**(11): 3473-3486.

Yang, S. H., J. P. Lee, H. R. Jang, R. H. Cha, S. S. Han, U. S. Jeon, D. K. Kim, J. Song, D. S. Lee and Y. S. Kim (2011). "Sulfatide-reactive natural killer T cells abrogate ischemia-reperfusion injury." J Am Soc Nephrol **22**(7): 1305-1314.

Yang, X., Y. Chen and D. Gabuzda (1999). "ERK MAP kinase links cytokine signals to activation of latent HIV-1 infection by stimulating a cooperative interaction of AP-1 and NF-kappaB." J Biol Chem **274**(39): 27981-27988.

Yarandi, S. S., M. R. Duggan and I. K. Sariyer (2020). "Emerging Role of Nef in the Development of HIV Associated Neurological Disorders." Journal of neuroimmune pharmacology : the official journal of the Society on NeuroImmune Pharmacology.

Yarandi, S. S., J. A. Robinson, S. Vakili, M. Donadoni, T. H. Burdo and I. K. Sariyer (2020). "Characterization of Nef expression in different brain regions of SIV-infected macaques." PloS one **15**(11): e0241667.

Yeager, M. and B. J. Nicholson (1996). "Structure of gap junction intercellular channels." Curr Opin Struct Biol **6**(2): 183-192.

Yilmaz, A., K. Blennow, L. Hagberg, S. Nilsson, R. W. Price, J. Schouten, S. Spudich, J. Underwood, H. Zetterberg and M. Gisslen (2017). "Neurofilament light chain protein as a marker of neuronal injury: review of its use in HIV-1 infection and reference values for HIV-negative controls." Expert Rev Mol Diagn **17**(8): 761-770.

Yin, F. (2022). "Lipid metabolism and Alzheimer's disease: clinical evidence, mechanistic link and therapeutic promise." FEBS J.

Young, A. C., C. T. Yiannoutsos, M. Hegde, E. Lee, J. Peterson, R. Walter, R. W. Price, D. J. Meyerhoff and S. Spudich (2014). "Cerebral metabolite changes prior to and after antiretroviral therapy in primary HIV infection." Neurology **83**(18): 1592-1600.

Yu, R. K., Y. T. Tsai, T. Ariga and M. Yanagisawa (2011). "Structures, biosynthesis, and functions of gangliosides--an overview." J Oleo Sci **60**(10): 537-544.

Yuan, L., A. Liu, L. Qiao, B. Sheng, M. Xu, W. Li and D. Chen (2015). "The relationship of CSF and plasma cytokine levels in HIV infected patients with neurocognitive impairment." Biomed Res Int **2015**: 506872.

Yuan, L., F. Wei, X. Zhang, X. Guo, X. Lu, B. Su, T. Zhang, H. Wu and D. Chen (2017). "Intercellular Adhesion Molecular-5 as Marker in HIV Associated Neurocognitive Disorder." Aging Dis **8**(3): 250-256.

Zaima, N., T. Hayasaka, N. Goto-Inoue and M. Setou (2009). "Imaging of metabolites by MALDI mass spectrometry." J Oleo Sci **58**(8): 415-419.

Zajonc, D. M. and M. Kronenberg (2009). "Carbohydrate specificity of the recognition of diverse glycolipids by natural killer T cells." Immunol Rev **230**(1): 188-200.

Zhan, X., G. C. Jickling, B. P. Ander, B. Stamova, D. Liu, P. F. Kao, M. A. Zelin, L. W. Jin, C. DeCarli and F. R. Sharp (2015). "Myelin basic protein associates with AbetaPP, Abeta1-42, and amyloid plaques in cortex of Alzheimer's disease brain." J Alzheimers Dis **44**(4): 1213-1229.

Zhang, X., F. Zhang, X. Ma, X. Zhao, W. Li, Z. Zhang, J. Zhang, X. E. Zhang and Z. Cui (2016). "Identification of interaction between HIV-1 glycoprotein 41 and integrase." Virologica Sinica **31**(5): 415-424.

Zhong, P., L. M. Agosto, A. Ilinskaya, B. Dorjbal, R. Truong, D. Derse, P. D. Uchil, G. Heidecker and W. Mothes (2013). "Cell-to-cell transmission can overcome multiple donor and target cell barriers imposed on cell-free HIV." PLoS One **8**(1): e53138.

Zhou, J., X. Chi, M. Cheng, X. Huang, X. Liu, J. Fan, H. Xu, T. Lin, L. Shi, C. Qin and W. Yang (2019). "Zika virus degrades the omega-3 fatty acid transporter Mfsd2a in brain microvascular endothelial cells and impairs lipid homeostasis." Sci Adv **5**(10): eaax7142.

Zimmerman, M., L. Blanc, P. Y. Chen, V. Dartois and B. Prideaux (2018). "Spatial Quantification of Drugs in Pulmonary Tuberculosis Lesions by Laser Capture Microdissection Liquid Chromatography Mass Spectrometry (LCM-LC/MS)." J Vis Exp(134).

Zonta, M., M. C. Angulo, S. Gobbo, B. Rosengarten, K. A. Hossmann, T. Pozzan and G. Carmignoto (2003). "Neuron-to-astrocyte signaling is central to the dynamic control of brain microcirculation." Nat Neurosci **6**(1): 43-50.

Zonta, M., A. Sebelin, S. Gobbo, T. Fellin, T. Pozzan and G. Carmignoto (2003). "Glutamate-mediated cytosolic calcium oscillations regulate a pulsatile prostaglandin release from cultured rat astrocytes." J Physiol **553**(Pt 2): 407-414.

Vita

Daniela D'Amico was born on May 12th, 1990 in Palermo, Italy, to Di Salvo Paola & D'Amico Santo. Daniela's older sister, Teresa, was born on June 20, 1985. Daniela attended Primary and Secondary school in nearby Bagheria, where she lived. Daniela earned her high school diploma from Scientific High School in 2009. She completed her Bachelor of Biotechnology at the nearby University of Palermo between 2009 and 2013 and her Master of Industrial Biotechnology between 2013 and 2016, from which she graduated Cum Laude. While at Palermo's University, Daniela completed an Honor's Thesis project comprised of original research, titled "Hspd1 gene over-expression in C_2C_{12} cells induces the expression of PCG1α" under the mentorship and guidance of Dr. Valentina Di Felice. After graduation, throughout the spring and summer of 2016, Daniela spent 6 months at the Biomedicine, Neuroscience and Advanced Diagnostic department at the University of Palermo and Catholic University in Rome for an unpaid internship developing a patent titled "Synthesis of exosomes containing Heat shock proteins and their use as a treatment for muscle atrophy and cachexia". In September 2016, Daniela applied for the combined pre-doctoral fellowship between the University of Palermo and the University of Texas Medical Branch, where she was offered a position in the Neuroscience Graduate Program. After the first year in Palermo, Daniela joined the lab of Dr. Fernanda Laezza and later the lab of Dr. Eugenin Eliseo and Dr. Prideaux Brendan at UTMB. She has been the recipient of awards including Best Oral Presentation at Neuroscience Graduate Program Symposium (2018), Early Career Support Award for International Gap Junction Conference (2019), Samuel N. Kolmen, Ph.D. and Barbara Kass Kolmen, M.D. Award (2019), Best Poster Award at the Neuroscience, Cell Biology, and Anatomy Department Retreat (2020), and Elferink

Scholarship for Academic Excellence Award (2020). She graduated from the University of Palermo in 2020. In the lab of Dr. Eliseo A. Eugenin and Dr. Brendan Prideaux, Daniela continued to undertake her project to evaluate the mechanism of HIV-Associated Neurocognitive Disorders, focusing on myelin structure and lipid dysregulation, which would develop into this dissertation project.

Manuscripts:

1. Mangano, G.D.; Fouani, M.; **D'Amico, D.**; Di Felice, V.; Barone, R. (2022) Cancer-Related Cachexia: The Vicious Circle between Inflammatory Cytokines, Skeletal Muscle, Lipid Metabolism and the Possible Role of Physical Training. Int. J. Mol. Sci. 23, 3004. https://doi.org/10.3390/ijms23063004
2. Di Felice, V.; Barone, R.; Trovato, E.; **D'Amico, D**.; Macaluso, F.; Campanella, C.; Marino Gammazza, A.; Muccilli, V.; Cunsolo, V.; Cancemi, P.; Multhoff, G.; Coletti, D.; Adamo, S.; Farina, F.; Cappello, F. (2022) Physiactisome: A New Nanovesicle Drug Containing Heat Shock Protein 60 for Treating Muscle Wasting and Cachexia. Cells 11, 1406. https://doi.org/10.3390/cells11091406
3. **D'Amico, D.**; Fiore, R.; Caporossi, D.; Di Felice, V.; Cappello, F.; Dimauro, I.; Barone, R. (2021) Function and Fiber-Type Specific Distribution of Hsp60 and αB-Crystallin in Skeletal Muscles: Role of Physical Exercise. Biology 10, 77. https://doi.org/10.3390/biology10020077
4. Malik S., Valdebenito S., **D'Amico D.**, Prideaux B., Eugenin EA. (2021) HIV infection of astrocytes compromises inter-organelle interactions and inositol phosphate metabolism: A potential mechanism of bystander damage and viral reservoir survival. Prog Neurobiol.;206:102157. doi: 10.1016/j.pneurobio.2021.102157.
5. **D'Amico D.**, Marino Gammazza A., Macaluso F., Paladino L., Scalia F., Spinoso G., Dimauro I., Caporossi D., Cappello F., Di Felice V., Barone R. (2021) Sex-based differences after a single bout of exercise on PGC1α isoforms in skeletal muscle: A pilot study. FASEB J.;35(2):e21328. doi: 10.1096/fj.202002173R.
6. **D'Amico D.**, Valdebenito S., Eugenin E.A. (2021) The role of Pannexin-1 channels and extracellular ATP in the pathogenesis of the human immunodeficiency virus. Purinergic Signalling 17, 563–576. https://doi.org/10.1007/s11302-021-09817-3
7. Wadsworth P.A., Folorunso O., Nguyen N., Singh A.K., **D'Amico D.**, Powell R.T., Brunell D., Allen J., Stephan C., Laezza F. (2019) High-throughput screening against protein:protein interaction interfaces reveals anti-cancer therapeutics as potent modulators of the voltage-gated Na+ channel complex. Sci Rep 9, 16890. https://doi.org/10.1038/s41598-019-53110-8
8. Valdebenito S., **D'Amico D**., Eugenin E. (2019) Novel approaches for glioblastoma treatment: Focus on tumor heterogeneity, treatment resistance, and computational tools. Cancer Rep (Hoboken);2(6):e1220. doi: 10.1002/cnr2.1220
9. Barone R., Sangiorgi C., Marino Gammazza A., **D'Amico D.**, Salerno M., Cappello F., Pomara C., Zummo G., Farina F., Di Felice V., Macaluso F. (2017)

Effects of Conjugated Linoleic Acid Associated With Endurance Exercise on Muscle Fibres and Peroxisome Proliferator-Activated Receptor γ Coactivator 1 α Isoforms. J Cell Physiol.;232(5):1086-1094. doi: 10.1002/jcp.25511

10. Barone R., Pitruzzella A., Marino Gammazza A., Rappa F., Salerno M., Barone F., Sangiorgi C., **D'Amico D.**, Locorotondo N., Di Gaudio F., Cipolloni L., Di Felice V., Schiavone S., Rapisarda V., Sani G., Tambo A., Cappello F., Turillazzi E., Pomara C. (2017) Nandrolone decanoate interferes with testosterone biosynthesis altering blood-testis barrier components. J Cell Mol Med.;21(8):1636-1647. doi: 10.1111/jcmm.13092

Manuscripts submitted or in preparation:

1. Donoso M., **D'Amico D.**, Valdebenito S., Hernandez C., Prideaux B. and Eugenin E.A. (2022) Identification, quantification, and characterization of HIV-1 reservoirs in the human brain. Submitted on Cell Report Medicine Journal, under second review.
2. **D'Amico D.**, Barone R., Di Felice V., Ances B. M., Prideaux B., Eugenin E. A. (2022) Chronic Brain Damage in HIV-Infected Individuals under Combined Anti Retroviral Therapy is Associated with Viral Reservoirs, Sulfatide Release, and Compromised Cell-to-Cell Communication". Submitted on Cells Journal, under second review.
3. **D'Amico D.**, Marcatti M., Fracassi A. Taglialatela G., Eugenin E.A., Prideaux B. (2022) MALDI-2 MSI Enhances Analytical Sensitivity for Triacylglycerides in Brain Tissue from an Alzheimer Mouse Model. In preparation.

Her final oral defense and examination commenced June 29th, 2022.

Permanent address: 56, Via Sant'Antonio, Bagheria, Italy, 90011

This dissertation was typed by Daniela D'Amico.